TECHNICAL REPORT S-72-4

PHYSICAL PROPERTY AND DYNAMIC COMPRESSIBILITY ANALYSIS OF THE WATCHING HILL BLAST RANGE

by

J. G. Jackson, Jr.

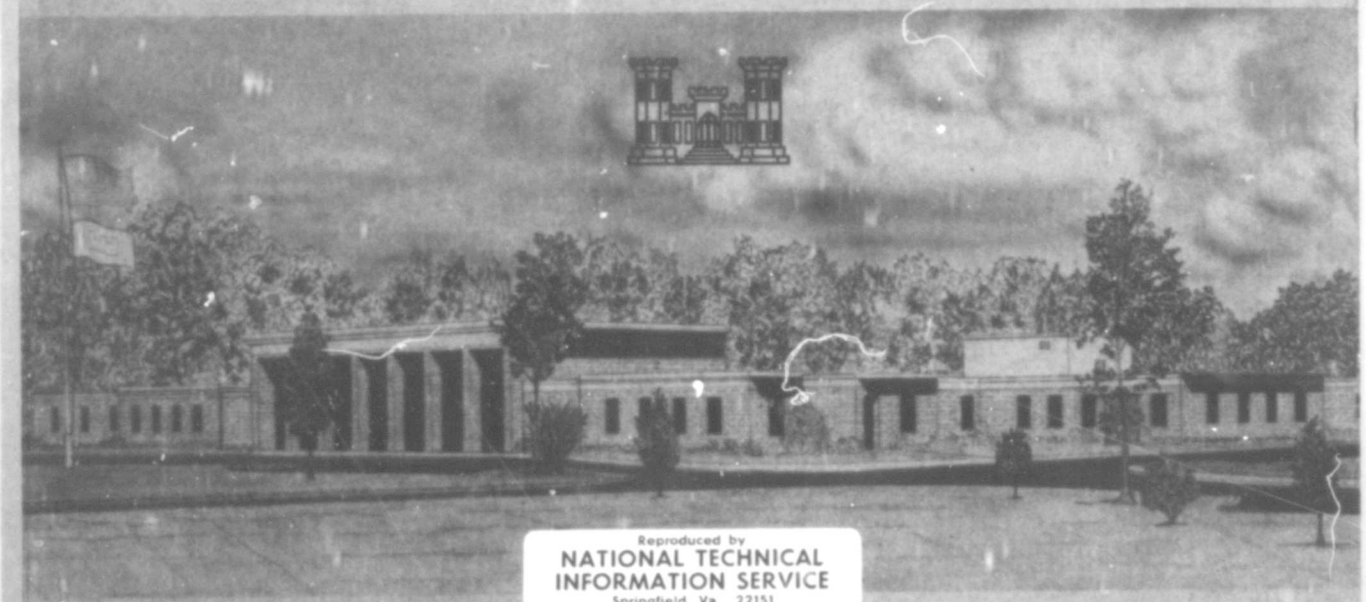

April 1972

Sponsored by Defense Nuclear Agency and Office, Chief of Engineers, U. S. Army

Conducted by U. S. Army Engineer Waterways Experiment Station, Vicksburg, Mississippi

Unclassified

Security Classification

DOCUMENT CONTROL DATA - R & D

(Security classification of title, body of abstract and indexing annotation must be entered when the overall report is classified)

1. ORIGINATING ACTIVITY (Corporate author) U. S. Army Engineer Waterways Experiment Station Vicksburg, Mississippi	2a. REPORT SECURITY CLASSIFICATION Unclassified 2b. GROUP

3. REPORT TITLE

PHYSICAL PROPERTY AND DYNAMIC COMPRESSIBILITY ANALYSIS OF THE WATCHING HILL BLAST RANGE

4. DESCRIPTIVE NOTES (Type of report and inclusive dates)

Final report

5. AUTHOR(S) (First name, middle initial, last name)

John G. Jackson, Jr.

6. REPORT DATE April 1972	7a. TOTAL NO. OF PAGES 169	7b. NO. OF REFS 60
8a. CONTRACT OR GRANT NO. b. PROJECT NO. c. d.	9a. ORIGINATOR'S REPORT NUMBER(S) Technical Report S-72-4 9b. OTHER REPORT NO(S) (Any other numbers that may be assigned this report)	

10. DISTRIBUTION STATEMENT

Approved for public release; distribution unlimited.

11. SUPPLEMENTARY NOTES Report was also submitted to University of Michigan, Ann Arbor, Michigan, as thesis for degree of Doctor of Philosophy in Civil Engineering	12. SPONSORING MILITARY ACTIVITY Defense Nuclear Agency and Office, Chief of Engineers, U. S. Army Washington, D. C.

13. ABSTRACT

In this study, geologic, physical property, and dynamic and static soil compressibility test data for the Watching Hill Blast Range at the Defence Research Establishment were analyzed. The site consists of a thick succession of glacial tills and lake deposits; the near-surface deposit is composed of thin interbedded layers of lacustrine silt, sand, and clay sediments. The problem was to furnish accurate profile information for ground shock calculations of explosive events and to select stress-strain curves to represent the in situ response of each stratum to transient uniaxial strain loading and unloading. Primarily, the analyses were conducted to determine if a simplified procedure could be developed whereby this could readily be done for any location within the site for which a field boring log and conventional soil classification test data were available. Such a procedure was developed. The Unified Soil Classification System was found to be too broad to adequately classify the various fine-grained sediments in the near-surface lacustrine deposit. However, an expanded grain-size and plasticity-based classification was established whereby all the sediments could be sorted into one of six soil groups. Specific gravity, water content, and density data for each of the groups revealed consistent patterns of variation with depth and/or elevation. Therefore, the calculated void ratios, porosities, saturations, and air void contents also exhibited characteristic profiles. However, due to geologic and climatic influences, these composition property profiles were quite site dependent. They were used as a basis for subdividing each of the groups into five generalized profile zones in which all the soil strata of the given soil group were expected to have similar compressibility characteristics. Based on laboratory loading history similarities, the available uniaxial strain (or compressibility) data for each group could be further categorized according to loading rate. By studying the records of field stress measurements obtained during explosive events, a rough correlation was established between laboratory loading rates and those expected at various depths and surface overpressure ranges. Based on an analysis of 130 measured strain-strain relationships, curves were drawn to represent in situ uniaxial strain response of each soil classification group-profile zone combination. These curves quantitatively define the compressibility of the various interbedded soil strata in the upper glacial lake deposit at Watching Hill.

DD FORM 1473 (PAGE 1) REPLACES DD FORM 1473, 1 JAN 68, WHICH IS OBSOLETE FOR ARMY USE.

Unclassified

Security Classification

14. KEY WORDS	LINK A		LINK B		LINK C	
	ROLE	WT	ROLE	WT	ROLE	WT
Compressibility (Soils)						
Ground shock calculations						
Soil classification						
Soil properties						
Stress-strain relations (Soils)						
Watching Hill Blast Range						

TECHNICAL REPORT S-72-4

PHYSICAL PROPERTY AND DYNAMIC COMPRESSIBILITY ANALYSIS OF THE WATCHING HILL BLAST RANGE

by

J. G. Jackson, Jr.

Details of illustrations in this document may be better studied on microfiche

April 1972

Sponsored by Defense Nuclear Agency and Office, Chief of Engineers, U. S. Army

Conducted by U. S. Army Engineer Waterways Experiment Station, Vicksburg, Mississippi

ARMY-MRC VICKSBURG, MISS.

ABSTRACT

This study was concerned with the analysis of geologic, physical property, and dynamic and static soil compressibility test data obtained for the Watching Hill Blast Range at the Defence Research Establishment Suffield, Alberta, Canada. The site profile consists of a thick succession of glacial tills and lake deposits with the near-surface deposit composed of thin interbedded layers of lacustrine silt, sand, and clay sediments. The problem posed was that of furnishing accurate profile information for ground shock calculations of explosive events and selecting stress-strain curves to represent the in situ response of each stratum in the profile to transient uniaxial strain loading and unloading. The primary purpose of the analyses was to determine if a simplified procedure could be developed whereby this could readily be done for any given location within the site for which a field boring log and conventional soil classification test data were available.

It was possible to develop such a procedure; two example applications are given for demonstration purposes. In the process of developing this procedure, it was found that the Unified Soil Classification System was too broad to adequately classify the various fine-grained sediments found within the near-surface lacustrine deposit. It was

possible, however, to establish an expanded grain size and plasticity based classification whereby all of the sediments, regardless of their elevation location within the deposit, could be sorted into one of six soil groups.

The specific gravity, water content, and density data for each of the six soil groups revealed consistent patterns of variation with depth and/or elevation. Therefore, the calculated void ratios, porosities, saturations, and air void contents also exhibited characteristic profiles. Evidence was presented, however, to show that, due to geologic and climatic influences, these composition property profiles were quite site dependent. They were used as a basis for subdividing each of the six soil classification groups into five generalized profile zones within which all the soil strata of the given soil group were expected to have similar compressibility characteristics.

As a result of laboratory loading history similarities, the available uniaxial strain (or compressibility) test data for each soil group could be further categorized according to loading rate. By studying the records of field stress measurements obtained during explosive events, a rough correlation was established between laboratory test loading rates and those expected at various depths and surface overpressure ranges.

Finally, based on the analysis of 130 measured stress-strain relationships (120 of which were from undisturbed specimens), a set of curves was drawn to represent, as a function of loading rate, the in situ uniaxial strain response of each soil classification group-profile zone combination. These curves quantitatively define the compressibility of the various interbedded soil strata in the upper glacial lake deposit at Watching Hill.

PREFACE

The work reported herein was conducted in the Soils Division of the U. S. Army Engineer Waterways Experiment Station (WES). It was sponsored by the Defense Nuclear Agency (DNA) under Nuclear Weapons Effects Research Subtask SB 209, "Propagation of Ground Shock Through Earth Media," and by the Office, Chief of Engineers (OCE), under Nuclear Construction and Engineering Task 08, "Ground Shock and Dynamic Earth Pressure Effects." The study primarily involved a collective analysis of conventional and special-purpose soil property test data obtained by WES over a four-year period from 1967 to 1971 in support of the DNA-sponsored high-explosive events at the Watching Hill Blast Range of the Defence Research Establishment, Suffield (DRES), Ralston, Alberta, Canada.

This report is essentially a dissertation submitted by Mr. J. G. Jackson, Jr., of the Soil Dynamics Branch to the University of Michigan in partial fulfillment of the requirements for the degree of Doctor of Philosophy in Civil Engineering. Mr. J. E. Windham and CPT R. W. Peterson assisted in conducting the experimental programs. The cooperation and assistance of many other WES associates who contributed in some way to the completion of this project are acknowledged. The work was performed under the general direction of Mr. J. P. Sale, Chief of the Soils Division, and Mr. R. W. Cunny, Chief of the Soil Dynamics Branch.

Director of WES during the conduct of this study and the preparation of this report was COL Ernest D. Peixotto, CE. Technical Director was Mr. F. R. Brown.

CONTENTS

LIST OF TABLES

LIST OF ILLUSTRATIONS

LIST OF ILLUSTRATIONS (CONTINUED)

LIST OF ILLUSTRATIONS (CONTINUED)

LIST OF ILLUSTRATIONS (CONTINUED)

LIST OF ILLUSTRATIONS (CONTINUED)

CONVERSION FACTORS, BRITISH TO METRIC UNITS OF MEASUREMENT

British units of measurement used in this report can be converted to metric units as follows:

Multiply	By	To Obtain
mils	0.0254	millimeters
inches	2.54	centimeters
feet	0.3048	meters
tons (2000 pounds)	907.185	kilograms
pounds per square inch	0.6894757	newtons per square centimeter
pounds per cubic foot	16.0185	kilograms per cubic meter
feet per second	0.3048	meters per second

CHAPTER 1

INTRODUCTION

1.1 BACKGROUND

Until nearly midway into the Twentieth Century, interest in the study of explosively induced earth motions centered primarily about prevention of blasting damage caused by construction excavation, tunneling, quarrying, and mining operations. The introduction during World War II of large high explosive bombs quickened interest in the effects of earth motion as a factor in the design of fortifications. But it was the development of nuclear explosives and the physical devastation demonstrated by their application over Japan that made it absolutely imperative that an intensive effort be mounted to understand the propagation and attenuation of explosively induced waves through the earth, how the earth is transformed under their influence, and how these waves affect buried structures.[1]

As part of this effort, under the auspices of the Technical Cooperation Program with participation by the United States, the United Kingdom, Canada, and Australia, an extensive program of large-scale, high explosive field tests has been conducted on the Watching Hill Blast Range at the Defence Research Establishment Suffield (DRES),[2] Alberta, Canada. The general site location is shown in Figure 1.1. The tests date back to 1959 when a 5-ton[3] charge of TNT was detonated; this was followed by a 20-ton event in 1960 and a 100-ton event in 1961.

---

[1] The status of this understanding as of the mid-1960's is presented in two excellent and comprehensive summaries by Sauer et al. (1964) and Whitman (1970).

[2] Formerly designated as the Suffield Experimental Station (SES).

[3] A table of factors for converting British units of measurement to metric units is presented on page xvii.

This early series, known as the Canadian Trials, was followed by the 500-ton Operation SNOW BALL event in 1964, by the 100-ton Event 6 and the 20-ton Event 1A of Operation DISTANT PLAIN in 1967, by the 500-ton Operation PRAIRIE FLAT event in 1968, and, most recently, by the 500-ton Operation DIAL PACK event in 1970. The ground zero (GZ) location for each of these eight detonations is shown on the site contour map in Figure 1.2.

The last five events, conducted by the U. S. Defense Nuclear Agency (DNA),[3] are of primary interest since each included one or more projects to measure the transient stresses and/or motions transmitted to various ranges and depths beneath the ground surface. Such basic information on explosive-induced ground shock phenomena is necessary in order to validate theoretical prediction techniques. The field measurements, however, reflect the effects of waves passed through the characteristic stratifications and unique soil media of the Watching Hill test site. Thus, in order to fully interpret these measurements and provide the proper input to theoretical calculation studies, detailed information must be made available regarding the subsurface soil profiles for the site and their related physical and mechanical properties. The mechanical property of primary interest is the stress-strain relation generated from an impulsive stress applied to an undisturbed specimen confined so as to deform in an undrained state of uniaxial strain, i.e., the dynamic compressibility (Jackson, 1968a).

Furnishing accurate data regarding soil profiles and properties for the various events at the Watching Hill site has proved to be by no

---

[3] Formerly designated as the Defense Atomic Support Agency (DASA).

means an easy task. The site is located on the relatively flat surface of an old glacial lake bed. The near-surface deposits consist of thin interbedded layers of silt, sand, and clay, as indicated by the photograph in Figure 1.3. In discussing their attempts to correlate cratering data from the different events, Jones et al. (1970) take note of the difficulties with rapidly varying soil properties by stating that "In the very incompetent material of the Suffield test sites, in which layers of free running sand alternate with soft clay-silts, any form of coherent motion of the surface layers as part of a cratering mechanism appears most improbable, and this lack of plausibility possibly explains why it has taken a decade to recognize it." Dynamic compressibility variations are specifically illustrated by the photographs in Figure 1.4. The left-hand photograph reveals four distinct and alternating stratums of silt and clay within the 12-inch-high sample. The adjacent uniaxial strain test Polaroids show that the relatively dry silt compressed 82 mils under a dynamically applied stress of 500 psi while the nearly saturated clay, just inches away, compressed only 2.5 mils under similar loading, i.e., a sudden decrease in dynamic compressibility by a factor of 33.

Field subsurface exploration and sampling programs of varying scope have been conducted in the vicinity of each of the Watching Hill events. In addition, a number of laboratory testing programs have been conducted to obtain both conventional and special-purpose soil property data in support of the various projects and agencies involved in the explosive experiments. The major portion of this work has been performed by the U. S. Army Engineer Waterways Experiment Station (WES), Vicksburg, Mississippi, and the data obtained is on file there. While

the data from any one project are generally somewhat limited, the total data obtained to date represent an unusually large assemblage of profile and property information. If analyzed collectively, these data should lead to a much better picture than has heretofore been possible of the overall site stratigraphy, the nature of the associated soil deposits, and the influence exerted by physical properties on the dynamic compressibility of near-surface glacial lake sediments.

1.2 PURPOSE AND SCOPE

The problem posed for the Watching Hill soils analyst is that of furnishing accurate profile information for ground shock calculations and selecting stress-strain curves to represent the in situ response of each layer in the profile to transient uniaxial strain loading and unloading. The primary purpose of this study was to develop a simplified procedure whereby the necessary calculation profiles and special-purpose soil properties can readily be established for any given location within the site for which a field boring log and conventional soil classification test data are available. In order to do this, the study proposes to:

1. Review the available geologic, field exploration, and laboratory soil property data to establish the overall stratigraphy of the Watching Hill Blast Range.

2. Critically examine the physical property data for the soils obtained from the most recent glacial lake deposit and relate the variation of their three-phase (air, water, solid) composition properties with depth to their conventional classification and index properties.

3. Assemble and analyze the available compressibility data for the interbedded clays, silts, and sands found in the near-surface

deposit. Present it in such a manner as to quantitatively illustrate the influence of particle gradation, density, natural structure, saturation, and rate of loading on their stress-strain behavior.

4. Illustrate the application of the above information by defining, from conventional boring and classification data, the basic soil profile and dynamic compressibility input required for theoretical ground shock calculations related to two specific HE events at the Watching Hill Blast Range.

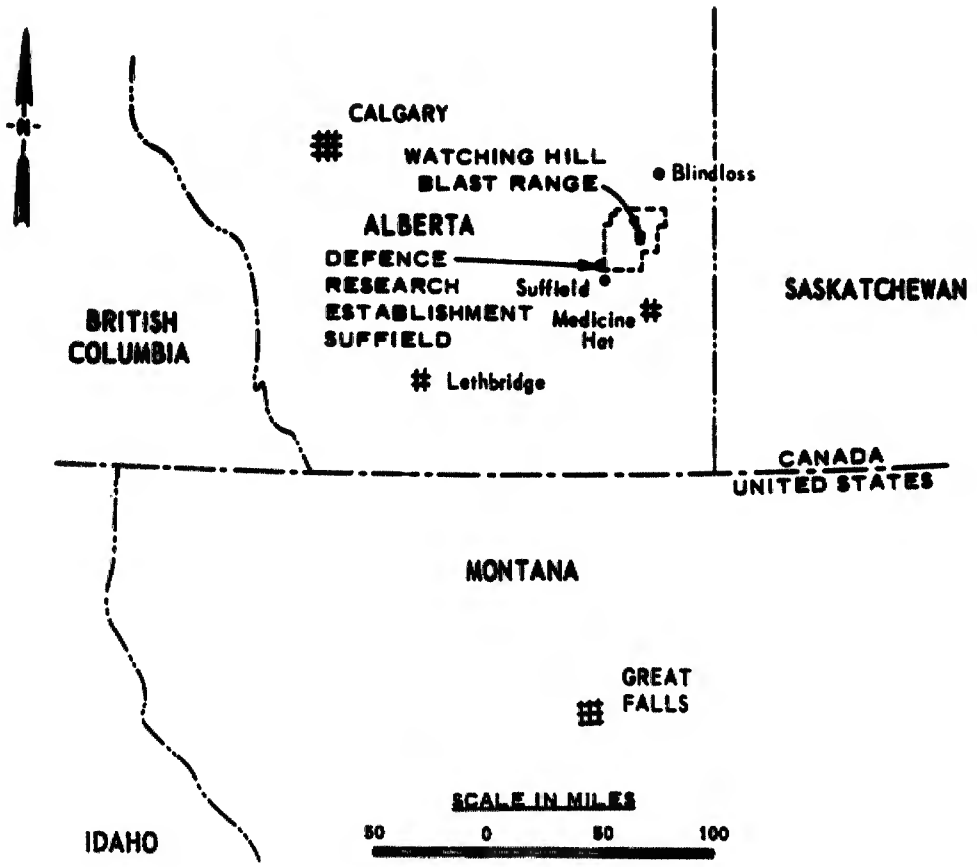

Figure 1.1 General site location map.

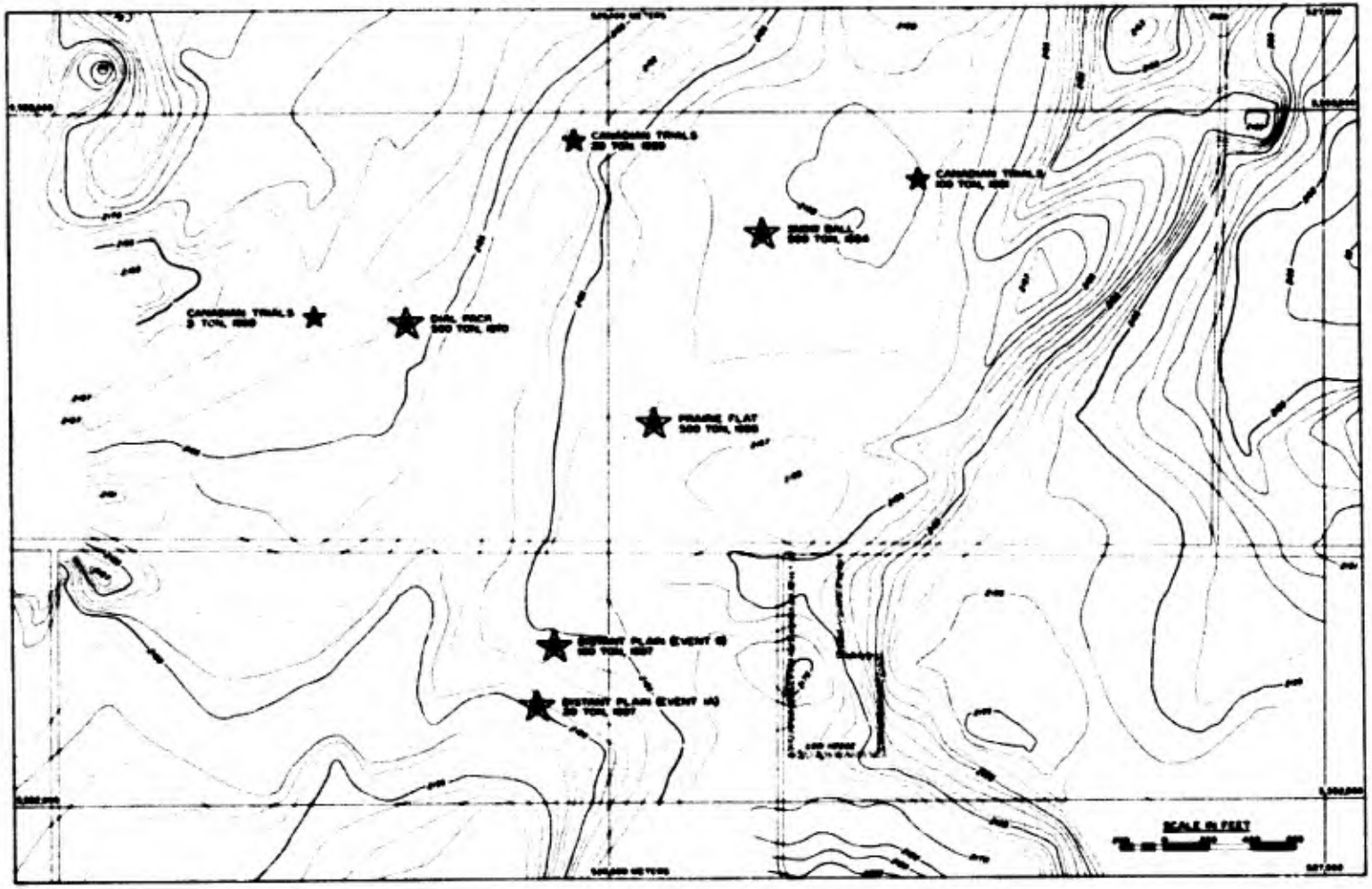

Figure 1.2 Location of high explosive field tests on the Watching Hill Blast Range.

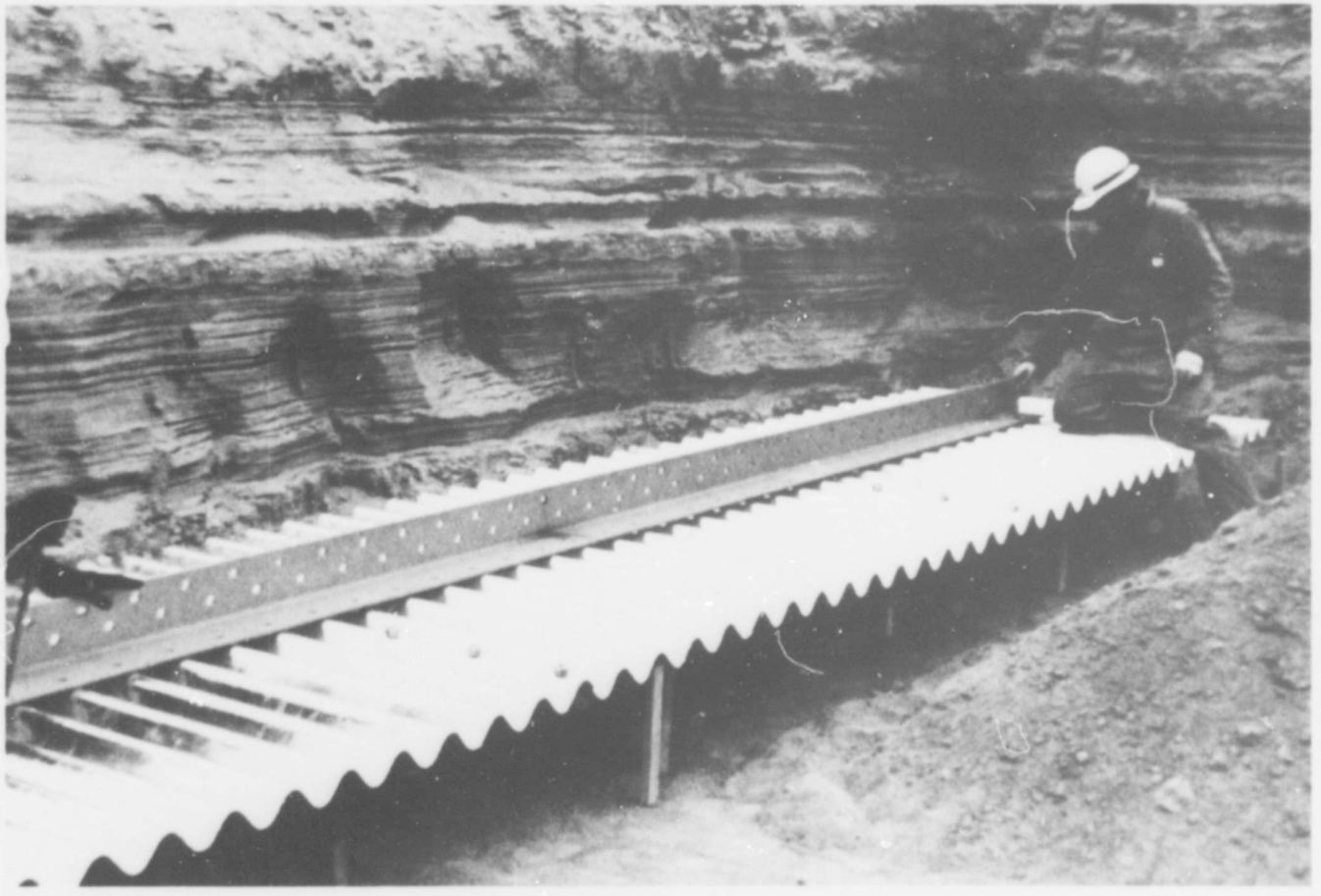

Figure 1.3 Interbedded glacial lake sediments exposed during excavation for DIAL PACK Project LN 313.

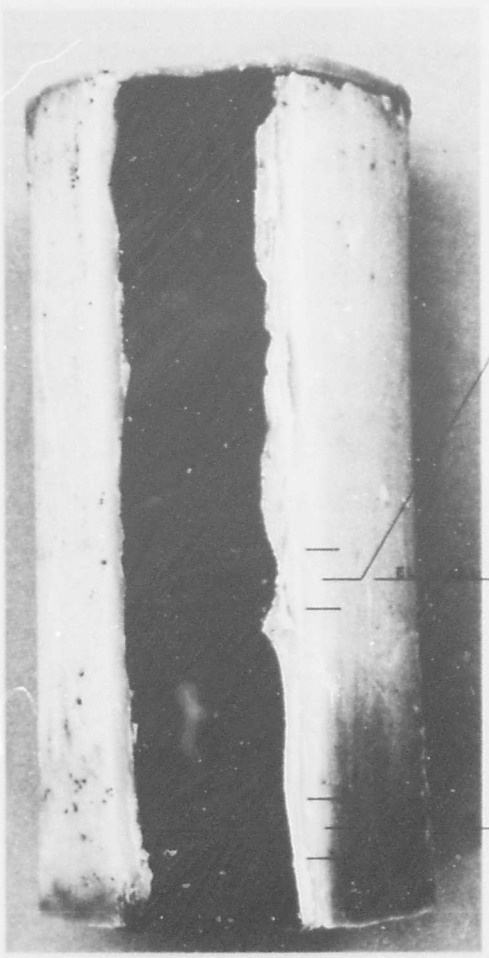

5-IN. DIAM SHELBY-TUBE SAMPLE NO. 10
DIAL PACK BORING NO. U3

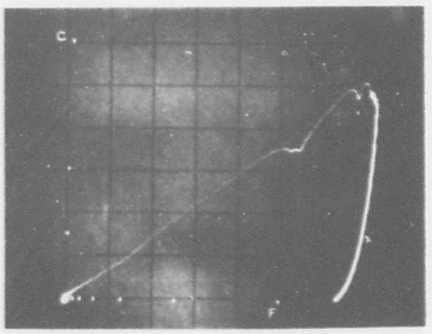

UNIAXIAL STRAIN TEST NO. DPK/3.10.3

VERTICAL SCALE: C=600 PSI
HORIZONTAL SCALE: F=62.0 MILS

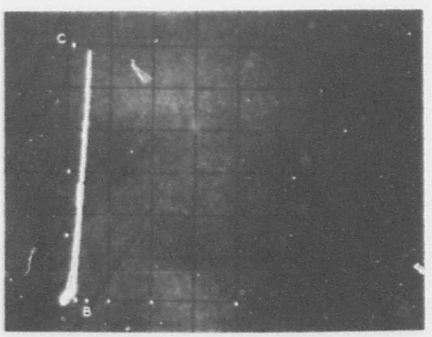

UNIAXIAL STRAIN TEST NO. DPK/3.10.4

VERTICAL SCALE: C=600 PSI
HORIZONTAL SCALE: B=3.9 MILS

Figure 1.4 Dynamic compressibility variations within 12-inch-high undisturbed soil sample.

CHAPTER 2

REVIEW OF SUBSURFACE INFORMATION

2.1 GEOLOGIC HISTORY OF THE AREA

The Watching Hill site is located in the rolling plains of southeastern Alberta in a region typical of western Canada's glacial topography, and overlies a large buried valley, probably the preglacial Milk River Channel (see Jones et al., 1970). Berg (1968) states that this northeast-southwest trending valley is a continuation of Geigers' (1965) Lethbridge Valley and joins another preglacial valley near Blindloss, Alberta (see Figure 1.1). The geologic history of the area since Precambrian time has been traced by Lewis (1970), who estimates that erosion removed approximately 2700 feet of sediment from the bedrock surface at the site prior to glaciation. This eroded surface was later subjected to loading and unloading by at least two ice sheets estimated to be 2200 feet or more thick (see Gravenor and Bayrock, 1961). The glaciers disrupted drainage systems throughout the plains, and formed many temporary lakes in former valleys. Berg's (1968) stratigraphic survey, conducted some 15 miles southwest of the Watching Hill site, reveals lacustrine deposits from at least three such Pleistocene lakes.

The topography of the area immediately surrounding the Watching Hill Blast Range is shown on the 25-foot-contour map in Figure 2.1. Jones (1963) notes that Juniper Flats to the southwest and Dishpan Lake to the northeast are probably nonperennial vestiges of the most recent glacial lake covering and observes what appears to be a late boundary of this lake running from the South Saskatchewan River circling north to northwest around the Ross Depression. This boundary has the form

of a distinct "shoreline" of heavy boulder drift, the boundary showing a sharp transition between the almost stone-free lacustrine deposit and the heavy drift beyond.

The Pleistocene succession of tills and lake deposits is underlain by Upper Cretaceous beds of either the lower Oldman or the upper Foremost formation. The lower Oldman is princially composed of freshwater sandstone and shale units, while the brackish water Foremost deposits are capped by a zone of coal seams and carbonaceous shales (see Crockford, 1949; and Lewis, 1970). In these beds, it is difficult to identify the contact between the Foremost formation and the overlying Oldman formation, but based primarily on elevation data, it appears that most if not all of the Oldman formation is absent in the Watching Hill area, so that bedrock beneath the test site is probably Foremost (see Jones, 1960, 1963; and Jones et al., 1970).

2.2 FIELD SEISMIC INVESTIGATIONS

Jones (1963) summarizes the results of a deep refraction seismic survey conducted in 1961 by the Century Geophysical Corporation of Canada with one of its primary objectives to determine depths to bedrock beneath the Watching Hill test site. The first shot point was located approximately 50 feet south of the Canadian Trials 20-ton GZ with geophones spaced at 250-foot intervals along a S 39° W bearing, passing within 130 feet of the GZ location for the DIAL PACK event (see Figure 1.2). Figure 2.2 shows the section of the refraction profile pertinent to this study, together with the lithology actually logged by the driller. This section indicates a 2200-ft/sec velocity to a depth of 40 to 45 feet followed by a 5500-ft/sec velocity stratum, which is presumed to extend to a bedrock formation having a 7500-ft/sec

velocity. On this basis, the calculated depth to bedrock varies between 225 and 275 feet across the site.

Downhole velocity measurements were made in two holes drilled to a depth of 230 feet. A velocity of 2100 ft/sec is given for the 0- to 42-foot depth range, but the data on which this interpretation is based is meager and scattered. From 42 to 130 feet, however, a 5500-ft/sec velocity fits the data quite well; from 130 feet to the top of the "hard gray clay" stratum at 215 feet, the velocity appears to gradually increase from 5500 to about 6000 ft/sec.

Reed, Zelman, and Coates (1964) report the results of a shallow refraction survey conducted using a sledgehammer source in conjunction with Operation SNOW BALL. This survey extended some 2100 feet across the test site from the SNOW BALL GZ along a S 44° W bearing, passing approximately 360 feet west of the GZ for Operation PRAIRIE FLAT. The data from this survey are plotted in Figure 2.3; the interpretation shown in the figure indicates an upper soil profile with two very distinct zones of material, i.e., a surface layer with an average seismic velocity of 1150 ft/sec overlying a second very dense or saturated layer, at a depth of about 21 feet, with an average velocity of 4850 ft/sec. Results of a similar but less extensive survey along a N 38° W bearing from the SNOW BALL GZ are reported by Zelman (1964). These data indicate an average velocity for the near-surface soils of 1070 ft/sec, changing at a depth of approximately 23 feet to an average velocity of 5330 ft/sec.

A composite seismic velocity profile for the Watching Hill site can be obtained by combining the results from the above studies as follows:

Depth Interval ft	Seismic Velocity ft/sec
0 to 21	1150
21 to 42	4850
42 to 130	5500
130 to 215	6000
>215	7500

Further comment on this field seismic information will be deferred for the present, since its accuracy in depicting the actual subsurface stratigraphy of the site and its usefulness in correlating with physical properties such as dynamic compressibility can best be assessed after results are presented from exploratory borings and laboratory soil property tests.

2.3 SITE STRATIGRAPHIC STUDIES

A search of the published literature and the WES files revealed the logs of over 150 exploratory and sample borings drilled on the Watching Hill Blast Range since 1959. These logs depict a pattern of ever increasing interest in obtaining deeper profile information and undisturbed samples for laboratory property testing. The 26 earliest, drilled in support of the Canadian Trials, were primarily shallow auger holes (5 to 50 feet deep) yielding disturbed samples for visual classification and water content determinations. (See Goode, 1959; Strange, Wallace, and Strohm, 1961; Strange and Sager, 1962; and Strange and Pinkston, 1962.)

Fifty-two logs are available from Operation SNOW BALL, with three of these extending to depths in excess of 80 feet (see Rooke and Chew, 1965; and Davisson and Maynard, 1965). While most of these were from

auger borings, a number of undisturbed samples were obtained for subsequent laboratory physical and mechanical property testing.

Diehl and Jones (1966) report results of seven bucket auger holes, all over 70 feet deep with one to 105 feet, drilled in 1966 during preliminary siting studies for Operations DISTANT PLAIN and PRAIRIE FLAT. An extensive subsurface investigation was conducted in 1967 prior to these operations. This investigation included 7 piezometer installations, 15 standard penetration test (SPT) and split spoon sample borings, and 12 undisturbed sample borings; 3 of these borings were drilled to a depth of 100 feet (see Gatz, 1968). Jones et al. (1970) report on a 1968 boring at the PRAIRIE FLAT GZ drilled to bedrock at 222 feet (see Figure 2.4). Logs from a number of miscellaneous shallow borings are also available (see Odello, 1971a; and Briosi, 1970).

After examining several logs from borings drilled by DRES in the vicinity of Operations DISTANT PLAIN and PRAIRIE FLAT, Jones et al. (1970) noted that, due to the very fine interleaving of strata, it was quite difficult to identify minor strata consistently from borehole data. They also observed, however, that the stratigraphic pattern was essentially coherent and concluded that no marked stratigraphic change occurs over the area. The validity of their observations is readily substantiated by the logs of borings drilled by WES at the GZ locations of the three events in these same two operations (see Figure 2.5). An integrated analysis of all the available data, however, has now led to a fairly clear picture of the overall stratigraphy and lithology of the Watching Hill site.

The subsurface exploration and soil property testing program conducted for Operation DIAL PACK was particularly instrumental in

developing this picture. Three piezometers were installed, and sample borings were drilled at six locations (Gatz, 1969). To illustrate the type of data available, the field classified log and SPT results for a 100-foot-deep split spoon sample boring are given in Figure 2.6 along with those for the GZ boring, which was drilled to obtain continuous 5-inch-diameter undisturbed samples to a depth of 150 feet, followed by split spoon samples and NX cores to 250 feet. These data appear to indicate the presence of nine different stratigraphic units within the site profile.

The usefulness of soil mechanics laboratory test data in geologic interpretation was classically illustrated for a similar problem by Rominger and Rutledge (1952) who used data on Atterberg limits, natural water contents, and preconsolidation stress in establishing five stratigraphic units within the lacustrine sediments of glacial Lake Agassiz. Terzaghi and Peck (1948) note that a knowledge of the shape of the grain-size curves may assist in determining the geologic origin of a soil and thereby reduce the risk of error in interpretation of data obtained by test borings. Over the years, an unusually large quantity of grain-size distribution and Atterberg limits data has been generated in order to properly classify[1] the various soil test specimens obtained from the numerous Watching Hill borings. In addition, extensive data have been obtained in order to permit calculation of three-phase composition properties for many of these specimens. Plots depicting the variation of specific gravity of soil solids G_s, water content w, dry unit weight γ_d, and wet unit weight γ with subsurface elevation

---

[1] According to the Unified Soil Classification System (WES, 1960).

are given in Figure 2.7 for the DIAL PACK event; the nine stratigraphic units are denoted for correlation with Figure 2.6. Similar plots are available for all of the events of primary interest.

The five DNA-conducted events were mentioned in Chapter 1 as being of primary interest because each included free-field ground shock measurements. The traverse shown on the detailed site contour map in Figure 2.8 passes through the GZ boring locations for each of these events plus a selection of other borings found to be particularly useful in establishing the overall site stratigraphy. A three-dimensional plot of this traverse and the included borings is given in Figure 2.9. The nine stratigraphic units previously observed for DIAL PACK Boring U1 are noted in the figure; corresponding units in the other 10 borings are similarly shaded and connected by peripheral lines. A description and discussion of each of these units follows:

2.3.1 Unit 1 - Bedrock. The glacially disturbed, weathered clay shale surface of the Foremost formation was encountered in DPK/U1 at a depth of 210 feet (elevation 1956). The "hard gray clay" shown at a depth of 215 feet (elevation 1950) in Figure 2.2 and the "almost black stiff sandy clay" shown at a depth of 222 feet (elevation 1943) in Figure 2.4 are presumed to represent similar encounters. The upper clay shale is interbedded with clayey, poorly cemented sandstone. A thin seam of very hard, very fossiliferous, clayey limestone was found at 237 feet followed by a 3-foot-thick seam of black, hard, brittle coal. Subsequent strata consisted of soft to moderately hard dark gray clay shale alternating with thin clayey silt lenses.

The reported seismic velocity of 7500 ft/sec is quite reasonable for these Cretaceous sedimentary deposits. The bedrock surface beneath

the site appears, based on the test boring depth variation of only 12 feet, to be horizontal for all practical purposes; the 50-foot-depth variation indicated by the seismic survey probably represents a variation in the degree of glacial disturbance and weathering of the upper strata.

2.3.2 Unit 2 - Outwash Sand and Gravel. A 5- to 9-foot-thick stratum of sand and gravel was found above the bedrock unit in all three deep borings. The only grain-size curve available is given in Figure 2.10a. Berg (1968) identified the 18 feet of sand and gravel which he encountered directly above Oldman bedrock as alluvial fill in the preglacial river valley. Jones et al. (1970), however, describe the deep gravel at the Watching Hill site as "angular" (see Figure 2.4); while Lewis (1970) notes that it contains "some rounded particles." Based on these descriptions, the unit is probably an outwash sand and gravel of glacial origin.

2.3.3 Unit 3 - Lacustrine Deposit. Entry into Unit 3 is designated in Figure 2.4 by a change from "stiff sandy clay" to "fairly stiff silty clay," in Figure 2.6 by a change from "moderately hard" to "moderately soft" and by a noticeable drop in penetration resistance, and in Figure 2.7 by a slight increase in water content, which for a saturated clay indicates a slight decrease in dry density. The material in this 40- to 43-foot-thick unit is described by Lewis (1970) as a calcareous silty clay that is more plastic than the material above. He noted the presence of some very fine-grained sand and silt with a maximum sand grain size in the upper 30 feet of 0.07 mm, increasing to 0.25 mm in the bottom 10 feet. More important perhaps in assigning a lacustrine origin to this unit are the facts that gravel and shale

fragments were not observed in the samples and that the grain-size curve given in Figure 2.10a is similar to those obtained for clays of like plasticity found in the near-surface lacustrine deposit.

2.3.4 Unit 4 - Glacial Till. A 41- to 42-foot-thick stratum of glacial till was encountered at a depth of 131 feet (elevation 2034) at the PRAIRIE FLAT GZ (see Figure 2.4) and at 120 feet (elevation 2045) at the DIAL PACK GZ (see Figure 2.6). This unit may be correlative with the 36-foot-thick till unit found by Berg (1968) at about elevation 2065. Lewis (1970) describes the Watching Hill site material as a slightly calcareous, silty, sandy clay containing many angular, dark gray shale fragments embedded in the clay matrix. He also observed gravel particles scattered throughout and in one sample noted the presence of two granite cobbles 3 to 4 inches in diameter. The data in Figure 2.7 denotes uniform, high densities, indicating substantial precompression. The four grain-size curves shown for this till unit in Figure 2.10a are all nearly identical. Flint (1971) notes that because of this distinctive character, it is often possible to distinguish, in a single district, between two tills that are similar in appearance. The reason given for this is that an ice sheet transports drift having a characteristic assortment of grain sizes, which it mixes as it travels into a rather uniform mechanical composition. Figure 2.12 gives a ternary diagram expressing grain-size distribution in four types of till found in Ontario (see Flint, 1971, Figure 7-5A); the Unit 4 till gradation falls in an overlapping zone for till consisting mainly of claystone and siltstone (i.e., shale) and till consisting chiefly of clay and silt derived from lacustrine sediments.

2.3.5 Unit 5 - Outwash Sand and Gravel. A 4-foot-thick stratum of sand and gravel was logged at a depth of 117 feet (elevation 2050) in Boring DPK/U1 (see Figures 2.6 and 2.7). Lewis (1970) describes the up-to-3-inch-diameter gravel particles as subrounded to rounded and the sand and silt grains as angular to subrounded. The only grain-size curve available for this unit is given in Figure 2.10b.

2.3.6 Unit 6 - Lacustrine Deposit. At least seven borings penetrated this relatively uniform deposit of fine silty sand and sandy silt at depths ranging from 61 to 95 feet. A thickness of 8 feet was recorded in Boring SB/A, 42 feet in PF/U7, and 36 feet in DPK/U1. The five grain-size curves shown in Figure 2.10b are representative of a number of curves obtained for this unit. The average sand grain size lies between 0.10 and 0.15 mm with the maximum size observed only 1.0 mm. Berg (1968) noted that a thick lacustrine sequence composed of sorted sands, clays, and silts separated the two tills observed in his area of study. This apparently well-sorted, fine-grained deposit at the Watching Hill site also appears to be of lacustrine origin, perhaps delta sediments.

2.3.7 Unit 7 - Glacial Till. Eight of the eleven borings shown in Figure 2.9 penetrated this unit, which varies from a 27-foot-thick stratum at a depth of 33 feet (elevation 2135) in Boring SB/A, to a 2-foot-thick stratum at a depth of 87 feet (elevation 2078) in the adjacent Boring PF/U7. The drillers generally noted traces of gravel in this sandy clay (see Figure 2.6), and the densities obtained were higher than those from any other unit except those from the lower till in Unit 4 (see Figure 2.7). The five grain-size curves shown in Figure 2.11a were obtained from samples taken from SNOW BALL, DISTANT

PLAIN and DIAL PACK borings and indicate a distinctive character to this till that is slightly different from that indicated for Unit 4. On the ternary diagram given in Figure 2.12, the average grain-size curve for this till falls well into the zone for till consisting chiefly of clay and silt derived from lacustrine sediments. Interestingly enough, Lewis (1970) did not observe shale fragments during his examination of this clay.

2.3.8 Unit 8 - Outwash Sand and Gravel. This unit was penetrated by ten of the eleven borings shown in Figure 2.9, at depths ranging from 9 feet (elevation 2159) in Boring SB/N1 to 80 feet (elevation 2085) in Boring DP/U3. Thicknesses recorded for eight of these borings ranged from 5 to 18 feet. The collection of 20 grain-size curves in Figure 2.11b are the best evidence for characterizing this unit as an outwash sand and gravel. Many have shapes quite similar to those which Terzaghi and Peck (1948) present as being typical of soils of glacial or fluvioglacial origin as well as common among sand-gravel mixtures deposited by swiftly flowing rivers.

2.3.9 Unit 9 - Lacustrine Deposit. There appears to be little doubt as to the general lacustrine origin of this deposit, although the frequent occurrence of lignite particles, weathered horizontal bedding surfaces, and oxide-stained vertical shrinkage cracks are indicative of numerous cycles of flooding and drying. Within the area of interest, the deposit is deepest along a NW-SE section between Boring DPK/G2 (70 feet to elevation 2095) and Boring DP/U3 (80 feet to elevation 2085). The shallowest regions of the deposit occur at the SW and NE corners of the traverse, i.e., 36 feet to elevation 2125 at Boring DPK/U2 and 9 feet to elevation 2159 at Boring SB/N1. This latter fact

is in agreement with observations by Jones et al. (1970) that the southern exposures of the SNOW BALL crater were uniform lacustrine sediments, while the northern edge of the crater reached into delta or shore deposits. Flint (1971) states that where glacial lakes have been completely filled with sediment, the deposits become coarser near the top, indicating gradual shoaling and correspondingly increased capacity of lake currents to sweep suspended sediment toward the outlet. This characteristic feature is evident in the Watching Hill logs; see Figure 2.6 for an example.

The deposit is also characterized by a relatively stable groundwater table and a corresponding distinct transition in color from brown to gray. The maximum variation noted in the borings on Figure 2.9 occurs along a SW-NE section, i.e., from elevation 2138.5 at Boring SB/D to 2143.8 at DPK/U2. The variation across the NW-SE section is less than one foot, i.e., from elevation 2142.8 at Boring DPK/U1 to 2141.9 at DPK/U3. The levels indicated were recorded at various times from mid-April to mid-December over a period of years beginning in 1963 and extending through 1970. The average surface elevation along the shallow seismic survey line (see Section 2.2) is approximately 2165 and the average groundwater level along this line is at elevation 2141, for an average depth of 24 feet. The seismic survey indicated an average first layer depth, presumably to the groundwater table, of 21 feet, which is certainly close; it may be even closer if a zone of capillary saturation extends above the water table.

Figure 2.7 indicates only minor scatter in the water contents and densities of test specimens obtained below the groundwater table, but extreme variations in the interbedded clay, silt, and sand regime just

above. In any event, the profile and properties from within this most recent stratigraphic unit, and especially those pertaining to the partially saturated regime in the upper 25 feet, undoubtedly dominate the ground shock phenomena observed during explosive events on the Watching Hill Blast Range. Thus, the remaining chapters will be specifically directed toward establishing an order to the extreme composition property variations in Unit 9 by first relating them to conventional classification and index properties and, subsequently, to dynamic compressibility.

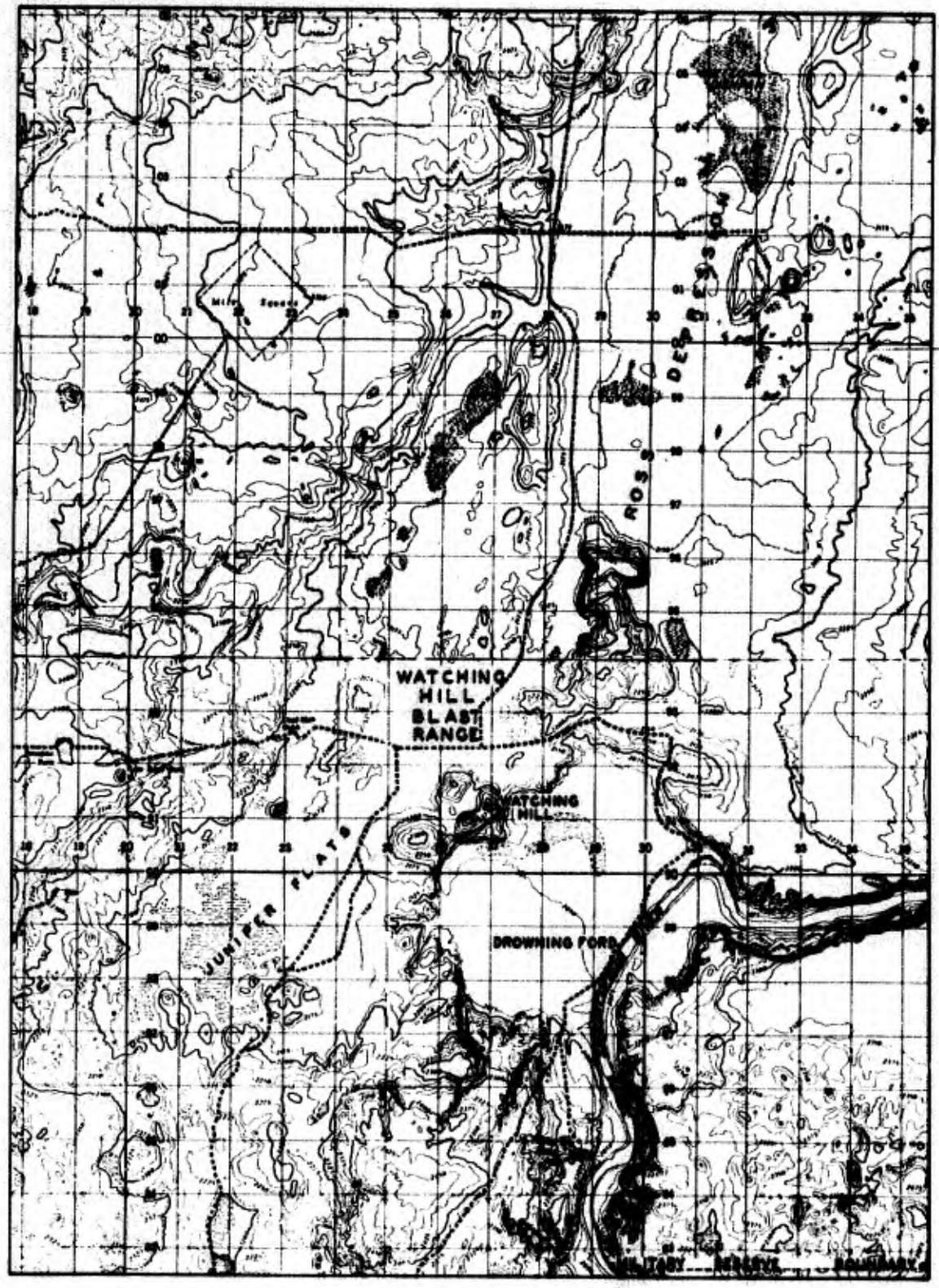

Figure 2.1 Topography of the area surrounding the Watching Hill Blast Range.

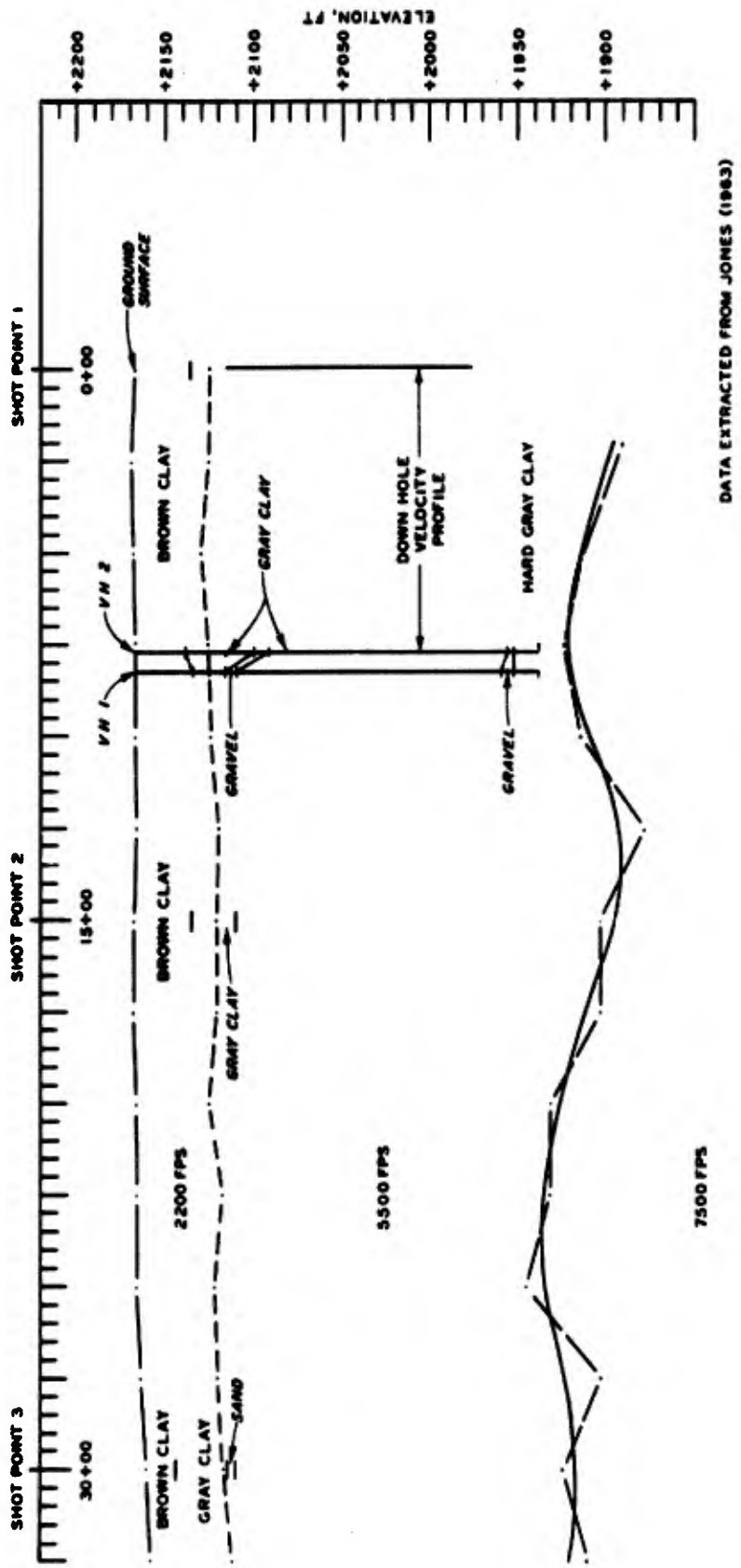

Figure 2.2 Seismic velocity section through the Watching Hill site from deep refraction survey.

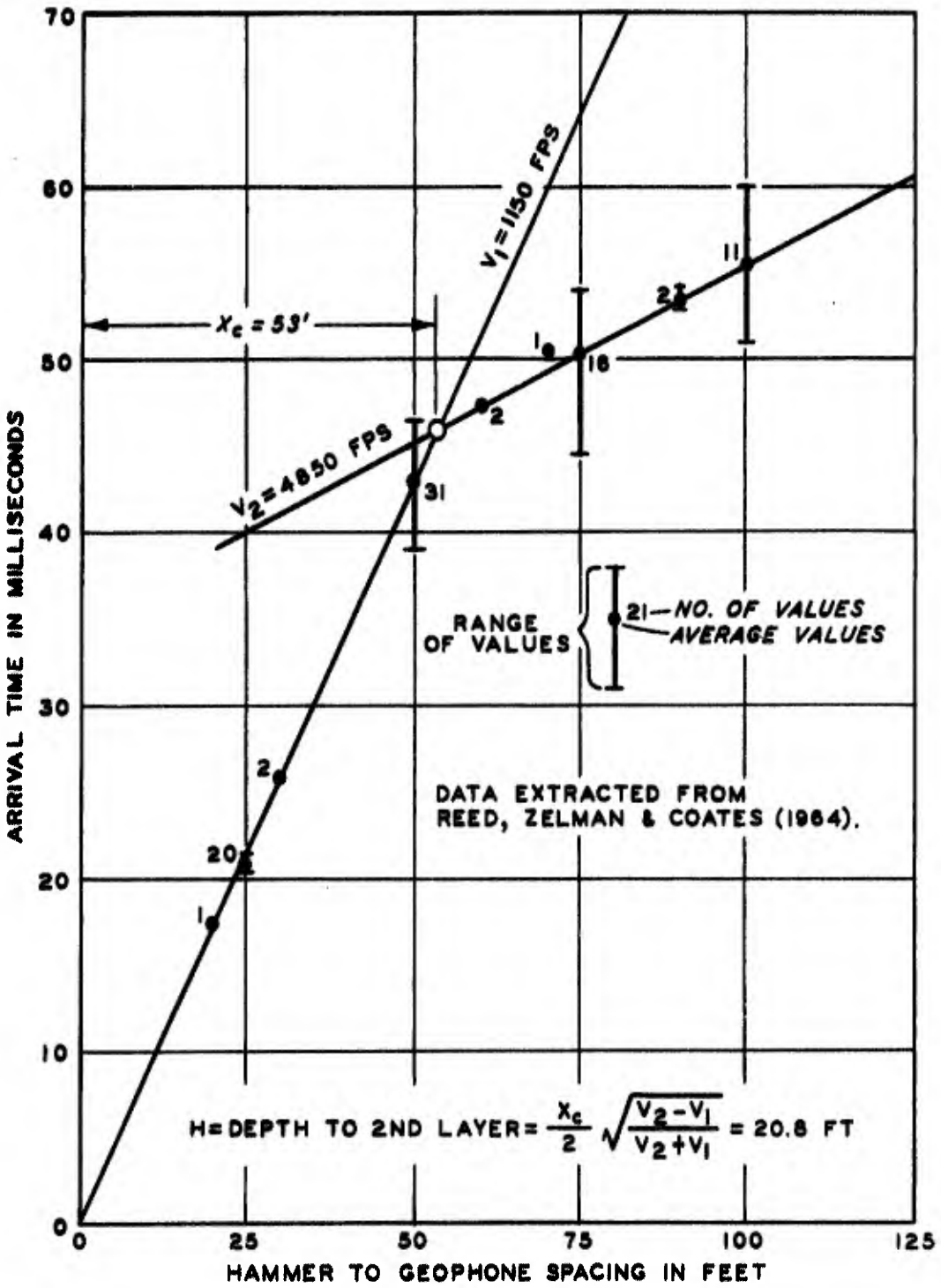

Figure 2.3 Data from shallow seismic refraction survey conducted for Operation SNOW BALL.

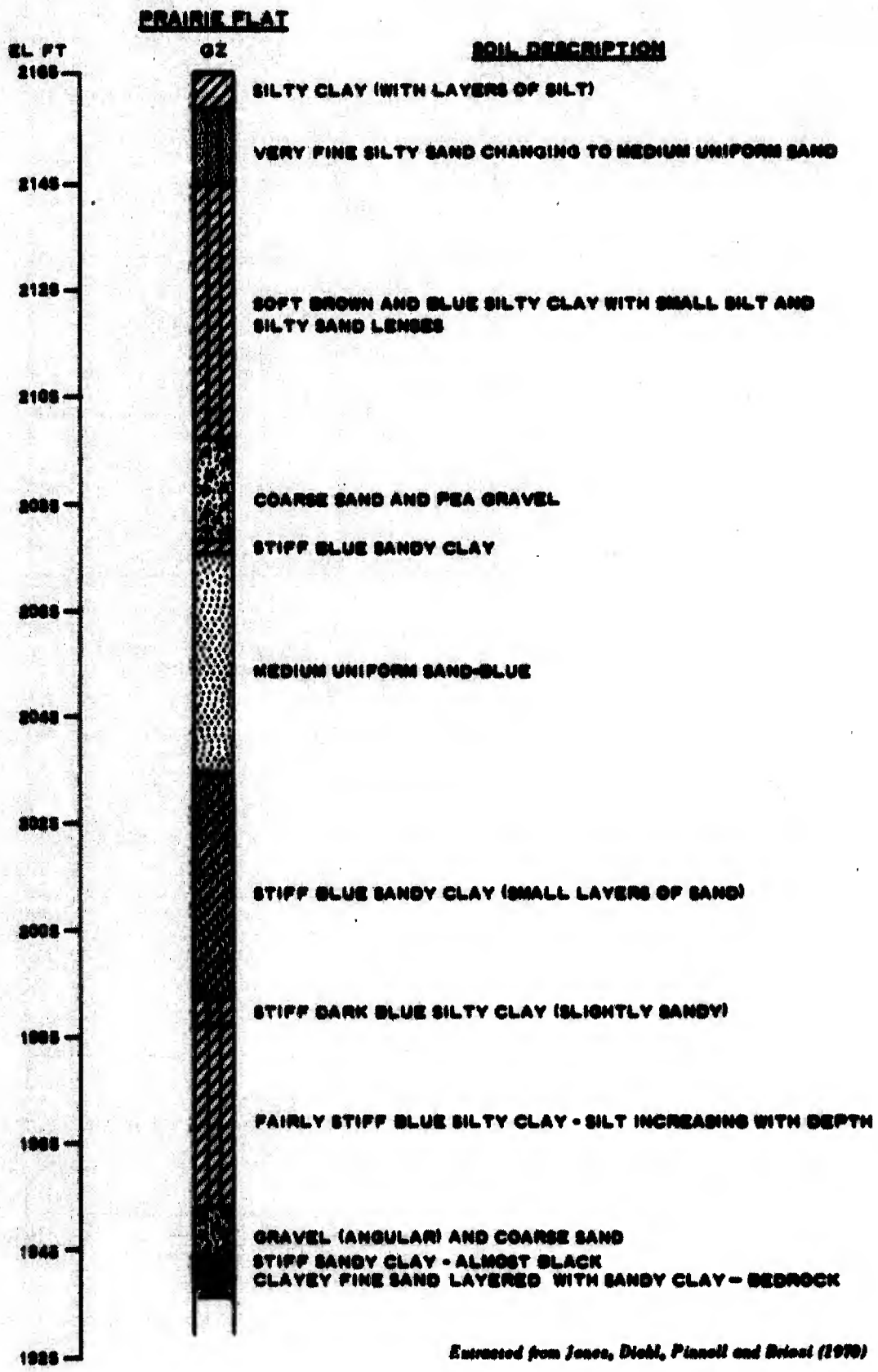

Figure 2.4 DRES boring log for the PRAIRIE FLAT GZ location.

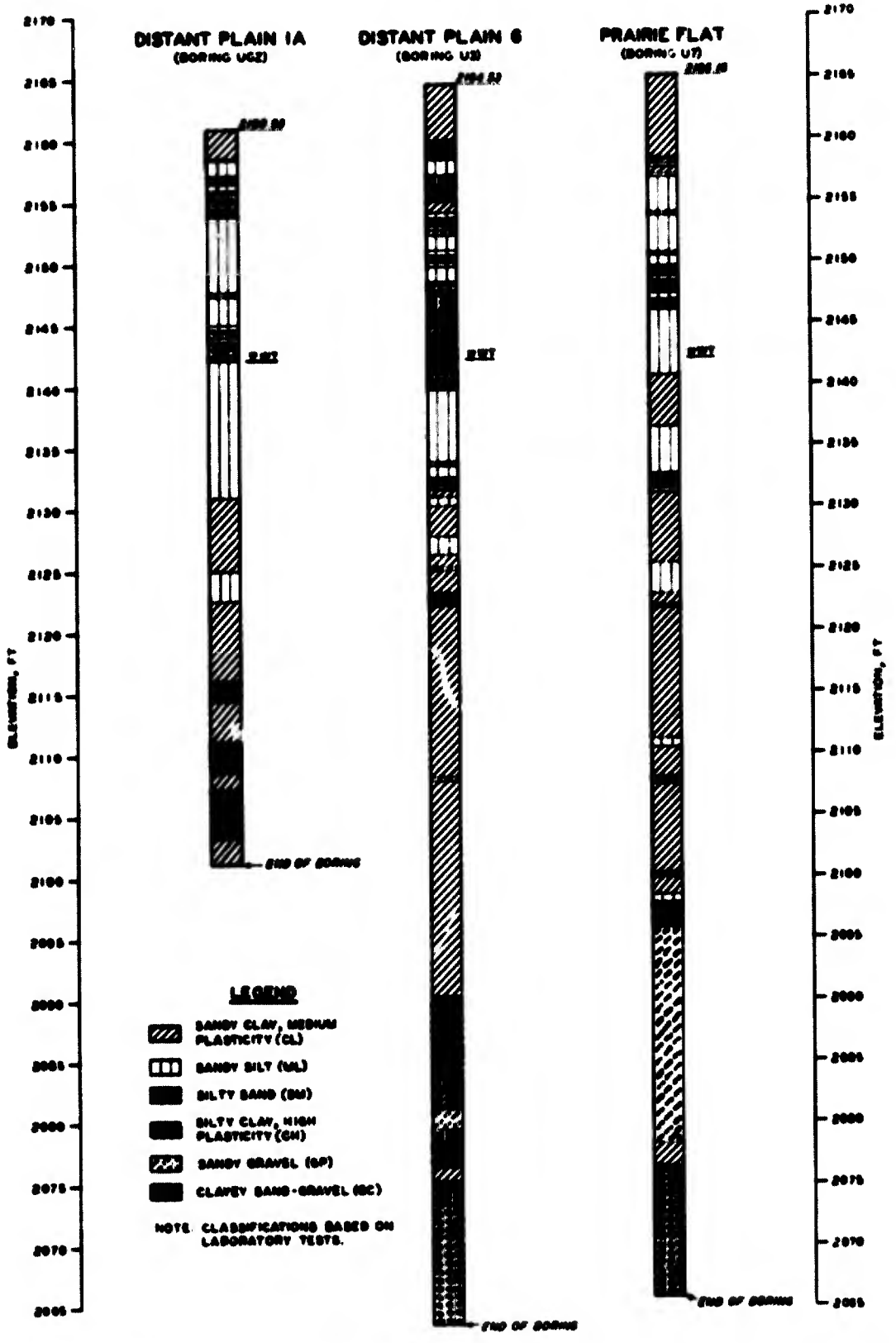

Figure 2.5 WES boring logs for the DISTANT PLAIN 1A, DISTANT PLAIN 6, and PRAIRIE FLAT GZ locations.

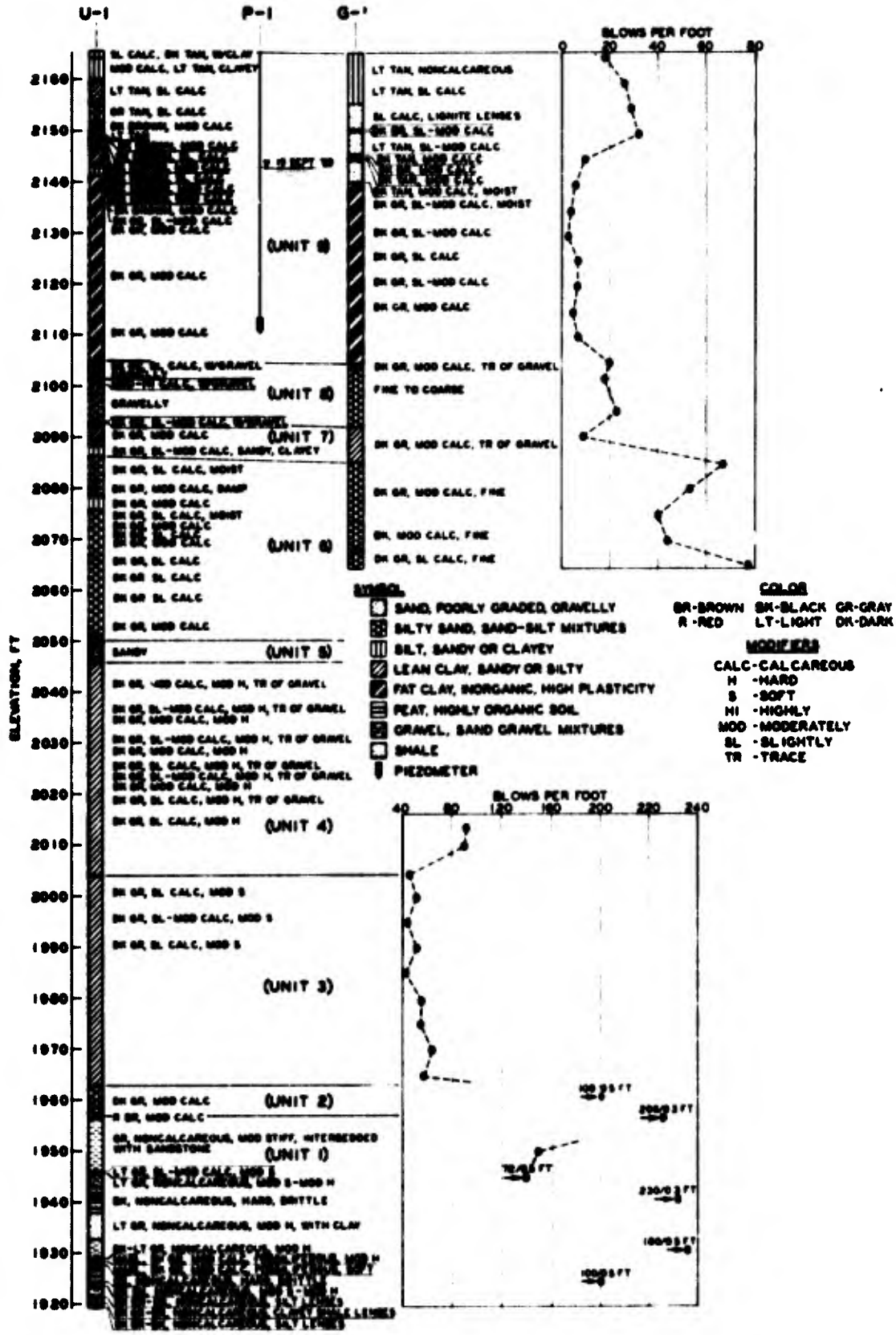

Figure 2.6 Field classification and standard penetration test data for DIAL PACK Borings U1 and G1.

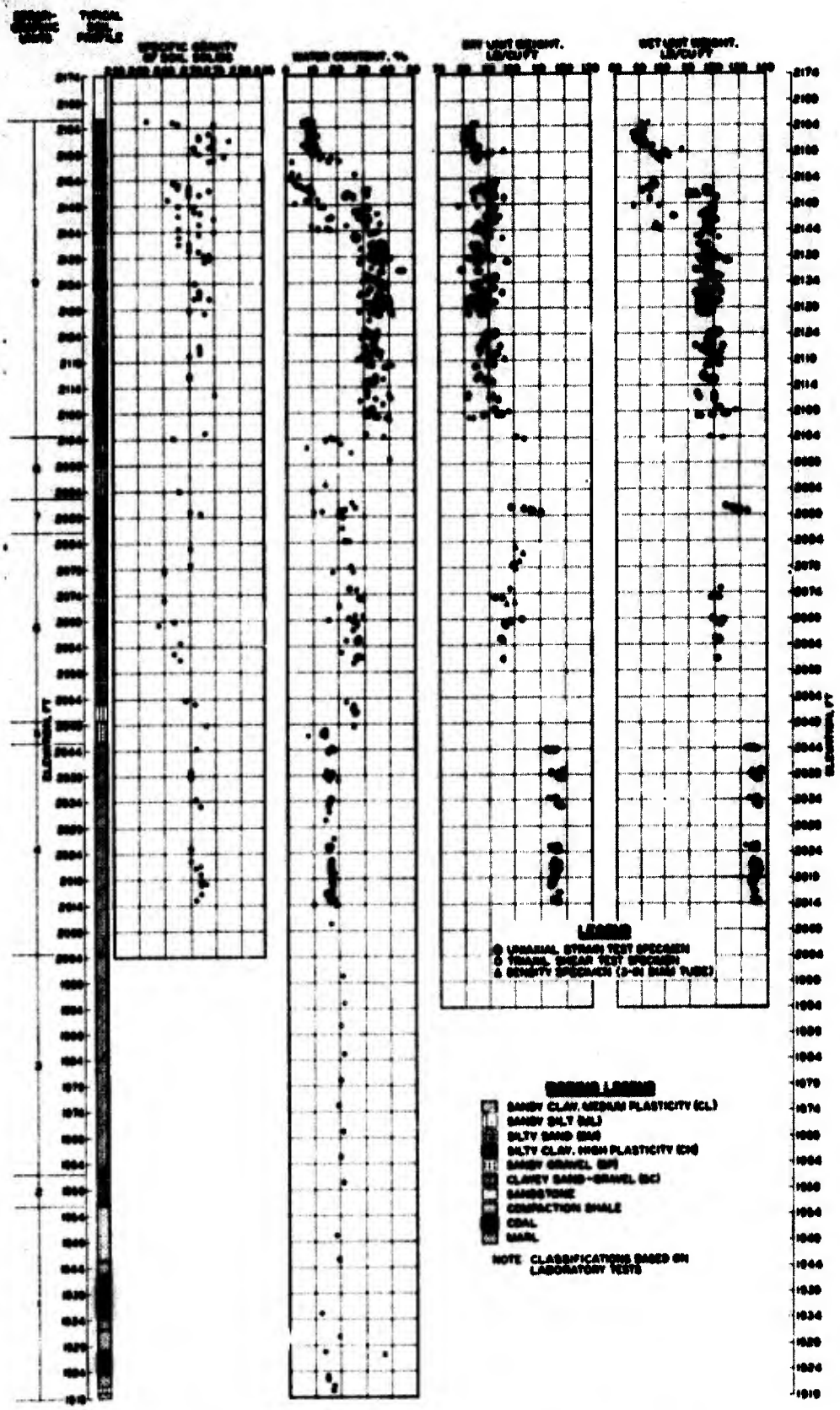

Figure 2.7 Laboratory classified soil profile and composition property data for DIAL PACK.

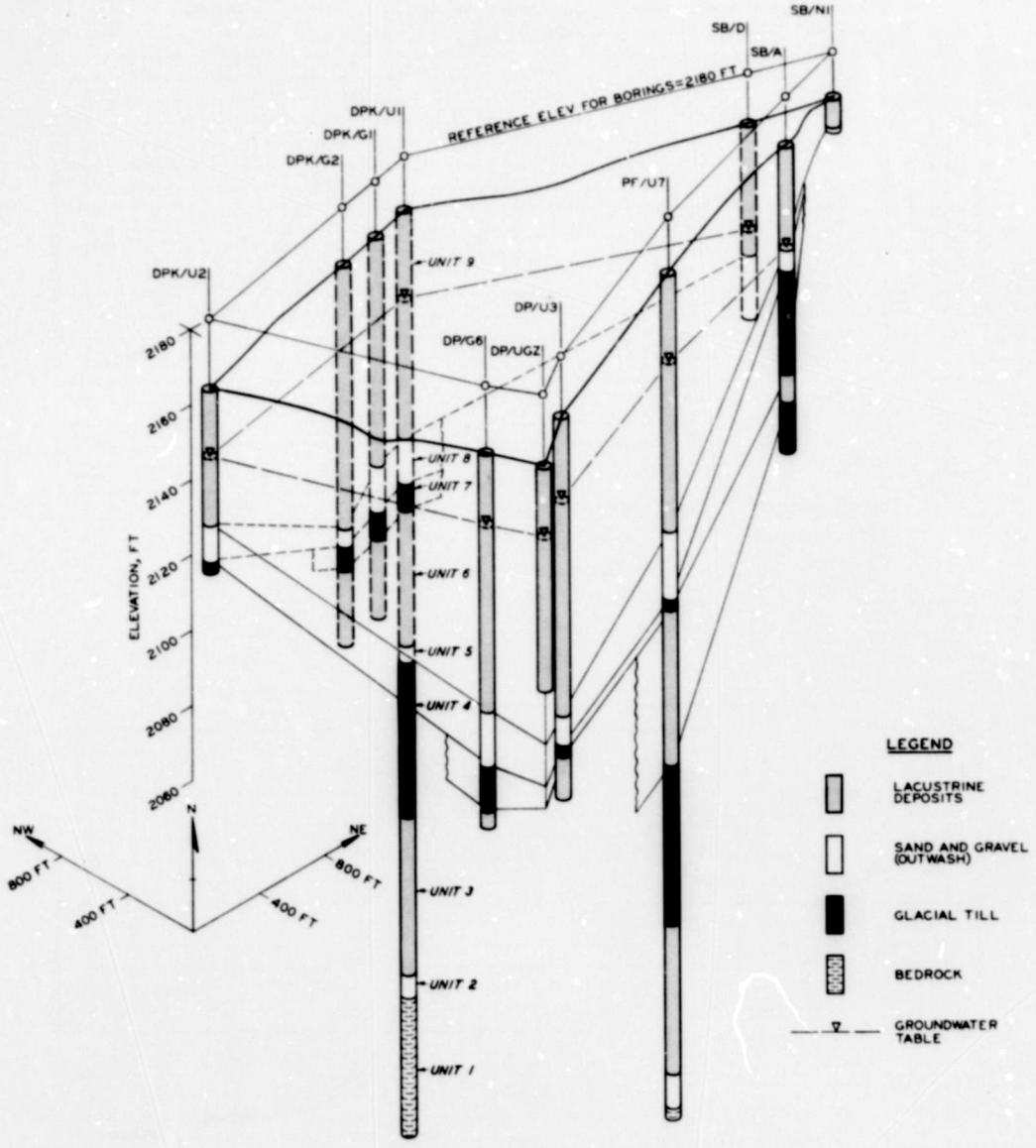

Figure 2.9 Three-dimensional plot depicting stratigraphic units encountered by borings.

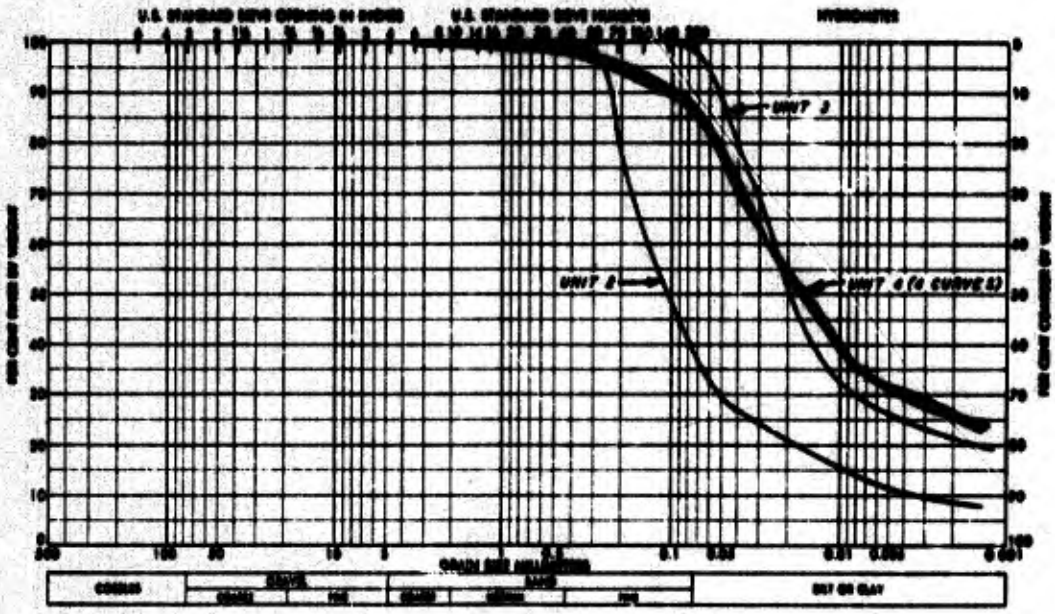

a. Units 2, 3, and 4.

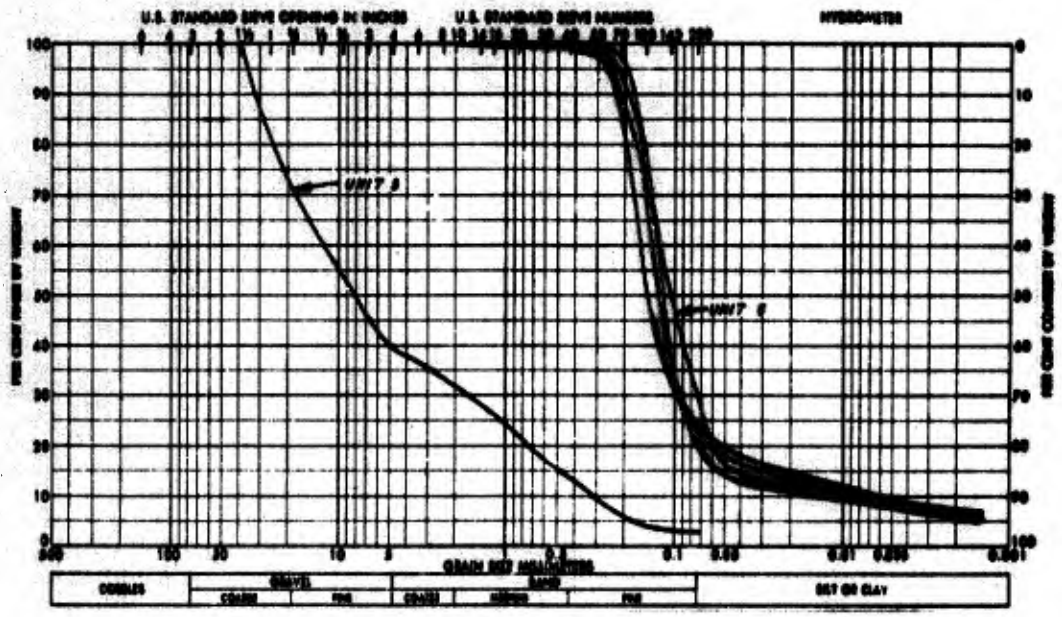

b. Units 5 and 6.

Figure 2.10 Grain-size distribution curves for Stratigraphic Units 2 through 6.

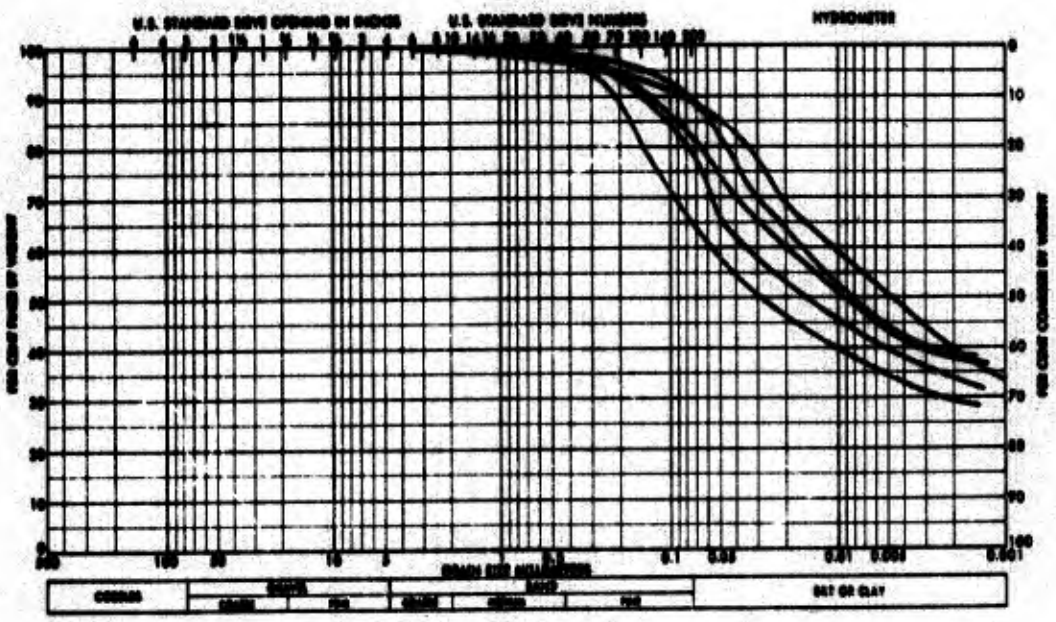

a. Unit 7.

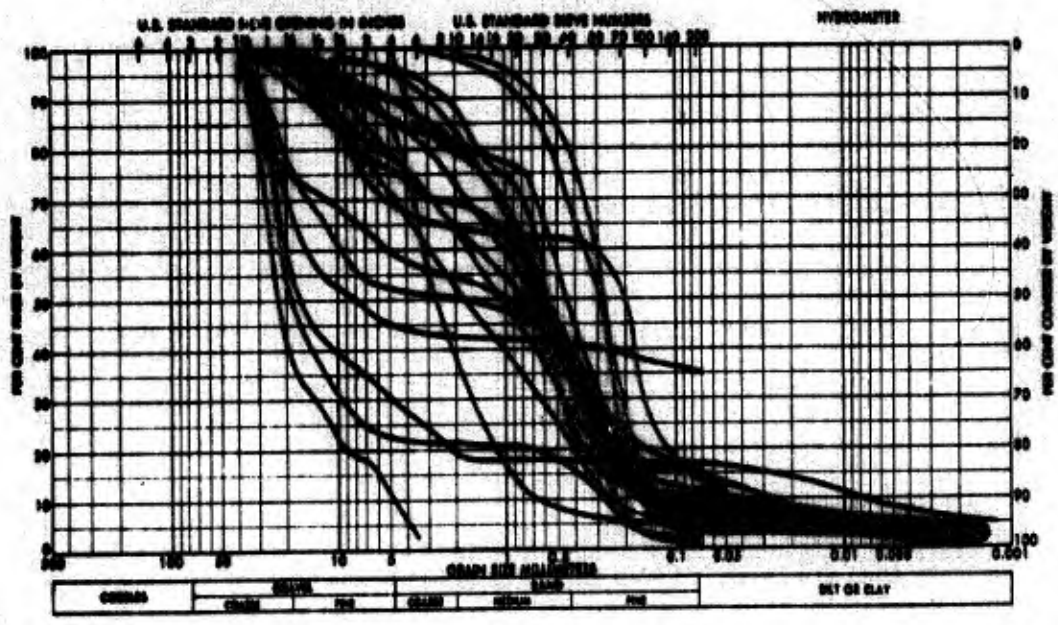

b. Unit 8.

Figure 2.11 Grain-size distribution curves for Stratigraphic Units 7 and 8.

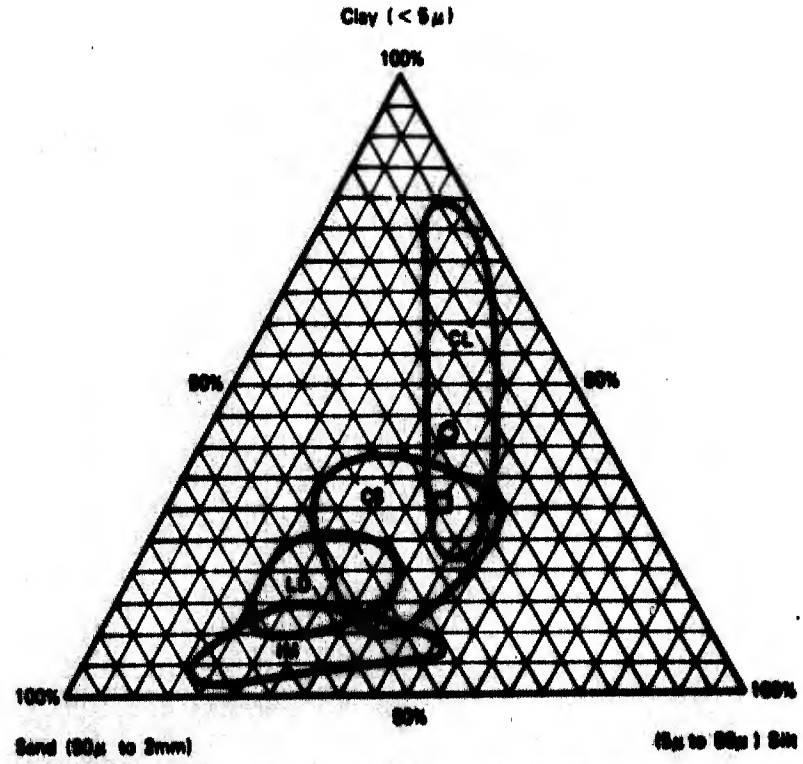

Figure 7-8.4 Ternary diagram expressing grain-size distribution in four types of till in Ontario, based on analyses of ~400 samples (Aichais D. cimanis).

IM = Tills consisting of particles of igneous and metamorphic rock. (Tills consisting of reworked glaciofluvial sediments are similar.)

LD = Tills consisting of particles of limestone and dolostone and containing as much as 60% particles of igneous, metamorphic, and clastic rocks.

CS = Tills consisting mainly of claystone and siltstone.

CL = Tills consisting chiefly of clay and silt derived from lacustrine sediments.

Extracted from Flint (1971)

□ WATCHING HILL STRATIGRAPHIC UNIT 4
○ WATCHING HILL STRATIGRAPHIC UNIT 7

Figure 2.12 Watching Hill till gradations compared with Ontario tills of different compositions.

CHAPTER 3

PHYSICAL PROPERTY ANALYSIS

3.1 PROPERTIES THAT AFFECT COMPRESSIBILITY

Soils, especially as they occur in situ, are exceedingly complex physical systems. For purposes of describing their mechanical response to applied loadings, however, a given volume of a soil mass can be characterized as a three-phase composition consisting of a structural skeleton of discrete mineral particles (solid phase) enclosing voids or interspaces filled with water (liquid phase) and/or air (gaseous phase). A piston and spring analogy is frequently used to explain the manner in which such a volume of saturated soil consolidates under drained, one-dimensional compression, i.e., uniaxial strain (see Taylor, 1948).

A similar analogy can be used to illustrate the principal mechanisms contributing to the uniaxial strain response of partially saturated, undrained soil specimens. In Figure 3.1a, a solid spring, representing the mineral skeleton, is shown inclosed in a watertight cylinder, partly surrounded by water and partly by air.[1] The schematic is drawn with the water and air completely separated to illustrate that at low degrees of saturation, soil moisture is primarily discontinuous, forming wedges of water between adjacent grains and moisture films around them (see Sowers and Sowers, 1970). The adjacent phase diagram indicates that, in overall composition, the hypothetical soil sample is composed of 28.0 percent air, 24.0 percent water, and 48.0 percent solids. Under an applied compressive stress, initial deformation of

---

[1] Any inclination to take this analogy too literally can be quickly dispelled by reading some of the early classic papers on soil mechanics such as those by Terzaghi (1925) and Casagrande (1932).

the frictionless piston is resisted almost exclusively by the stiffness of the soil "spring," since the bulk modulus of free air is negligible (i.e., approximately 20.6 psi at atmospheric pressure).

Soil mineral skeletons are usually quite deformable, even though the individual particles are very rigid. Their compressibility is governed by many factors, such as the type of structural arrangement, the size and shape of the soil particles, the number of particles (i.e., density) and their distribution, the nature and strength of the cohesive bonds at the intergranular contacts, the size and content of the void spaces, and previous stress conditions. Quantitatively, skeleton stiffnesses for soils similar to those of interest at Watching Hill can vary at low stress levels from several hundred psi to several thousand psi. Bishop and Eldin (1951), for instance, report typical structural stiffnesses for soft clay, stiff clay, compact silt, loose sand, and medium dense sand as 100, 1430, 500, 1760, and 3330 psi, respectively. Compression index data from drained oedometer or consolidation tests[2] reported by Lambe and Whitman (1969) imply similar values.

As the specimen densifies under the applied load, the "spring" stiffens considerably. In addition, the pore water will, at some point, become continuous, with the remaining air existing in the form

---

[2] The compression index C_c, which expresses the slope of the stress-void ratio curve, is commonly used to compare compressibilities of soils in the virgin compression range. The slope of the straight-line portion of the curve is

$$C_c = \frac{-\Delta e}{\Delta \log \bar{\sigma}_z}$$

Where: Δe = change in void ratio
$\bar{\sigma}_z$ = effective vertical stress

of bubbles, as illustrated in Figure 3.1b, so that the compressibility of air-water mixtures becomes a factor for consideration. According to Schuurman (1966), the work of Sparks (1963) indicates that free air will form bubbles in the pore water at a degree of saturation of about 85 percent. Richart, Hall, and Woods (1970) give a formula for the combined bulk modulus of an air-water mixture[3] which indicates that 1.0 percent of air bubbles in the pore water will result in a mixture modulus of only 2050 psi, and a further reduction to just 0.1 percent air bubbles only increases the air-water mixture modulus to 19,500 psi. Results from other theoretical studies which further refine the analysis by taking into account such realistic features as solubility and/or the effects of surface tension in small bubbles, do not appreciably alter the above values (see Koning, 1963; Bishop and Eldin, 1951; and Schuurman, 1966).

The situation changes rapidly with just a little additional strain; i.e., the last bubbles collapse, V_a becomes zero, and the bulk modulus of water becomes approximately 300,000 psi. This stage of 100 percent

---

3

$$B_{aw} = \frac{B_w}{1 + V_a\left(\frac{B_w}{B_a} - 1\right)}$$

Where: B_{aw} = combined bulk modulus of air-water mixture
B_w = bulk modulus of water
B_a = bulk modulus of air
V_a = volume of air expressed as a fraction of the total volume of air and water

By noting that $(B_w - B_a) \approx B_w$ and that $1/B_w \approx 0$, the above equation can be reduced to an easily remembered rule-of-thumb, which even for V_a values as low as 0.0005 is accurate to about 10%, i.e.

$$B_{aw} \approx \frac{B_a}{V_a} \approx \frac{20 \text{ psi}}{V_a}$$

saturation in which the voids of the mineral skeleton are completely filled with water is illustrated in Figure 3.1c. It is no longer the stiffness of the soil "spring" which resists further compression (Figure 3.1d), but rather the bulk modulus of the mineral particles composing the "spring." Using the Wood equation as given by Richart, Hall, and Woods (1970) for the combined compressibility of solid particles suspended in water, a bulk modulus of 4.45×10^6 psi for the particles (i.e., quartz) and a void ratio of 0.75, a modulus of 640,000 psi is computed for the mixture.

The above discussion should amply emphasize the importance of including three-phase weight-volume relationships in any attempt to correlate physical properties with undrained compressibility. The grain-size distribution of the particles comprising the soil skeleton is also an obvious candidate for such correlations, especially the percentage of sand-size particles (i.e. >0.074 mm in diameter) which are most likely to be rigid, bulky grains of quartz and the percentage of soil colloids or clay-size particles (i.e. <0.002 mm in diameter) which consist principally of flake-shaped particles of secondary minerals (Terzaghi, 1927). Terzaghi and Peck (1948) state that within relatively small regions where all soils in the same category, such as all the clays or all the sands, have a similar geologic origin, grain-size characteristics can be used as a basis for judging the significant properties of the soils. They also note that Atterberg limit data from different samples from the same soil stratum define a straight line on a plasticity chart that is roughly parallel to Casagrande's A-line, and that as the liquid limits (LL) of soils represented by such a line increase, the plasticity and the compressibility of the soils also

increase. Presumably then, soils whose skeletal structures are composed of particles of like size and consistency, and who have similar three-phase compositions achieved under similar geologic conditions, will have similar dynamic stress-strain properties. The next step, therefore, for the Watching Hill site analysis, is to establish classification groups based on gradation and limits for the lacustrine soils found in the upper stratigraphic unit and attempt to relate the variation of their three-phase composition properties to depth or elevation.

3.2 SOIL GROUPS BASED ON GRADATION AND LIMITS

The Unified Soil Classification System (WES, 1960) is an outgrowth of the Airfield Classification System developed by A. Casagrande (1948). It has proved very useful in grouping soils not only for airfield construction, but also for embankments and foundations; only tests for grain size and plasticity are necessary for accurate classification. This system thus provided a logical beginning for grouping the Watching Hill glacial lake sediments. Results of well over 500 classifications made for samples obtained from throughout the Unit 9 deposit showed that all were basically inorganic fine-grained materials, being classified as either CL (silty clays of low to medium plasticity), CH (clays of high plasticity), ML (sandy or clayey silts with slight or no plasticity), or SM (silty sands with appreciable fines, i.e. more than 12 percent passing the No. 200 sieve).

Grouped according to the above classifications, plots were made of measured composition properties (i.e., water content and density) versus elevation. While these plots depicted definite trends, the data bands were considered too broad for making quantitative predictions of properties at specific boring locations. The problem appeared to stem

primarily from two sources. First, the CL grouping included samples having a considerable variation in gradation which overlapped gradations obtained for CH classified soils. The former undoubtedly occurred because LL values for the CL materials ranged from 22 up to the limiting value of 50 used to distinguish CL soils from CH soils and the latter because almost all of the CH soils had LL values equal to or less than 55 whereas a large group of the CL soils had values equal to or greater than 45. Second, many of the ML and SM gradations were almost identical. Distinction is made between these two classifications solely on the basis of whether more or less than 50 percent of the particles pass the No. 200 sieve. Indeed a large number of the ML gradation curves indicated less than 70 percent of minus-200 particles while an equally large number of the SM curves indicated a minus-200 fraction greater than 30 percent. An expanded grouping was therefore considered necessary in order to adequately sort the interbedded soils found in the near-surface lacustrine deposit at Watching Hill.

Six soil groups were finally established based on the following somewhat arbitrarily selected criteria for liquid limit, the percentage of sand-size particles, and the percentage of clay-size particles:

Group Number	Liquid Limit	% Retained 200 Sieve	% Finer 0.002 mm
1	>45	NA	35 to 60
2	38 to 45	NA	20 to 40
3	30 to 38	NA	10 to 25
4	<30	<30	5 to 15
5	NA	30 to 70	5 to 10
6	NA	>70	<5

The composition properties usually determined by laboratory test are the specific gravity of soil solids G_s , the water content in percent by weight of soil solids w , dry unit weight in weight of solids per

total volume of soil γ_d, and/or wet unit weight in weight of water and solids per total volume of soil. These property values can be used to calculate other weight-volume relationships of interest. In order to realistically depict in situ compositions, the unit weight measurements should be obtained from high-quality undisturbed specimens which have been recompressed under static stresses approximately equal to the geostatic overburden stress at the depth from which the sample was obtained. The Watching Hill soil specimens of interest to the physical property analysis, therefore, were those for which sufficient data were obtained both to classify the specimen according to the above group criteria and to measure one or more of its three-phase composition properties.

A search of the WES data files for Operations DISTANT PLAIN, PRAIRIE FLAT, and DIAL PACK produced a list of 477 such specimens. One hundred twenty-three of these met the criteria for Group 1; their classification and composition data are tabulated according to depth and elevation in Table 3.1. The listing for Group 2 includes 126 specimens (Table 3.2), 47 for Group 3 (Table 3.3), 105 for Group 4 (Table 3.4), 43 for Group 5 (Table 3.5), and 33 for Group 6 (Table 3.6). The relative number of specimens listed in each table does not, of course, provide information on the relative quantity of soils from each group that will be found in the site profiles; it only attests to the fact that one is always able to recover and test more samples from a cohesive soil stratum than from a noncohesive one.

Gradation curves obtained by averaging the grain-size data given in Tables 3.1 through 3.6 are plotted for each soil group in Figure 3.2; all of the tabulated curves fall within the shaded bands of their

respective groups. The fact that these relatively narrow bands depict gradation characteristics without regard to elevation tends to confirm the previous conclusion that the samples were all obtained from deposits of similar geologic origin. The average gradation curves for each of the six groups are plotted together for comparison in Figure 3.3; they separate distinctly with a well-established trend of increasing grain size and uniformity. Average plasticity values for the first four groups are also shown in Figure 3.3; the three clay values do indeed define a straight line that is "roughly" parallel to the A-line. The average LL value of 50.4 for the Group 1 clays is indicative of the fact that this group includes an almost equal number of both CL and CH classified soils. The position on the plasticity chart of the average Group 4 data well illustrates that this group included soils from the ML, CL, and the borderline CL-ML groups of the Unified Soil Classification System. Group 5, with an average minus-200 fraction of 50.2 percent obviously includes both ML and SM materials, as expected. From the analysis presented thus far, it is concluded that the interbedded lacustrine sediments beneath the Watching Hill Blast Range can be sorted into six groups, each of which is readily identifiable by its grain-size and plasticity characteristics. Having presumably eliminated the influence of these physical properties, it is hoped that predictable variations in other properties, such as those defining three-phase composition, can now be established with depth and/or elevation.

3.3 SPECIFIC GRAVITY, WATER CONTENT, AND DENSITY DATA

Although specific gravity is generally considered as an auxiliary property whose primary usefulness is in computing other property values, it can, if accurately measured, provide some information about the

constituency of the test specimen. While one would hesitate to make physical property inferences about a soil specimen based on a single specific gravity test, the unusually large quantity of G_s data that exists for the well-defined Watching Hill soil groups should contain some trends. The G_s values given in Tables 3.1 through 3.3 for the clay groups are plotted versus elevation in Figures 3.4a, 3.4b, and 3.4c. The heavy solid lines are considered to be the most representative fits to these data while the shaded bands define ± 0.02 variations in the representative G_s values. The data below elevation 2140 (i.e., near the water table) indicate values of 2.72, 2.71, and 2.70 for Groups 1, 2, and 3, respectively. All of the groups, however, show distinct increases in the region between elevation 2140 and elevation 2158, with the largest variations occurring in the most plastic soils, i.e., Group 1. This may be a reflection of the iron oxide coatings observed in the clay samples obtained from this zone (see Lewis, 1970). The sharp decreases which occur in the upper 5 to 6 feet may reflect increased organic content due to near-surface vegetation and climatic alteration or maturing.[4] The G_s values given in Tables 3.4 through 3.6 for the silt and sand groups are plotted in Figures 3.5a, 3.5b, and 3.5c. The most representative fits to these data are constant values of 2.69, 2.68, and 2.67 for Groups 4, 5, and 6, respectively. The graduated variation in G_s between 2.72 for the unweathered Group 1 clays

---

[4] Tschebotarioff (1951) states that irrespective of their original composition, most soils tend to lose their original characteristics under the influence of various climatic factors prevailing in a certain region. As a result, all the surface soil layers of this region tend to assume the same type of chemical composition. It is interesting to note that the G_s data from the upper 5 feet of all three clay groups is indistinguishable (see Figure 3.4d).

and 2.67 for the Group 6 sands provides added confidence in the data if not new information about typical G_s values. What has not been heretofore recognized about the Watching Hill site, however, are the apparent effects due to the chemical products of weathering on the G_s values for clay strata caught between a moisture source (i.e., the water table) and a drying source (i.e., the ground surface).

While reasonable estimates of specific gravity can often be made without the benefit of tests, such is not the case with water content and density, since the variations of both within a given site are strong functions of geologic history and present environmental conditions. The w, γ_d, and γ data for each of the six groups are plotted versus elevation to a depth of about 20 feet below the water table in Figures 3.6 through 3.11; the solid lines are considered to be the most representative fits to these data. A composite plot of the representative fits is given in Figure 3.12. The plots are characterized by a number of features which appear to be related to geologic processes.

Presumably, all of the material was deposited under water. The lowest in an apparent sequence of lake levels appears to have been at about elevation 2140, i.e., just below the present groundwater table. A change in color from brown to gray has been consistently observed in the field borings at this approximate elevation and a recent examination of the samples from all of the DIAL PACK borings revealed no evidences of oxidation below elevation 2139. The density and water content data slightly increase and decrease, respectively, with increasing depth below this level, indicating that these deposits are still normally consolidated. Based on the previously recommended G_s values, the w and γ fits shown between elevations 2140 and 2120 for all groups are

compatible with a theoretical saturation value of precisely 100.0 percent. The same is true for the Group 1 and Group 2 sediments found below elevation 2120 to the bottom of the stratigraphic unit (see Figure 3.13).

As noted in Section 2.3.9, the frequent occurrence of lignite particles, weathered horizontal bedding surfaces, and oxide-stained vertical shrinkage cracks observed in the samples above elevation 2140 are indicative of numerous cycles of flooding and drying. The substantial increase in dry density measured for the clay specimens between this elevation and about elevation 2155 can be attributed to capillary stresses developed during these periods of dessication. Densification of this type is not evident in the coarser-grained silts and sands. Their dry density pattern is consistent with normal consolidation under the bulk unit weight of material above the water table and submerged or bouyant unit weights below.

The water content profiles in this region depict a classic pattern of increasing capillary attraction or suction capacity with decreasing effective pore diameter. Moisture attracted from the water table is mostly in a liquid state, though part of it is in the form of water vapor (see Krynine and Judd, 1957). Thus, even though the suction capacity of the sand and silt groups is insufficient to maintain high degrees of saturation above the water table, their air voids undoubtedly are maintained at a high relative humidity. Terzaghi and Peck (1948) note that water will evaporate only if the relative humidity of the air is less than the relative vapor pressure of the water, and that the relative vapor pressure in pore water decreases with increasing tensile or suction stresses. The combination of these phenomena probably

explains why the clay strata do not drain, but rather maintain high degrees of saturation even though interbedded with the relatively dry sands and silts.

Evaporation from the wind-swept surface, however, is another matter. The area is semiarid, with an annual rainfall of only 12 to 14 inches (Lewis, 1970), and is essentially void of vegetation except for range grass that grows only a few inches high (Gatz, 1968). With the exception of perhaps a foot of lean topsoil, the soil layer to an elevation of 2158±1 consists of a dry, almost brittle, crumbly, crust containing numerous cracks and fissures. Krynine and Judd (1957) note that crusts on the order of 5 feet thick, formed apparently by dessication during exposure, often cover glacial clay deposits. All of the samples obtained from this stratum were clays from Groups 1 and 2, with a few from Group 3. Their light tan color attests to the fact that they have been dried below their shrinkage limit. Their dry densities, however, are extremely low, which in addition to shrinkage cracks, may reflect a structure altered by frost action. Soil temperature measurements made at the nearby Drowning Ford Blast Range during the winter of 1967 indicated a maximum frost penetration depth of 8 to 9 feet (Smith, 1968). The WES laboratory measurements for near-surface densities were confirmed by the in situ measurements shown in Figure 3.14 made during several projects by the Naval Civil Engineering Laboratory (Allgood, 1967; Odello, 1971a; and Odello, 1971b).

In summary, the G_s , w , γ_d , and γ data exhibit remarkably little scatter within each group, and it appears that they have been successfully correlated with conventional classification and index data. Ample evidence has also been presented, however, to indicate that

due to geologic and climatic influences, these correlations are quite site dependent. Nevertheless, since the data were obtained from a number of different borings, these and other three-phase composition property profiles calculated from them should be valid for any location within the confines of the traverse shown in Figure 2.8.

3.4 VOLUME RELATIONSHIPS AND GENERALIZED PROFILE ZONES

Values of G_s , w , γ_d , and γ all express unit weight relationships. Presuming that the unit weight of water γ_w is also known, these quantities can be used to compute many other soil composition properties using formulas readily available in any standard soil mechanics textbook; a particularly complete listing is given by Jumikis (1962). As indicated by the discussion in Section 3.1, for compressibility problems we are particularly interested in unit volume relationships. Two of the most common are void ratio e , expressing the ratio between the volume of voids V_v and volume of solids V_s , and porosity n , expressing the volume of voids as a percentage of the total volume V , where

$$e = \frac{V_v}{V_s} = \left(\frac{G_s \gamma_w}{\gamma_d} - 1 \right)$$

and

$$n = \frac{V_v}{V} \times 100 = \left(1 - \frac{\gamma_d}{G_s \gamma_w} \right) \times 100$$

Plots of these calculated quantities are given as a function of elevation in Figure 3.15. Since γ_w is a constant and G_s is almost constant, it is obvious from the above formulas why these relationships bear such a remarkable resemblance to the γ_d versus elevation relationships given in Figure 3.12.

Two other volume properties of interest are the degree of saturation S, expressing volume of water V_w as a percentage of the total volume of voids, and the volume of air voids V_a, expressed as a percentage of the total volume of soil, where

$$S = \frac{V_w}{V} \times 100 = \left(\frac{w\gamma_d}{n\gamma_w}\right) \times 100$$

and

$$\frac{V_a}{V} \times 100 = \left(1 - \frac{S}{100}\right) n$$

At relatively low degrees of saturation, before the pore water becomes continuous, water serves primarily as a form of lubricant to the soil skeleton so that in a given soil of a given density, increased saturation means increased compressibility (see Hendron, Davisson, and Parola, 1969). The total volume percentage of air voids is a particularly useful quantity since it readily gives a reasonable approximation to the maximum strain that can occur under undrained conditions. Plots of these calculated quantities are given as a function of elevation in Figure 3.16; the tic marks denote the elevations below which the various soil strata are theoretically 100 percent saturated (or contain zero air voids). These relationships strongly resemble the water content relationships given in Figure 3.12.

With the variation of composition properties thus established as a function of soil type and profile elevation, the next step was to employ the factors discussed in the compressibility analogy of Section 3.1 to subdivide the site profile into five generalized zones within which it would be reasonable to expect that all the soil strata of a given type

would exhibit similar compressibility characteristics. The results of this analysis are given in Figure 3.17, in which the boundary elevations separating Profile Zones A through E are given for each soil group along with distinguishing values of w, γ_d, S, and V_a. Saturations within the first two zones are less than 50 percent, and it is assumed that the dominant physical property influencing their compressibility is the density of the soil skeleton. Saturations within Zone C generally range between 50 percent and 85 percent and lubrication of the soil skeleton should become a significant factor. Between 85 percent and 100 percent saturation, i.e. Zone D, air-water compressibility deserves consideration, but the dominant feature is the effective limitation on strain set by the small V_a values. And the response of Zone E, of course, is characterized by the bulk compressibility of water and solid mineral.

The fact that soil compressibility cannot be quantitatively evaluated based on physical properties alone is well established (Sowers and Sowers, 1970; Terzaghi and Peck, 1948; etc.). The profile zoning given in Figure 3.17, however, does establish a framework within which the combined effect of physical properties, natural structure, and rate of loading on the compressibility of undisturbed specimens obtained from throughout the Watching Hill site can be analyzed. Such an analysis is the purpose of the next chapter.

Table 3.1

Classification and Composition Data--Lacustrine Deposit: Group 1

Specimen No.	Depth ft	Elevation ft	Percent Finer by Weight: Sieve No. 10	20	40	60	Diameter in Millimeters: 0.1000	0.0500	0.0250	0.0100	0.0050	0.0020	Atterberg Limits: LL	PL	PI	G_s	w %	γ_d pcf	γ pcf
Operation DISTANT PLAIN																			
4.6X	1.7	2161.8	100	100	100	99	98	97+	93	80	59	40	45	21	24	2.70	11.0		
2A.1.4	3.6	2160.6	100	100	100	99	97+	96	92	77	57	35	46	17	29	2.76	12.1	83.4	93.5
1A.1.3	3.9	2160.6	100	100	100	99	96	94	90	80	59	38+				2.77	11.7	81.7	91.3
2A.1.3	3.9	2160.3	100	100	100	99+	98	96+	90	79	59	39+				2.73	11.3	82.0	91.3
1A.1.1	4.5	2160.0	100	100	100	99+	98+	98	96	87+	65	38	50	20	30		12.9	83.2	93.9
2A.1.2	4.3	2159.9	100	100	100	99	96+	93+	90	80	60	37				2.77	12.5	84.0	94.5
2A.1.1	4.5	2158.7	100	100	100	99	95	93+	91	80	57	38	48	18	30	2.76	12.7	84.8	95.6
GZ.2.3	1.7	2159.2	100	100	100	97+	90+	87+	83+	75+	58	37	60	24	36	2.69	13.4	80.3	95.9
GZ.2.2	1.9	2159.0	100	100	100	97	92+	90	87	80	58	36+	55	24	31	2.71	13.7	84.7	99.7
GZ.2.1	2.8	2158.7											48	20	28	2.70	16.8	86.3	100.8
1A.2.2	11.2	2153.3	100	100	100	99+	99	98	95+	84	63	40	48	19	29		27.8	90.7	115.9
3A.3.3C	18.1	2145.6	100	100	100	99+	99	98	95	81	61	39+	57	24	33	2.70			
1.20B	33.4	2131.8	100	100	100	99	96+	93	86	70	53	35+	48	17	31	2.74	34.9		
3.19	35.0	2121.5	100	100	100	99+	97+	96	89+	75	59	39	45	23	22	2.71	37.1		
3.20	36.3	2120.2	100	100	100	99	97	93+	89	75+	58	35+	49	23	26	2.72	37.1		
GZ.20A	35.8	2125.1	100	100	100	100	95	92+	88	75	57+	37+	49	21	28	2.71	34.8		
1A.5.3	41.8	2122.7	100	100	100	99+	98+	97+	95+	88+	65	42+	54	22	32	2.73	35.7	84.7	114.9
3A.5.4	41.2	2120.5	100	100	100	99	97	94	87+	71	48+	33	47	22	25	2.68	35.0	88.0	118.8
3A.5.2	42.0	2121.7	100	100	100	99	98	96	91+	75+	56	37	48	21	27	2.74	35.1	86.7	117.1
GZ.23A	39.4	2121.5	100	100	100	99	95	92	84	70	51+	35	47	22	25	2.72	34.5		
3A.5.1	42.3	2121.4	100	100	100	99+	98+	96+	90	75	57+	38	46	21	25	2.69	34.7	86.4	116.4
1.22A	44.1	2121.1	100	100	100	99	98	96+	92+	82	64	42	51	21	30	2.73	36.1		
2.26A	44.4	2120.6	100	100	100	99	97+	95+	90	75+	55	41+	47	22	25	2.71	33.5		
3.26	45.9	2119.2											49	23	26	2.72	36.7		
GZ.25A	43.7	2117.2	100	100	100	100	94	89+	82+	70	53+	35	48	20	28	2.73	34.5		
GZ.27A	46.2	2114.7	100	100	100	100	97	93+	89	77+	59	38	51	23	28	2.75	37.6		
GZ.30A	49.9	2111.0	100	100	100	100	96+	94+	91+	80	57	41	52	22	30	2.72	37.7		
GZ.31A	51.2	2109.7	100	100	100	100	95	93	90	78	60	40	52	24	28	2.74	34.5		
3.35	56.1	2108.4	100	100	100	100	97	96	92	80	64	45	49	20	29	2.70	36.2		
GZ.33A	53.7	2107.2	100	100	100	100	97+	96	94	81	62+	42	51	22	29	2.69	33.8		
GZ.34A	54.9	2106.0	100	100	100	100	95	92+	89+	75+	57	38+	49	19	30	2.73	34.1		
GZ.35A	56.2	2104.7	100	100	100	99+	94+	92	90	83+	70+	52	62	24	38	2.74	37.9		
GZ.36A	57.4	2103.5	100	100	100	100	95+	93	90+	80	62	46+	51	21	30	2.74	35.8		
GZ.37A	58.7	2102.2	100	100	100	100	98+	89	87	78	60	40	54	20	34	2.76	35.6		
3.40	62.8	2101.7											54	22	32	2.72	37.4		
3.47	71.3	2093.2											56	26	30	2.73	38.6		
3.49A	74.4	2090.1											57	22	35	2.70	35.4		
3.50A	76.2	2086.3	100	100	100	99	96+	95	94	87	69	50	56	24	32	2.72	35.3		
3.51	78.8	2085.7	100	100	100	99	95	92	89	80	64	44	54	22	32	2.72	33.6		
3.51A	79.4	2085.1	100	100	100	99	95	91	87+	80	66	45	56	21	35	2.71	33.4		
Operation PRAIRIE FLAT																			
7.2.2	3.5	2161.7	100	100	100	100	95+	93+	90	78+	58	38	48	22	26	2.72	9.7	84.1	92.3
7.3A	5.0	2160.2	100	100	100	99+	93+	89+	85	75	54	35	46	19	27	2.79	12.2		
7.4T	5.3	2159.9	100	100	100	99+	95	92	90	78	61+	45	46	22	24	2.77	12.5		
7.4N	5.7	2159.5	100	100	100	99	94	91+	90	87	77+	61	51	21	30	2.78			
7.16A	28.7	2136.5	100	100	100	99+	95	91+	85	72	55	35+	47	20	27	2.73	35.2		
7.25.2	39.1	2126.1	100	100	100	99+	96+	94	89	75	56	38	47	18	29	2.70			
7.29A	45.5	2119.7	100	100	100	100	95	91+	87+	75	57	40	45	18	27	2.72	32.6		
7.39A	57.9	2107.3	100	100	100	100	95	94	91+	82	65	45	53	21	32	2.73	35.1		
7.42.6	60.9	2104.3	100	100	100	99+	91+	86+	80+	68+	55	38+	49	18	31	2.72			
7.42.5	61.1	2104.1	100	100	100	99+	94	92	90	82	61+	47+	49	19	30	2.73			
7.42.4	61.3	2103.9	100	100	100	99	92+	87	78	65	53	38	49	20	29	2.73	33.9	88.4	118.4
7.42.3	61.5	2103.7	100	100	100	99	93+	90	85	76	60	42	49	21	28	2.71	32.8	91.4	121.4
7.42A	62.0	2103.2	100	100	100	100	91	87+	85	76	60	43	49	19	30	2.74	33.2		
7.43.3	62.6	2102.6	100	100	100	100	95	92	88+	78+	61	39+				2.74	34.8	88.1	118.7
7.44A	64.5	2100.7	100	100	100	100	96	93	86	74	56	40	46	20	26	2.73	31.8		
7.45A	65.7	2099.5	100	100	100	100	95+	94	91	84	70	49	54	22	32	2.74	36.1		

(Continued)

Table 3.1 (Concluded)

Specimen No.	Depth ft.	Elevation ft.	Percent Finer by Weight: Sieve No. 40	100	140	200	Diameter by Hydrometer 0.050	0.030	0.020	0.010	0.005	0.002	Atterberg Limits LL	PL	PI	G_s	w %	γ_d pcf	γ pcf
Operation DIAL JACK																			
1.2.1	1.9	2163.9											52	19	33	2.75	9.5		
1A.A2	2.3	2162.8	100	99+	99+	99	94	90	86	78+	57+	37	49	20	29		9.9		
1.3.1	2.7	2162.7											46	19	27	2.74	10.1	82.8	91.2
3.2.1	2.0	2162.5											48	17	31	2.75	9.9		
2A.A2	3.1	2162.0	100	100	99+	99	97	93	87+	77	55+	38	48	18	30	2.72	8.3		
2.2	1.6	2160.0											50	19	31		11.1		
3.3A	4.7	2159.8											46	14	32		8.6		
2.3.1	2.7	2158.9											47	21	26	2.72	11.2	91.2	101.4
2.3.3	3.3	2158.3	100	100	100	99+	96	94	90	79	42+	35	47	23	24	2.77	14.6	89.7	102.8
2.4.1	5.1	2156.5	100	99+	99	98	94	90+	85	71+	53	35	49	19	30	2.81	24.9	95.2	119.1
2.4.2	5.4	2156.2	99+	99+	98+	97+	94+	91	84	66	48+	34	47	23	24	2.80	24.7	90.4	112.8
2.5.1	6.1	2155.5	100	99	98+	98	94+	92	87+	77+	58	38	52	20	32	2.78	26.3	96.1	121.3
2.5.2	6.3	2155.3	100	99+	99	98	95	91+	85	73	59	43	52	18	34	2.78	26.7	97.7	123.8
2.5.3	6.6	2155.0	100	99+	99+	98	94	88+	80	66+	54	39	55	19	36	2.77	26.6	97.7	123.7
2.5A	6.8	2154.8											60	19	41		27.0	95.1	121.0
3.7.7	12.8	2151.7											49	23	26	2.74	30.4	91.2	118.9
1.8.8	14.5	2150.9											48	20	28	2.73	31.7	90.8	119.6
3.9.1	13.9	2150.6	100	100	100	99+	97+	94	85+	65+	50	35	47	18	29	2.76	34.9	87.5	118.0
1A.10.3	14.9	2150.2	100	100	99	98	95	92	86	77	60	38	53	20	33	2.75			
2A.7.4	15.3	2149.8	100	100	100	99	97	95	90+	76	58	38+				2.74	31.5	89.4	117.6
2A.7.4B	15.4	2149.7	100	100	100	100	98	94	87+	72+	55+	37	50	19	31	2.74			
2.7.3	10.1	2149.5	100	99	98	97+	96+	93+	89	81	65	45	58	20	38	2.78	33.0	88.9	118.2
1A.12.1	15.8	2149.3	100	100	99+	99	94	88	80	68	46	29				2.75			
1A.12.3	16.3	2148.8	100	100	100	99	95	88	76	65	45	40	49	22	27	2.73	32.4		
3.10.4	15.7	2148.8	100	100	99+	99	97	93	85	70	55	39	47	20	27	2.75	35.8	86.3	117.1
1.10.2	17.2	2148.2											47	17	30	2.73	31.1		
2.8.1	13.5	2148.1	100	100	100	99	96+	94+	91	84	70	49+	40	21	19	2.80	31.5	89.6	118.7
3.11.2B	16.6	2147.9	100	99+	99	98+	95	91+	86	77	60+	43				2.81			
2A.A10	17.4	2147.7	100	100	99+	99	97	93	86	72+	53+	35	48	20	28	2.74	31.6		
3.11.4	17.0	2147.5	100	100	100	99	97+	95	90+	77	57+	40				2.76			
3.12.1	17.4	2147.1	100	100	100	99	95	91	82	65	50	35	48	21	27	2.75	34.9	86.8	117.0
2.10.2	16.6	2145.0											50	19	39	2.76	34.0	87.3	117.4
2A.10.2B	20.3	2144.8	100	100	100	99	97+	95+	90+	77+	60	42	52	20	32	2.76	33.7	88.2	117.9
2A.10.2T	20.5	2144.6	100	100	99+	99	96+	94	89	76+	60	40	53	21	32	2.76			
1A.15.3	20.7	2144.4	100	100	100	99	97	93	86	77	60	40	46	20	26	2.75	33.9		
3.13.2	20.3	2144.2	99+	99+	99	98+	95	90+	87+	78	60+	42	52	20	32	2.77	38.6	83.1	115.1
1.12.2	20.2	2144.2											52	19	33	2.72	36.4	86.2	117.5
1A.A16	21.0	2144.1	99	99	98	98	97	92	86	75	60	42	54	21	33	2.75	38.5		
3.13.2	20.5	2144.0	100	100	100	99	97	93	87	75	55+	39	48	21	27	2.76	38.4	83.5	115.6
1.12.6	21.5	2143.9											53	26	27	2.75	39.6	86.7	117.5
1A.16.3	22.2	2142.9	100	100	100	99	95	91	87	77	59	40	50	22	28	2.75	37.4		
2.11.1	20.2	2141.4											50	22	28	2.70	35.7		
2.12.1	21.4	2140.2											46	21	25	2.70	38.2		
1.15.2	25.4	2140.0											50	15	35	2.72	37.9	85.0	117.2
1A.18.3	25.1	2140.0	100	100	100	99	98	94	87	77	60	40	53	21	32	2.74	38.5		
1A.A19	25.4	2139.7	100	100	100	99	95	89	77	66	58	40	52	23	29	2.72	35.6		
2.13.4	23.6	2138.0	100	100	100	99	98	96	92	80	63	46	53	24	29	2.73	34.1	86.2	115.6
2.14.1	25.3	2136.3											53	16	37				
1.17.1	31.5	2133.9											51	18	33		36.0		
3.20.3	33.2	2131.3											49	22	27	2.72	37.0	85.7	117.4
3.20.4	33.5	2131.0	100	100	100	99+	96	94+	92	83	60	43+	49	22	27	2.74	39.2	83.4	116.1
2.16.1	30.6	2130.8											52	19	33		39.7		
1.18A	34.8	2130.6											48	19	29		38.2		
2.17.1	31.4	2130.2											48	20	28		36.6		
1.19.2	35.5	2129.9											47	15	32		36.3		
3.20A	34.7	2129.8											53	22	31		39.6		
2.18.2	33.0	2128.6											47	21	26	2.70	32.5	88.4	117.1
2.18.4	33.5	2128.1	100	100	100	99+	96	93+	86	68+	50	35	47	23	24	2.73	34.8	88.4	118.8
3.22.2	36.8	2127.7											51	15	36		36.0		
3.23A	41.0	2123.5											54	22	32		35.0		
1.23.5A	43.8	2121.6	100	100	100	100	98	97	93+	80	62+	42+	51	20	31	2.73	34.2		
1.23.6	44.1	2121.3											52	20	32	2.72	35.0	86.1	116.2
3.25.6A	44.0	2120.5	100	100	100	99+	94	88+	82	73	52+	37+	46	21	25	2.73			
3.28.4	40.5	2116.0											56	16	40	2.70	34.5	86.5	116.4
3.28.5	48.8	2115.7	100	100	100	99+	95	90	83	68	51	35	44	22	22	2.70	35.0	86.0	116.1
1.28.2	53.0	2112.4											60	18	42	2.75	39.9		
1.32.2	60.5	2104.9											48	19	29	2.73			
		Total:	8698	8693+	8684+	8625	8333+	8078+	7650+	6646	5110	3486	5797	2351	3446				
		Number of Samples:	87	87	87	87	87	87	87	87	87	87	115	115	115				
		Average:	100.0	99.9	99.8	99.1	95.8	92.9	87.9	76.4	58.7	40.1	50.4	20.4	30.0				

Table 3.8

Classification and Composition Data--Lacustrine Deposit: Group 2

Specimen No.	Depth ft.	Elevation ft.	Percent Finer by Weight: Sieve No. 10	40	100	200	Hydrometer 0.020 mm	0.005 mm	0.002 mm	0.002 mm	Atterberg Limits: LL	PL	PI	G_s	w %	γ_d pcf	γ pcf
Operation DISTANT PLAIN																	
2.1.2	0.8	2164.1									38	18	20	2.66	19.1	83.3	99.2
2.1A	1.1	2163.8									40	20	20	2.69	8.8		
3.1A	1.1	2163.4	100	100	100	98+	92	84+	73+	57+	42	28	37	22	15	2.64	6.3		
2.2.3	1.5	2163.4	100	100	100	99	98	96	88	70	46	33	42	21	21	2.69	8.3	77.5	83.9
1.2A	1.9	2163.3	100	100	100	99	98	96	88	73	50	33	45	20	25	2.74	8.2		
2.2.4	2.0	2162.9									44	23	21	2.69	9.0	76.2	83.1
3.2	1.7	2162.8	100	100	100	99	98	96	88+	70	49	31	40	21	19	2.67	9.3		
2.3X	1.7	2162.7	100	100	100	98	95+	93	87+	71+	50	35	45	22	23	2.71	9.0		
2.3Z	3.2	2161.7	100	100	100	99	95	91	84	72	55+	39	44	19	25	2.78	11.5		
5.1Z	0.9	2161.3	100	100	100	98+	94	88+	80	65	50	35	42	22	20	2.72	10.8		
GZ.1.2	0.6	2160.3									38	20	18	2.66	12.1	80.5	90.2
GZ.1.1	0.8	2160.1									39	22	17	2.66	12.3	78.2	87.8
GZ.1A	1.0	2159.9	100	100	100	97	92	88	80	69+	55	38	43	25	18	2.66	15.8		
1.4A	13.4	2151.8									40	17	23	2.70	26.5		
1.13.1	19.2	2146.0	100	100	100	99+	96+	93	84	70	50+	36+	42	19	23	2.71	32.2	89.9	118.8
GZ.11B	16.7	2144.2	100	100	100	100	94	91	84	70	50	34	42	19	23	2.72			
1.21B	34.6	2130.6	100	100	100	99+	96+	91+	80	63	45+	31+	43	20	23	2.70	33.9		
1.22A	37.0	2128.2	100	100	100	99	95+	90	78+	57+	42	28+	41	17	24	2.72	33.9		
2.20A	36.9	2128.0	100	100	100	99	95	89	78+	62	41+	32+	39	18	21	2.70	31.0		
3.20A	36.9	2127.6	100	100	100	99	96+	93+	85	59	41	28+	36	21	15	2.71	34.1		
1.23A	37.8	2127.4	100	100	100	100	98	95	88	73	52	33+	41	19	22	2.70	32.2		
GZ.18A	33.6	2127.3	100	100	100	100	95	91+	83+	68	51+	35+	42	19	23	2.72	33.9		
GZ.19A	34.9	2126.0	100	100	100	100	98+	87	75+	56+	40+	25+	40	19	21	2.72	30.6		
GZ.22A	38.4	2122.5	100	100	100	100	95	92	87	74	56	37+	45	22	23	2.71	31.5		
3.21B	39.3	2125.2	100	100	100	99	97	94+	86	67+	45	33	46	20	26	2.70	30.0		
1.25A	40.4	2124.8	100	100	100	99+	97	93+	84+	66	48	33+	44	18	26	2.68	32.9		
2.23A	40.6	2124.3	100	100	100	99+	98	94	85	70	50+	36+	44	21	23	2.67	29.1		
GZ.21A	36.8	2124.1	100	100	100	98+	96	92	82	62+	45	29	42	21	21	2.70	30.3		
3.22A	40.7	2123.8	100	100	100	99	98	93+	80	62	43	28+	42	19	23	2.70	29.9		
2.24A	41.8	2123.1	100	100	100	99	97+	95+	87	66	46+	34+	43	19	24		30.0		
1A.5.4	41.5	2123.0	100	100	100	99+	97	93+	87	70	52+	35				2.72	30.7	92.1	120.4
1A.5.2	42.0	2122.5	100	100	100	99	97	93	82+	66	51	35	39	20	19	2.73	30.4	91.9	119.8
1.27A	42.9	2122.3	100	100	100	99	97	93+	86+	69+	50+	33+	45	22	23	2.74	32.1		
1A.5.3	41.5	2122.2	100	100	100	99	95	86+	63	45+	32	21+	42	20	22	2.71	30.7	90.7	118.5
2.25A	43.1	2121.8	100	100	100	99+	97+	94+	87+	74+	55	40	44	18	26	2.68	30.7		
GZ.24A	41.5	2119.4	100	100	100	100	93	89+	80+	63	46	29	40	21	19	2.71	30.0		
4.25X	50.0	2113.5	100	100	100	99	94	88+	80	65	51	37+	42	20	22	2.70	34.0		
GZ.25A	48.7	2112.2	100	100	100	100	92	86	76	62+	46+	31	41	19	22	2.73	31.5		
6.30.1	52.2	2112.2	100	100	100	99+	94+	89	80	66	49	32	44	21	23	2.72	32.9	89.3	118.7
GZ.32A	52.4	2108.5	100	100	100	100	92	86	72	55	42	28+	40	18	22	2.69	31.2		
1.38A	57.3	2107.9	100	100	100	100	98	94	84	69	50	32	44	21	23	2.71	30.9		
2.40A	61.8	2103.1	100	100	100	99	97+	93+	85	70	50	34+	44	19	25	2.68	31.9		
GZ.38A	59.9	2101.0	100	100	100	100	95+	92	85+	72+	55	36+	45	21	24	2.73	33.5		
Operation PRAIRIE FLAT																	
7.1.2	1.9	2163.3	100	100	100	99	90	86+	80	64+	45	31	39	20	19	2.71			
7.1A	2.5	2162.7	100	100	100	99	92	90	80	58+	40	26	40	22	18	2.71	10.5		
7.2.3	3.3	2161.9	100	100	100	100	94+	92	87+	70	47+	29	46	23	23	2.73	9.2	76.6	83.6
7.2.1	3.7	2161.5	100	100	100	99+	95	90+	80+	67	47	30+	41	19	22	2.74	9.9	82.8	91.0
7.2A	3.8	2161.4	100	100	100	99	94	90	82	64+	45+	29+	44	21	23	2.76	9.2		
7.3.5	3.9	2161.3	100	100	100	100	86+	80+	74+	56	36+	20	38	20	18	2.80	11.3	82.9	92.3
7.3.4	4.1	2161.1	100	100	100	100	90	84+	79	65	45	30	42	21	21	2.81	12.2	79.9	89.6
7.3.3	4.3	2160.9	100	100	100	100	94	87	76+	59	42	27+	40	20	20	2.80	11.3	82.7	92.0
7.3.2	4.5	2160.7	100	100	100	99+	93	90	86	71+	49	28	42	22	20	2.78			
7.3.1	4.6	2160.6	100	100	100	99+	96	90+	84+	66+	46+	28	44	21	23	2.76	11.1	82.1	91.2
7.4A	6.3	2158.9	100	100	100	98	92+	86+	75+	60	45	32+	39	18	21	2.72	10.5		
7.6.5	7.8	2157.4	100	100	100	99	92+	85+	75+	59	43+	29+	39	19	20	2.74	14.8	88.9	102.1
7.14A	24.9	2140.3	100	100	100	99+	91	83+	74	57+	40	28+	43	19	24	2.74	33.0		
7.19A	32.4	2132.8	100	100	100	99	91	85	72+	54	39	25	40	19	23	2.75	34.4		
7.21.4	33.5	2131.7	100	99+	98	95	79	68	60	50	39	26	40	18	22	2.72	31.6	89.6	117.9
7.21.3	33.8	2131.4	100	100	100	99	95	88+	75	56	39	24	40	19	21	2.73	32.2	89.8	118.7
7.21.1	34.4	2130.8	100	100	100	99	93	85	71	52+	38	24	38	19	19	2.67	34.8	86.3	116.3
7.25A	39.8	2125.4	100	100	100	99+	94	88	80	64	49+	32+	40	19	21	2.73	30.7		
7.27A	42.9	2122.3	100	100	100	100	93+	89	80+	66+	49	34	42	20	22	2.75	33.9		
7.30A	46.8	2118.4	100	100	100	99+	88+	78+	65	50	39	30	40	19	21	2.75	30.2		
7.38A	56.7	2108.5	100	100	100	100	90	81	68+	52+	39	26+	40	18	22	2.70	28.0		
7.41A	60.3	2104.9	100	100	100	100	93	87+	78	63	47	34	40	19	21	2.73	29.6		
7.43.2	62.8	2102.4	100	100	100	100	94+	92	88	77	57+	36+	36	19	17	2.73	29.2	95.1	122.9
7.43A	63.3	2101.9	100	100	100	100	97+	94	88	78+	63	40	38	18	20	2.75	28.5		

(Continued)

Table 3.2 (Concluded)

Specimen No.	Depth ft	Elevation ft	Percent Finer by Weight: Sieve No. 40	100	140	200	Diameter by Hydrometer 0.050	0.030	0.020	0.010	0.005	0.002	Atterberg Limits LL	PL	PI	G_s	w %	γ_d pcf	γ pcf
Operation DIAL PACK																			
1.1.2	0.6	2164.8											40	20	20	2.67	10.3		
1A.1.1	0.4	2164.7											43	19	24	2.67	11.8		
1.1.3	0.9	2164.5											38	18	20	2.68	9.3		
1.1A	1.1	2164.3											41	17	24		8.4		
3.1.1	0.2	2164.3											44	20	24	2.69	[illegible]	80.9	88.2
1A.1.2	0.9	2164.2											43	17	26	2.68	[illegible]		
1A.A1	1.1	2164.0	99+	99+	99	99	92+	82+	74	58	45	32+	43	25	18		8.2		
3.1.2	0.5	2164.0											39	20	19	2.68	8.9	79.8	86.9
3.1.3	0.8	2163.7											42	20	22	2.70	8.2	75.3	81.5
1.3.3	3.2	2162.2											41	21	20	2.72	9.8	81.7	89.7
1A.3.1	3.0	2162.1	100	100	100	99	97	93	85	74	55	34	44	20	24	2.74	7.3		
3.3.1	2.7	2161.8											38	20	18	2.75	11.0		
1.3.5	3.7	2161.7	100	100	100	99	94+	88	75	60	46+	34	40	19	21	2.72	9.8	82.2	90.3
1A.A3	3.5	2161.6	100	99+	99	99	95+	90	80	60	44+	31+	38	21	17		9.0		
2A.2.1	3.6	2161.5	100	100	100	99	95	92	85	69	50	37	45	19	26	2.72	10.0	84.6	93.0
3.3.3	3.2	2161.3	100	100	100	99+	95	90	81	68	54+	30	41	21	20	2.78	10.3	83.4	92.0
2A.2.2	3.9	2161.2	100	100	100	99+	95	90	82	65	50	35+	45	17	28	2.72	9.0	83.2	90.7
2A.2.3	4.2	2160.9	100	100	100	99	94+	89	80	68	53	42	44	17	27	2.72	9.2	82.6	90.1
1A.4.1	4.3	2160.8	100	100	100	99	93	86	75	60	45	32	40	19	21	2.74	7.5		
2A.3.1	4.6	2160.5	100	100	100	99+	95	88+	79	63	50	35	43	18	25	2.72	10.0	84.8	93.3
2.1A	1.2	2160.4											44	15	29		9.8		
1A.A4	4.8	2160.3	100	99	99	97+	93	87+	72	59+	43+	28	42	25	17		9.7		
1A.5.1	5.3	2159.8	100	99	98	97	90	83	72	57	44	30+	38	16	22	2.74	6.8		
1A.A5	5.6	2159.5	99	97	96	95+	89+	81	74	62	47+	31+	42	25	17		9.7		
1.4A	5.9	2159.5											40	19	21		10.3		
1.5.1	6.2	2159.2	100	100	99+	99	94	88	75+	59+	43	30	40	17	23	2.73	10.6	86.4	95.6
1.5.2	6.4	2159.0	100	99+	99+	99	93	86	75	57	41	27+	39	18	21	2.73	10.1	88.8	97.8
1.5.3	6.7	2158.7	100	100	99+	99+	95	91	84	67	49	35	43	20	23	2.73	12.1	81.6	91.5
1A.6.1	6.5	2158.6	100	99	99	97	92	86	78	64	50	33	41	18	23	2.79	11.0		
1A.A6	6.8	2158.3	100	99+	99+	99	95	91	85	73+	56	40	42	24	18		11.2		
2A.A5	6.9	2158.2	97	96	95+	94+	89+	83	72+	56+	44	29+	36	19	17	2.79	11.4		
2.3.6	4.0	2157.6											44	21	23	2.75	15.9	85.8	99.4
1A.7.1	7.6	2157.5	100	100	99	99	96	90	76	55	43	28	39	17	22	2.78	8.3		
2.3.7	4.2	2157.4											44	20	24	2.74	16.8	85.0	99.5
2.3A	4.3	2157.3	100	100	100	98	91	83+	72+	57	46	36+	44	19	25	2.78	19.2		
1A.A7	8.0	2157.1	99+	99	98+	96+	90	79+	69	57	45+	32+					13.9		
1A.9.2	11.7	2153.4	100	100	99	99	95	88	76	55	43	30	42	21	21	2.75			
2A.6.1	12.2	2152.9	100	100	100	99+	95	89	78	59	43	32				2.74	13.3	97.7	120.5
1.8A	14.8	2150.6											37	17	20		26.3		
2A.7.1	14.6	2150.5	99+	99	99	98	94	87+	76	57+	43	30+					28.3		
3.12.2	17.5	2147.0	100	100	100	99	94	87+	77	59+	44	30+	44	19	25	2.76	30.6	88.8	117.8
1A.A14	18.1	2147.0	100	100	100	99	98	94	85	58	43	32	41	18	23	2.73	33.4		
1A.14.1	18.8	2146.3	100	100	99+	99	96	92	81	60	43	30	42	18	24	2.73	33.4		
2.10.3	16.9	2144.7											44	17	27	2.75	31.7	90.9	119.6
2A.10.3	20.6	2144.5	100	100	100	99	95+	91	83	64	44+	32	42	22	20	2.74	34.0	88.2	118.2
3.13.3	20.8	2143.7	100	100	100	99+	93	84	71	53	39	26+	39	21	18	2.74	34.2	88.8	118.3
1.12.8	22.0	2143.4											38	21	17	2.72	32.4	90.3	119.6
1A.A17	22.6	2142.5	100	100	100	99	94	88	80	67	51	35	45	22	23	2.75	34.2		
1A.18.1	24.6	2140.5	100	100	100	100	96	88	75	55	43	30	40	18	22	2.72	30.6		
1.15.5	26.2	2139.2	100	100	100	99+	93	79	64+	47	34+	24+	39	20	19	2.73	33.9	89.9	120.3
2.13.2	23.1	2138.5											40	20	20	2.74	32.7	91.7	121.8
1.16.2	30.5	2134.9											41	19	22		33.2		
3.19.2	31.7	2132.8											43	15	28		32.4		
3.23.1	40.3	2124.2											41	17	24		32.1		
1.22.2	41.6	2123.8											40	14	26		31.7		
1.26.2	50.5	2114.9											42	16	26		32.7		
1.27A	52.3	2113.1											44	15	29		31.5		
1.30.1	55.8	2109.6											43	17	26		33.0		
1.31.1	57.0	2108.4											40	15	25		31.2		
		Total:	9394+	9389+	9376+	9308+	8852	8349	7458+	5331	4366	2977+	5009	2378	2671				
	Number of samples:		94	94	94	94	94	94	94	94	94	94	122	122	122				
		Average:	99.9	99.8	99.7	99.0	94.2	88.8	79.3	56.1	46.4	31.7	41.4	19.5	21.9				

Table 3.3

Classification and Composition Data--Lacustrine Deposits: Group 1

Specimen No.	Depth ft.	Elevation ft.	Percent Finer by Weight: Sieve No. 50	100	140	200	Diameter by Hydrometer 0.020	0.005	0.002	0.001	0.0005	0.0002	Atterberg Limits: LL	PL	PI	γ_s	w	γ_d sat	γ sat
Operation DIVERT PLAIN																			
2.1.1	0.3	2164.6											47	19	18	2.64	19.9	86.2	103.4
1.1A	0.8	2164.4	100	100	100	47+	40+	82	24	47	33+	24	36	19	17	2.68	16.2		
GE.3B	3.2	2157.7	100	100	100	99	80+	62+	47+	45	32	22+	34	19	15	2.77	9.1		
GE.3B	3.5	2157.4	100	100	100	95	80+	78	43	36	29+	17+	32	22	10	2.73	7.8		
5.4	8.4	2153.8	100	100	100	99	85	45	40	25	18	14	40	24	6		14.1		
3.12C	16.2	2148.3	100	98+	97+	84	69	34	20	34	30	21				2.71	26.9		
GE.10A	15.6	2145.3	100	100	100	99	80	45+	47+	25+	18	13+	31	27	4	2.70	33.8		
3A.3.2	18.5	2145.2	100	100	100	99+	84	80+	62+	43	30	21	36	23	13	2.73	31.9	90.2	119.0
1.18A	32.0	2132.5	100	100	100	86+	80	72+	58	36+	25	17+	34	22	12	2.68	31.8		
2.17A	33.4	2131.5	100	100	100	99	85+	61	44+	28+	18	13	34	21	13		29.8		
3.18C	36.4	2130.1	100	100	100	86+	33	14	14	42	27+	20	33	18	15	2.70	30.7		
1.21C	35.9	2129.3	100	100	100	86+	35	18	10+	17+	12	17	36	21	15		30.4		
2.22A	38.7	2126.2	100	100	100	86+	90	69+	42	25+	13+	10	30	21	9	2.67	29.5		
1.26A	41.6	2123.6	100	100	100	100	87+	49	33+	25	14	11+	28	20	8	2.67	28.1		
Operation PRAIRIE FLAT																			
7.5.3	6.5	2158.7	100	100	100	98	68	36	27	19+	17+	20	40	19	11	2.71	7.5	80.8	97.6
7.5.1	7.1	2158.1	100	100	100	99	80	75	40	27	18	13	41	22	9	2.72	7.0	88.4	96.2
7.7A	11.4	2153.8	100	100	100	99+	86	70	48	23+	20	17	44	22	11	2.70	11.4		
7.10.1	14.6	2150.6	100	100	100	99+	89	75	50	30	20	14	42	20	12	2.69	17.1	88.9	104.1
7.15A	20.2	2139.0	100	100	100	82+	73	58+	40	15	10+	12+	31	24	7	2.71	33.1		
7.23.1	37.1	2126.1	100	100	100	99	83+	72+	59+	45	33	22+	41	20	11	2.70			
7.24.1	38.3	2120.9	100	100	100	85	55	75+	67+	55	43	27	40	17	13	2.70	29.6	89.5	118.4
7.25.1	39.4	2129.8	100	100	100	99	86	74	56	38	26	18+	43	17	16	2.69			
7.27.3	42.4	2128.8	100	100	100	99	80+	82+	68	52+	37+	25	4	20	16	2.69	33.0	87.4	118.2
7.28.1	44.1	2121.1	100	100	100	99+	89	74+	58	42	31	22+	46	14	15	2.71	30.1	93.6	120.8
7.28A	44.6	2120.7	100	100	100	100	86	91	84	65	45	27+	32	20	12	2.71	28.4		
Operation DIAL BACK																			
1.1.1	0.3	2165.1											34	16	18	2.62	8.2		
1.3.8	4.5	2160.9											36	17	19	2.75	10.3	84.1	99.0
2A.A3	4.4	2160.7	99	98+	97+	97	91+	84	70	53	35	25	36	16	20	2.73	9.7		
1.3A	4.8	2160.6											32	17	15		7.4		
2A.3.2	4.3	2160.2	100	100	99+	97	91	84+	70	60+	45	29	37	17	20	2.72	9.5	85.3	98.5
1.4.1	5.3	2160.1											34	15	19	2.74	10.2		
1.4.2	5.7	2159.7											36	19	17	2.75	10.7		
2A.A4	5.5	2159.6	100	100	99+	99	90+	78	58	43	32	23	37	18	19	2.73	12.5		
1.7.3	12.0	2153.4	100	99+	99	98+	80	80	70	55+	43	30					12.5	95.7	107.7
2A.6.1B	12.2	2152.9	100	100	99+	99	85	70	50	35+	25	18+				2.73			
1A.A12	15.2	2149.9	100	99+	99+	98+	90	77+	54	48	40	24				2.71	20.4		
1A.13.1	17.2	2147.9	100	99+	99	86+	82	83+	65	49	32	22	40	19	17	2.71			
1A.13.2	17.4	2147.7	100	99+	99+	99	82	81	60	35	25	20	41	20	13	2.72	29.8		
1.11.1	17.8	2147.6											37	16	21	2.71	27.2		
1.12A	22.3	2143.1											34	17	17		26.4		
1A.17.1	23.1	2142.0	100	100	100	99	88	75	56	40	27	20	34	22	12	2.74	34.0		
1A.17.2	23.4	2141.7	100	100	100	99	81	64	44	28	21	16	30	21	9	2.71	34.5		
2.14A	26.1	2135.5	100	100	100	98+							32	16	16		30.8		
1.18.4	33.5	2131.9	100	100	100	98+	87	67+	50	30	24	18	34	16	15	2.72	29.0	95.5	123.2
1.23.8	43.8	2126.6	100	100	100	99+	90+	80	60+	44	32	23	34	17	17	2.71	26.7	94.0	121.7
3.25.8	44.5	2120.0											34	20	14	2.70	29.7		
3.27.1	46.4	2118.1											34	15	19		32.5		
		Total:	3699	3695	3690	3484	3134	2716	2028+	1393+	1004+	710+	1432	692	700				
	Number of Samples:		37	37	37	37	36	36	36	36	36	36	43	43	43				
		Average:	100.0	99.9	99.7	98.5	86.4	75.4	57.5	38.9	27.9	19.7	33.3	19.4	14.0				

Table 3.4

Classification and Composition Data—Lacustrine Deposit: Group 4

Specimen No.	Depth ft	Elevation ft	Sieve No. 40	Sieve No. 100	Sieve No. 140	Sieve No. 200	Hydrometer 0.050	Hydrometer 0.030	Hydrometer 0.020	Hydrometer 0.010	Hydrometer 0.005	Hydrometer 0.002	Atterberg Limits LL	Atterberg Limits PL	Atterberg Limits PI	G_s	w %	γ_d pcf	γ pcf
Operation DISTANT PLAIN																			
GZ.4A	4.9	2156.0	100	100	100	98	80	54+	35+	25+	19	14+	29	24	5	2.71	4.8		
1.5A	9.5	2155.7	100	99	99	96	59	44	30	12	8	8+	25	19	6	2.70	5.5		
1.7A	10.6	2154.8	100	99	97+	97	77+	45	27+	17+	13+	12	25	21	4	2.68	14.7		
GZ.5.3	5.2	2154.7											24	21	3		5.5	78.8	84.7
GZ.5.2	6.6	2154.5											20	22	1	2.69	7.0	86.5	93.1
1.6A	11.3	2153.6	100	99+	89+	81+	72	52	33+	20	15	11+			NP	2.69	15.7		
GZ.GZ.2.5	10.5	2153.5	99+	97	89	75	52+	37+	18	14	10	7	23	18	5	2.69	10.1	87.9	96.8
4.4X	10.5	2152.9	100	98+	86+	67+	49	31	41	21+	19	15	25	19	6	2.68			
GZ.GZ.1.5A	11.2	2152.8	100	99	97	77+	46	28	37	13+	12	9+			NP	2.68	5.7	88.5	93.7
7.7A	12.4	2152.5	100	100	100	98	82+	50	27	20	15	12+			NP	2.67	10.1		
3.9	12.4	2152.2	99+	99	98+	91+	72	50	33+	22+	13	14			NP	2.69	7.9		
4.7.1	11.8	2151.7	100	99+	98	87+	50	28	19+	14+	11	8			NP	2.69	5.2	88.7	94.8
3.8	12.3	2151.5	99+	99	98	92	73+	46	27	20+	18	13	25	20	5	2.68	7.0		
2.9A	13.5	2151.4	99+	99	98+	96	42	27+	17+	14	10	8			NP	2.67	7.4		
1.9.1	12.9	2151.3	100	100	100	98	80	59	41+	30+	18	11	30	20	10	2.67	11.1	90.4	100.5
GZ.7A	9.9	2151.0	99+	99	98+	95	64	46	29+	16	12	7+	35	24	4	2.71	11.0		
5.6	11.6	2150.6	100	99+	99	93+	73	49	33+	21+	14+	12+	35	24	8	2.69	11.6		
5.7	12.7	2149.5	100	100	99	94	76	47	25+	19	17+	12+	28	17	11	2.67	11.4		
3.11A	15.1	2149.6	100	100	100	98+	73	50	27	16	12	8	28	24	4	2.68	9.4		
1.10A	15.9	2149.4	99+	99	99	90+	74	50	27	13+	11+	11+	27	25	2	2.69	8.4		
GZ.7A	12.1	2148.8	100	99+	99	96	80	44+	14+	15+	12+	10			NP	2.71	12.3		
6.8	14.0	2148.2	100	99+	99	95+	82	58	45+	27+	21+	11	27	24	3	2.67	11.0		
GZ.9A	12.9	2148.0	100	99	97+	97	76	46	30	25	20+	14+	25	20	5	2.72	16.6		
GZ.8A	13.4	2147.5	100	100	100	97+	75	45	34	24+	21+	15	26	20	6	2.68	17.2		
2.11.2	15.6	2146.5	100	100	100	96+	72	52+	34+	23+	19+	13	25	24	1	2.73	21.5	85.1	103.4
2.11.1	18.2	2146.2	99+	97	96	88	60	41	28+	15	10	8			NP	2.68	22.4	88.4	108.3
GZ.10.1	17.6	2145.5	100	100	100	99+	77	58	37	16	10	7	27	24	3	2.70	17.7	85.3	100.3
3A.1.1	18.8	2144.9	100	100	100	98+	72+	43	31	24+	14	9				2.67	40.4	80.1	111.4
5.11	18.3	2144.1	100	99+	97	91	42	26	13+	12+	14	11	24	20	4	2.69	24.1		
1.12A	24.3	2141.9	100	99+	97	94	42+	27+	20+	16+	14+	10+			NP	2.67	FW		
3.13	26.2	2138.2	99+	98	97	94	71+	51	42+	25+	20+	15			NP		30.2		
3.14A	29.4	2135.1	100	99+	99+	96+	65	37	30	15+	13	8			NP	2.68	34.4		
1.15A	30.8	2134.6	100	99	99+	98+	66	46	25+	14	14	11+	24	21	3	2.69	FW		
GZ.15A	27.8	2133.2	100	99	99+	94+	70+	41	17+	14	11	7	23	22	1	2.71	FW		
3.16B	32.5	2132.0	100	100	100	97+	87	55	35	20+	17	12	26	22	4	2.68	35.0		
1.20A	33.2	2132.0	100	99+	99	96+	70	41	30	20	14+	11+	24	21	3	2.69	34.2		
1.21A	33.7	2131.1	100	100	100	99+	68	41	29+	19	15	12	25	24	1	2.68	FW		
GZ.17A	34.3	2131.0	100	100	100	98+	61	36+	22+	14+	12+	8	27	25	2	2.70	FW		
2.18A	36.0	2130.1	99+	99	98+	96+	57	40	25	17+	14	11+			NP	2.68	FW		
2.19A	35.7	2129.2	100	100	99	97+	71	41	25+	17	17	14	26	22	4	2.67	FW		
3.19A	35.6	2128.4	100	100	100	99	75	40	32+	17	15	11+	27	20	7	2.67	31.0		
4.21A	37.4	2127.2	100	99	97	91	58+	42+	23	17+	13+	10			NP	2.67	29.5		
2.21A	36.0	2126.9	100	100	100	99	76	43	35	24	19	14	25	24	1	2.69	32.4		
1.24A	35.2	2126.0	100	100	99+	98+	67	44	30	21	16+	13	24	23	1	2.67	FW		
3.21C	38.4	2125.1	100	100	100	98+	75	49	40	22	17	13+			NP	2.67	32.2		
Operation PRAIRIE FLAT																			
7.5.2	6.8	2158.4	99	98+	97+	94+	80	45	40	26+	16	10+	27	21	6	2.69	5.2	84.0	88.8
7.5A	7.5	2157.7	100	100	100	99	71	58	35	26	12	10	25	24	1		4.4		
7.6.2	8.5	2156.7	99+	99	97+	81	56	37	27+	21	15	9	26	22	4	2.70	5.2	80.8	85.4
7.6.1	8.7	2156.5	100	99+	97+	84	56	42	22	15	10+	7+			NP	2.67	5.9	83.4	89.1
7.8.2	11.8	2155.4	100	100	100	99+	67	43	30	18+	12	10+	27	26	1	2.69	5.7	85.2	90.1
7.8.1	12.1	2153.1	99+	98	98	94+	60	34	22	12	9	7	24	22	2		9.5	81.4	89.7
7.9A	12.5	2152.7	100	99	97	96	67+	29	17	12+	9+	7			NP	2.69	9.5		
7.9A	13.8	2151.4	100	100	100	99	74	41	24	15	11	8	28	26	2	2.72	11.0		
7.10A	15.0	2150.2	100	100	100	98	68	37+	23+	14+	12	8	27	26	1		10.4		
7.12.1	16.9	2148.3	100	100	100	97	70	44	30	24+	17	14	28	23	5	2.68	10.0	82.4	90.2
7.12B	17.7	2147.5	100	100	100	97	70+	42+	28	18+	13+	10+	26	25	1	2.68	12.6		
7.13A	20.2	2145.0	100	100	100	98+	67	46	30	25	20	14					25.8		
7.16.2	22.6	2142.6	100	100	100	99+	72	50	34	21	15	9	24	22	2	2.68	40.4	80.1	121.0
7.16.1	28.0	2137.2	100	99	98	90	56	44	23	14+	11	8			NP		31.1	90.0	118.0
7.17A	29.7	2135.5	100	100	99	98	58	44	24	17	12	9	25	23	2	2.69	FW		
7.18A	31.1	2134.1	100	99	99	95+	60	41	25	15	12	9	27	26	1	2.70	FW		
7.20A	32.5	2132.7	100	100	100	99	76	45	32+	20	13	8	29	23	6	2.73	28.7		
7.21.2	34.1	2131.1	100	100	100	99	69	42	40	22	15	10+	29	24	5	2.69	31.1	91.0	119.3
7.23.2	37.9	2128.3	100	100	100	98	75	47	39+	23	15	11	28	21	7	2.69			
7.26A	41.9	2123.3	100	100	100	98+	69	38+	25	17+	13	9	28	24	4	2.70	34.2		
7.27.4	42.1	2123.1	100	100	100	99	74	53	38	25	18	13	29	22	7	2.69	30.5	93.9	122.4
7.27.2	42.7	2122.5	100	100	100	99+	64+	40+	29+	17	13	9	30	22	8		31.4	91.1	120.0
7.36A	54.3	2110.9	100	100	100	99	75	58	37+	22	16+	12	24	24	0	2.68	29.7		
7.40A	59.1	2106.1	100	100	100	99+	68	40	35	23	16	13	29	22	7	2.70	29.2		

(Continued)

Table 1.4 (Concluded)

Specimen No.	Depth ft	Elevation ft	Percent Finer by Weight: Sieve No. 50	100	140	200	Hydrometer by Hydrometer: 0.020 mm	0.010 mm	0.005 mm	0.002 mm	0.001 mm	0.000 mm	Atterberg Limits: LL	PL	PI	G_s	w %	γ_d pcf	γ pcf
Operation DIAL DATE																			
1A.A9	9.8	2155.3	100	99	98	97	63	50	30	20	15	10	21	16	5	2.70	5.5		
1.7.2	11.8	2153.4	100	99	98	88	60	41	25	16	12	9	26	22	4	2.70	5.7	89.5	94.4
1A.9.3	11.9	2153.2	100	99+	98	91	70	45	30	19+	14	10	28	19	9	2.71	6.9		
2A.6.2	12.4	2152.7	100	99+	98+	96	58	45	35	[illegible]	18	13	27	17	10	2.71	8.4	82.5	89.4
1.8.5	13.7	2151.7	100	99+	98+	98										2.70	10.0	86.0	95.7
1A.A11	13.8	2151.5	100	99	98	95	70	42	21	15	11	8			NP	2.69	9.8		
3.7A	13.3	2151.2				70											10.4		
1A.10.1	14.3	2150.8	100	99	99+	74	60	36	19	12	9+	7	23	20	3	2.70	9.7		
1A.10.2	14.5	2150.6	100	99	99	97	80	50	30	19	14	10	29	25	7	2.71			
3.9.2	14.8	2150.3	99+	99	99	83	70	53	37	25	18	12	28	19	9	2.72	9.5	84.8	92.9
2A.7.2	14.8	2150.3	100	99	97	76	45	34+	27	20	15+	11+				2.69	10.4	84.0	92.7
2A.7.3	15.1	2150.0	100	99+	99	87	54	39+	30	15	12	9+	24	25	1	2.70	10.1	84.2	92.7
1.9.3	15.5	2149.9	99+	98+	95	71	54+	40+	37	28	21	15	27	26	1	2.[illegible]	12.5	84.2	94.7
2.7.2	11.8	2149.8	100	99+	98+	93	70	60	29+	18+	15	11	27	20	7	2.73		95.7	
3.10.1	14.9	2149.6	100	99+	99	91	70	60	26+	17	13+	9+	23	21	2	2.71	11.7	84.9	94.9
2A.A9	15.0	2149.5	99+	99	97+	73	70	58+	37	23	16	11				2.70	10.5		
3.10.2A	15.3	2149.2	100	99	98+	85+	70	52+	34	20+	14+	12+	24	20	4	2.72			
3.10.3	15.6	2149.1	100	100	99	91	70	62+	21+	15	12	9+	25	19	6	2.69	11.0	84.7	94.0
1A.10.2	16.0	2149.1	100	99	98	85	63	39	18	12	10	8	22	20	2	2.70	10.8		
1.10A	16.9	2148.5	99+	99	98+	94+							28	15	13	2.71	14.1		
1A.A13	16.6	2148.5	100	99	98	95	81	60	36	24	16	13+	27	26	1		14.4		
3.11.2	16.5	2148.0	100	99+	98+	90	65	44	30	21	17	13	25	18	7	2.71	12.8	87.4	98.6
3.11.3	16.7	2147.8	100	99	99+	79+	64	39	18+	13+	10	7	22	19	3	2.70	9.5	84.7	92.7
1A.11.2	17.0	2147.5	100	99+	99	89	70	49	29	19	10+	8	27	23	4	2.70	11.2		
1.12B	18.0	2146.5	99+	99	98	90							22	14	8	2.68	17.4		
3.12A	18.3	2146.2				70+											14.5		
1A.14.2	19.5	2145.0	100	99	98	88+	54	32	22	14	10	8	25	22	3	2.70	14.9		
1A.A15	19.6	2145.7	100	99+	97	81	48	31	22	17	13	9	28	21	7	2.69	17.4		
2.10.1A	19.2	2145.4	100	99+	98+	89	62+	38	33	21	16	12	26	19	7	2.69			
2A.10.1	20.0	2145.0	100	99+	99	97	70	60	29	17	13	10+	29	21	4	2.72	20.3	97.2	104.9
1A.15.2	20.4	2144.7	100	100	99+	80	55	39	25	15+	12	9	25	20	5	2.71	12.2		
1A.16.2	21.0	2144.1	100	99	98	82	48	34	19	14+	11+	8+			NP	2.70	27.0		
1.13.1	22.7	2142.7	99+	98	93	61+							28	21	7	2.[illegible]	21.[illegible]		
1A.17.2	23.7	2141.4	100	99	96	77+	45	29+	21+	17	13+	10			NP	2.69			
1.14.1	24.1	2141.3	100	99	96	76+							28	24	5	2.68	33.5		
2A.A14	24.7	2140.4	100	99	95+	81	64	29	18+	13+	9	7+	34	20	4	2.69	28.1		
		Total:	10,099+	10,035+	9894+	9128	4350+	4103	2478	1800	1392	1000	2042	1677	555				
		Number of Samples:	101	101	101	101	[illegible]	[illegible]	[illegible]	[illegible]	[illegible]	[illegible]	78	78	78				
		Average:	99.9	99.4	98.0	90.4	[illegible]	40.4	27.9	18.9	14.1	10.5	26.4	21.5	4.5				

Table 3.9

Classification and Composition Data--Lacustrine Deposits, Group 5

Specimen No.	Depth ft	Elevation ft	Percent Finer by Weight: Sieve No. 50	100	140	200	Diameter by Hydrometer 0.05?	0.01?	0.00?	0.00?	0.00?	0.00?	Atterberg Limits LL	PL	PI	G_s	w %	γ_d pcf	γ pcf
Operation DISTANT PLAIN																			
GE.4.2	4.4	2156.5	100	93+	73	48+	25	20	15	11	9	6+			NP	2.69	5.2	84.2	90.7
5.3	5.8	2156.4	99	89	70+	51	34+	23+	15	11+	10	8+			NP	2.67	4.9		
5.3A	7.1	2155.1	99+	90	63	38	23+	15	12	10+	9	7+			NP	2.66	5.7		
GE.5B	6.0	2154.9	99+	90	61	46	25	19	15	12	9	6+			NP	2.68	7.3		
GE.5.1	6.7	2154.2	100	91	64	37	17+	13+	11	9	7+	6			NP	2.68	4.7	86.6	90.7
GE.5C	7.1	2153.8	99+	81+	58+	38	15	11	9+	7+	6	4			NP		5.0		
5.9B	10.7	2153.8	99+	94+	68	58	33	24+	15+	11+	9	7			NP	2.68	4.9		
1.7A	12.1	2152.9	100	99	69	40+	32+	21	14+	13+	11	8+			NP	2.67	6.1		
2.10C	16.8	2148.1	98	78+	47+	40+	25	18	11	9	7+	6+			NP	2.66	7.1		
3.12D	19.9	2147.0	99	89	64	49	30	19	10	7+	5+	5			NP	2.66	6.3		
1.12A	18.4	2146.8	99	88+	62+	35+	19	12+	9+	8	6+	5+			NP	2.67	5.9		
GE.9A	14.5	2146.4	100	95	84+	60	29+	20	13+	10+	8+	6			NP	2.68	9.9		
1.13A	19.7	2145.5	100	97+	80+	59+	42+	26	18	15	12	9	24	21	3	2.69	12.3		
GE.11A	16.6	2144.1	100	77+	49	30+	18	14+	12+	8+	5+	4+			NP		17.5		
GE.12.3	17.7	2143.2	99	80	54	32+	19	11+	10	8+	7+	6			NP	2.69	23.1	93.7	110.9
Operation PRAIRIE FLAT																			
7.6A	8.9	2156.3	100	97	84	58+	28+	19+	14+	11	9	6+			NP	2.64	4.7		
7.20B	33.2	2132.0	100	95+	86	62+	33+	21	15	11	9	6+			NP	2.67			
7.20.1	33.3	2131.9	100	88+	66	49	26	18	8	5+	4	3			NP	2.69	24.6	95.9	119.5
7.47A	61.6	2097.6	100	97	84+	62	31+	25	20	15	12	9+			NP	2.66	FW		
Operation DEAD MAN																			
3.4.1	6.5	2156.0	99+	94	75	42+	20	15+	13	10	7+	6			NP		4.6		
1.7.4	12.1	2153.3	99+	97+	84+	55	41	28+	18	13	10	8			NP	2.67	6.2		
1.7.5A	12.2	2153.2	99+	89	68+	44+	30	21	12+	10	8+	6+			NP	2.67	5.5		
1.7.5E	12.2	2153.2	99+	85	67+	45+	26	20+	16	12+	9+	7+			NP		5.0		
1A.9.4	12.0	2153.1	99+	92	67	43	34	21	16	13	10	7	23	20	3	2.71			
1A.A10	12.2	2152.9	100	95	75	44+	20	13	10	7	6	4+			NP		4.5		
2A.6.2B	12.4	2152.7	100	97	82	62	30	22	15	12	9+	7+				2.71			
2A.6.4	12.6	2152.5	100	91+	70+	41	22+	14+	11+	8+	6+	5				2.70	2.9		
1.7.4	12.0	2152.5	100	97+	84+	52+	25	17	13+	10+	8+	6+			NP	2.70	5.7	92.2	97.4
2A.A7	12.8	2152.3	99+	70+	49	34+	25	19+	16	13	10+	8+				2.69	1.9		
1.8.3	13.2	2152.2	99+	95	81	61+										2.68	6.7	89.5	95.5
1A.11.1	13.4	2151.7	100	96	71	41+	24	16+	13	10+	8	6+			NP	2.68	3.0		
2A.A8	14.3	2150.8	99+	89	55	28+	29+	17	11	8	6	4				2.71	4.4		
2A.7.2B	14.8	2150.3	100	99	80	48+	40	25+	19	15	12	8				2.67			
2.7.1	11.5	2150.1	100	97+	82	51+	29	19	16	13	10+	8+	21	20	1	2.71		90.1	
3.9A	14.7	2149.8				47											7.8		
1A.13.4	17.9	2147.2	100	92	83	50	24	16	12+	9+	7+	6			NP	2.69	9.1		
2A.A11	18.7	2146.4	98+	75	58	40	25	18	14	10+	8+	6				2.66	10.8		
1A.15.1	20.2	2144.9	100	99	93	68	40	26+	18	13	10	7	21	18	3	2.70	8.7		
3.13A	20.0	2144.5				30											15.9		
1.12.4	21.0	2144.4	100	91	65	38										2.68	12.8		
2A.A13	21.8	2144.3	99	98	90	68+	37	29+	17	11	9	6+				2.67	21.1		
1A.16.1	21.6	2143.5	100	87	60	34	18	14+	12	10	8+	7			NP	2.70	17.9		
1A.A16	23.9	2141.2	100	96+	91	56+	29+	21	17	14	11	8+	21	18	3		FW		
		Total:	4089+	3768+	3085	2057	1140	720+	542+	420	335	247+							
		Number of Samples:	41	41	41	41	39	39	39	39	39	39							
		Average:	99.6	91.9	75.2	50.2	29.2	18.5	13.9	10.8	8.6	6.4							

Table 3.6

Classification and Composition Data--Lacustrine Deposits, Group 6

Specimen No.	Depth ft	Elevation ft	Percent Finer by Weight: Sieve No. 10	40	100	200	Diameter in Millimeter: 0.050	0.030	0.020	0.010	0.005	0.002	Atterberg Limits: LL	PL	PI	G_s	W %	γ_d pcf	γ pcf
Operation DISTANT PLAIN																			
1.1B	5.6	2159.6	99+	53+	25+	15+	13+	11+	9+	7+	6+	5			NP	2.66	2.8		
RCHL-2.4	8.7	2155.3	9[illegible]	57	36	20+	13+	11	9+	8	6	5			NP	2.67	4.1	94.8	104.1
1.3A	14.4	2150.8	98+	44	24+	14	8+	6	5	4	3+	2+			NP	2.68	1.7		
2.3A	14.7	2150.2	98+	63+	44	29	17+	10+	7+	5+	4	3			NP	2.68	4.1		
2.10B	15.4	2143.5	97+	55	34	21	11	9	7+	6	4	2+			NP	2.66	4.0		
1.11A	17.1	2148.1	95+	44	24+	13	7+	5	4	3+	2+	1+			NP	2.67	2.3		
2.11A	17.6	2147.3	97+	41	26+	20	15+	13+	11	9	7+	6			NP	2.65	3.0		
2.11B	19.1	2145.8	99	54	26+	13+	8	6+	6	5+	5	4			NP	2.65	4.4		
5.10	16.8	2149.4	99	78+	43	23	13+	11	9+	7	6	5			NP	2.66	4.6		
1.14A	20.9	2144.3	99+	58	28+	13+	7+	5+	5	4	3	2+			NP	2.66	6.1		
3.14	20.5	2144.0	98+	49	33+	14	10	7+	6	5	4+	3+			NP	2.67	8.7		
2.12A	21.2	2143.7	99	30+	15+	8+	6	5	4	3+	3	2+			NP	2.66	14.2		
GE.12.2	17.9	2143.0	99+	71	41	21	10+	8	6+	6	5+	4+			NP	2.68	24.8	96.8	120.8
GE.12.1A	18.1	2142.8															25.9	94.5	118.9
GE.12.1	18.4	2142.5	99+	70	39+	21	10+	8	7+	7	6	5			NP	2.69	25.5	91.9	115.3
GE.12A	18.6	2142.3	99	66+	22	12	8+	6+	5+	4	3+	2+			NP	2.68	23.7	-	
Operation PRAIRIE FLAT																			
7.11.1	15.9	2149.3	99+	72	45	22+	11	7+	6	5+	4	3			NP	2.69			
7.11A	16.3	2148.9	100	69+	36	18	7+	6	4+	4	3+	2+			NP	2.67	2.9		
7.12C	19.2	2146.0	100	70	39	20+	9	6+	5+	5	4	3			NP	2.67	3.8		
Operation DIAL JACK																			
3.4.2	6.7	2157.8	99+	81+	50+	26	17	13	10	8	6+	5				2.68	3.8		
3.4.3	6.9	2157.6	99+	68	38+	19+	10	7+	6+	5+	4	3			NP	2.70	1.8		
3.4A	7.3	2157.2				18											2.2		
1A.A8	9.3	2155.8	99+	56	33+	21	15	12+	10+	9	8	6+			NP	2.70	3.0		
3.5	10.2	2154.3				27											3.2		
1.6	11.1	2154.3	99+	49	21	10+	8	7	6	4+	3+	2					1.6		
3.6	10.6	2153.9	99+	68	32+	15+	12+	9+	8	7+	5+	3+					2.1		
1.7.1	11.6	2153.8	99+	45+	23	15+	12+	10+	9+	8	6+	5				2.66	3.2		
1A.9.1	11.4	2153.7	100	86	50	25+	12	8+	7	6	6+	4+	20	19	1	2.70	2.3		
3.7.1	11.2	2153.3	100	84+	52+	25										2.67	3.6	93.0	96.4
3.7.2	11.5	2153.0	100	80	51+	18+										2.68	4.4	92.2	96.2
3.9.3	14.4	2150.1	99+	73+	43	22	12	9	7+	6	4+	3				2.66	2.6	96.0	98.4
1.9A	16.1	2149.3				21											3.4		
3.14A	21.9	2142.6				22+											26.1		
		Totals:	2770	1732	980+	519+	288	222	184	154+	127	98							
	Number of Samples:		28	28	28	28	26	26	26	26	26	26							
		Average:	98.9	61.9	35.0	18.6	11.1	8.5	7.1	5.9	4.9	3.7							

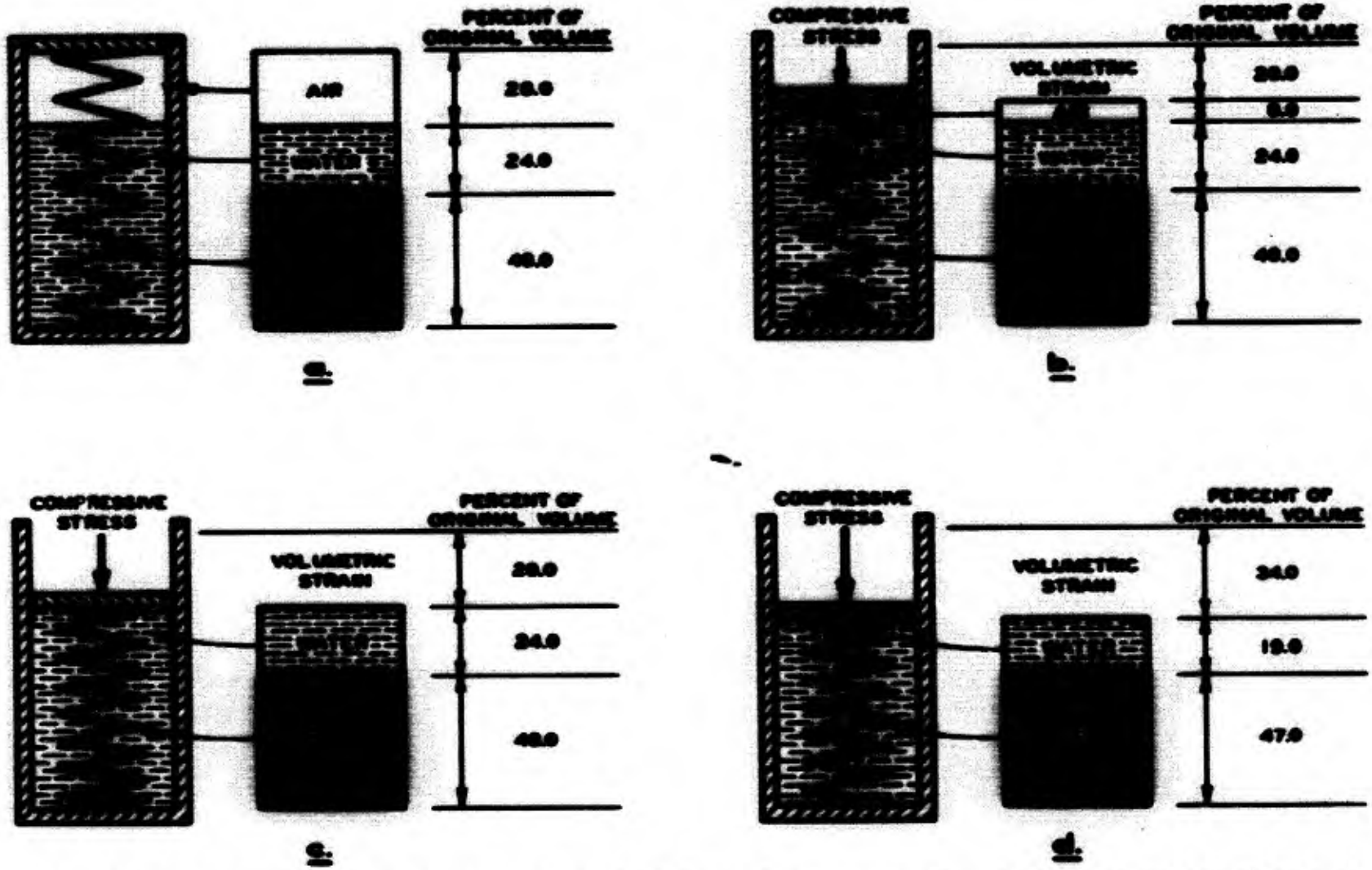

Figure 3.1 Piston and spring analogy for uniaxial strain response of partially saturated, undrained soil specimens.

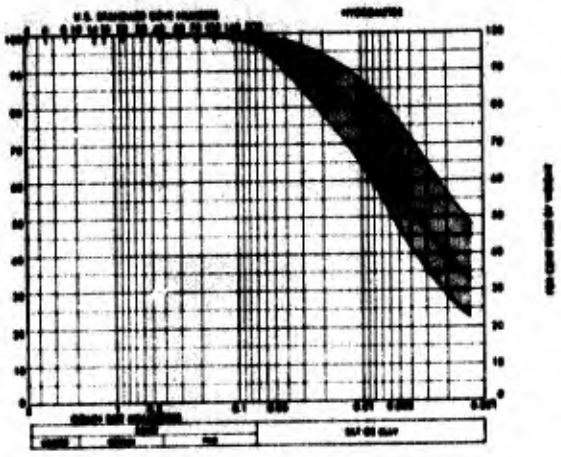

a. Group 1.

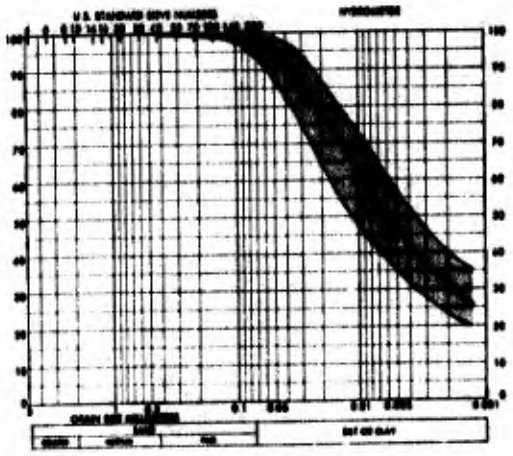

b. Group 2.

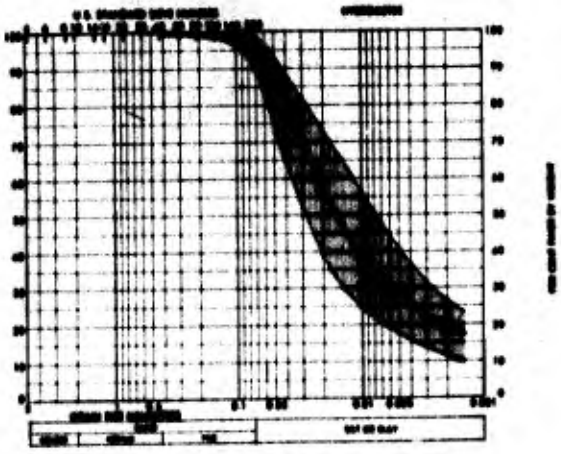

c. Group 3.

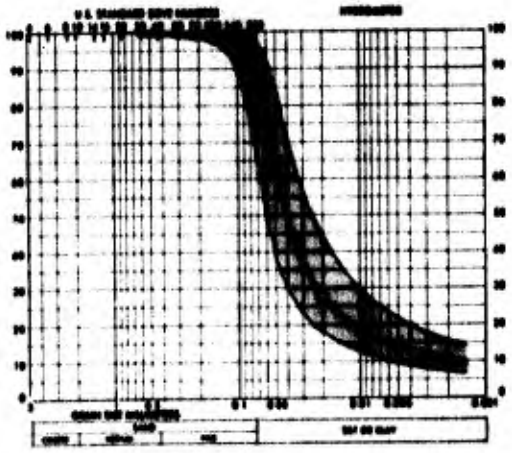

d. Group 4.

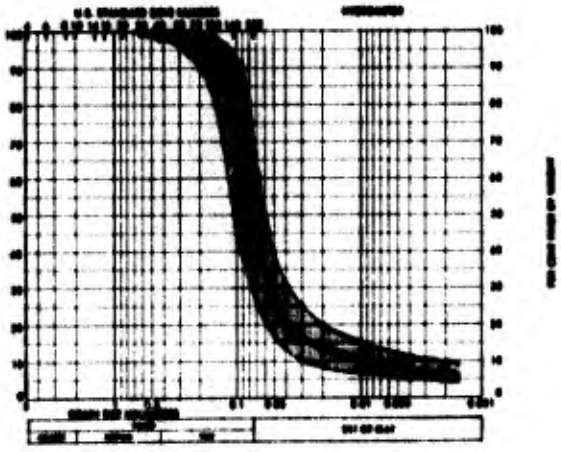

e. Group 5.

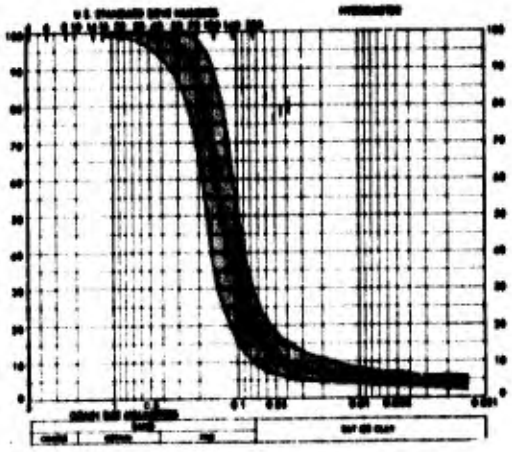

f. Group 6.

Figure 3.2 Average gradation curves and band-spreads for six soil groups.

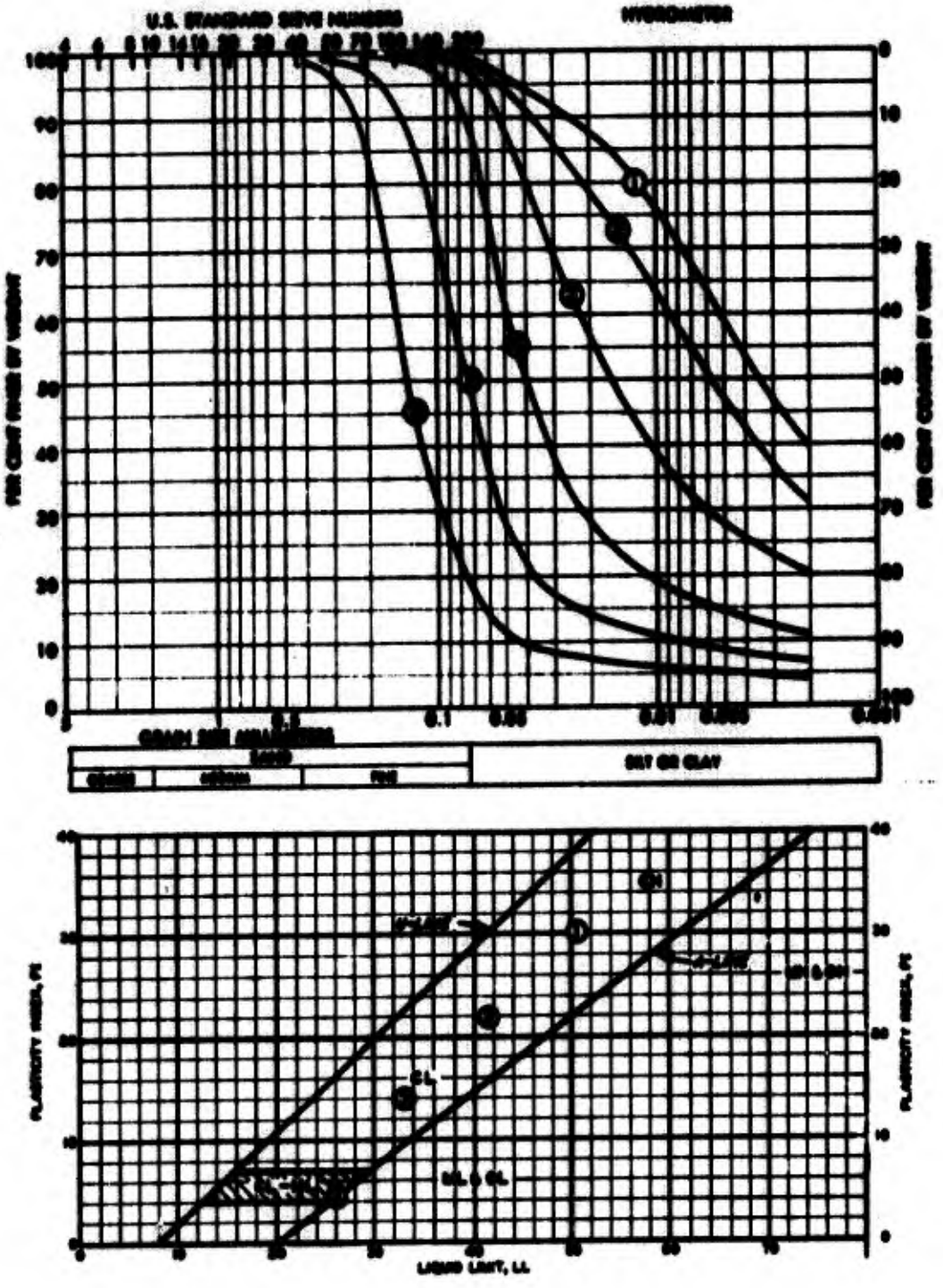

Figure 3.3 Average gradation and plasticity characteristics of lacustrine soil groups.

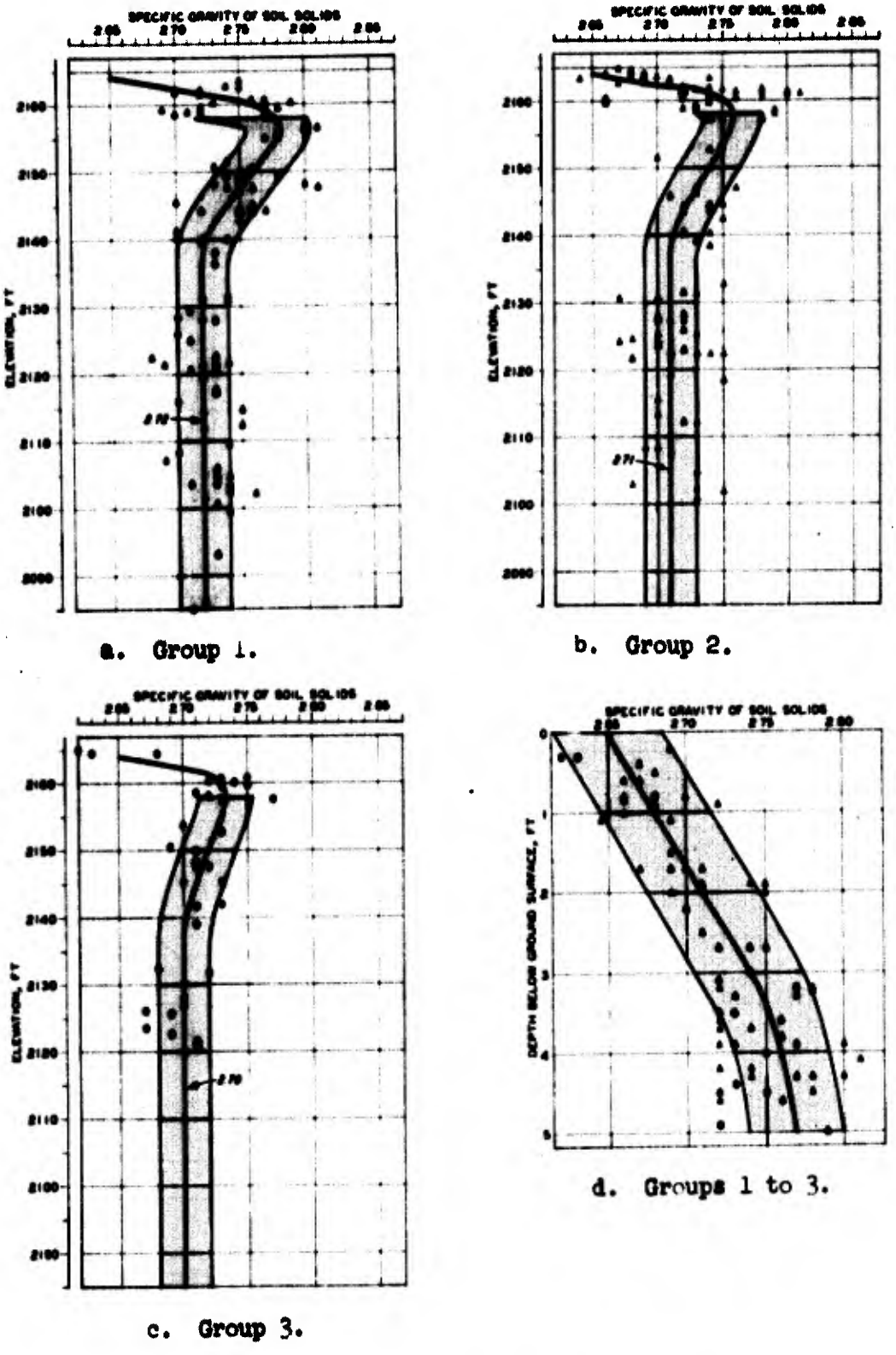

a. Group 1.

b. Group 2.

c. Group 3.

d. Groups 1 to 3.

Figure 3.4 Specific gravity data and recommended profiles for Soil Groups 1, 2, and 3.

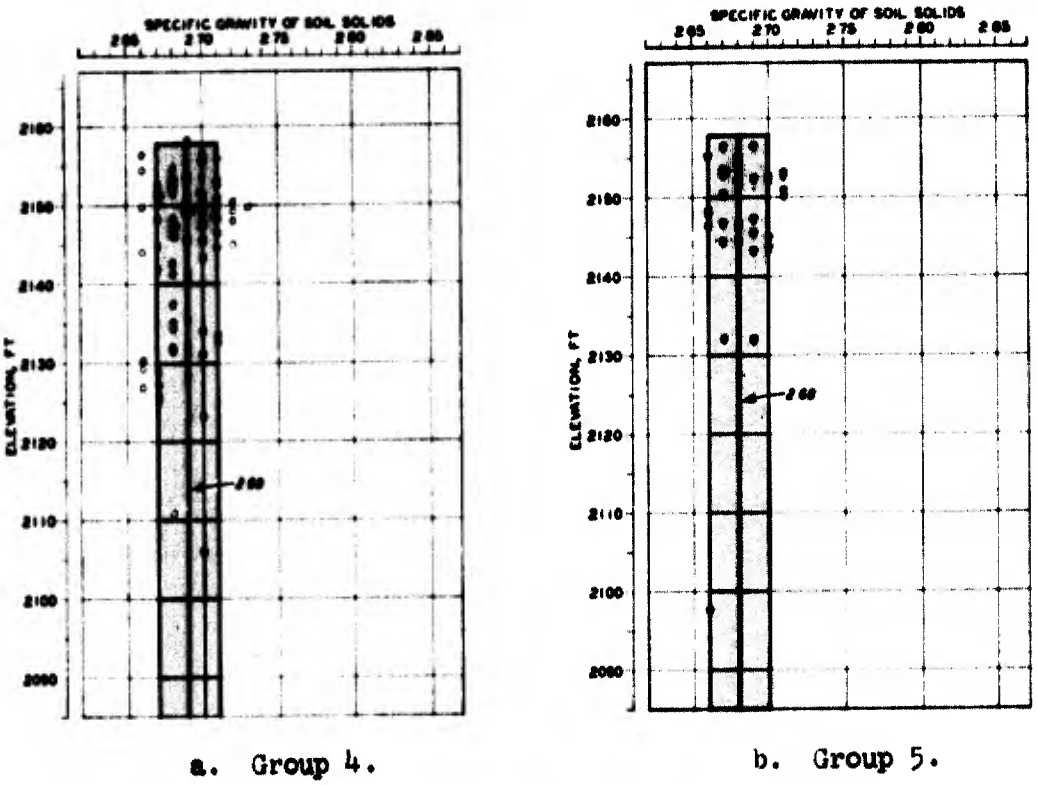

a. Group 4.

b. Group 5.

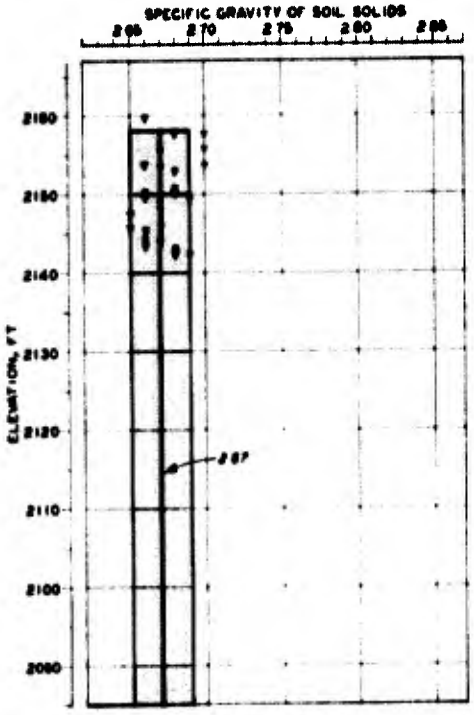

c. Group 6.

Figure 3.5 Specific gravity data and recommended profiles for Soil Groups 4, 5, and 6.

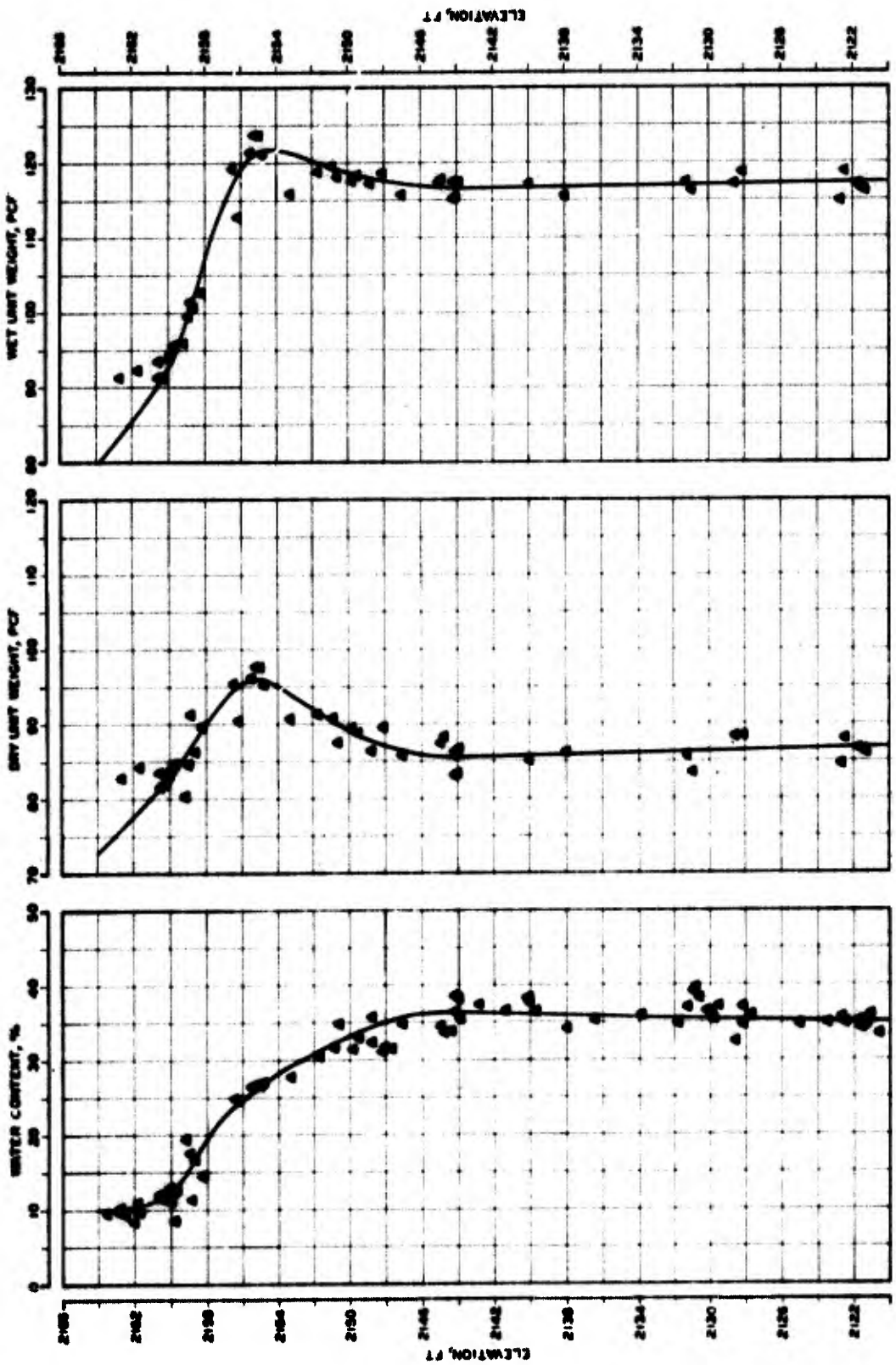

Figure 3.6 Water content, dry unit weight and wet unit weight data, and recommended profiles for Soil Group 1.

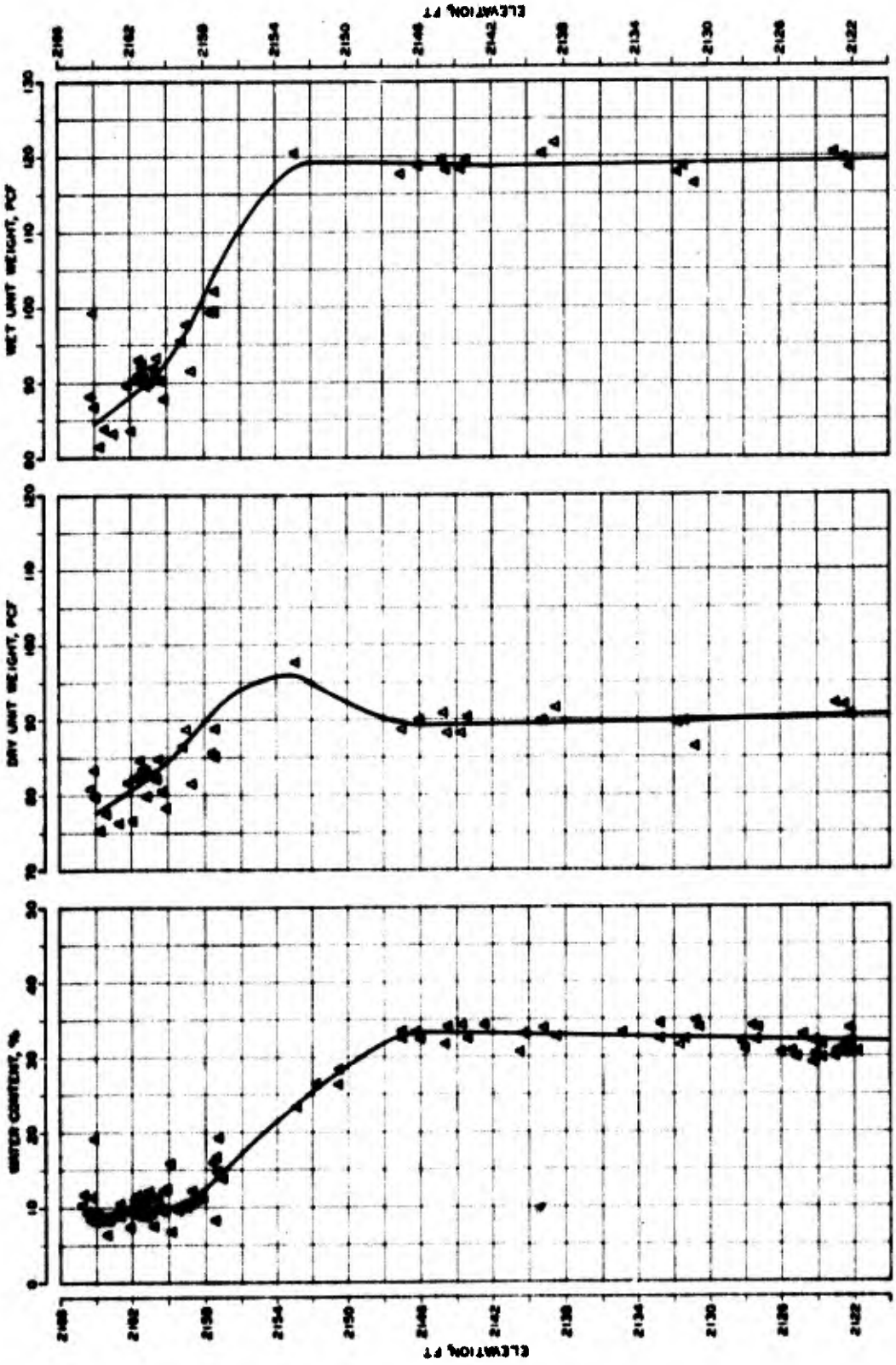

Figure 3.7 Water content, dry unit weight and wet unit weight data, and recommended profiles for Soil Group 2.

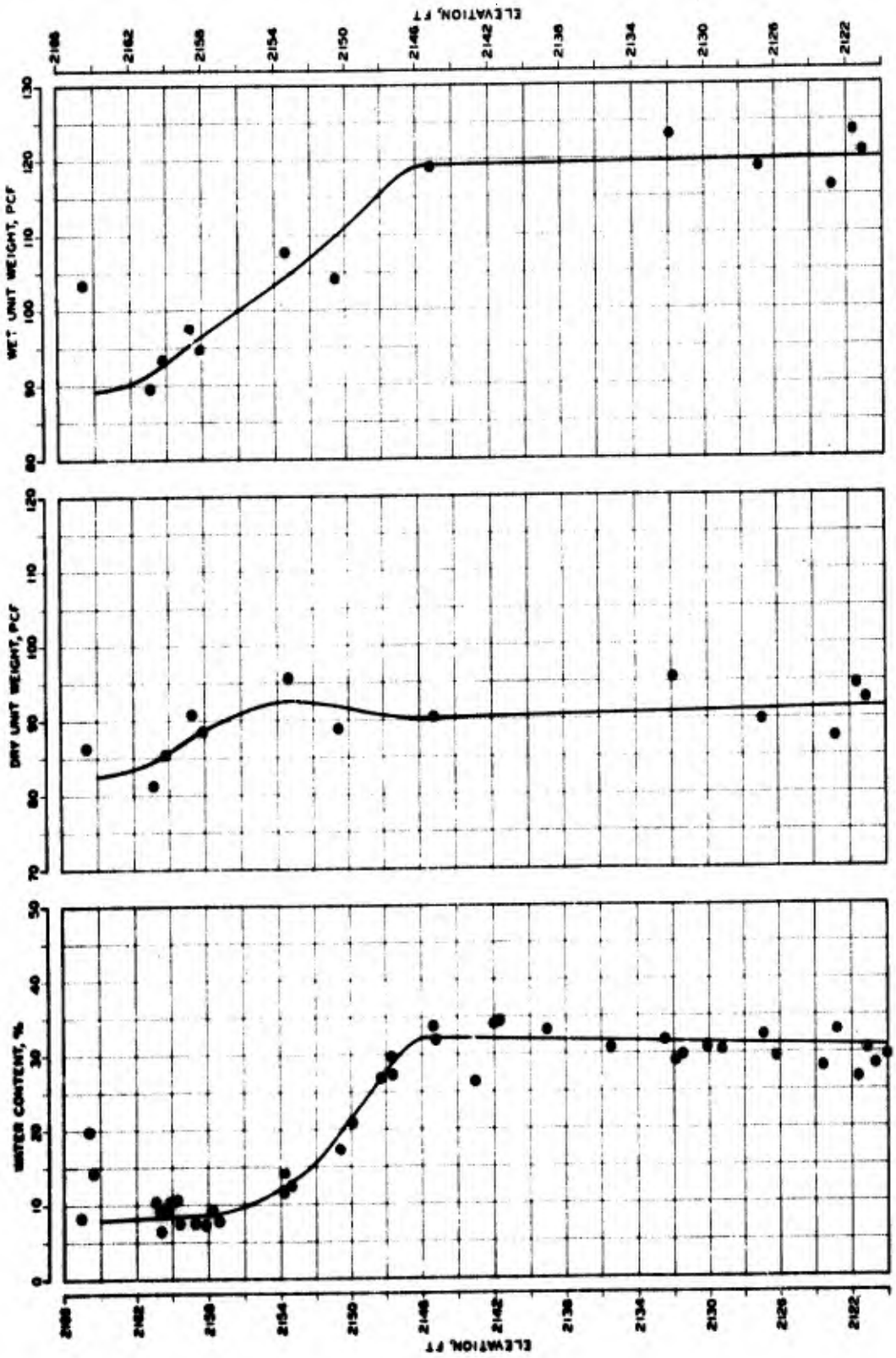

Figure 3.8 Water content, dry unit weight and wet unit weight data, and recommended profiles for Soil Group 3.

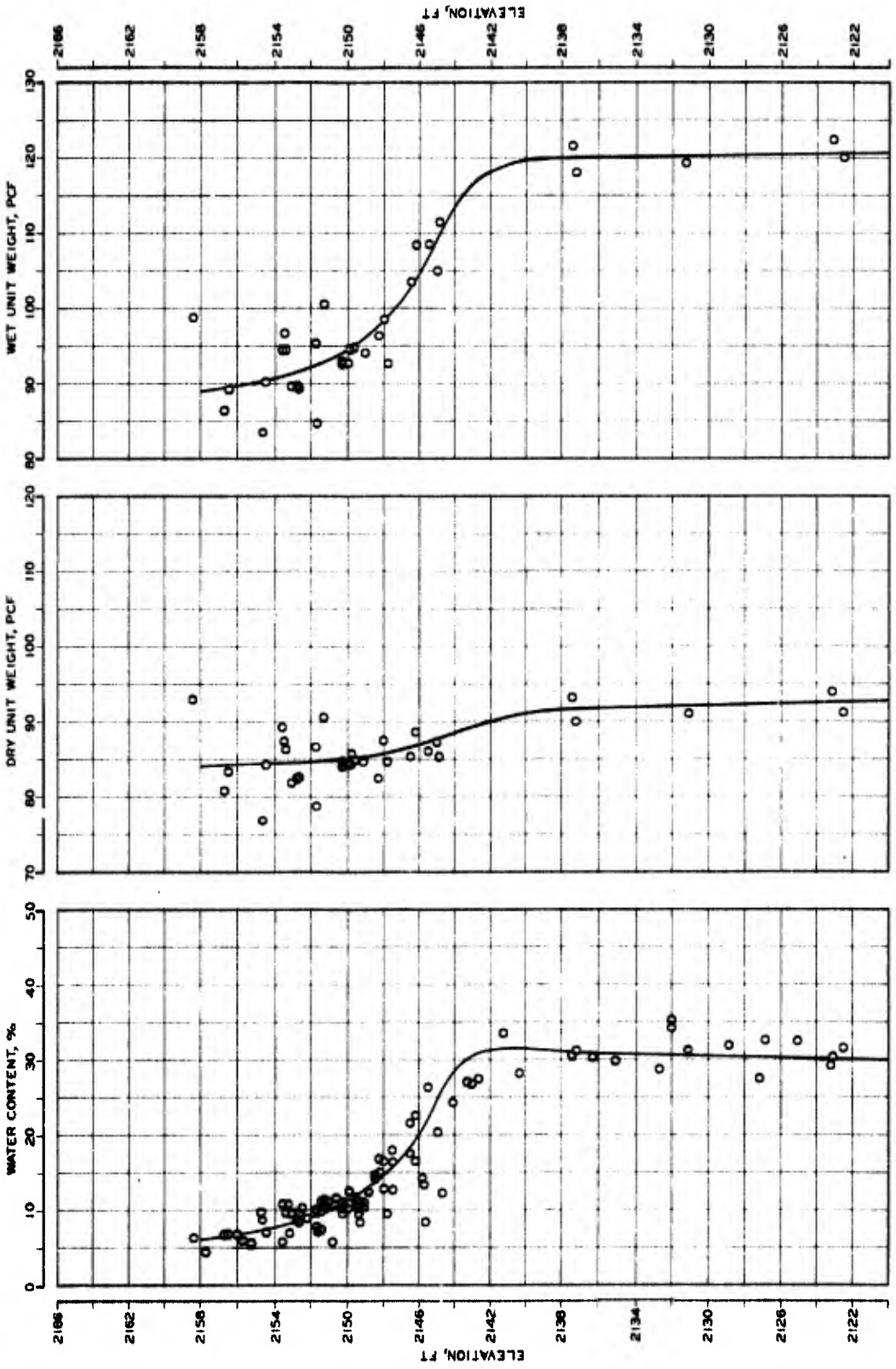

Figure 3.9 Water content, dry unit weight and wet unit weight data, and recommended profiles for Soil Group 4.

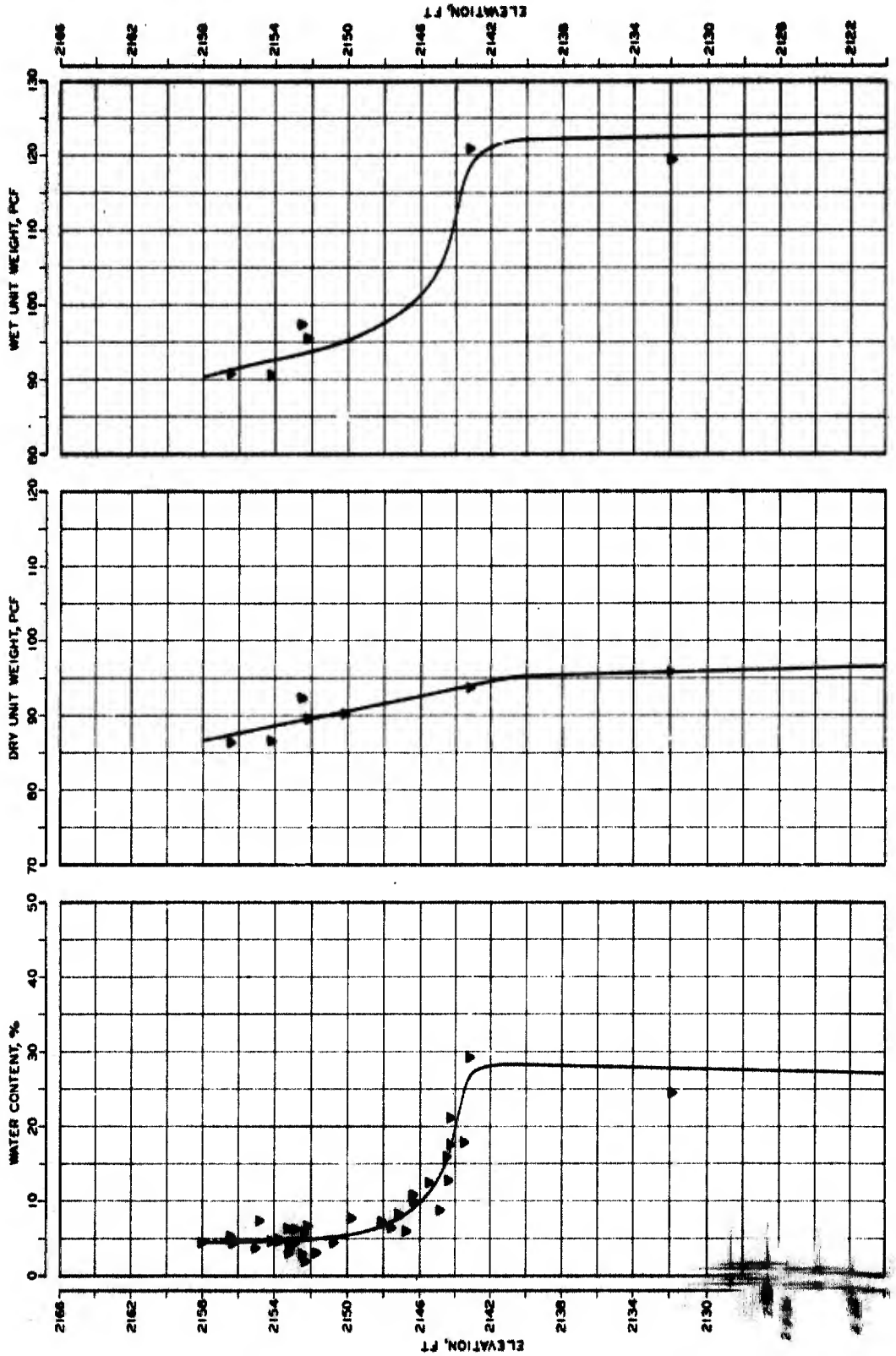

Figure 3.10 Water content, dry unit weight and wet unit weight data, and recommended profiles for Soil Group 5.

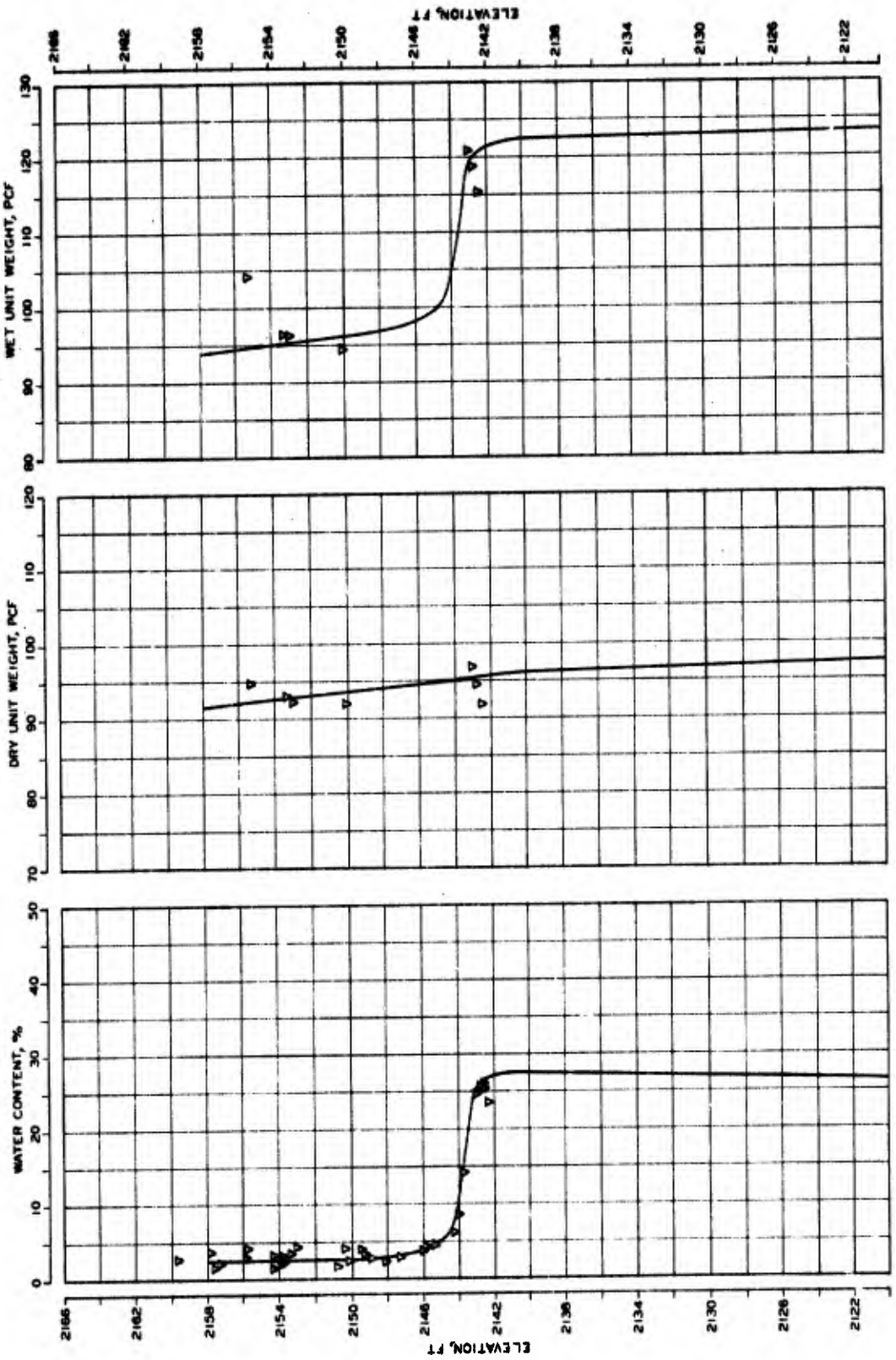

Figure 3.11 Water content, dry unit weight and wet unit weight data, and recommended profiles for Soil Group 6.

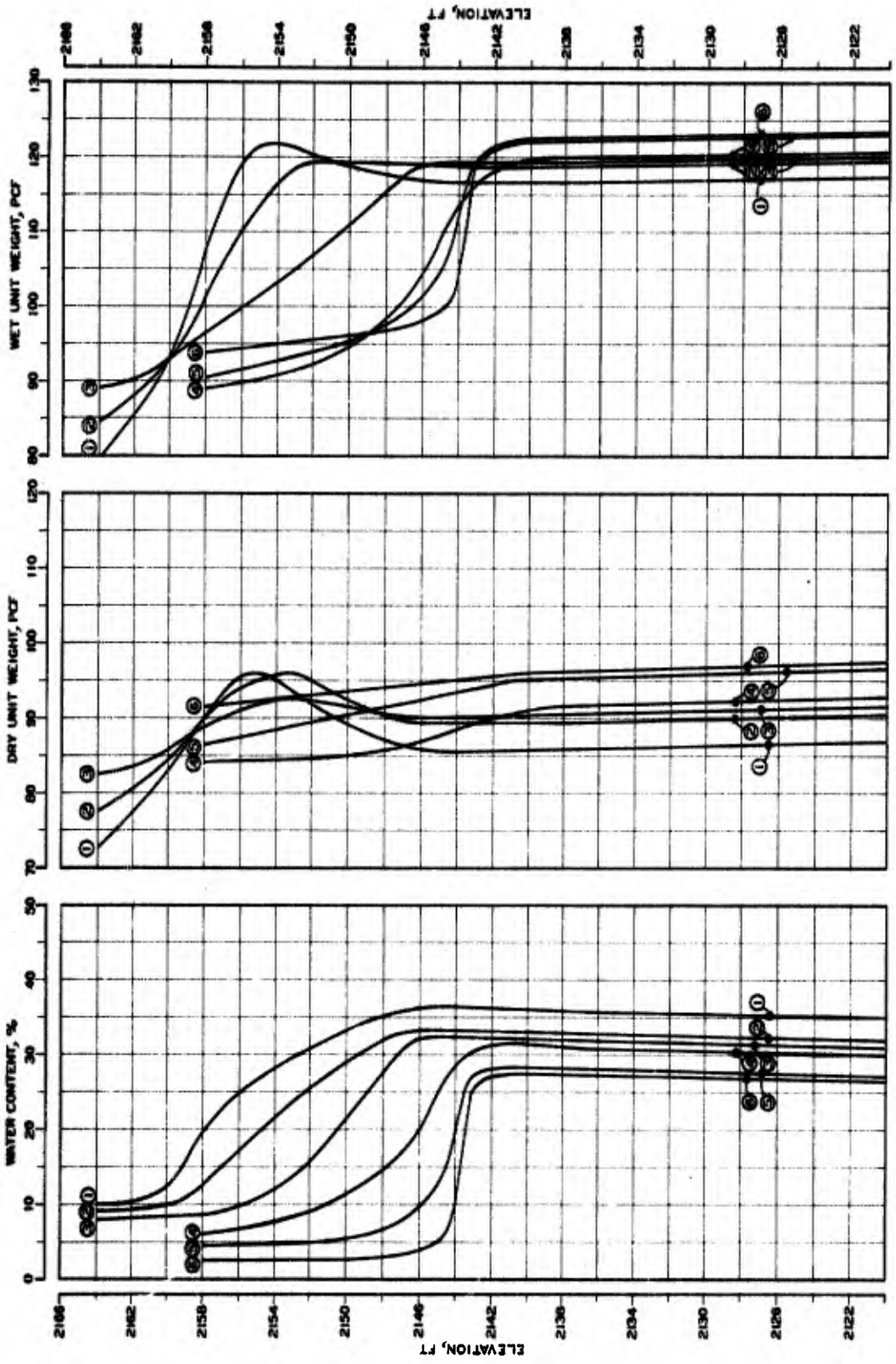

Figure 3.12 Composite plot of recommended water content and density profiles for six soil groups.

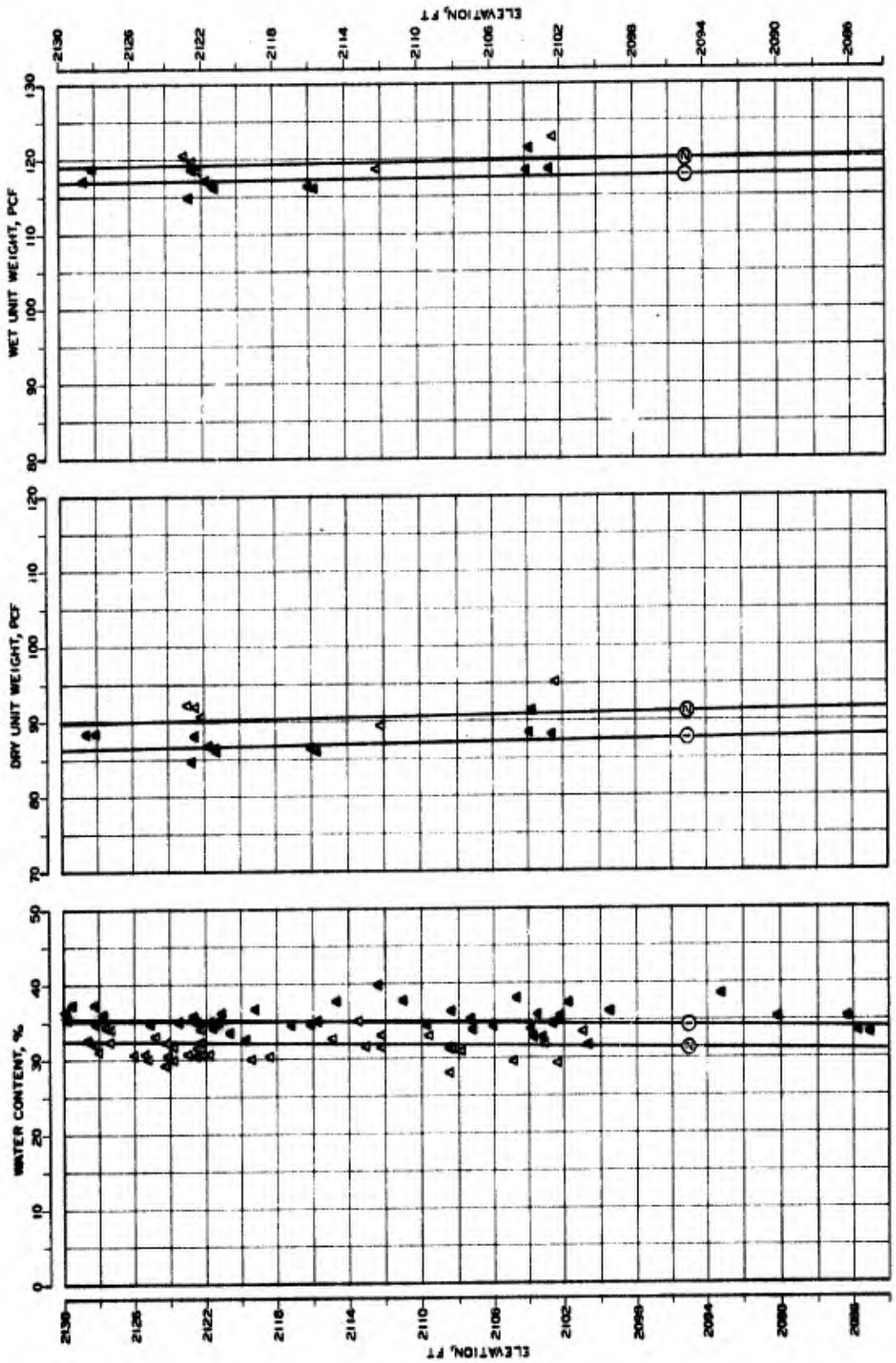

Figure 3.13 Water content, dry unit weight, and wet unit weight profiles for saturated clays below elevation 2130 feet.

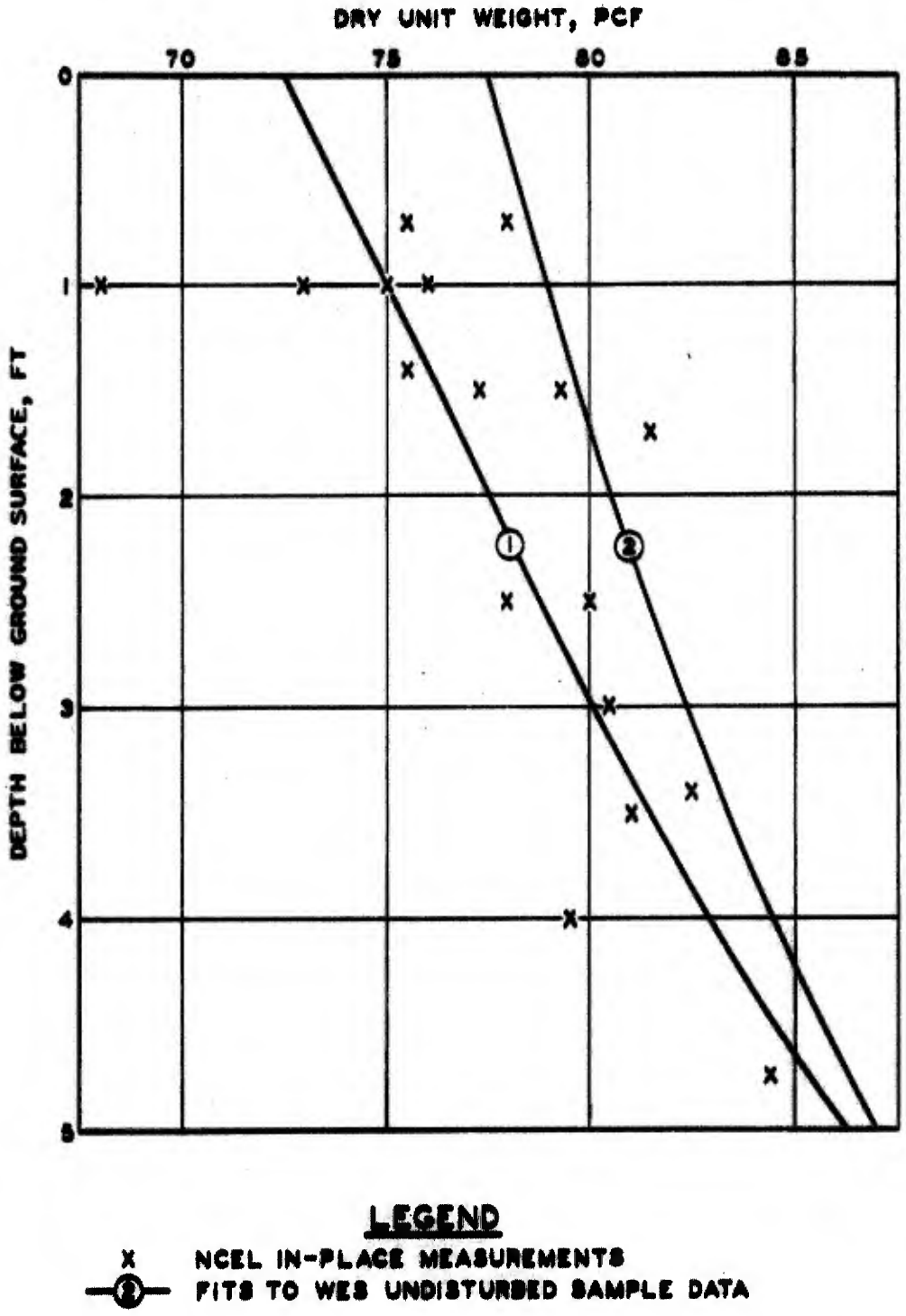

Figure 3.14 Comparison of near-surface laboratory and field dry unit weight measurements.

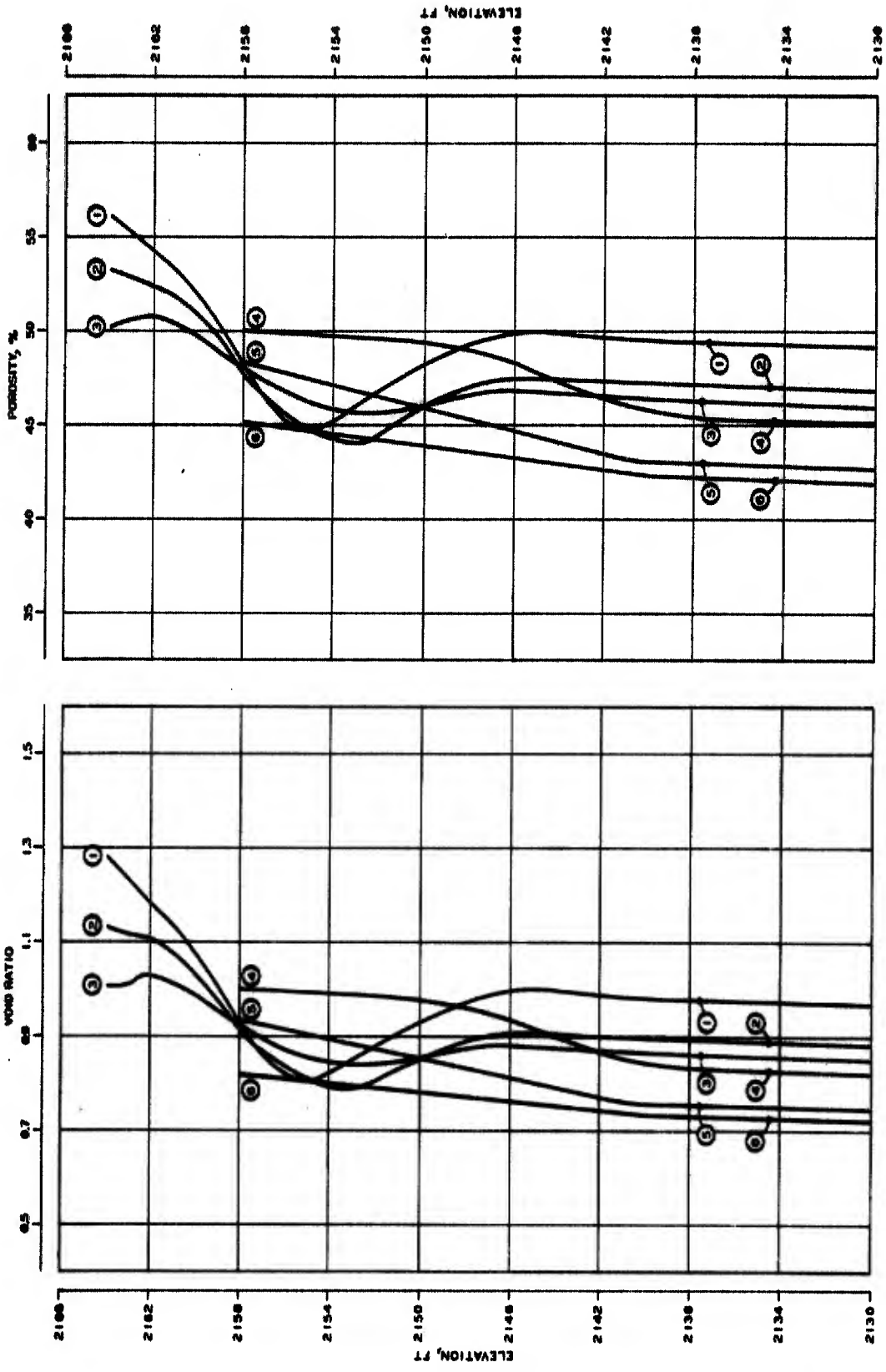

Figure 3.15 Calculated void ratio and porosity profiles for six soil groups.

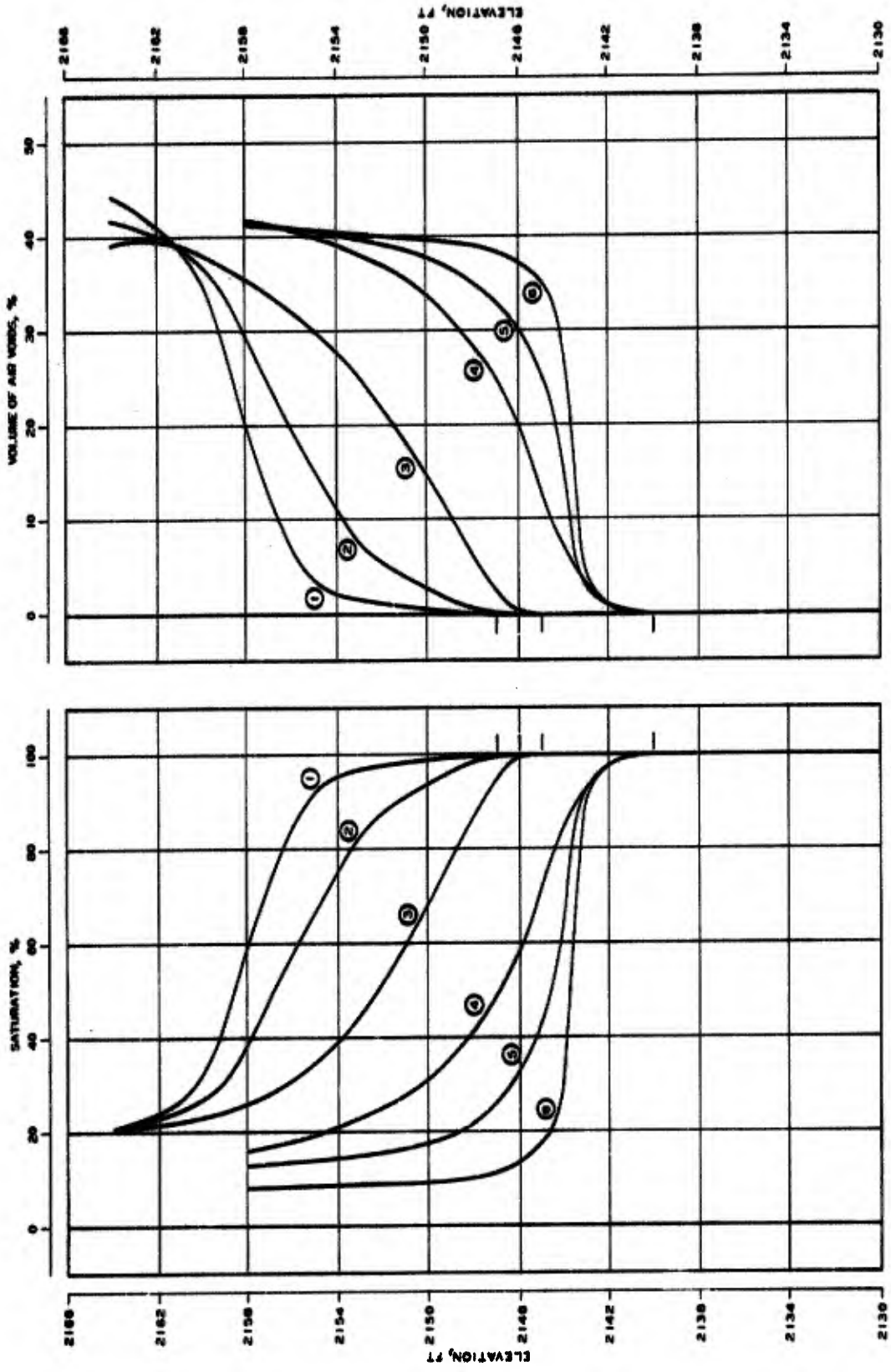

Figure 3.16 Calculated saturation and volume of air voids profiles for six soil groups.

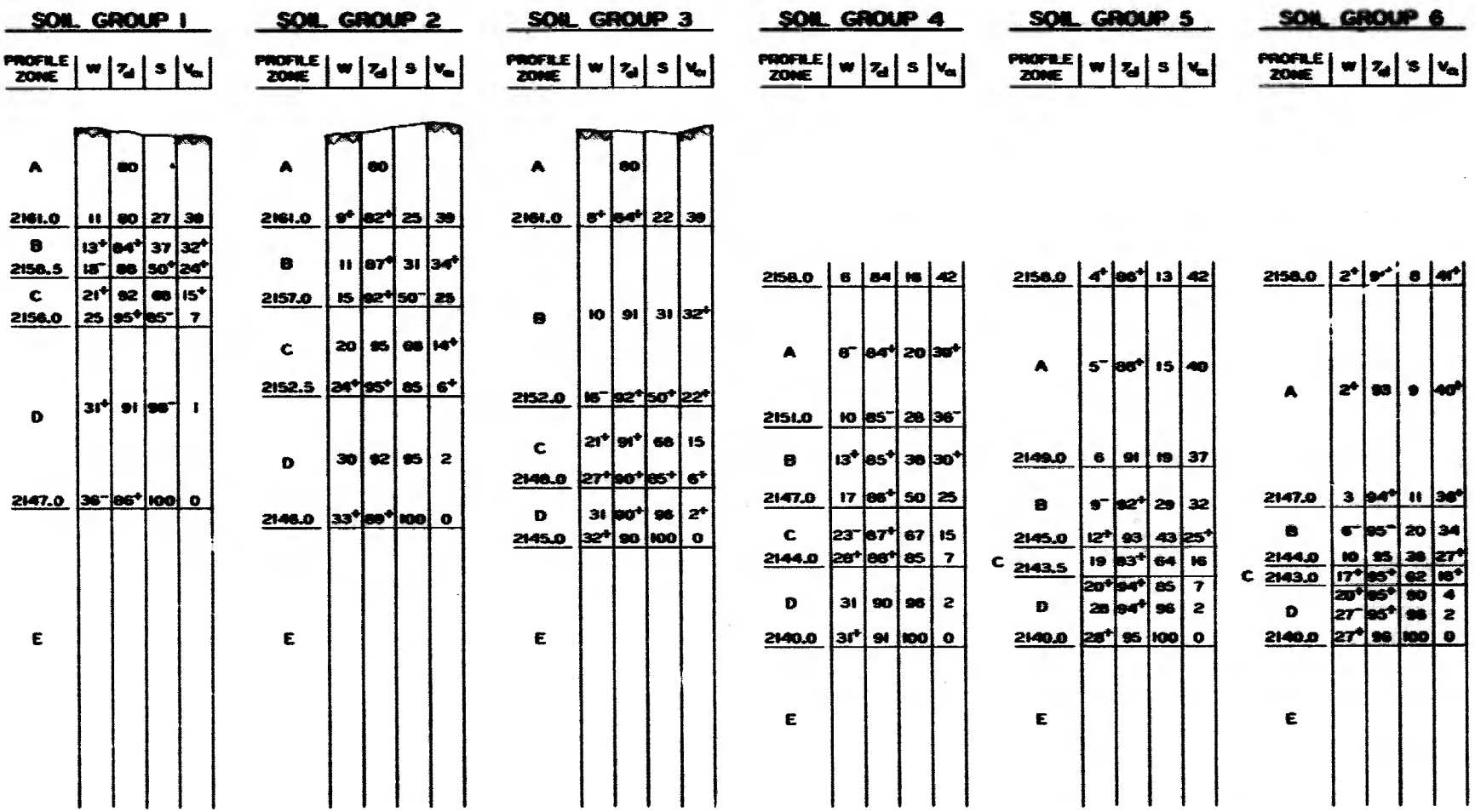

Figure 3.17 Generalized profile zones for six soil groups with boundary elevations and distinguishing values of w, γ_d, S, and V_a.

CHAPTER 4

DYNAMIC COMPRESSIBILITY ANALYSIS

4.1 TYPE OF DATA AVAILABLE

Laboratory measurements of soil compressibility are usually made in a uniaxial strain device,[1] in which a condition of zero radial strain is imposed as a boundary restraint on the specimen while a controlled axial or vertical stress σ_z is applied to it. The response of the specimen is measured in terms of a vertical surface displacement, which is converted to vertical strain ϵ_z by dividing by the original height of the specimen. Compressibility is evaluated as the ratio of a change in vertical strain to a corresponding change in vertical stress. It can also be expressed as a stiffness by the reciprocal term, constrained modulus M, i.e., $\Delta\sigma_z$ divided by $\Delta\epsilon_z$.[2]

Constrained modulus has an especially significant role in soil dynamics due to its direct linkage with the velocity of compression waves in continuous media. In an infinite elastic medium

$$v_p = \sqrt{\frac{M}{\rho}}$$

---

[1] Although frequently referred to in conventional soil mechanics practice as a consolidometer, oedometer, confined compression or one-dimensional compression device, the test boundary conditions are most accurately described from a continuum mechanics viewpoint by the term uniaxial strain (see Eringen, 1967).

[2] M is related to other, more common elastic parameters as follows:

$$M = \lambda + 2\mu = K + \frac{4}{3}G = \frac{(1 - \nu)E}{(1 + \nu)(1 - 2\nu)}$$

Where:

λ and μ = Lamé constants
K = bulk modulus
G = shear modulus
E = Young's modulus
ν = Poisson's ratio

Where:

v_p = compression wave velocity

and

ρ = mass density

As pointed out by Whitman (1970), there is really no such thing as the constrained modulus of a soil, since the stress-strain curves whose slope M defines are by nature extremely nonlinear and hysteretic. This poses no real problem, however, for current wave propagation codes, which readily accept nonlinear hysteretic stress-strain data as direct input (see Radhakrishnan and Rohani, 1971, for example). The stress-strain curves furnished as input to blast-oriented problems though, should reflect the behavior of the soil media when subjected to rapidly applied impulsive loads of high intensity. As a result, extensive efforts have been made to develop laboratory facilities capable of applying loadings of this type to soil specimens confined so as to deform in an undrained state of uniaxial strain.

Schindler (1968), after a critical review of previous developments, designed and evaluated a significantly improved device of the multiple-reflection type which utilized a unique gas-actuated ram loader to subject 10-inch-diameter uniaxial strain specimens to millisecond-scale stress pulses with peak intensities up to 300 psi. Jackson (1968b) describes modifications and extensions made for the express purpose of testing undisturbed field specimens obtained from 5-inch-diameter Shelby tubes at pressures up to 15,000 psi; specimen preparation procedures designed to minimize sample disturbance, including those specifically

devised for use with relatively fragile lacustrine silts and sands, are also described. The equations and assumptions used for analysis of uniaxial strain test data have been outlined by Jackson (1969). A summary of the WES dynamic uniaxial strain equipment, specimen preparation, and test procedures is given in Appendix A.

Although some dynamic compressibility data were obtained by other agencies for analysis of SNOW BALL ground motions (see Davisson and Maynard, 1965; Seknicka and Druebert, 1965; and Hendron, 1965), use of the above described WES facilities to study the dynamic compressibility of soils from the Watching Hill Blast Range began in the summer of 1967 with a limited series of tests on samples obtained in the vicinity of DISTANT PLAIN Event 6 (Jackson and Windham, 1967). Since that time, additional test series have been conducted on samples from DISTANT PLAIN Event 1A, from PRAIRIE FLAT, and several on samples from DIAL PACK, the most recent being completed in May of 1971. Each of these series utilized a single loading device with its control settings fixed so as to subject all specimens in the series to an essentially common stress history. Thus, each of the actual test loading histories shown by the dashed lines in Figure 4.1 are characteristic of a number of other tests.

As a result of the loading history similarities, it was possible to categorize each dynamic test according to loading rate using four somewhat arbitrarily selected stress-time zones; boundaries for the four dynamic loading categories are shown by the solid line segments in Figure 4.1. They incorporate loading rates at various stress levels ranging from more than 1000 psi/msec in Category IV to less than 10 psi/msec in Category I. A number of static tests were also conducted. The time to peak load was on the order of several minutes for most of these tests,

several hours for some, and several days for a couple. These general static loading categories are designated as S, SS, and C, respectively.

In addition to the normal precautions of checking test data sheets and driller's logs for evidence of specimen disturbance or test irregularities, special attention was given the specimen trimmer's original written notes and Polaroid record photographs. This was done in order to be reasonably confident that the trimmings used for classification and index tests matched the specimen tested, or that the specimen slice did not include the transition boundary between two different strata. The sample photographs shown in Figure 1.4 readily illustrate the reasons for these concerns, especially in view of the fact that only a few of the sample tubes were opened and mapped prior to making specimen cuts, as was obviously the case with the Figure 1.4 sample. After this screening, results from 130 uniaxial strain tests were assembled into Figures 4.2 through 4.11 for subsequent analysis. It should be kept in mind, however, that in spite of all precautions, variations from specimen to specimen will exist even though obtained from the most homogenous of natural deposits. Thus, the proposed analysis must, of necessity, be based on considerable individual judgment.

As previously mentioned, the partially saturated region above the water table undoubtedly dominates ground shock phenomena at the Watching Hill site. The attempt to define compressibility in this complicated region will include 125 of the 130 test results; behavior in the saturated region beneath the water table can be adequately depicted with the results from five tests. Each of the σ_z versus ϵ_z relations from these tests is identified in the subsequent figures by a plot number, consecutively listed as 1 through 120 for tests on undisturbed

specimens and R1 through R10 for tests on remolded sands. A table is given with each figure listing the specimen number,[1] elevation, water content, dry unit weight, saturation, percentage of air voids, loading rate category, and soil classification group associated with each of the various stress-strain plots in that figure.

4.2 RESULTS OF TESTS ON CLAYS

Seventy-nine of the tests were conducted on clay specimens classified as belonging either in Soil Group 1, Group 2, or Group 3. In examining the results of these tests, it was observed that, while the composition properties for the three groups vary somewhat with elevation, specimen compressibilities for all three groups were essentially the same if their composition properties were approximately the same; i.e., five sets of stress-strain curves could probably be used to represent 15 profile zone-soil group categories.

Data from less-than-40-percent-saturated specimens with γ_d values less than 83 pcf are plotted for Loading Rates IV and III in Figure 4.2a and for γ_d values greater than 83 pcf in Figure 4.2b. Similar data are given in Figure 4.3 for Loading Rate Categories II and I and in Figure 4.4 for static categories. Considering the fact that these specimens were obtained from the near-surface region of intense weathering, they exhibit remarkably consistent stress-strain behavior and depict distinguishable trends of increasing stiffness with increasing density and increasing loading rate. Their loading behavior is characteristic

---

[1] Test specimens are generally identified by a four-part number, i.e., DPK/2A.2.3, where DPK refers to Operation DIAL PACK, the 2A to undisturbed Boring No. U2A, the 2 to Shelby tube Sample No. 2, and the 3 to Specimen No. 3 trimmed from Sample DPK/2A.2.

of cohesive materials, i.e., initially stiff due to structural bonding, followed by a softening as the bonds are sheared and a subsequent stiffening with further densification. The principal feature of this group of soils is their extremely high air voids percentage (i.e., greater than 30 percent), which results in exceptionally large, nonrecoverable strains under intense loading; this unusually large energy-absorbing characteristic should play a dominant role in Watching Hill blast-induced ground shock phenomena.

Based on the data given in Figure 3.14, a γ_d value of 80 pcf is considered representative of Profile Zone A; based on this dry density, the most representative stress-strain curves for Zone A are believed to be those shown in Figure 4.12. They illustrate behavior under stress levels up to 1000 psi; data are available on which to base extensions to considerably higher levels if necessary. A single unloading curve is given for the static plot which can be translated along the strain axis to define unloading behavior from all of the other plots. The curves indicate loading rate effects in terms of dynamic stress to static stress ratios at equal strains that are relatively insignificant for Rates I and II, but which rapidly increase to surprisingly large values for the faster rates of loading.

Based on an average dry density of 87 to 88 pcf, the most representative stress-strain curves for Profile Zone B are believed to be those shown in Figure 4.13. They are slightly stiffer than the Zone A curves, reflecting their increased density; i.e., Zone B strains at 200 psi are approximately 70 percent of the Zone A strains at this stress level, approximately 75 percent at the 500-psi level and 85 percent at 1000 psi. The pattern of loading rate influence observed for

the Zone A clays is essentially repeated for the Zone B clays.

Zone C contains strata that are 50 to 85 percent saturated with a representative air voids value of about 15 percent. The available data spanning this zone is given in Figures 4.5a, 4.5b, and 4.6a. The representative stress-strain curves deduced from these data are shown in Figure 4.14. Although denser than the Zone B soils, their initial moduli are softer due to decreased intergranular friction and bonding effected by the added moisture. They rapidly stiffen, however, reflecting a characteristic crossover pattern with the Zone B soils as strains approach air void closure. The previously observed pattern of loading rate influence is generally maintained in Zone C, but the effect appears to be diminishing quantitatively, especially on the initial moduli values.

Zone D contains strata that are 85 to 100 percent saturated with a representative air voids value of only 2 percent. Data for this regime are given in Figures 4.6a and 4.6b. The dominant role played by air void content on the response of these specimens is readily apparent; with the lone exception of Plot No. 55, there is excellent agreement between the "locking" strains exhibited during the compression tests and the theoretical values of V_a calculated from other specimen data. The stress-strain curves selected to represent Zone D are shown in Figure 4.15a. Rather than continue to soften with increasing saturation, the initial moduli are roughly twice as stiff as those for Zone C; presumably this is due to added resistance now being provided by the pore water. The previously noted trend of diminishing influence of loading rate with increasing saturation continues, however.

Entry into the zone of 100 percent saturation, Zone E, occurs

between elevation 2147 and 2145. Data available between this latter elevation and the water table at about elevation 2142 are given in Figure 4.7a; data from five tests conducted on specimens obtained from beneath the water table are given in Figure 4.7b. Both the calculated V_a values and the stress-strain data indicate small amounts of air or gas in the specimens. Although most of it can probably be attributed to sampling-induced processes, it is also quite unlikely that any natural soil is theoretically pure in terms of air voids, at least until subjected to some pressure. In any event, if lack of a measurable hysteretic effect is any indicator, then the data above a stress of 200 psi in Figure 4.7b would certainly qualify as representing fully saturated specimens. The maximum moduli calculated from the slopes of Plots 75 through 79 are 495,000, 360,000, 640,000, 680,000, and 435,000 psi, respectively, for an average bulk modulus of 522,000 psi. The soils obtained below the water table were predominately Group 1 and Group 2; using the void ratio values at elevation 2142 shown for these soils in Figure 3.15, a bulk modulus for water of 300,000 psi, and a bulk modulus for quartz of 4.45×10^6 psi, the bulk modulus of the Watching Hill mixture is calculated as 577,000 psi with the equation given by Richart, Hall, and Woods (1970). If a bulk modulus of 1.8×10^6 psi is assumed for the clay minerals instead of the quartz-related value of 4.45×10^6 psi, a mixture modulus of 525,000 psi is calculated, which is exceptionally close to the average measured value of 522,000 psi.

The stress-strain curve recommended for use with all soil groups and all loading rates is given in Figure 4.15b. This curve uses as an initial modulus the stiffest initial value measured during any test, i.e., 150,000 psi. The modulus subsequently increases to a value of 550,000 psi at a vertical stress of 200 psi, reflecting a slight air

void content of 0.05 percent. For those who prefer to hypothesize a V_a value of zero, the dashed line through the origin should suffice.

4.3 RESULTS OF TESTS ON CLAYEY SILTS

Twenty-nine tests were conducted on clayey silt specimens from Group 4. Profile Zone A was defined as the region between elevation 2158 and 2151; the most representative dry density for this zone is between 84 and 85 pcf, but as can be seen in Figure 3.9, there is considerable scatter in the γ_d data . Results from all tests on specimens with γ_d values less than 85 pcf are plotted in Figure 4.8a; those with γ_d values greater than 85 pcf are plotted in Figure 4.8b. Comparison of these two figures reveals the expected trend of increasing stiffness with increasing density, but since the average γ_d value for all of these tests was 85.2 pcf, they were combined to establish representative curves for the zone.

Profile Zone B was defined as the region between elevation 2151 and 2147 with a representative γ_d value just a little above 85 pcf. In contrast to the data from Zone A, densities from the test specimens obtained from Zone B were very tightly grouped with an average value of 84.9 pcf; test results are plotted in Figure 4.9a. The set of curves selected to represent this zone were only marginally different from those selected for Zone A. This is really not surprising in view of the fact that both zones have essentially the same representative γ_d value and representative saturations less than 40 percent. It is, nonetheless, an opportunity to further reduce the number of sets of stress-strain curves required to characterize site behavior; the set selected to represent both Zones A and B is given in Figure 4.16.

The influence of loading rate is even more pronounced in these dry silt zones than in the comparable zones of dry clay. The silt series even included two week-long tests in static Loading Rate Category C, which adds a further dimension to the overall results. Finding data to corroborate specialized test results on undisturbed specimens from an isolated location, while usually quite fortuitous, nevertheless is always welcome. Hendron and Davisson (1964) report the results of static and dynamic uniaxial strain tests on silt specimens obtained from an undrained desert basin within the Nevada Test Site known as Frenchman Flat. The water contents, dry densities, and saturations of their test specimens were almost in perfect agreement with those from Watching Hill Zones A and B. Static loading rates were analogous to those of Category S; their two dynamic loading rates, as evidenced by comparing the typical examples presented with those in Figure 4.1, are analogous to Categories II and IV. The playa silts of Frenchman Flat have a cemented structure which precludes a valid comparison with the Watching Hill silts at low stress levels, but Hendron and Davisson note that this natural structure has generally been destroyed after application of 1000 psi, so perhaps a comparison at that level is meaningful. In this stress regime, their data indicate a band of static-to-dynamic Rate II strain ratios ranging from 1.00 to 1.40, or an average ratio of 1.20. Ratios of static strains at 1000 psi to dynamic Rate IV strains at this stress level for the playa silts fall within a band ranging from 1.35 to 2.35 with an average value of 1.85. Watching Hill silt strains at 1000 psi in Figure 4.16 are 18.7, 15.3, and 10.4 percent for curves representing Loading Categories S, II, and IV, respectively, giving a II/S ratio of 1.22 and a IV/S ratio of 1.80.

Profile Zone C extends over a narrow reach between elevation 2147 and 2144 within which saturations rapidly increase from 50 to 85 percent and the representative air void value is 15 percent. Data for this zone is plotted in Figure 4.9b; as observed for the clay data, there is excellent correlation between strain "lock-up" and calculated V_a values. The set of stress-strain curves believed to best represent behavior in this zone are given in Figure 4.17. Even though the specimens were slightly more dense than those in Zones A and B, initial moduli, like those for the counterpart Zone C clays, were softer. But, as expected, they rapidly stiffen prior to reaching the 15 percent strain effective limit.

Profile Zone D ranges from elevation 2144 to 2140. No silt specimens were recovered from this zone, but since the dominant feature is the low average air void content, i.e., only 2 percent, the stress-strain curves recommended for Zone C clay strata in Figure 4.15a should also suffice for any clayey silts found between the above elevations. As already mentioned, response in the saturated Zone E regime is defined by the curve in Figure 4.15b.

4.4 RESULTS OF TESTS ON SILTY SANDS

Obtaining undisturbed specimens of sand for laboratory testing is seldom a very rewarding task, and the Watching Hill site investigation was no exception as only 12 such specimens were obtained. Not even all of these were strictly applicable to the problem at hand, as evidenced by those plotted in Figure 4.10a. These specimens appear to be representative of a borderline classification; i.e., while their gradation (as noted in the percentage passing the 200 sieve column added to the descriptive tables for the sand tests) indicates a Group 5 silty sand,

their dry densities indicate a Group 4 clayey silt based on their elevation and their water contents fall almost precisely in between. Nevertheless, they give some information on possible loading rate effects as do Plot Nos. 112 and 113 in Figure 4.10b. Comparison of Plot 113 with Plot 114 in the same figure indicates an influence of grain-size distribution while the data in Figure 4.10c gives information on the effect of increased saturation.

By supplementing the undisturbed data with results from remolded tests, other factors can be given quantitative consideration. For example, comparing Plot 119 with Plots R1 and R2 in Figure 4.11a gives some information on the effect of natural structure on Group 6 sands while R1 and R2 with R3 gives information on loading rate effects in the same materials. Comparing R3 with R4 through R8 indicates the magnitude of dry density and grain-size effects. Loading rate effects in a Group 5 sand are evidenced in the R9 and R10 plots of Figure 4.11b and natural structure effects in an R10 versus 120 comparison.

By analyzing the above results, quantitative conclusions could be made regarding the effects of natural structure, as indicated by undisturbed versus remolded response, and the effects of loading rate on the stress-strain behavior of the two sand groups. Natural structure effects are shown in Figure 4.18a. The shaded zone defines the quantitative effect, in terms of a differential in strain as a function of stress level, between remolded R and undisturbed U tests. The actual positions of the R curves are not intended to define stress-strain within any particular profile zone of the two classification groups; rather they are intended as reference lines from which the relative strain for a compatible undisturbed specimen can be estimated.

The bands in Figure 4.18a readily depict the fact that compressibility as well as natural structure effects decrease as the amount of fines in the specimens decrease, i.e., Soil Group 5 was defined as having between 30 and 70 percent of its particles pass the 200 sieve, while less than 30 percent pass for Group 6 sands.

Loading rate effects are shown in Figure 4.18b where the shaded bands define the quantitative differential expected between static tests of rate S and dynamic tests with loading rates in Category IV. A decreasing influence of loading rate can be noted with a decreasing percentage of silt- and clay-size particles. The bands in this figure, as well as those in Figure 4.18a, were each derived from two compatible sets of test data; good agreement was observed between the two sets in all cases. While two of anything can hardly be considered as a basis for statistical confidence, it was nonetheless quite comforting not to contend with diverse trends.

Profile Zone A for Group 5 ranges from elevation 2158 down to elevation 2149 with a dry density average of about 88 to 89 pcf. Based on the data given in Table 3.5, Group 5 soils are composed, on the average, of 50 percent minus-200 particles. Based on the data given in Figure 4.11a, the estimated remolded static stress-strain curve for the above density and gradation is shown by the dashed line in Figure 4.19a. The natural structure effects shown in Figure 4.18a were superimposed to obtain the S-designated solid line estimated to be representative of in situ static response. Loading rate effects from Figure 4.18b were then superimposed on this curve to establish the upper bound for the recommended set of dynamic curves. Similar rationale was used to devise the Group 5-Zone B recommendations in Figure 4.19b,

those for Group 6-Zone A in Figure 4.20a, and for Group 6-Zone B in Figure 4.20b.

As defined in Figure 3.17, the air void content at the bottom boundary for Group 5-Zone C is 7 percent. Plot No. 116, albeit from Group 6, was determined from a sand specimen with 7.7 percent air voids tested at Loading Rate IV. This plot, with the exception of a lower initial modulus, roughly corresponds to the Category IV curve for Group 5-Zone B. The bottom boundary for Group 6-Zone C is listed as 4 percent; Plot 115 was determined from a Group 6 sand specimen with 3.6 percent air voids. This Category IV test roughly corresponds, with the same initial modulus exception as before, to the Category IV curve for Group 6-Zone B. Since the average Zone C air voids value of 16 percent well exceeds the maximum strain predicted at 1000 psi in Zone B with either sand type, it is believed that the Zone B curve can also be used to represent the behavior of any stratums found in Sand Zones C, i.e., Figure 4.19b for Group 5-Zone C and Figure 4.20b for Group 6-Zone C.

As previously discussed, Zone D behavior is governed almost exclusively by the low air void percentage, and as with the silts, it is believed that the clay-based Zone D curves in Figure 4.15a will adequately depict sand behavior in this regime. Saturated Zone E behavior for all groups was previously given in Figure 4.15b. Completion of these sand response definitions also completes the analysis as intended by the purpose set forth in Section 1.2. Presumably now, for any given location at the Watching Hill Blast Range for which a field boring log with conventional soil classification and index data exists, the soils can be grouped according to the criteria given in Section 3.2, an

idealized profile suitable for ground shock calculations established using the zoning outlined in Figure 3.17, and stress-strain curves selected from Figures 4.12 through 4.20 to represent the in situ response of each zone in the profile to transient uniaxial strain loading and unloading. An illustration of the application of this procedure will be given in the concluding chapter.

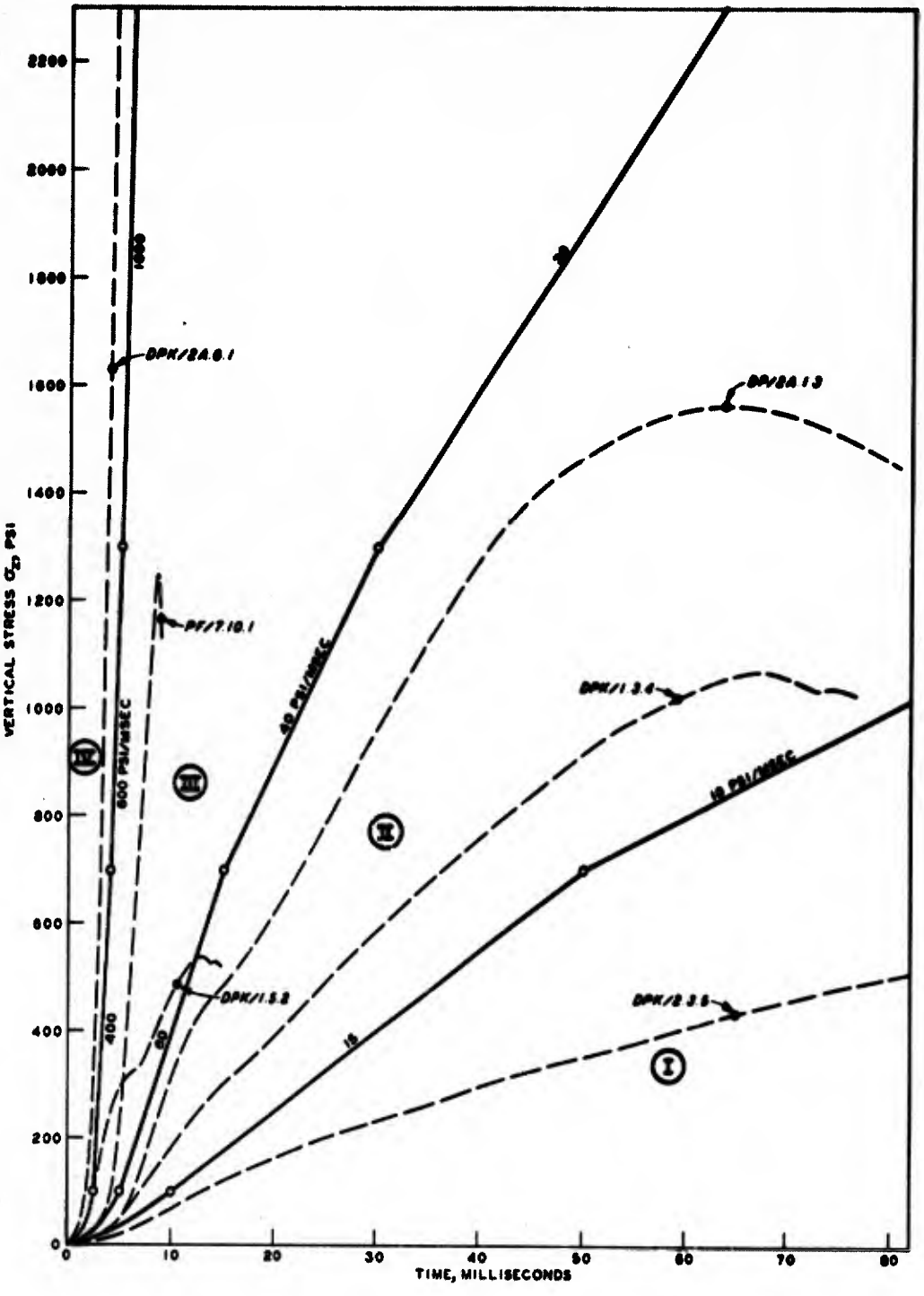

Figure 4.1 Stress-time zones for four dynamic loading categories.

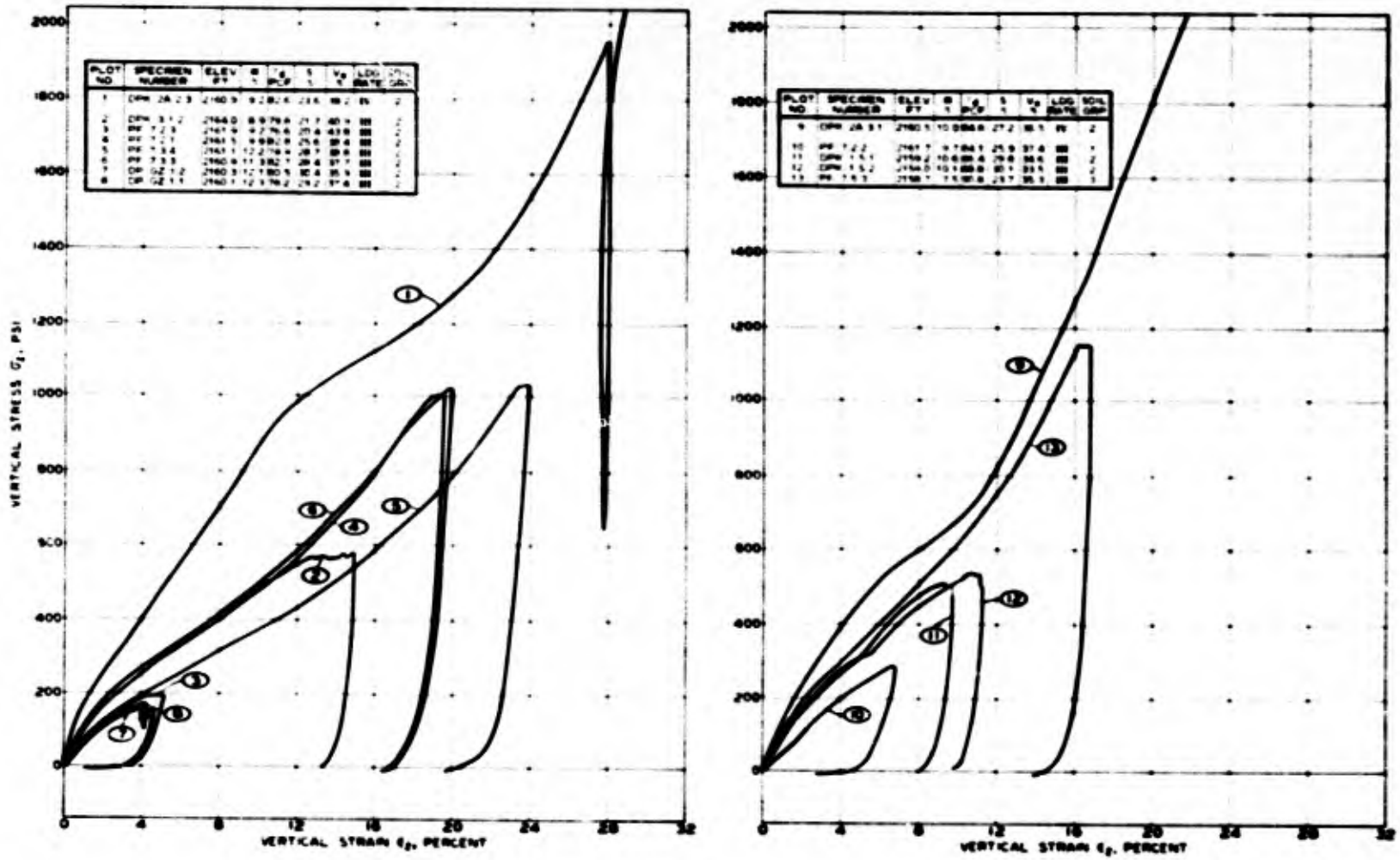

a. $\gamma_d < 83$ pcf.

b. $\gamma_d > 83$ pcf.

Figure 4.2 Uniaxial strain results for tests on clays--S < 40 percent, Loading Rate Categories IV and III.

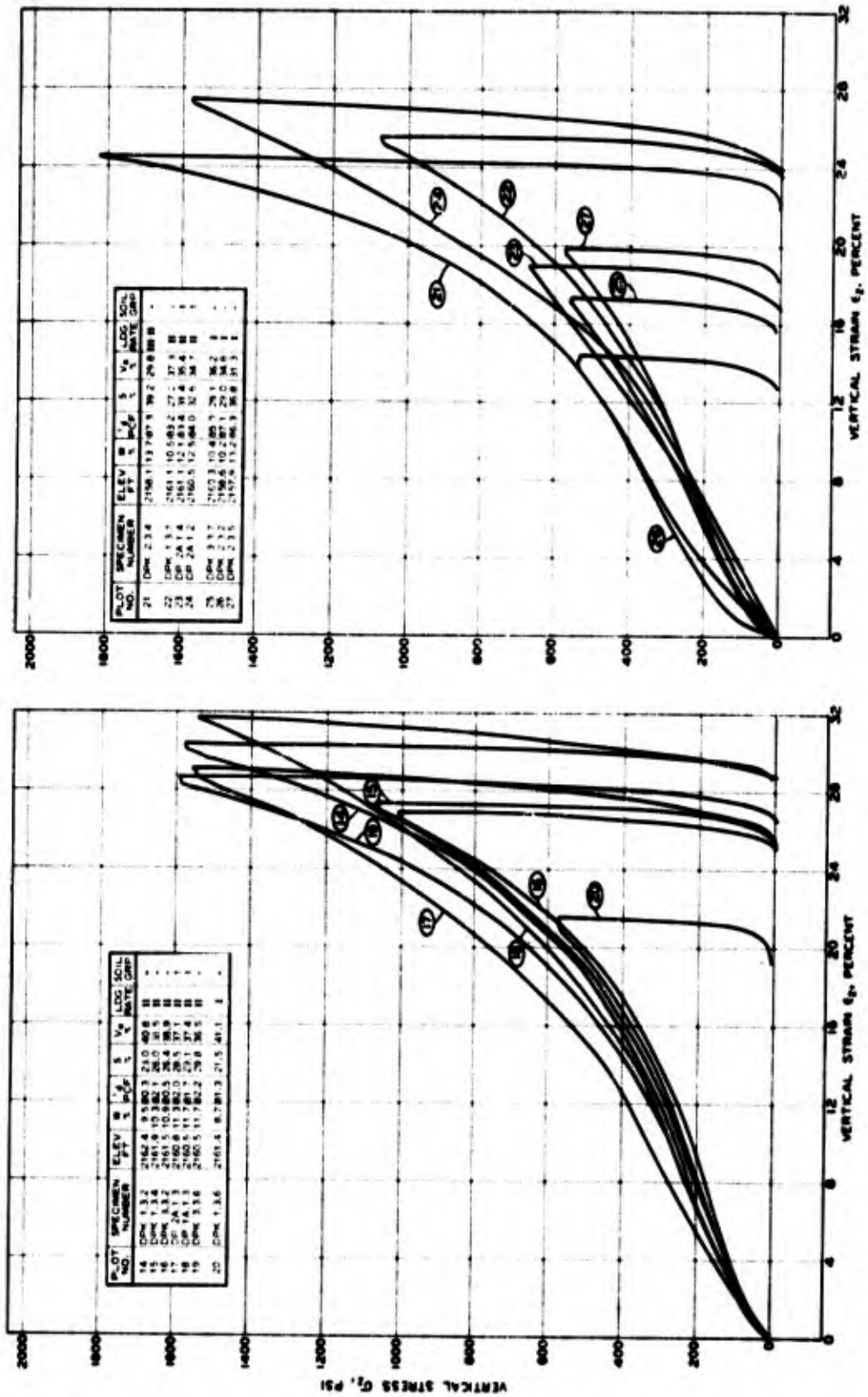

a. $\gamma_d < 83$ pcf.

b. $\gamma_d > 83$ pcf.

Figure 4.3 Uniaxial strain results for tests on clays--S < 40 percent, Loading Rate Categories II and I.

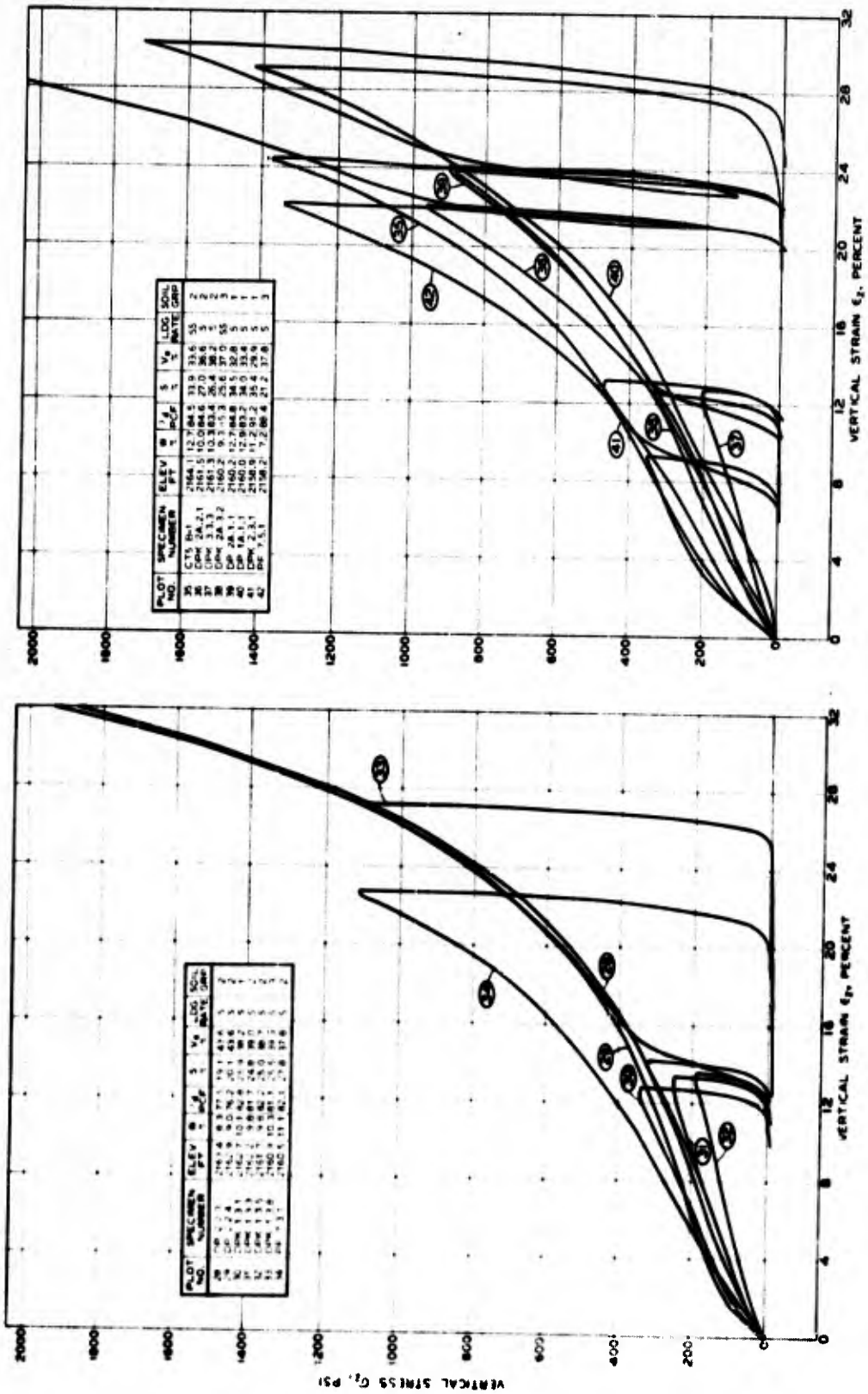

a. $\gamma_d < 83$ pcf.

b. $\gamma_d > 83$ pcf.

Figure 4.4 Uniaxial strain results for tests on clays--S < 40 percent, Loading Rate Categories S and SS.

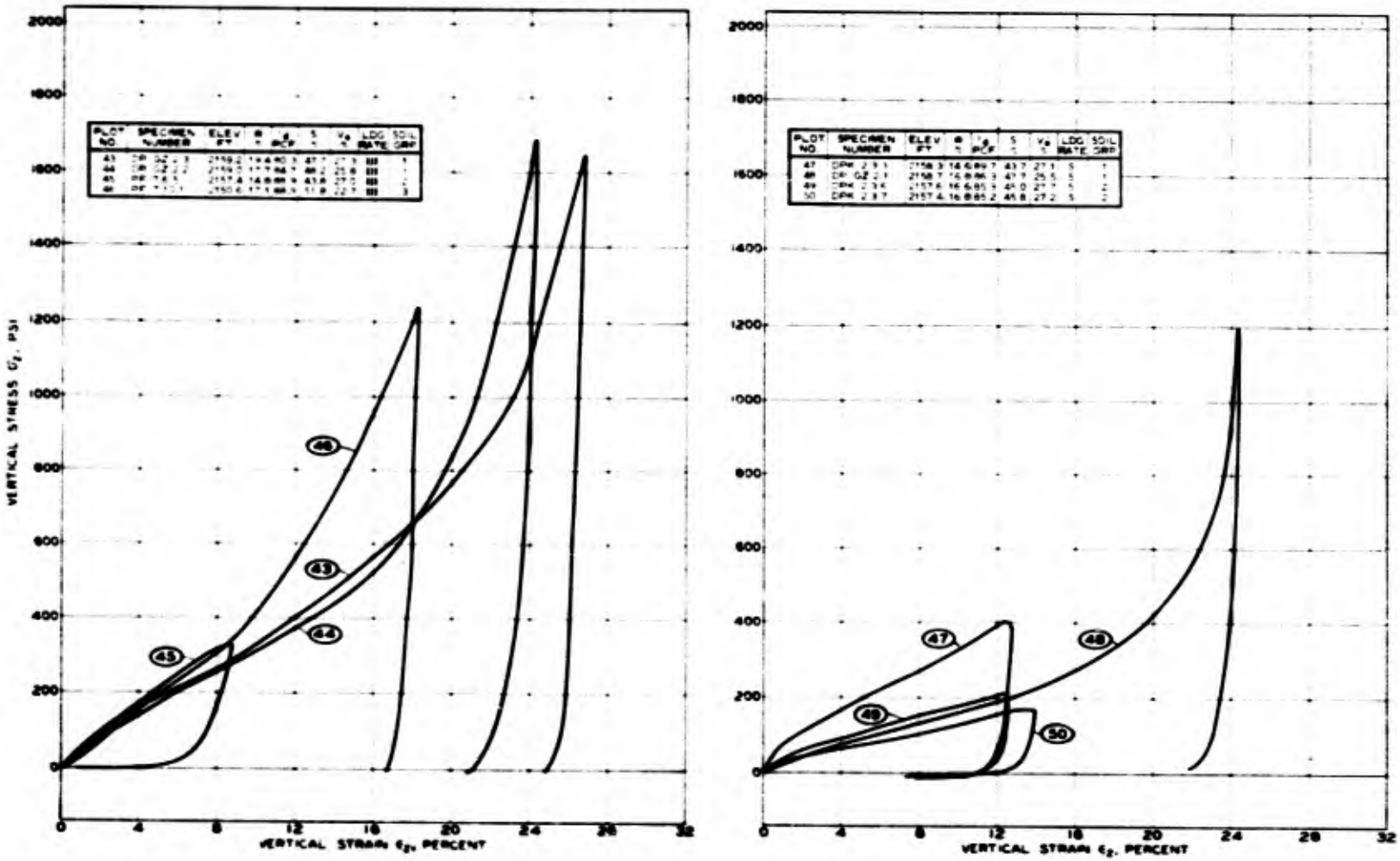

a. Loading Rate Category III.

b. Loading Rate Category S.

Figure 4.5 Uniaxial strain results for tests on clays--40 percent < S < 85 percent.

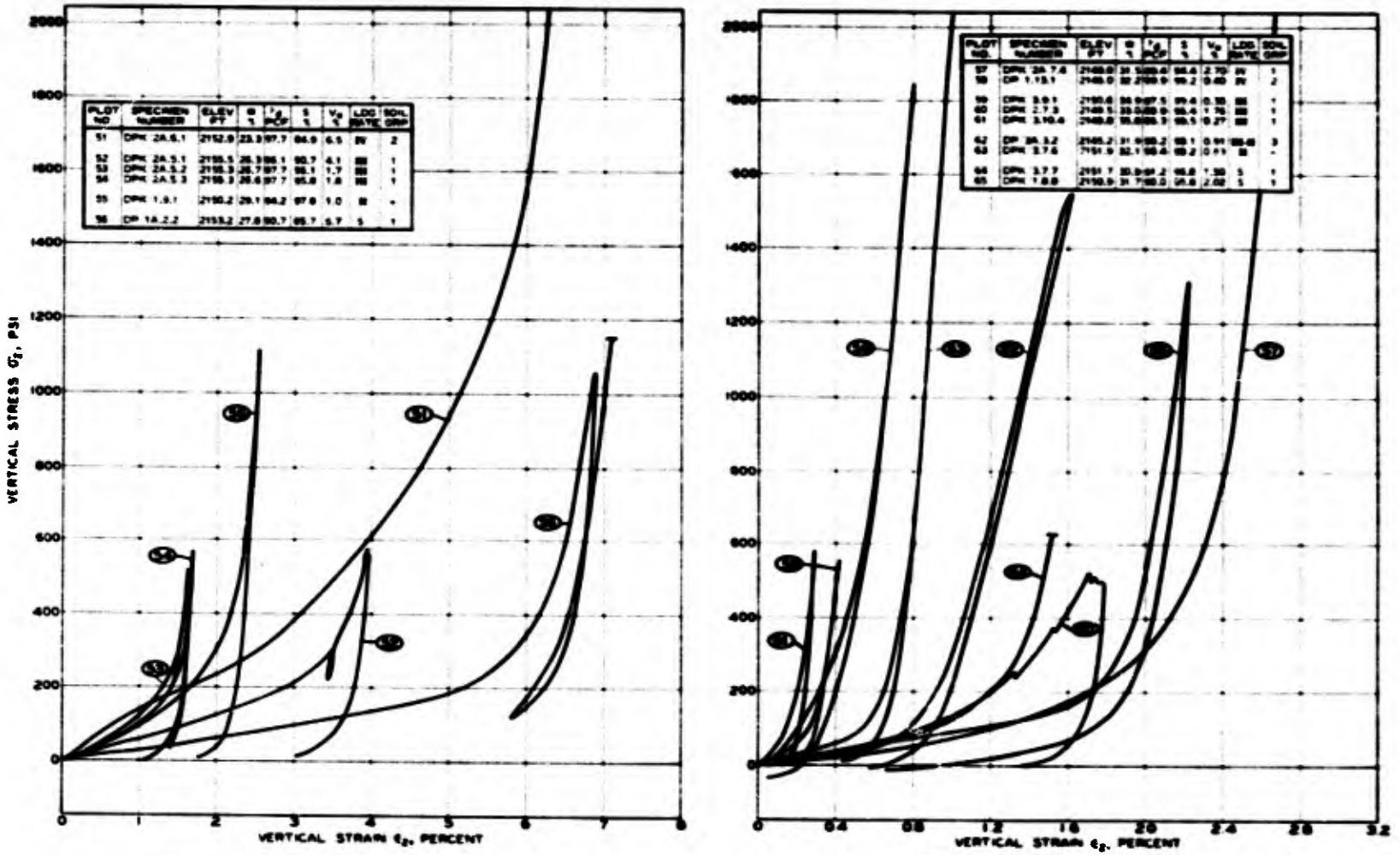

a. w < 30 percent.

b. w > 30 percent.

Figure 4.6 Uniaxial strain results for tests on clays--85 percent < S < 100 percent.

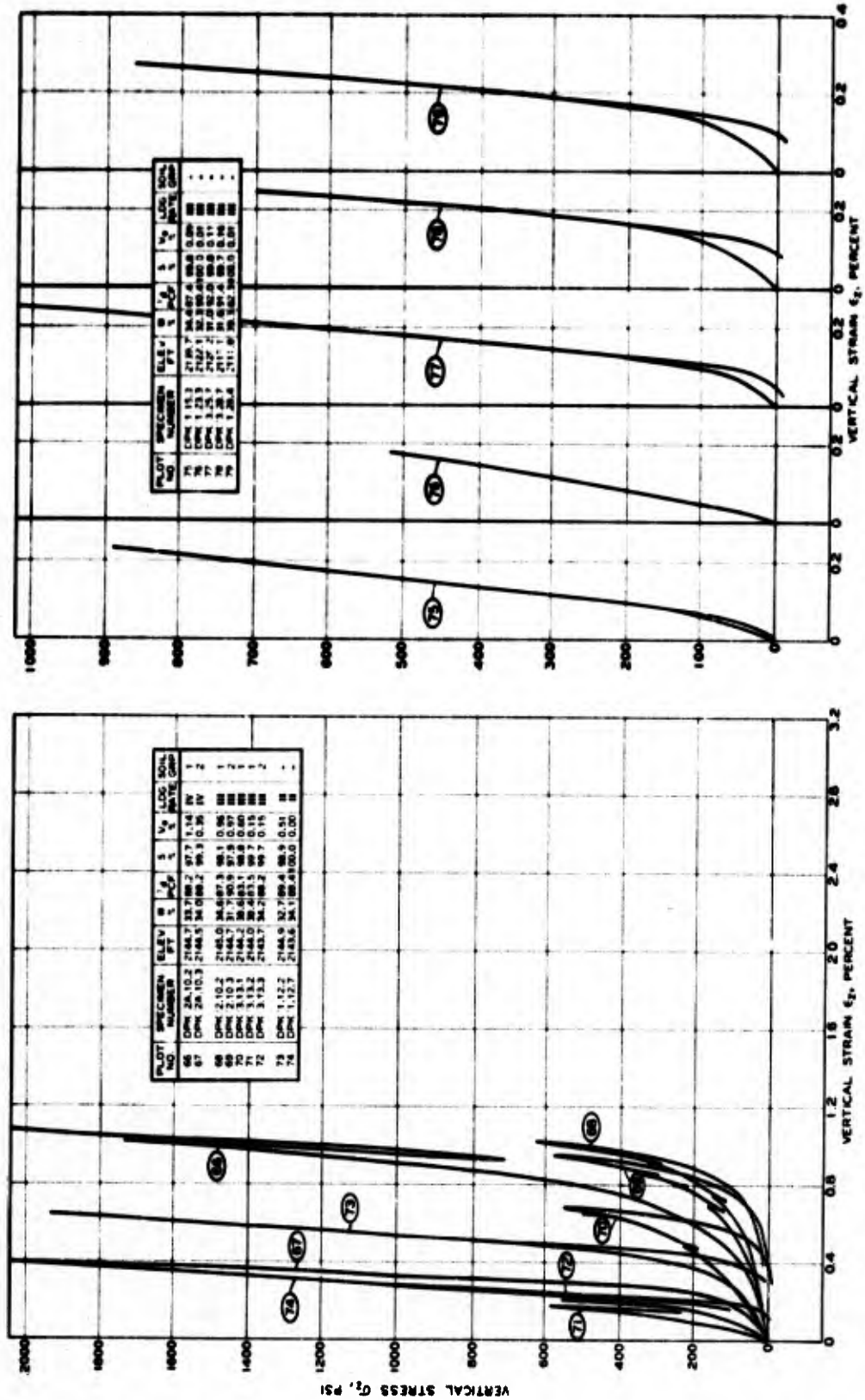

a. 2142 feet < elevation < 2145 feet.

b. Elevation < 2142 feet.

Figure 4.7 Uniaxial strain results for tests on clays from zone of 100 percent saturation.

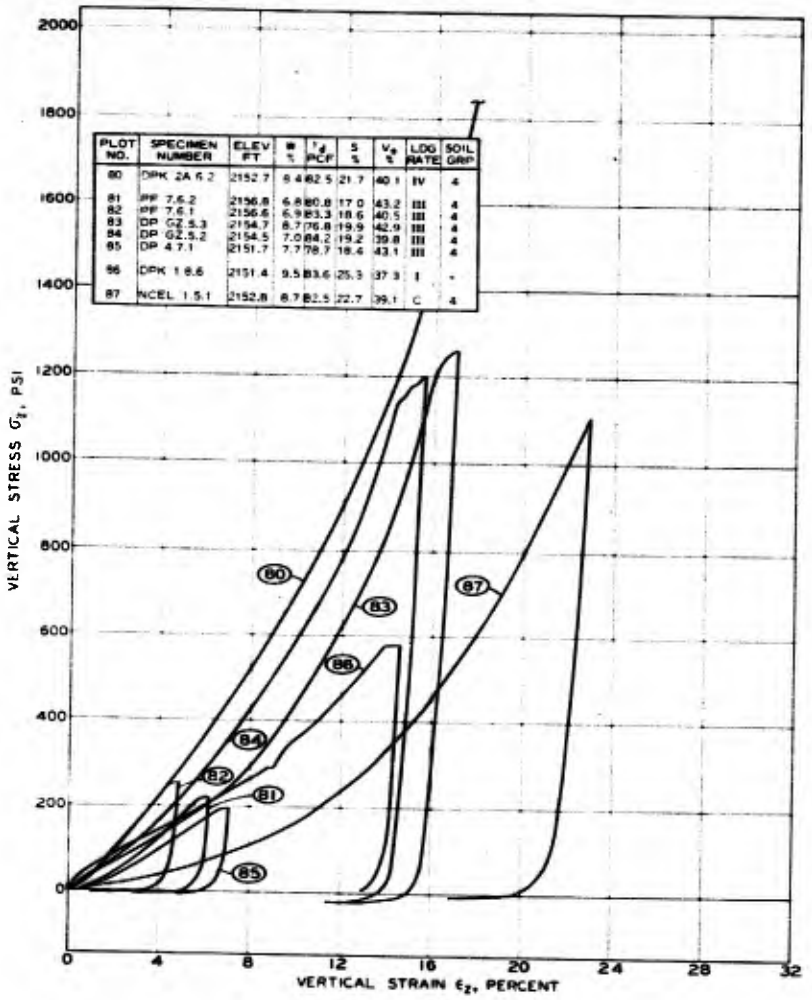

a. $\gamma_d < 85$ pcf.

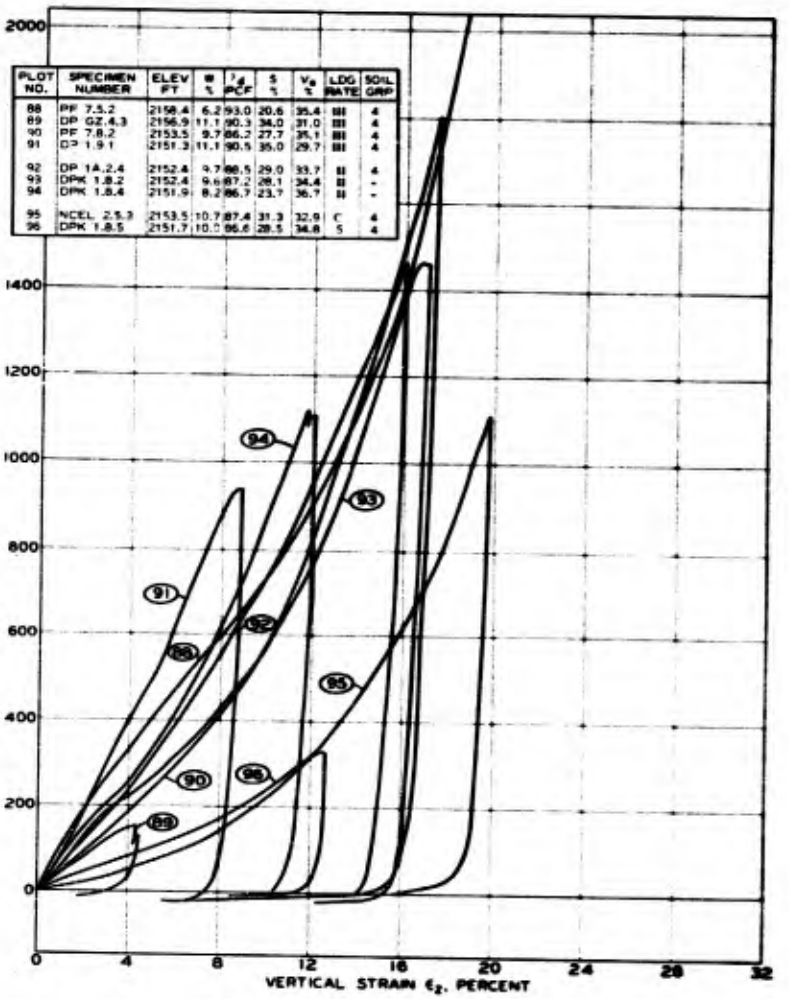

b. $\gamma_d > 85$ pcf.

Figure 4.8 Uniaxial strain results for tests on clayey silts above elevation 2151 feet.

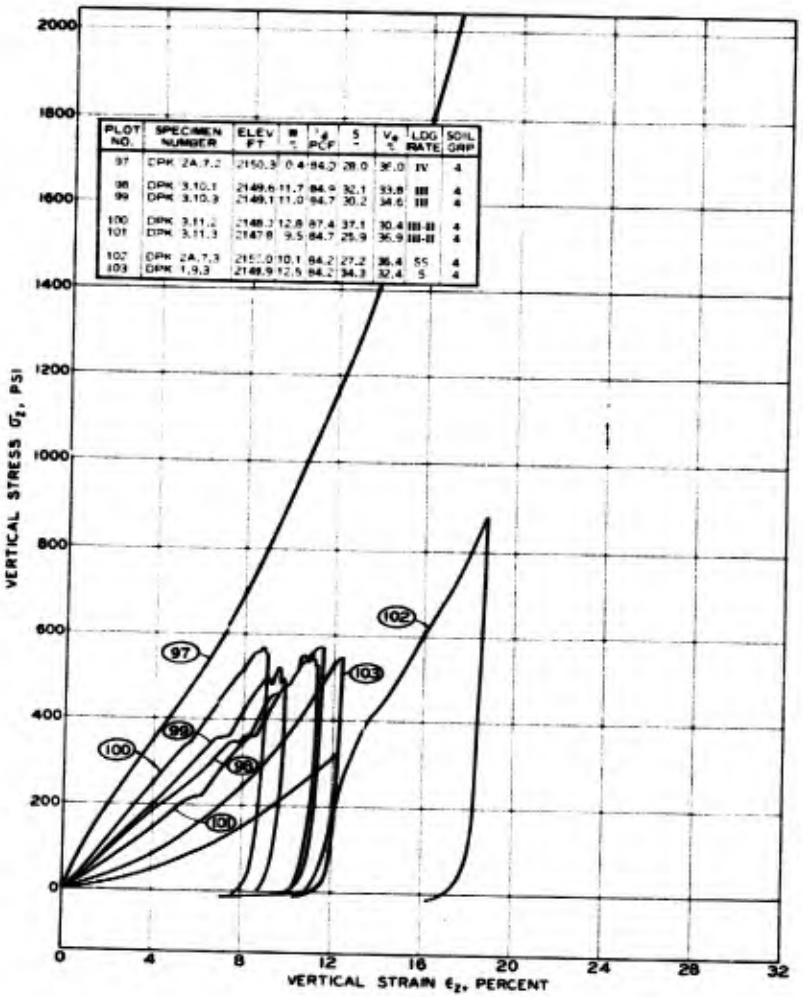

a. 2147 feet < elevation < 2151 feet.

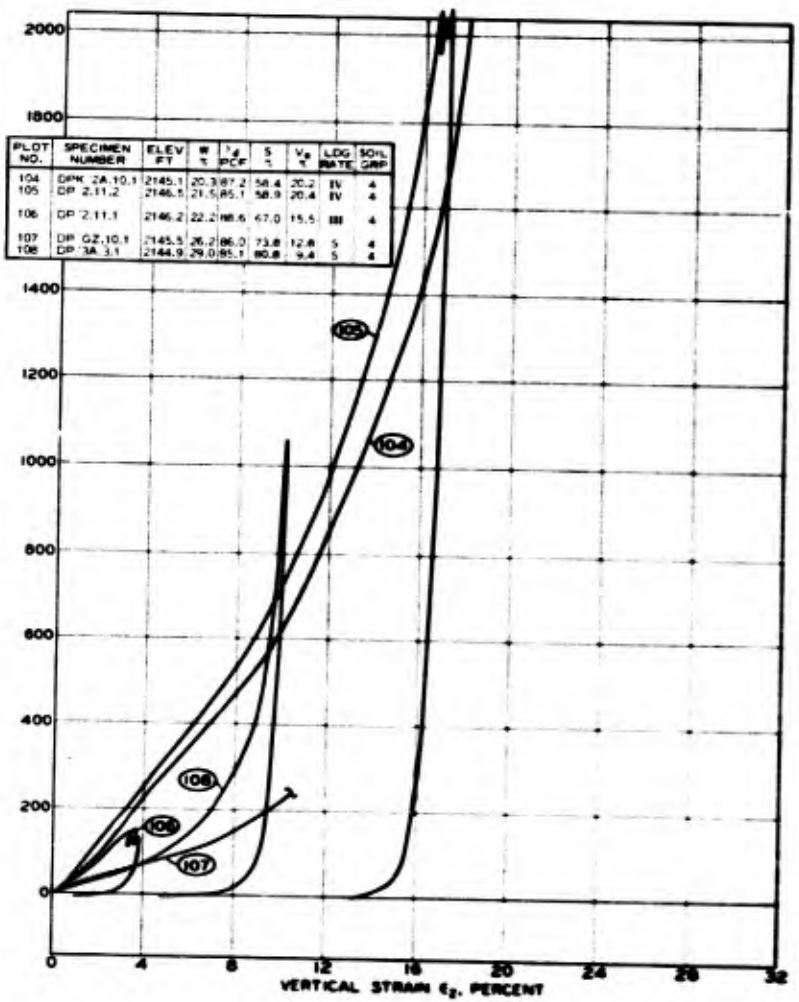

b. 2144 feet < elevation < 2147 feet.

Figure 4.9 Uniaxial strain results for tests on clayey silts between elevation 2151 feet and 2144 feet.

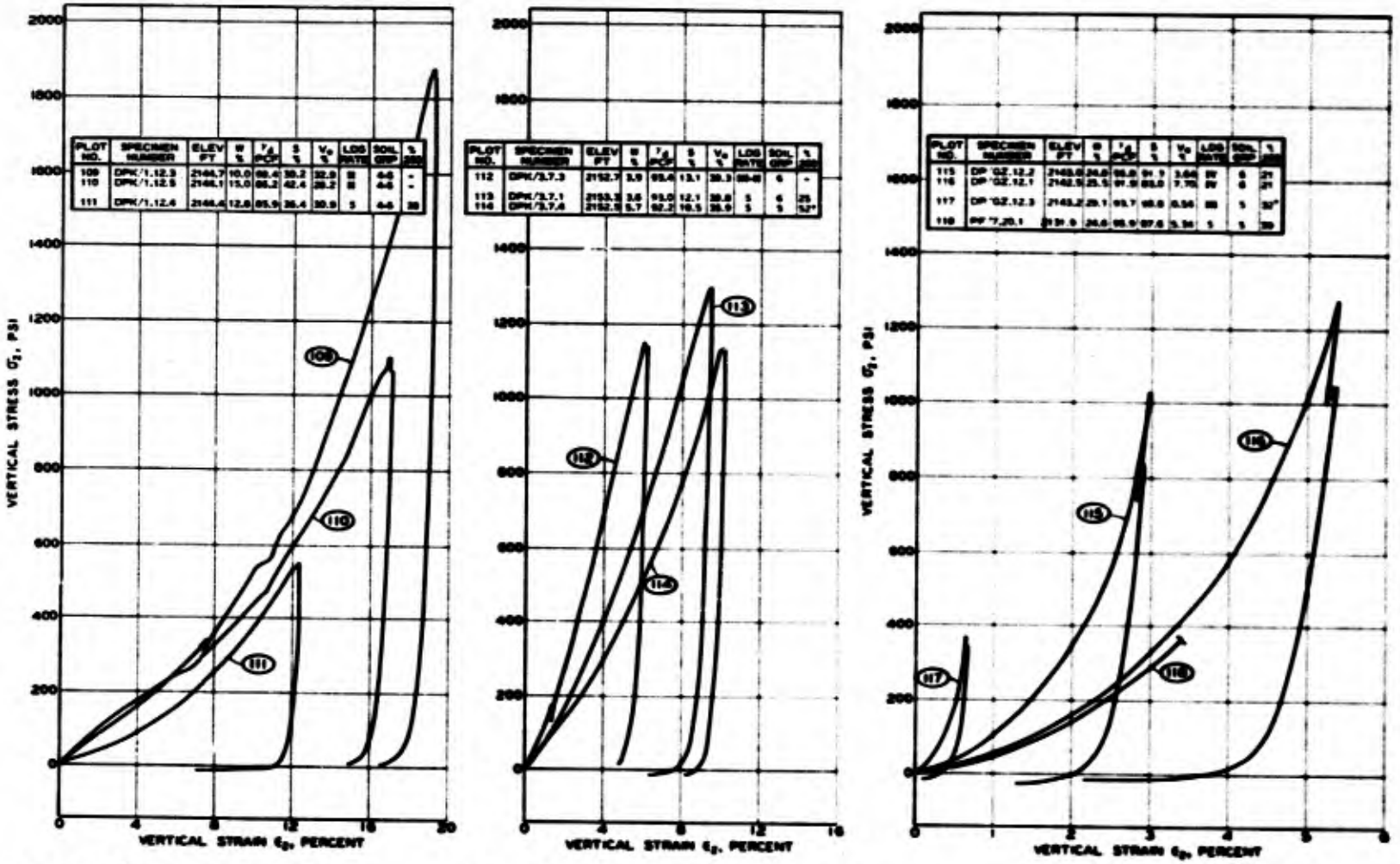

a. Loading rate effects.

b. Loading rate and grain-size effects.

c. Saturation effects.

Figure 4.10 Uniaxial strain results for tests on undisturbed specimens of silty sand.

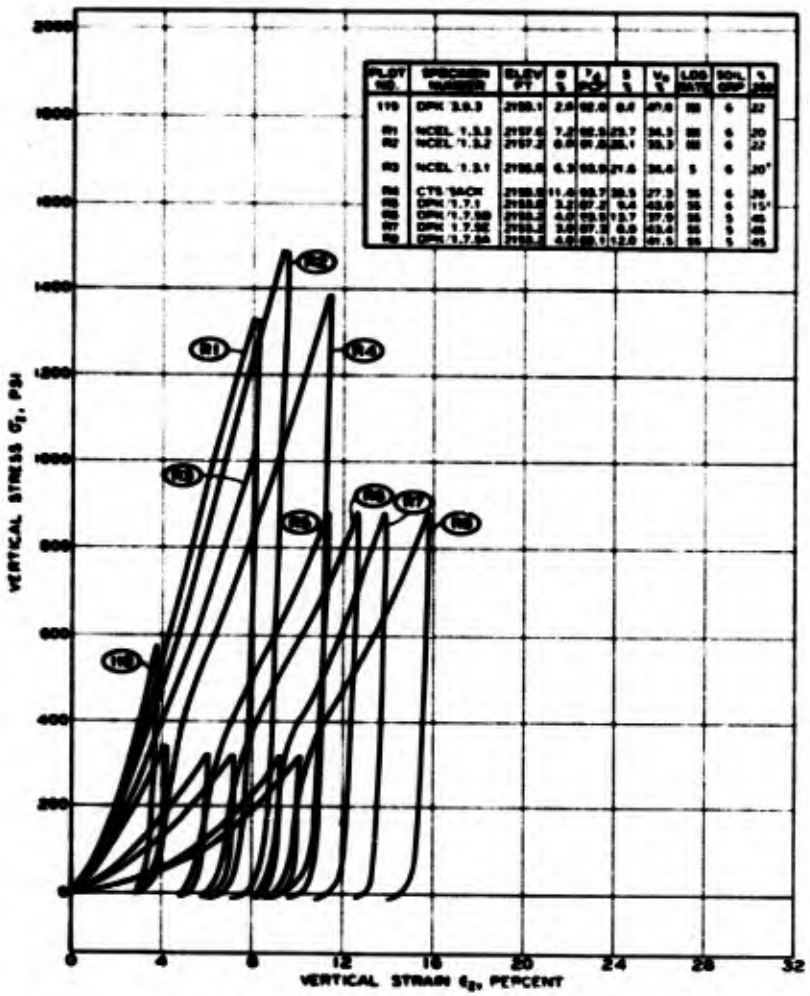

a. Natural structure, loading rate, dry density, and grain-size effects.

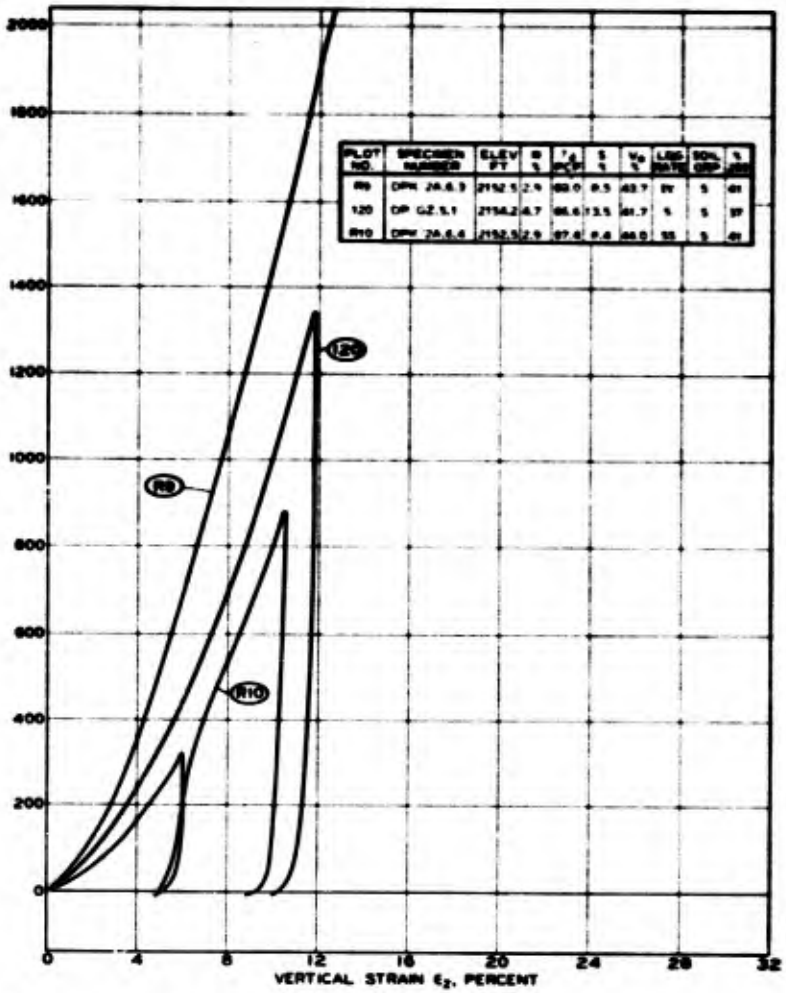

b. Natural structure and loading rate effects.

Figure 4.11 Uniaxial strain results for tests on undisturbed and remolded specimens of silty sand.

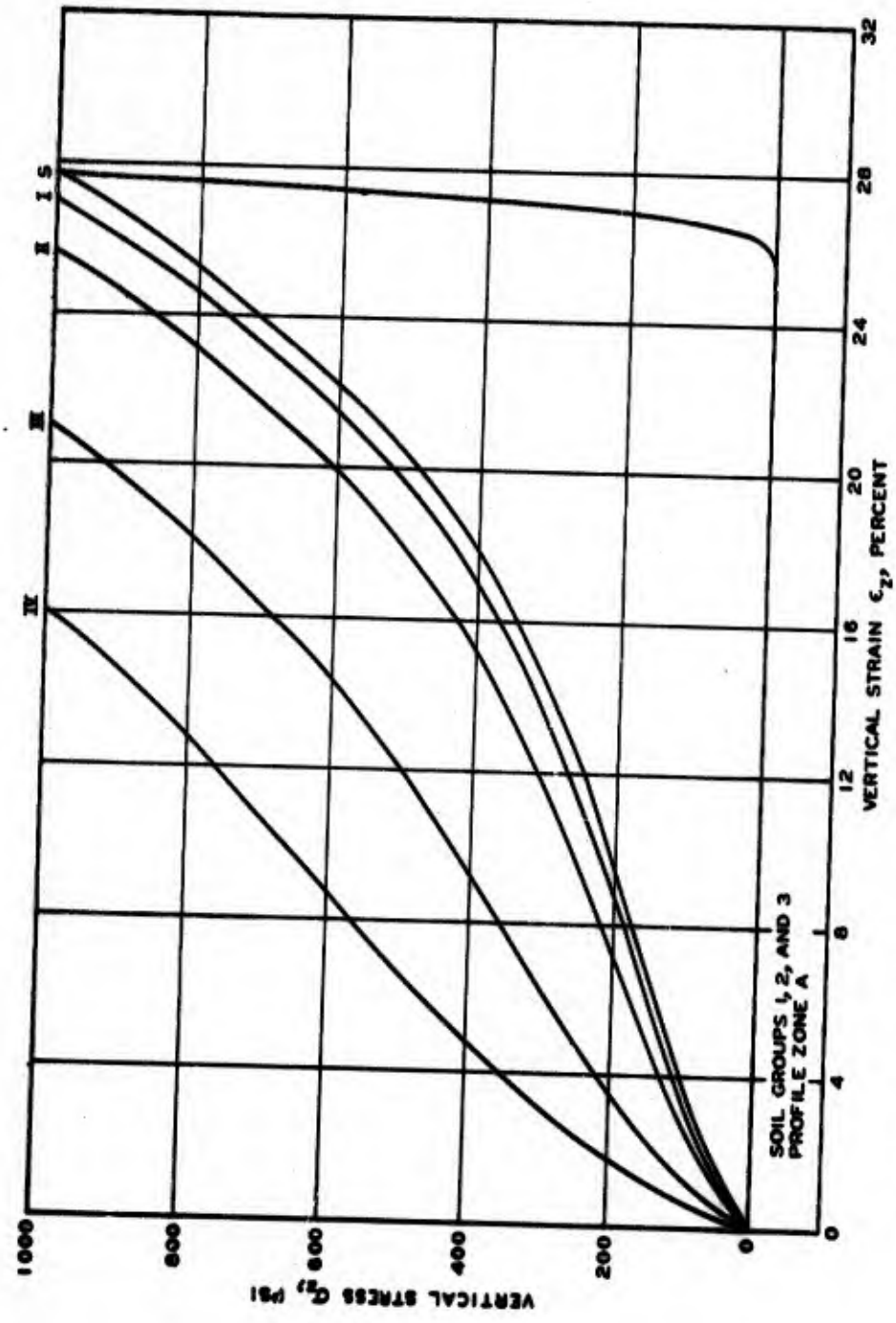

Figure 4.12 Recommended uniaxial strain σ_z versus ϵ_z relations for Soil Groups 1, 2, and 3--Profile Zone A.

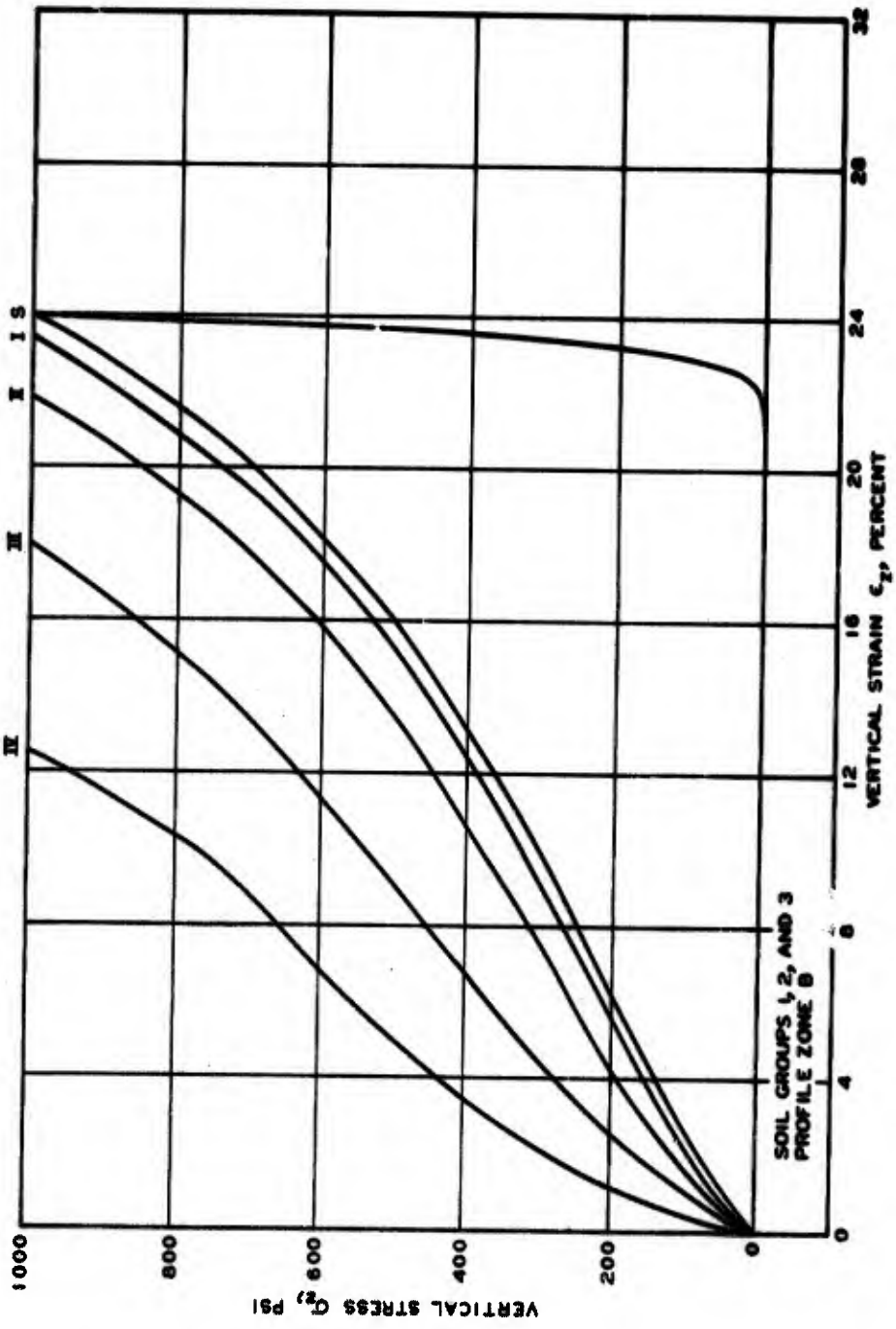

Figure 4.13 Recommended uniaxial strain σ_z versus ϵ_z relations for Soil Groups 1, 2, and 3--Profile Zone B.

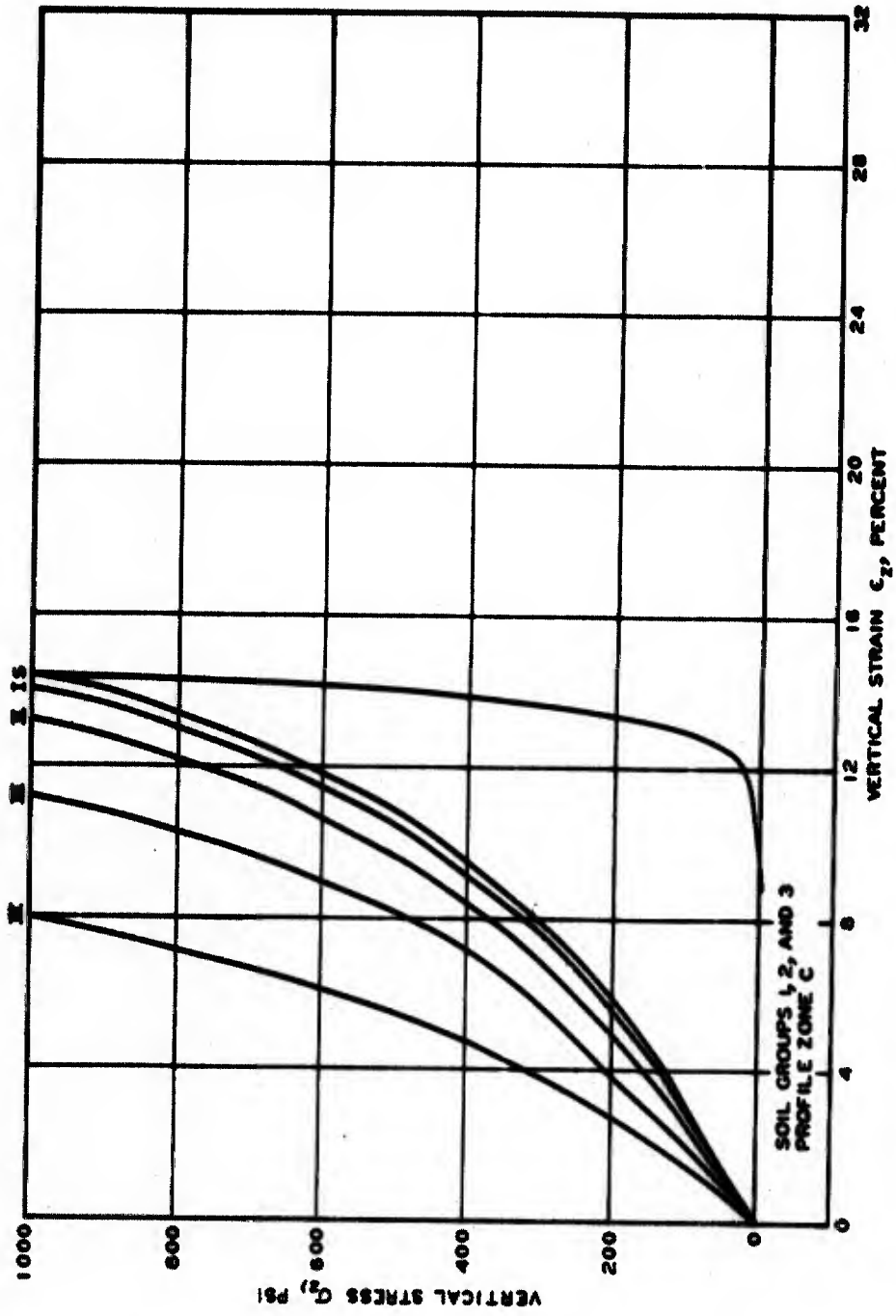

Figure 4.14 Recommended uniaxial strain σ_z versus ϵ_z relations for Soil Groups 1, 2, and 3--Profile Zone C.

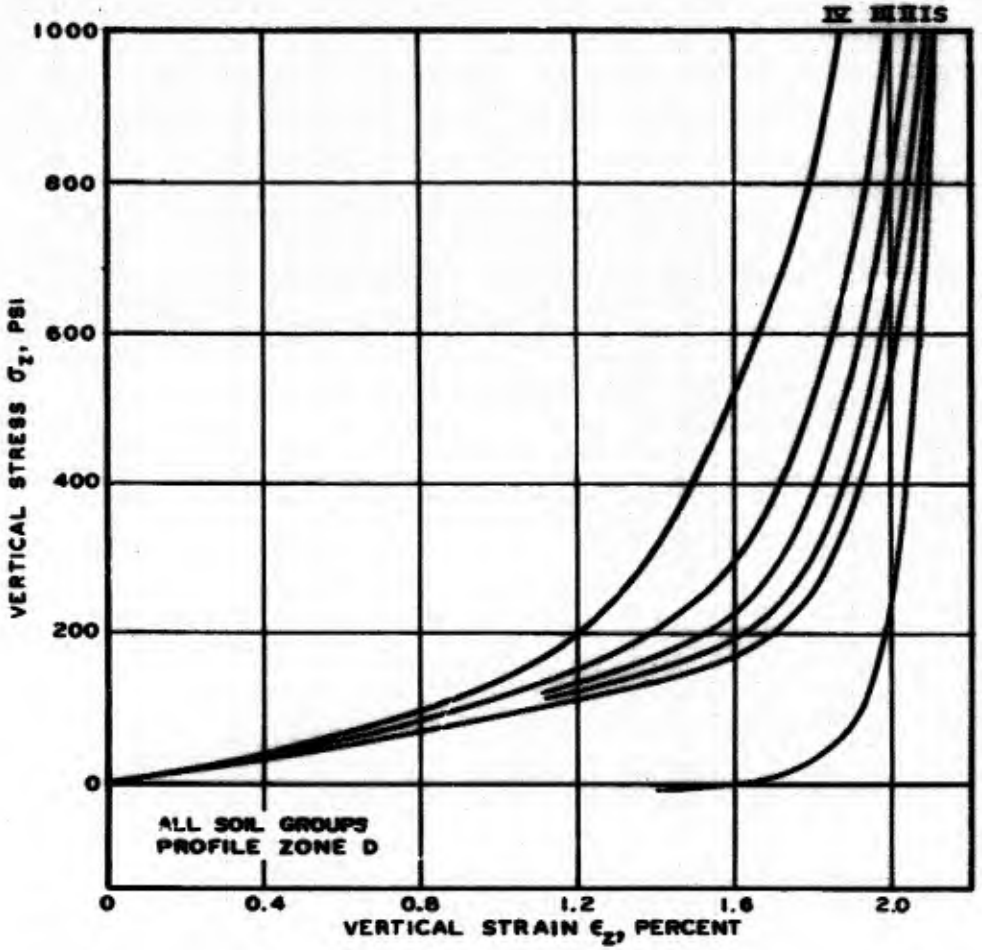

a. Profile Zone D.

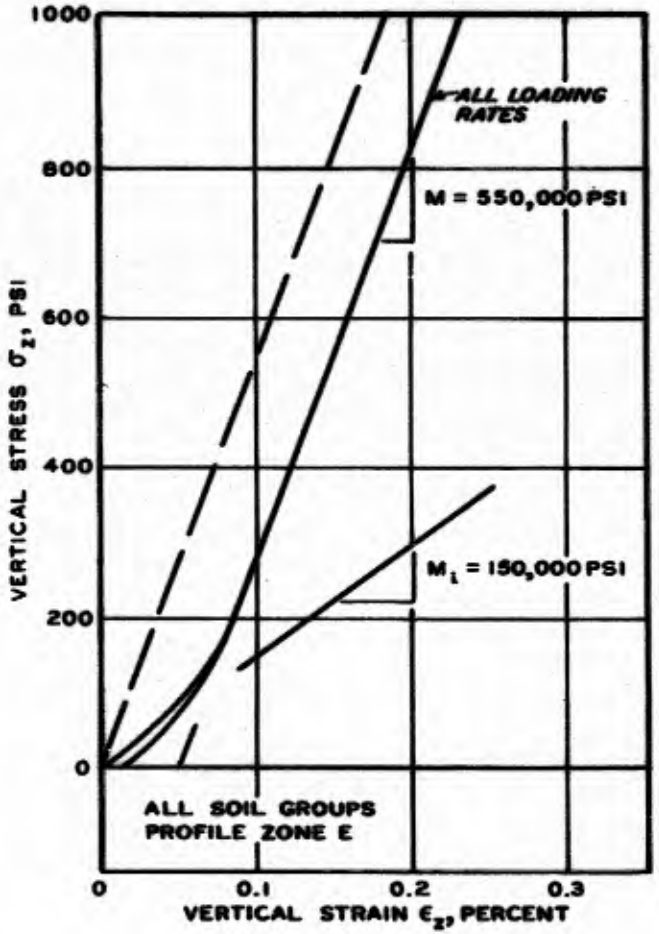

b. Profile Zone E.

Figure 4.15 Recommended uniaxial strain σ_z versus ϵ_z relations for all soil groups--Profile Zones D and E.

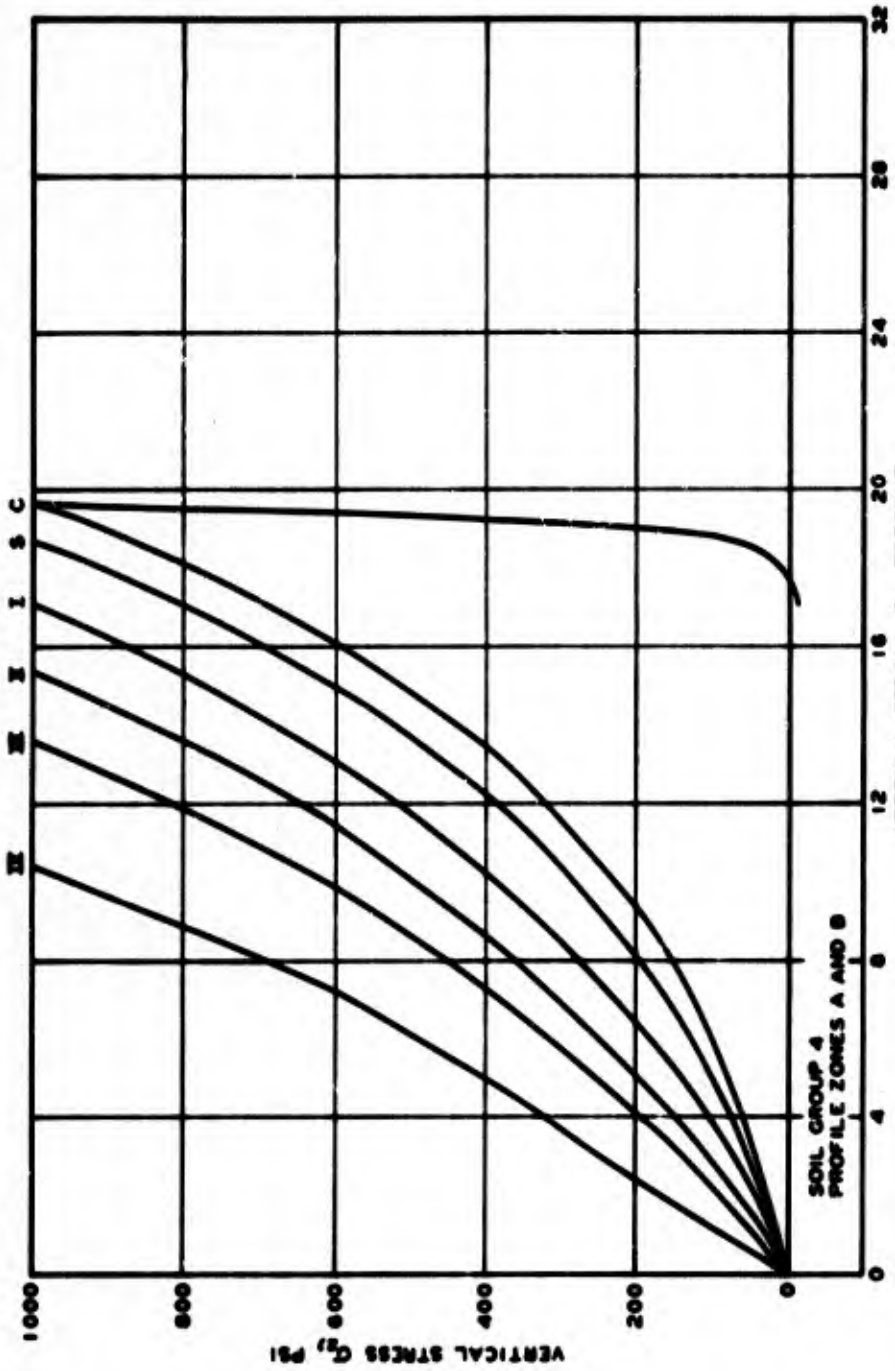

Figure 4.16 Recommended uniaxial strain σ_z versus ϵ_z relations for Soil Group 4--Profile Zones A and B.

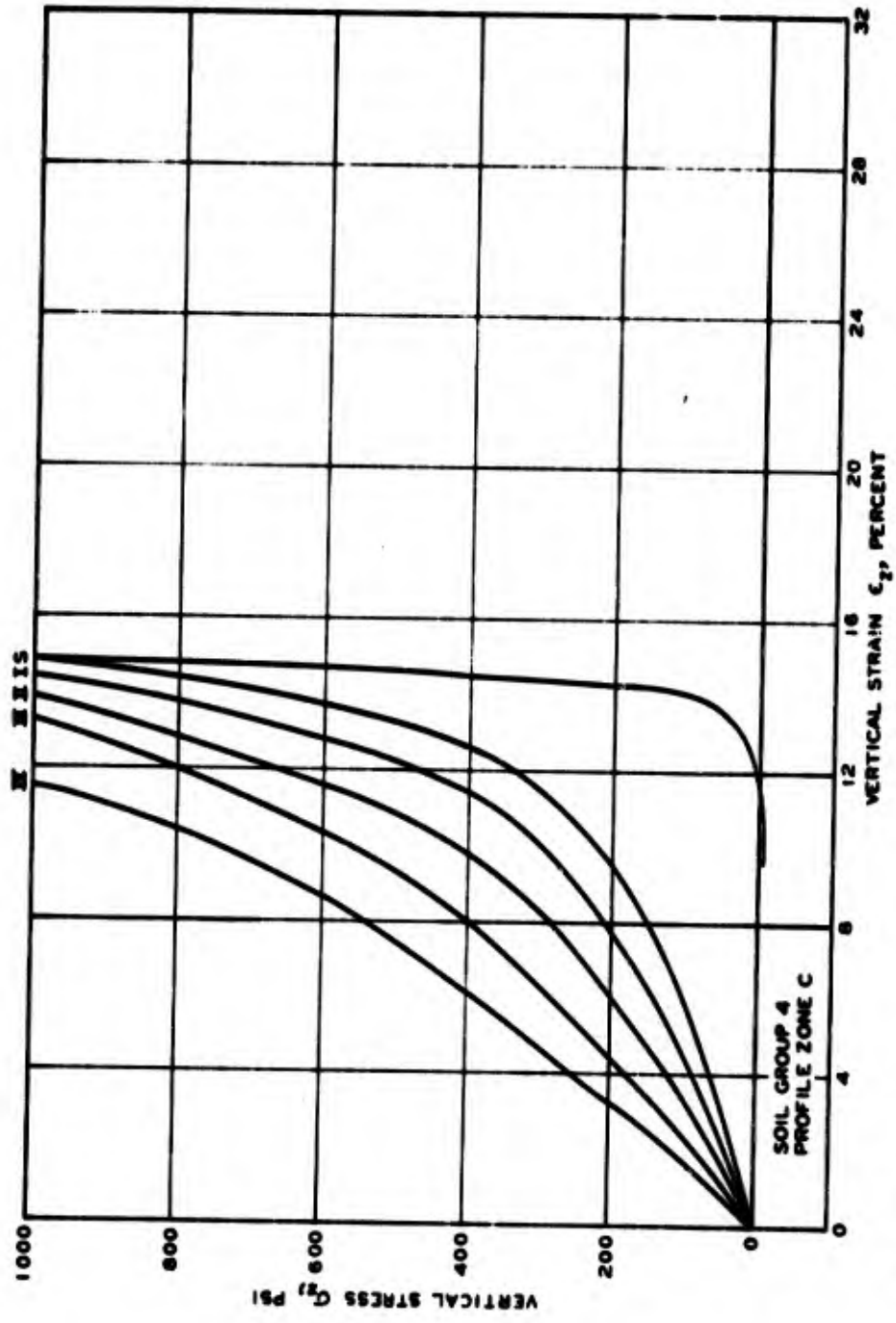

Figure 4.17 Recommended uniaxial strain σ_z versus ϵ_z relations for Soil Group 4--Profile Zone C.

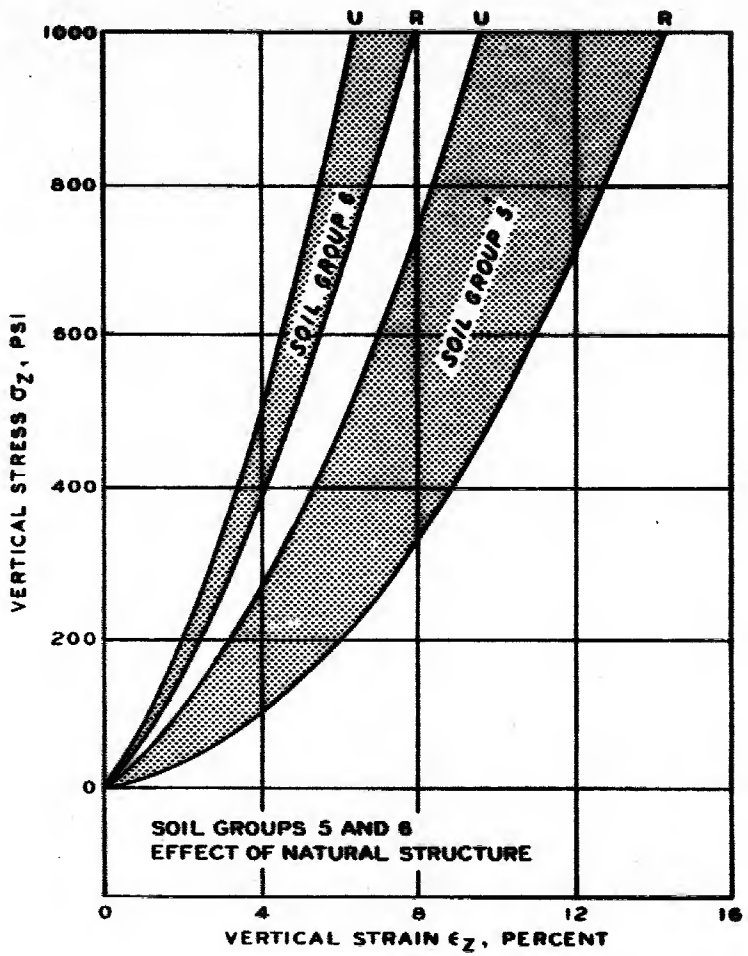

a. Effect of natural structure.

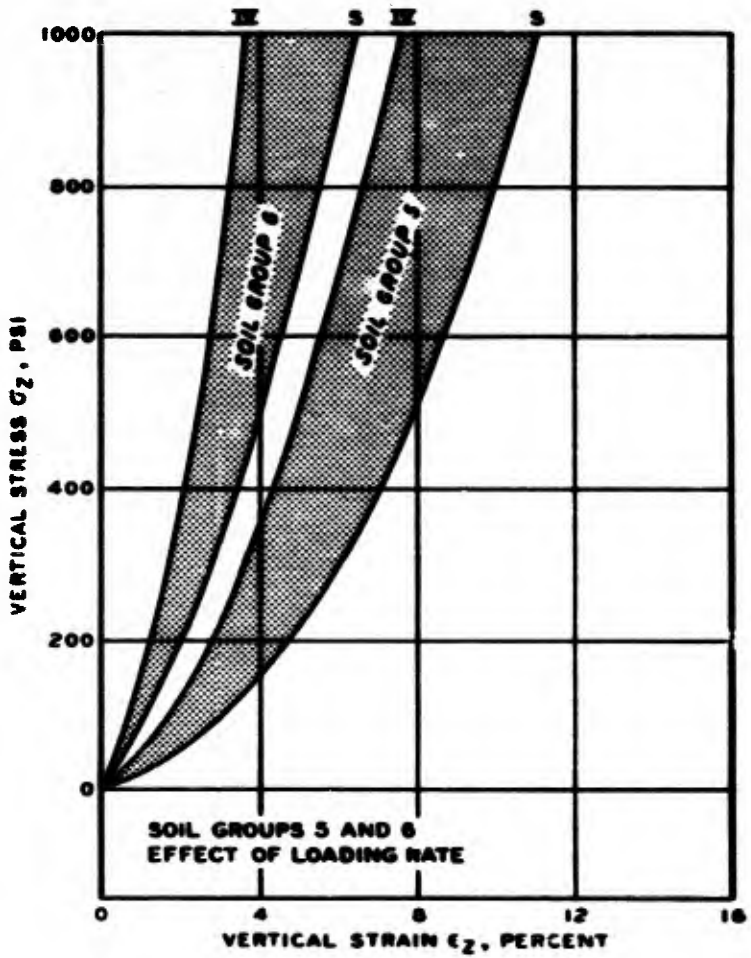

b. Effect of loading rate.

Figure 4.18 Effects of natural structure and loading rate for Soil Groups 5 and 6.

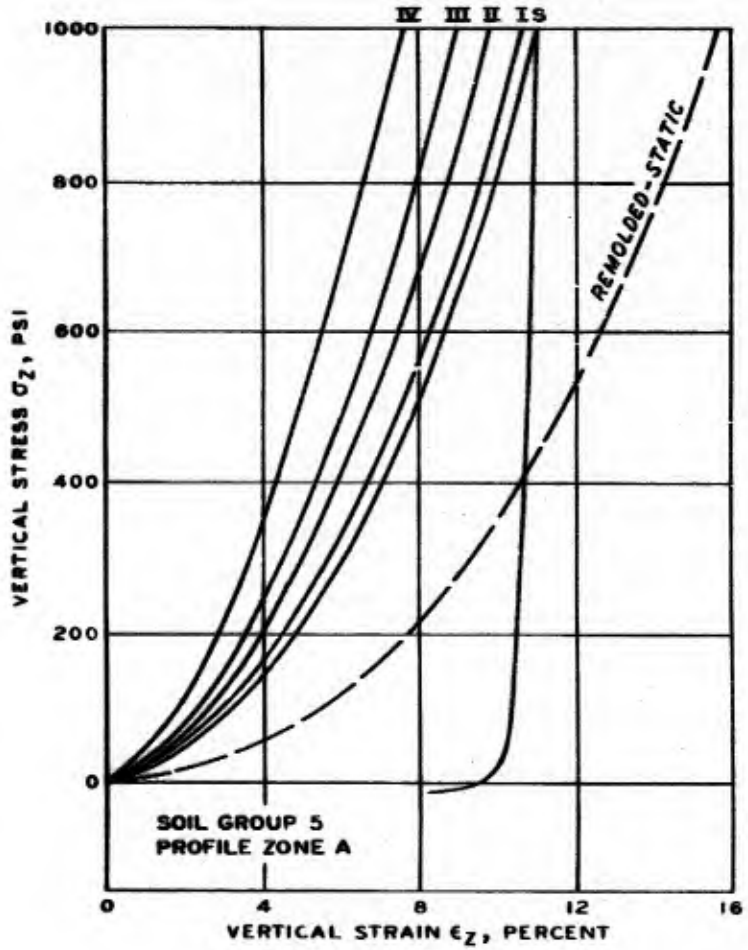

a. Profile Zone A.

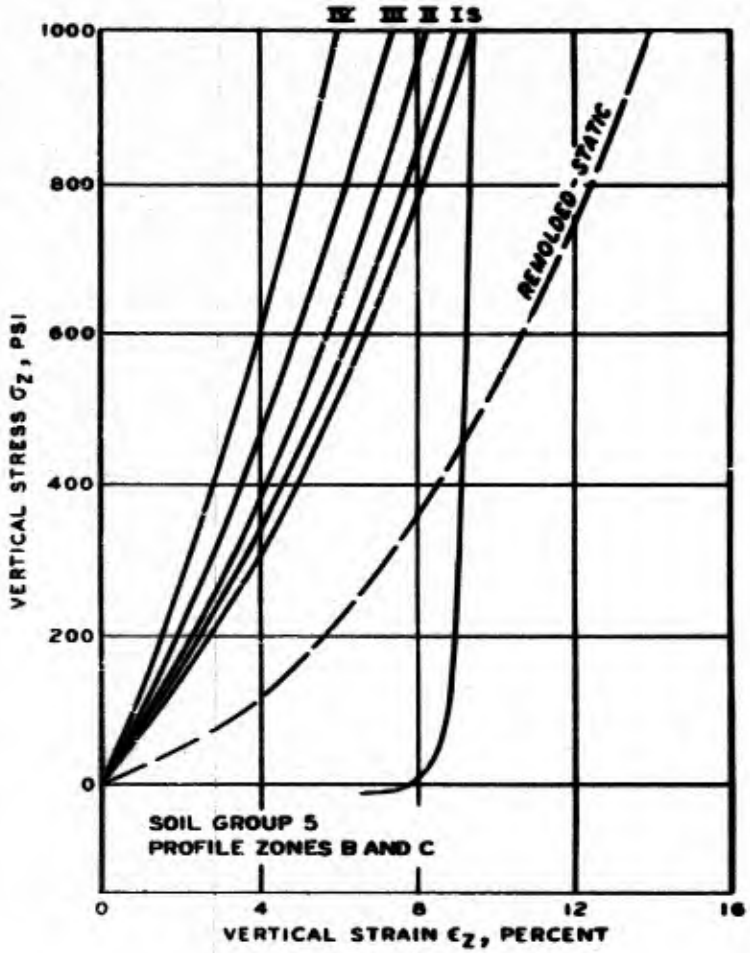

b. Profile Zones B and C.

Figure 4.19 Recommended uniaxial strain σ_z versus ϵ_z relations for Soil Group 5--Profile Zones A, B, and C.

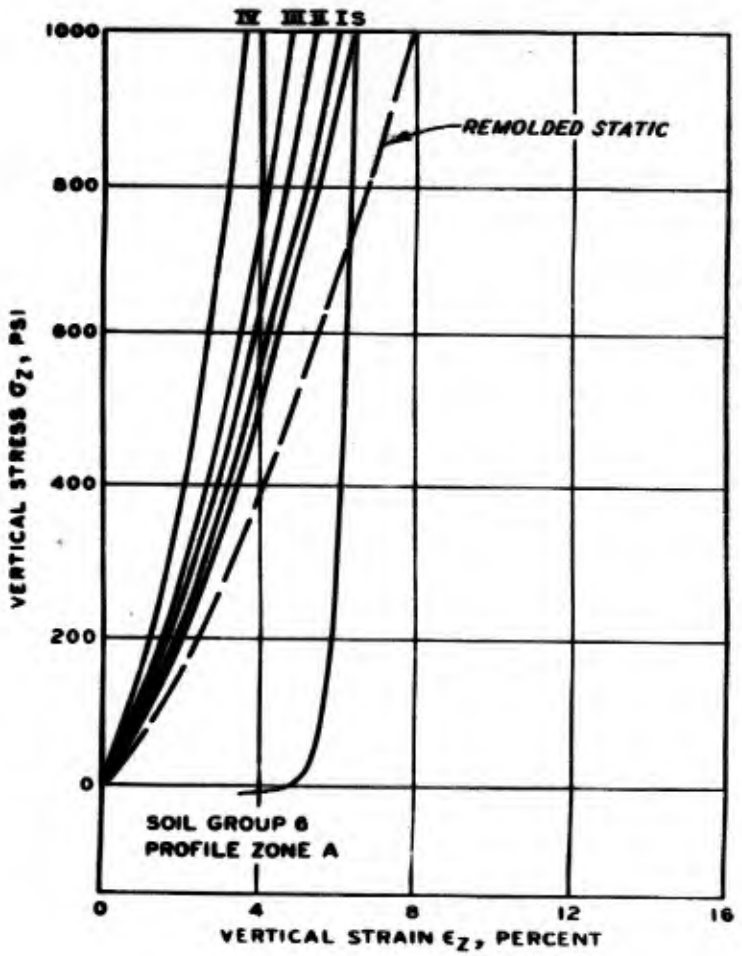

a. Profile Zone A.

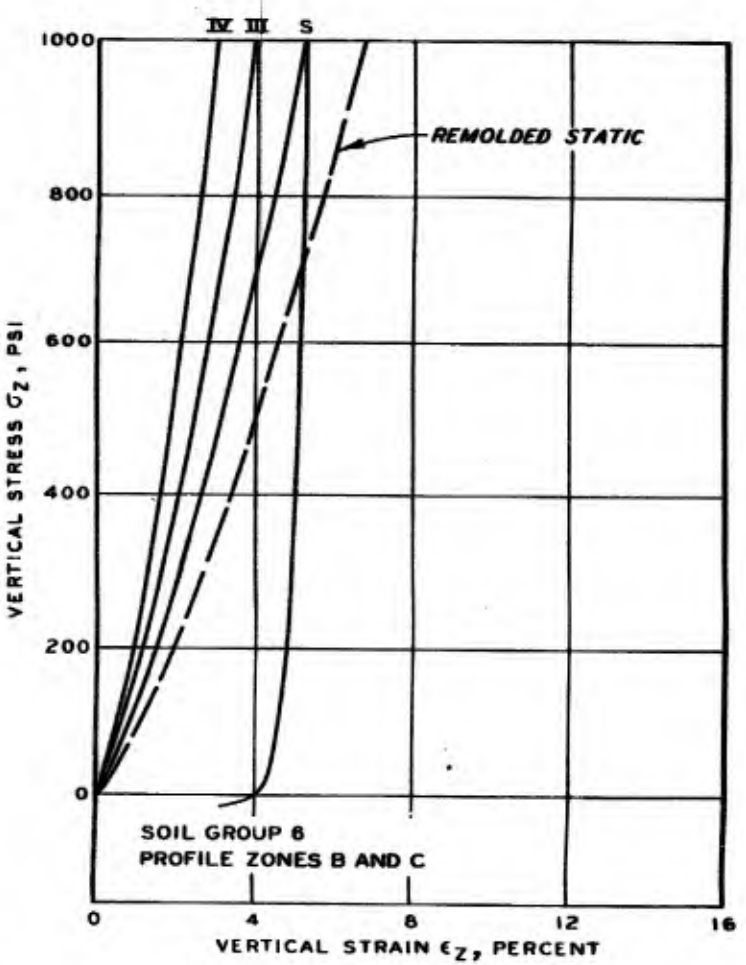

b. Profile Zones B and C.

Figure 4.20 Recommended uniaxial strain σ_z versus ϵ_z relations for Soil Group 6--Profile Zones A, B, and C.

CHAPTER 5

CONCLUSION

5.1 EXAMPLE APPLICATION OF RESULTS

Before the representative dynamic compressibility relations given in the preceding chapter can be applied in ground shock calculations for the Watching Hill site, a correlation must be established between the laboratory loading rate categories which form the basis for the different stress-strain curves and the explosive-induced loading rates anticipated at various depths within the profile. Although explosive-produced airblast pulses are characterized by extremely fast loading rates (i.e., times to peak stress on the order of microseconds), the rate at which a subsurface soil stratum is stressed as a result of such a pulse can be considerably altered by the stress-strain properties of the intervening soil strata. If these strata are extremely inelastic or hysteretic, as has been shown to be the case with the partially saturated soils at Watching Hill, then loading rates should be sharply attenuated with depth. And if, in addition, the virgin stress-strain relations initially soften under an applied stress, as is particularly evident in the case of the clays found just below the ground surface at Watching Hill (see Figures 4.12 and 4.13), the process of loading rate attenuation is further enhanced.

Stress gage measurements were made by WES at the 1.5, 5.0, 10.0, or 17.0 foot depths during DISTANT PLAIN Events 6 and 1A, Operation PRAIRIE FLAT, and Operation DIAL PACK (Murrell, 1970a, 1970b, and 1971). Most of these measurements were made at ground ranges subjected to peak airblast overpressures P_{so} ranging from 100 to 1600 psi. Vertical stress

versus time data recorded at the four different depths by these gages are plotted in Figure 5.1. Since these stress-time histories are influenced by the intensity and duration of the surface overpressure pulse, they are grouped into two overpressure ranges, i.e., 1600 psi > P_{so} > 400 psi and 400 psi > P_{so} > 100 psi. Boundaries for the loading rate categories used to distinguish stress pulses applied in the laboratory are superimposed on each of the eight field measurement plots. Based on these data, rough approximations to the variation of explosive-induced loading rates with depth at the Watching Hill Blast Range are given in the following tabulations:

1600 psi > P_{so} > 400 psi		400 psi > P_{so} > 100 psi	
Depth ft	Loading Rate Category	Depth ft	Loading Rate Category
0 to 2	IV	0 to 1	IV
2 to 5	III	1 to 2	III
5 to 10	II	2 to 5	II
>10	I	>5	I

It should be noted that loading rate attenuation will cease (or more than likely reverse) when the nonhysteretic saturated regime near the water table is encountered. But since a single, rate-independent stress-strain relation was specified for this regime, further definition with depth is unnecessary.

With the above field loading rate profiles established, it is now possible to illustrate with specific examples the manner in which soil profile and dynamic compressibility input can be selected for theoretical ground shock calculations. For the first example, assume that the location of interest is the 1000-psi surface overpressure contour for DISTANT PLAIN Event 1A. The nearest subsurface log and conventional

soil classification and index data is that from Boring DP/UGZ (see Figure 2.8). This information is plotted to a depth just below elevation 2140 feet in Figure 5.2. Using the available gradation and plasticity data in conjunction with the criteria established in Section 3.2, the conventional log can readily be reclassified into the six groups which characterize the near-surface lacustrine deposit at Watching Hill.

Translating the reclassified log into the first three columns of Table 5.1 facilitates the remaining steps. Profile zone designations for each soil stratum are entered in column four based on the boundaries given in Figure 3.17. The set of stress-strain curves applicable to each soil group-profile zone combination is referenced from Figures 4.12 through 4.20 in column five. The appropriate curve within the set in each figure is singled out by the loading rate category selected from the 1600 psi > P_{so} > 400 psi tabulation above and entered in column six. Finally, calculation layers are identified by number, depth, and thickness. These layers do not necessarily coincide with the soil stratum depths listed in column two. For instance, the stratum boundary at a depth of 1.3 feet can be omitted as a layer boundary since Soil Group 2-Profile Zone B has the same set of stress-strain curves as Soil Group 1-Profile Zone B. But a layer boundary must be inserted at 2.0 feet even though a stratum change does not occur at this depth because of the loading category change from IV to III. If it is necessary or desirable to use fewer layers in the calculation, then several layers and their stress-strain curves can be combined proportionally to define a composite layer of equal overall compressibility.

Because of its location on an apparently eroded slope (see contour map in Figure 2.8), Boring DP/UGZ exposed a clay crust only 2.5 feet

thick. This is in contrast to the second example, where the overlying clay crust was found to be 8.1 feet thick. This latter example assumes that the location of interest is the 300-psi surface overpressure contour on a SW bearing from the GZ of Operation DIAL PACK. The nearest subsurface log and conventional soil property data is that from Boring DPK/U1A. The conventional and reclassified logs are shown in Figure 5.3. Following the same steps outlined in the first example, with the single exception of using the 400 psi > P_{so} > 100 psi field loading category tabulation instead of the 1600 psi > P_{so} > 400 psi tabulation, the calculation layers and their respective dynamic compressibility relations were defined in Table 5.2.

It is clear from the above examples that the process of selecting Watching Hill profile and compressibility input for theoretical ground shock calculations has been reduced to a simple, almost-mechanical procedure. It should also be clear, however, that this simplification was bought at the expense of numerous averages, generalizations, idealizations, and assumptions. It should not be used to the exclusion of other data or information pertinent to specific problem situations.

5.2 SUMMARY OF FINDINGS AND CONCLUSIONS

This study was concerned with the analysis of a large quantity of soil property data obtained intermittently over a four-year period from the Watching Hill Blast Range at DRES, Canada. Through this collective analysis, a clear picture has been established, for the first time, of the overall site stratigraphy, the nature of the associated soil deposits, and the influence exerted by physical properties on the dynamic compressibility of the near-surface glacial lake sediments.

The specific problem posed regarding application of this newfound understanding was that of furnishing accurate profile information for sophisticated ground shock calculations and selecting stress-strain curves to represent the in situ response of each layer in the profile to transient uniaxial strain loading and unloading. The primary purpose of the study was to determine if a relatively simple procedure could be outlined whereby this could readily be done for any given location within the site for which a field boring log and conventional soil classification test data were available. The principal conclusion, therefore, is that it was possible to develop such a procedure, as demonstrated in the above examples. In the process of developing this procedure, it was found that:

1. The site overlies a large buried preglacial valley, the floor of which is composed of a zone of coal seams and carbonaceous shales, probably representing the Upper Cretaceous Foremost formation. The soil profile consists of a 210- to 220-foot-thick succession of Pleistocene tills and lake deposits.

2. The available field seismic survey data were useful primarily in that they denoted the general lines of demarcation between major changes in the deposit, i.e., the water table separating the highly compressible partially saturated soils from the relatively incompressible saturated regime and the soil-bedrock interface. They were of no help in depicting detailed subsurface stratigraphy and of little quantitative use with regard to dynamic compressibility under intense blast-induced loadings.

3. The site profile appears to consist of nine different stratigraphic units, i.e., three units of stratified lacustrine sediments,

three units of outwash sands and gravels, two units of unstratified glacial till, and the bedrock unit. The upper lacustrine deposit is characterized by a relatively stable groundwater table, above which the soils have apparently been subjected to numerous cycles of flooding and drying.

4. The primary physical properties affecting soil compressibility were grain-size distribution, Atterberg limits, and the various three-phase weight-volume relationships produced as a result of the specific geologic environment. The principal mechanisms contributing to the uniaxial-strain response of partially saturated, undrained soil specimens could be reasonably represented by the analogy of a spring, partly surrounded by water and partly by air, compressing within a sealed cylinder.

5. The Unified Soil Classification System was too broad to adequately classify the various fine-grained sediments found within the near-surface lacustrine deposit. It was possible, however, to establish an expanded grain size and plasticity based classification whereby all of these sediments, regardless of their elevation location within the deposit, could be sorted into six soil groups.

6. The specific gravity, water content, and density data for each of the six soil groups revealed consistent patterns of variation with depth and/or elevation. There was ample evidence to indicate that, due to geologic and climatic influences, these composition property profiles are quite site dependent.

7. The calculated volume relationships of void ratio, porosity, saturation, and air void content also exhibited characteristic profiles for each soil group. The elevations below which the various soil strata

were calculated to be 100 percent saturated agreed very well with those anticipated due to the observed position of the groundwater table. By analyzing these property profiles, it was possible to subdivide the site into five generalized zones (A, B, C, D, and E) within which all the soil strata of a given group were expected to have similar compressibility characteristics.

8. As a result of loading history similarities, the available uniaxial strain test data for each soil group could be further categorized according to loading rate (i.e., Categories IV, III, II, and I for dynamic tests and S, SS, and C for static tests).

9. Based on the analysis of 130 measured stress-strain relationships (120 of which were from undisturbed specimens), a set of curves could be drawn to represent, as a function of loading rate, the in situ uniaxial strain response of each soil classification group-profile zone combination. These curves quantitatively define the compressibility of the various interbedded soil strata in the upper glacial lake deposit at Watching Hill.

10. By studying the records of field stress measurements obtained during different explosive events, a rough correlation could be established between laboratory test loading rates and those to be expected at various depths and surface overpressure ranges. This correlation permits selection of specific compressibility curves for input to specific ground shock calculation problems related to the Watching Hill HE tests.

5.3 RECOMMENDATIONS FOR FUTURE STUDIES

Completion of this physical property and dynamic compressibility analysis will obviously materially assist with the soil mechanics

aspects of numerous projects involved in the series of explosive events at Watching Hill. It also opens the way for some fundamental studies of ground shock phenomena within multilayered geologic media. Several such follow-on studies readily come to mind. The first involves using a one-dimensional wave propagation code such as that described by Radhakrishnan and Rohani (1971) to calculate the effects of a given surface overpressure pulse within the soil profiles found at various site locations. The two used in the Section 5.1 examples should be included since the DP/UGZ location had only a thin clay crust and almost no highly saturated clay strata interspersed with the dry silts and sands. On the other hand, the DPK/U1A location had a number of such strata as well as being overlaid by a relatively thick dry clay crust. A second study of interest would be to compare the results from a calculation on a many-layered profile (such as the 36-layer DPK/U1A profile) with those from calculations on a series of composite-layer profiles using successively fewer layers in the profile representation.

Studies could also be conducted to ascertain the impact of incorporating the deeper stratigraphic units into ground shock calculations. Additional uniaxial strain data is available which can be analyzed to determine if suitable dynamic compressibility relations can be established for these units. Establishment of soil property input for two-dimensional calculations requires the analysis of lateral earth pressure coefficient and triaxial shear data (see Jackson, 1969). Although by no means as complete as the basic uniaxial strain test data, some test data are available for such analyses within the soil classification group framework established herein.

Table 5.1

Input Data for 1000-psi Calculation at Boring DP/UGZ

Stratum Elevation ft	Stratum Depth ft	Soil Group	Profile Zone	σ - ε Selection: Figure Reference	σ - ε Selection: Loading Rate
2160.9	0.0				
		2	B	4.13	IV
2159.6	1.3				
		1	B	4.13	IV
2158.6	2.3				
		3	B	4.13	III
2158.4	2.5				
		5	A	4.19a	III
2157.9	3.0				
		3	B	4.13	III
2157.3	3.6				
		4	A	4.16	III
2156.7	4.2				
		5	A	4.19a	III
2156.4	4.5				
		4	A	4.16	III
2155.9	5.0				
		3	B	4.13	II
2155.6	5.3				
		5	A	4.19a	II
2154.8	6.1				
		4	A	4.16	II
2154.4	6.5				
		5	A	4.19a	II
2152.8	8.1				
		6	A	4.20a	II
2152.0	8.9				
		5	A	4.19a	II
2151.4	9.5				
		4	A/B	4.16	II
2150.8	10.1				
		5	A	4.19a	I
2150.2	10.7				
		4	B	4.16	I
2149.5	11.4				
		6	A	4.20a	I
2148.8	12.1				
		4	B	4.16	I
2147.8	13.1				
		6	A	4.20a	I
2147.6	13.3				
		4	B	4.16	I
2147.4	13.5				
		5	B	4.19b	I
2146.0	14.9				
		2	E	4.15b	NA
2145.8	15.1				
		4	C	4.17	I
2145.4	15.5				
		3	D	4.15a	I
2145.1	15.8				
		4	C	4.17	I
2144.9	16.0				
		5	C	4.19b	I
2144.1	16.8				
		2	E	4.15b	NA
2143.3	17.6				
		5	D	4.15a	I
2143.1	17.8				
		6	D	4.15a	I
2140.9	20.0				
		1	E	4.15b	NA
--	--				

Calculation Layers: Number	Depth ft	Thickness ft
	0.0	
1		2.0
	2.0	
2		0.5
	2.5	
3		0.5
	3.0	
4		0.6
	3.6	
5		0.6
	4.2	
6		0.3
	4.5	
7		0.5
	5.0	
8		0.3
	5.3	
9		0.8
	6.1	
10		0.4
	6.5	
11		1.6
	8.1	
12		0.8
	8.9	
13		0.6
	9.5	
14		0.6
	10.1	
15		0.6
	10.7	
16		0.7
	11.4	
17		0.7
	12.1	
18		1.0
	13.1	
19		0.2
	13.3	
20		0.2
	13.5	
21		1.4
	14.9	
22		0.2
	15.1	
23		0.4
	15.5	
24		0.3
	15.8	
25		0.2
	16.0	
26		0.8
	16.8	
27		0.8
	17.6	
28		2.4
	20.0	
29		--
	--	

Table 5.2

Input Data for 30-psi Calculation at Boring DIK/UIA

Stratum Elevation ft	Stratum Depth ft	Soil Group	Profile Zone	σ - ε Selection: Figure Reference	σ - ε Selection: Loading Rate
2165.1	0.0				
		2	A	4.12	IV
2163.3	1.8				
		1	A	4.12	I.I
2162.6	2.5				
		2	A	4.12	II
		2	B	4.13	II
		2	B	4.13	I
2157.4	7.7				
		3	B	4.13	I
2157.0	8.1				
		4	A	4.1[illegible]	I
2156.2	8.9				
		6	A	4.20a	I
2159.6	9.5				
		4	A	4.1[illegible]	I
2155.1	10.0				
		[illegible]	A	4.20a	I
2154.4	10.7				
		4	A	4.1[illegible]	I
2153.8	11.3				
		[illegible]	A	4.20a	I
2153.5	11.6				
		2	[illegible]	4.14	I
2153.3	11.8				
		4	A	4.1[illegible]	I
2153.1	12.0				
		5	A	4.19a	I
2151.5	13.6				
		4	A/B	4.1[illegible]	I
2150.5	14.6				
		1	D	4.19a	I
2150.0	15.1				
		3	C	4.14	I
2149.7	15.4				
		[illegible]	A	4.20a	I
2149.4	15.7				
		1	D	4.19a	I
2149.2	15.9				
		4	B	4.1[illegible]	I
2149.0	16.1				
		1	D	4.19a	I
2148.[illegible]	16.[illegible]				
		4	B	4.1[illegible]	I
2148.2	16.9				
		3	C	4.14	I
			D	4.19a	I
2147.6	17.5				
		4	B	4.1[illegible]	I
2147.3	17.8				
		5	B	4.19b	I
2147.1	18.0				
		2	D	4.19a	I
2146.0	19.1				
		4	[illegible]	4.17	I
2145.4	19.7				
		5	A/B	4.19b	I
2144.8	20.3				
		4	C	4.17	I
2144.5	20.6				
		1	E	4.19b	IIA
2143.8	21.3				
		5	C	4.19b	I
		5	D	4.19a	I
2143.4	21.7				
		4	D	4.19a	I
2143.2	21.9				
		1	E	4.19b	IIA
2142.7	22.4				
		2	E	4.19b	IIA
2142.2	22.9				
		3	E	4.19b	IIA
2141.6	23.5				
		4	D	4.19a	I
2141.3	23.8				
		5	D	4.19a	I
2140.9	24.2				
		2	E	4.19b	IIA
--	--				

Calculation Layers: Number	Depth ft	Thickness ft
	0.0	
[illegible]	1.0	[illegible]
2	2.0	1.0
3	4.1	2.1
4	5.0	0.9
[illegible]	[illegible]	[illegible]
[illegible]	[illegible]	[illegible]
[illegible]	[illegible]	[illegible]
[illegible]	[illegible]	[illegible]
9	10.7	0.7
10	11.3	0.6
11	11.6	0.3
12	11.8	0.2
13	12.0	0.2
14	[illegible]	1.6
15	[illegible]	1.5
[illegible]	14.[illegible]	[illegible]
[illegible]	15.1	[illegible]
17	[illegible]	0.3
18	[illegible]	0.3
19	[illegible]	0.2
20	[illegible]	0.2
21	[illegible]	0.4
22	[illegible]	0.4
23	[illegible]	0.2
24	[illegible]	0.4
25	[illegible]	0.3
26	[illegible]	0.2
27	[illegible]	0.1
28	[illegible]	0.[illegible]
29	[illegible]	0.[illegible]
30	[illegible]	0.3
31	[illegible]	0.[illegible]
32	[illegible]	0.[illegible]
[illegible]	[illegible]	[illegible]
33	[illegible]	0.3
[illegible]	24.[illegible]	[illegible]
34	[illegible]	1.[illegible]
[illegible]	24.[illegible]	[illegible]
35	[illegible]	0.[illegible]
[illegible]	24.2	[illegible]
36	--	--

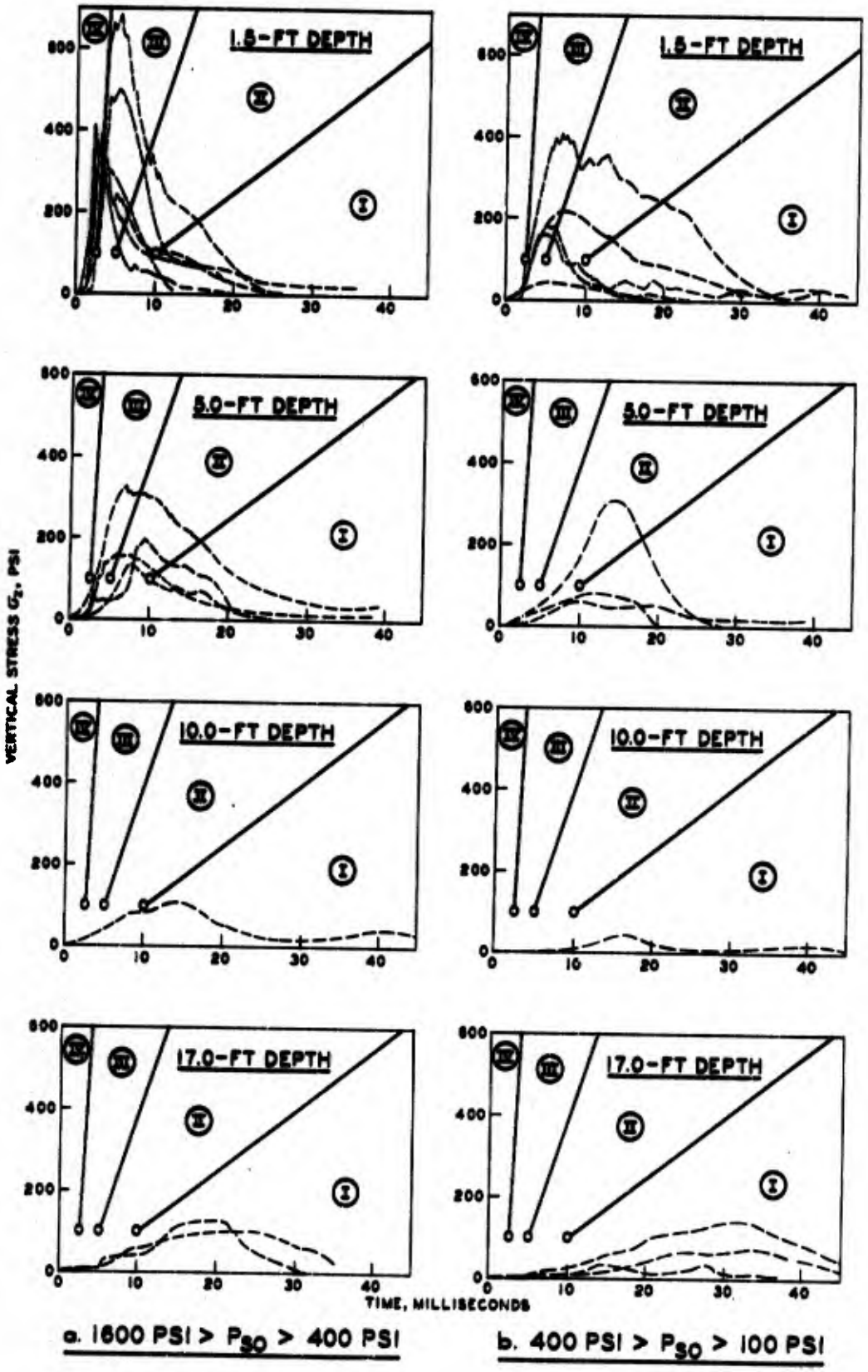

Figure 5.1 Comparison of field stress measurements with laboratory loading rate categories.

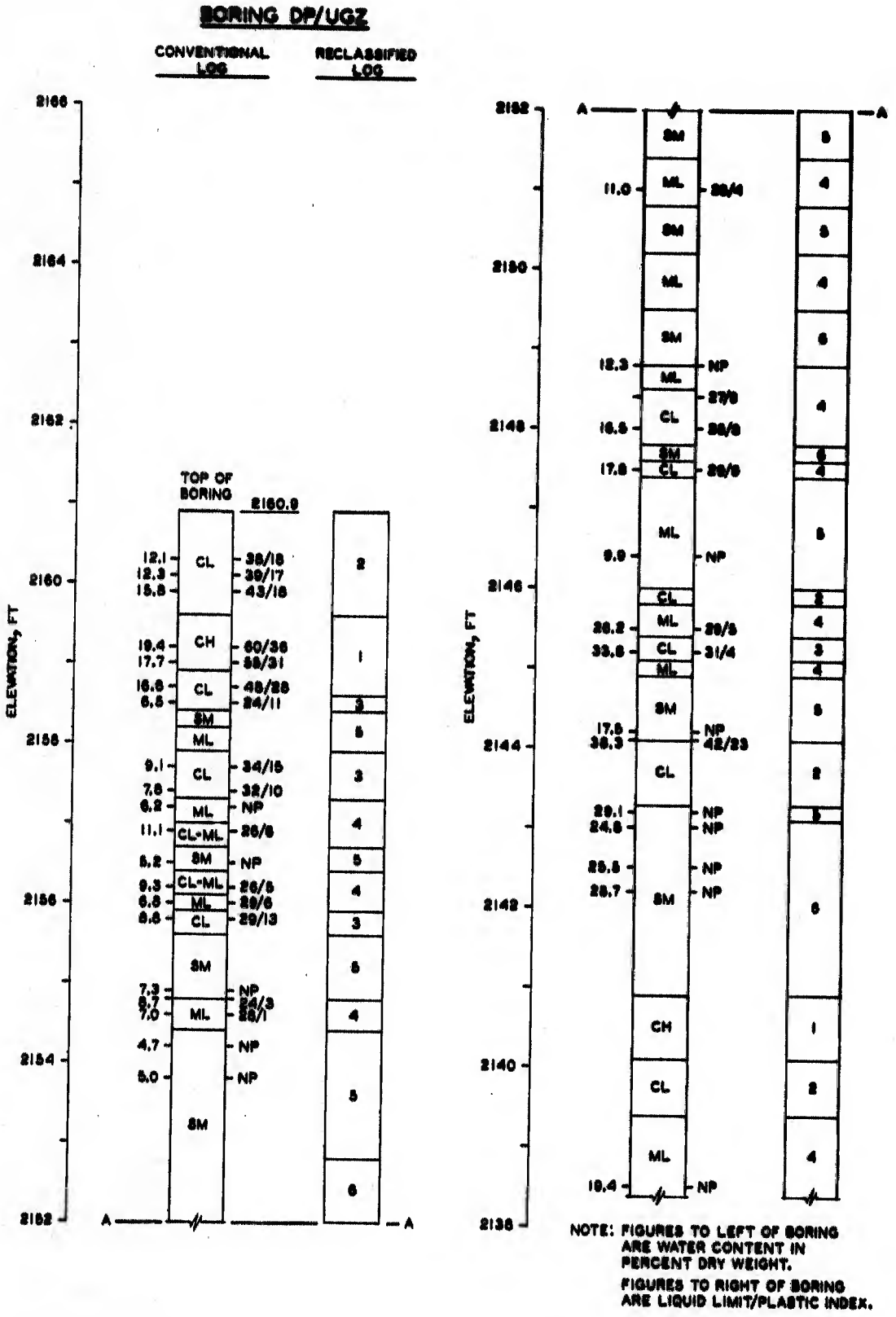

Figure 5.2 Conventional and reclassified logs for Boring DP/UGZ.

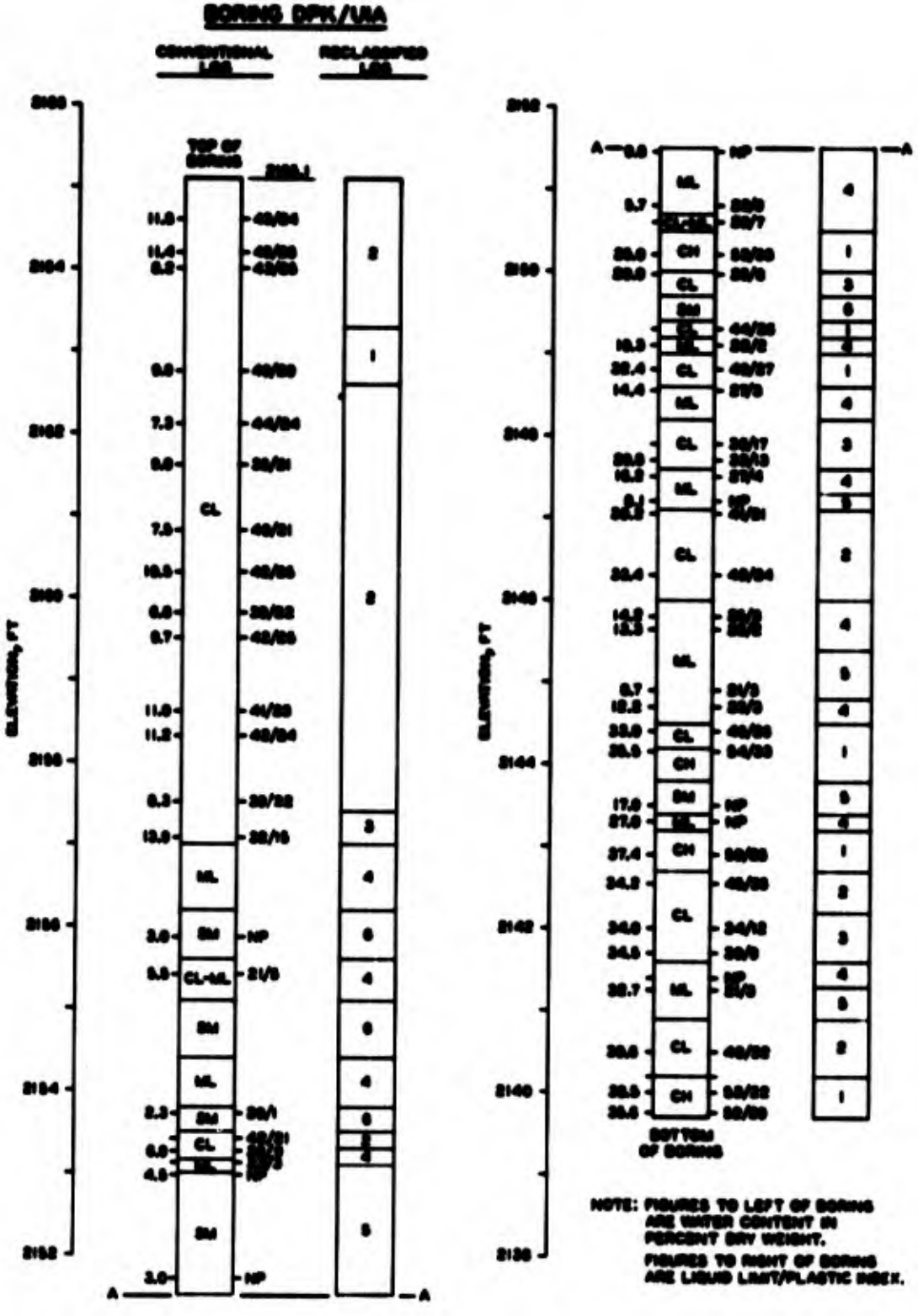

Figure 5.3 Conventional and reclassified logs for Boring DFK/U1A.

REFERENCES

Allgood, J. R. (1967), "In-Place Density Data from DISTANT PLAIN Event 6 Test Site," Private Communication, 5 October.

Berg, T. E. (1968), "Preliminary Report on Surficial Deposits in Proposed Blast Area, Suffield Experimental Station, Alberta," Research Council of Alberta, Canada.

Bishop, A. W., and Eldin, G. (1951), "Undrained Triaxial Tests on Saturated Sands and Their Significance in the General Theory of Shear Strength," Geotechnique, Vol II, No. 1.

Briosi, G. K. (1970), "Soil Profiles of Two Field Sites at DRES Proposed for Surface Burst Explosive Trials-Watching Hill and Juniper Flats," Project No. D-16-01-27, Suffield Memorandum No. 94/69, Defence Research Establishment Suffield, Ralston, Alberta, Canada, March.

Casagrande, A. (1932), "The Structure of Clay and Its Importance in Foundation Engineering," Journal of the Boston Society of Civil Engineers, April.

Casagrande, A. (1948), "Classification and Identification of Soils," Transactions of the American Society of Civil Engineers, Vol 113, p 901.

Crockford, M. B. B. (1949), "Oldman and Foremost Formations of Southern Alberta," Bulletin of the American Association of Petroleum Geologists, Vol 33, No. 4, April.

Davisson, M. T., and Maynard, T. R. (1965), "Static and Dynamic Compressibility of Suffield Experimental Station Soils," Technical Report No. 64-118, Air Force Weapons Laboratory, Kirtland Air Force Base, New Mexico, April.

Diehl, C. H. H., and Jones, G. H. S. (1966), "A Preliminary Soil Survey for DISTANT PLAIN 6 and the 1968 Trial," Suffield Special Publication No. 62, Suffield Experimental Station, Ralston, Alberta, Canada, 9 December.

Eringen, A. C. (1967), Mechanics of Continua, John Wiley & Sons, Inc., New York.

Flint, R. F. (1971), Glacial and Quaternary Geology, John Wiley & Sons, Inc., New York.

Gatz, J. L. (1968), "Soil Survey and Support Activities, Operation DISTANT PLAIN Event 6," Miscellaneous Paper No. 3-990, U. S. Army Engineer Waterways Experiment Station, CE, Vicksburg, Mississippi, April.

Gats, J. L. (1969), "Soils Investigation, Project DIAL PACK," Internal Report, U. S. Army Engineer Waterways Experiment Station, CE, Vicksburg, Mississippi, December.

Geiger, K. W. (1965), "Bedrock Topography of Southwestern Alberta," Preliminary Report 65-1, Research Council of Alberta, Canada.

Goode, T. B. (1959), "Soils Survey, Canadian HE Tests, SES, Ralston, Alberta, Canada," Internal Memorandum for Record, U. S. Army Engineer Waterways Experiment Station, CE, Vicksburg, Mississippi, 27 October.

Gravenor, C. B., and Bayrock, L. A. (1961), "Glacial Deposits of Alberta," Soils in Canada, Geological, Pedalogical, and Engineering Studies, The Royal Society of Canada Special Publications, No. 2, University of Toronto Press.

Hendron, A. J., Jr. (1965), "Correlation of Operation SNOWBALL Ground Motions with Dynamic Properties of Test Site Soils," Miscellaneous Paper No. 1-745, U. S. Army Engineer Waterways Experiment Station, CE, Vicksburg, Mississippi, October.

Hendron, A. J., Jr., and Davisson, M. T. (1964), "Static and Dynamic Constrained Moduli of Frenchman Flat Soils," Proceedings of the Symposium on Soil-Structure Interaction, University of Arizona, Tucson, September.

Hendron, A. J., Jr., Davisson, M. T., and Parola, J. F. (1969), "Effect of Degree of Saturation on Compressibility of Soils from the Defence Research Establishment Suffield," Contract Report No. 5-69-3, U. S. Army Engineer Waterways Experiment Station, CE, Vicksburg, Mississippi, April.

Jackson, J. G., Jr. (1968a), "Factors that Influence the Development of Soil Constitutive Relations," Miscellaneous Paper No. 4-980, U. S. Army Engineer Waterways Experiment Station, CE, Vicksburg, Mississippi, July.

Jackson, J. G., Jr. (1968b), "Uniaxial Strain Testing of Soils for Blast-Oriented Problems," Miscellaneous Paper S-68-17, U. S. Army Engineer Waterways Experiment Station, CE, Vicksburg, Mississippi, September.

Jackson, J. G., Jr. (1969), "Analysis of Laboratory Test Data to Derive Soil Constitutive Properties," Miscellaneous Paper S-69-16, U. S. Army Engineer Waterways Experiment Station, CE, Vicksburg, Mississippi, April.

Jackson, J. G., Jr., and Windham, J. E. (1967), "Soil Property Investigation for Project 3.10, Soil Sampling and Testing, Preliminary Report, Operation DISTANT PLAIN, Event 6," U. S. Army Engineer Waterways Experiment Station, CE, Vicksburg, Mississippi, December.

Jones, G. H. S. (1960), "Suffield Seismic Studies, Part I Introductory Paper with Some Notes on 10,000 lb Ground Burst Charges," Suffield Technical Paper No. 180, Suffield Experimental Station, Ralston, Alberta, Canada, 31 October.

Jones, G. H. S. (1963), "Strong Motion Seismic Effects of the Suffield Explosions," Suffield Report No. 208, Part I (Text, Tables, and Appendices) and Part II (Seismograms and Figures), Suffield Experimental Station, Ralston, Alberta, Canada, 15 November.

Jones, G. H. S., et al. (1970), "Operation PRAIRIE FLAT Project Officers' Report-Project LN3.01, Crater and Ejecta Study," POR-2115 (WT-2115), Defence Research Establishment Suffield, Ralston, Alberta, Canada, 10 December.

Jumikis, A. R. (1962), Soil Mechanics, D. Van Nostrand Company, Inc., Princeton, New Jersey.

Koning, H. L. (1963), "Some Observations on the Modulus of Compressibility of Water," Proceedings of the European Conference on Soil Mechanics and Foundation Engineering, Vol I, Weisbaden.

Krynine, D. P., and Judd, W. R. (1957), Principles of Engineering Geology and Geotechnics, McGraw-Hill Book Company, Inc., New York.

Lambe, T. W., and Whitman, R. V. (1969), Soil Mechanics, John Wiley & Sons, Inc., New York.

Lewis, J. T. (1970), "General Geology of the DIAL PACK Site," Internal Report, U. S. Army Engineer Waterways Experiment Station, CE, Vicksburg, Mississippi, 28 July.

Murrell, D. W. (1970a), "DISTANT PLAIN Events 6 and 1A Project 3.02A, Earth Motion and Stress Measurements," Technical Report N-70-14, U. S. Army Engineer Waterways Experiment Station, CE, Vicksburg, Mississippi, September.

Murrell, D. W. (1970b), "Project LN302, Earth Motion and Stress Measurements," Operation PRAIRIE FLAT Symposium Report - Vol I (Part I), DASA 2377-1 and DASIAC SR 92, General Electric Company, TEMPO, p 242, Santa Barbara, California, January.

Murrell, D. W. (1971), "Projects LN302-LN305: Earth Motion and Stress Measurements," paper presented at the DASA Operation DIAL PACK Symposium, Ottawa, Canada, 25 March.

Odello, R. J. (1971a), "Field Notes from Operation PRAIRIE FLAT Soil Tests," Private Communication, 12 April.

Odello, R. J. (1971b), "Field Notes from Soil Tests During DIAL PACK Silo Construction," Private Communication, 12 April.

Radhakrishnan, N., and Rohani, B. (1971), "A One-Dimensional Plane Wave Propagation Code for Layered Nonlinear Hysteretic Media," Technical Report S-71-12, U. S. Army Engineer Waterways Experiment Station, CE, Vicksburg, Mississippi, September.

Reed, A. S., Zelman, M., and Coates, D. F. (1964), "Unlined Tunnel Failures From Ground Shock-Appendix: Soil Tests and Seismic Velocities," RCAF Experiment in Operation SNOWBALL, Mining Research Laboratories, Fuels and Mining Practices Division, Mine's Branch, Dept. of Mines and Technical Surveys, Ottawa, Canada, December.

Richart, F. E., Jr., Hall, J. R., Jr., and Woods, R. D. (1970), Vibrations of Soils and Foundations, Prentice-Hall, Inc., Englewood Cliffs, New Jersey.

Rominger, J. F., and Rutledge, P. C. (1952), "Use of Soil Mechanics Data in Correlation and Interpretation of Lake Agassiz Sediments," The Journal of Geology, Vol 60, January-February.

Rooke, A. D., Jr., and Chew, T. D. (1965), "Operation SNOW BALL Project 3.1, Crater Measurements and Earth Media Determinations; Interim Report," Miscellaneous Paper No. 1-764, U. S. Army Engineer Waterways Experiment Station, CE, Vicksburg, Mississippi, December.

Sauer, F. M., Editor-in-Chief (1964), "Nuclear Geoplosics; A Sourcebook of Underground Phenomena and Effects of Nuclear Explosions," DASA-1285 (Five Vols), Defense Atomic Support Agency, Washington, D. C., May.

Schindler, L. (1968), "Design and Evaluation of a Device for Determining the One-Dimensional Compression Characteristics of Soils Subjected to Impulse-Type Loads," Technical Report S-68-9, U. S. Army Engineer Waterways Experiment Station, CE, Vicksburg, Mississippi, November.

Schuurman, I. E. (1966), "The Compressibility of an Air/Water Mixture and a Theoretical Relation Between the Air and Water Pressures," Geotechnique, Vol XVI, No. 4, December.

Seknicka, J. E., and Druebert, H. H. (1965), "Operation SNOWBALL Ground Displacement Study," Technical Report No. 64-175, Air Force Weapons Laboratory, Kirtland Air Force Base, New Mexico, August.

Smith, J. L. (1968), "Frozen Soil and Snow Studies, Operation DISTANT PLAIN, Event 5, Project 3.05," DASIAC SR 83, Operation DISTANT PLAIN Symposium II, DASA 2207 and DASIAC SR 83, DASA Information and Analysis Center, General Electric, TEMPO, p 164, Santa Barbara, California, May.

Sowers, G. B., and Sowers, G. F. (1970), Introductory Soil Mechanics and Foundations, Third Edition, The MacMillan Company, New York.

Sparks, A. D. (1963), "Theoretical Considerations of Stress Equations for Partly Saturated Soils," Third Regional Conference for Africa on Soil Mechanics and Foundation Engineering, Salisbury.

Strange, J. N., and Pinkston, J. M., Jr. (1962), "Crater Measurements from a 100-Ton Surface Explosion, U. S. Project 3, Canadian HE Test Program, 1961," Miscellaneous Paper No. 2-529, U. S. Army Engineer Waterways Experiment Station, CE, Vicksburg, Mississippi, October.

Strange, J. N., and Sager, R. A. (1962), "Crater Measurements from a Twenty-Ton Surface Explosion," Miscellaneous Paper No. 2-490, U. S. Army Engineer Waterways Experiment Station, CE, Vicksburg, Mississippi, June.

Strange, J. N., Wallace, W. L., and Strohm, W. E. (1961), "Crater and Permanent Displacement Measurements from a Five-Ton Surface Explosion, U. S. Project 1.6, Canadian HE Test Program, 1959," Miscellaneous Paper No. 2-424, U. S. Army Engineer Waterways Experiment Station, CE, Vicksburg, Mississippi, April.

Taylor, D. W. (1948), Fundamentals of Soil Mechanics, John Wiley & Sons, Inc., New York.

Terzaghi, C. A. (Karl) (1925), "Principles of Soil Mechanics," Engineering News-Record, Vol 95, Nos. 19-23, 25-27, pp 742-746, 796-800, 832-836, 874-878, 912-915, 987-990, 1026-1029, 1064-1068.

Terzaghi, C. A. (Karl) (1927), "Concrete Roads--A Problem in Foundation Engineering," Journal of the Boston Society of Civil Engineers, Vol 14, No. 5, pp 265-282, May.

Terzaghi, K., and Peck, R. B. (1948), Soil Mechanics in Engineering Practice, John Wiley & Sons, Inc., New York.

Tschebotarioff, G. P. (1951), Soil Mechanics, Foundations, and Earth Structures, McGraw-Hill Book Company, Inc., New York.

Waterways Experiment Station (1960), "The Unified Soil Classification System," Technical Memorandum No. 3-357, U. S. Army Engineer Waterways Experiment Station, CE, Vicksburg, Mississippi, April (reprinted May 1967).

Whitman, R. V. (1970), "The Response of Soils to Dynamic Loadings, Report 26, Final Report," Contract Report No. 3-26, U. S. Army Engineer Waterways Experiment Station, CE, Vicksburg, Mississippi, May.

Zelman, M. (1964), Emergency Measures Organization, Canada, Letter Report on "Seismic Survey Results, Watching Hill Blast Range, Suffield, Canada," to Kingery, C. N., U. S. Co-ordinator, Operation SNOWBALL, 21 July.

APPENDIX A

WES DYNAMIC UNIAXIAL STRAIN TESTING EQUIPMENT AND PROCEDURES

A.1 TESTING EQUIPMENT

The WES facilities for uniaxial strain soil property testing consist of two gas-actuated ram loaders capable of applying variable-intensity impulsive loads that are characteristic of airblasts and various test chambers which convert the ram load to a uniform axial pressure applied to the top surface of a laterally constrained soil specimen. The WES Dynapak ram loader in position for a uniaxial strain test is shown in Figure A.1. The Dynapak loader is used to apply preprogrammed dynamic loads of up to 50 kips with rise times to peak load ranging from 1 to 40 msec, hold times from 0 to ∞, and decay times from 25 to 10,000 msec. The SECO loader can be used to apply similar impulsive loads of up to 100 kips; this loading machine is shown in Figure A.2.

A.1.1 10-Inch-Diameter Device. A cutaway drawing of the WES 10-inch-diameter uniaxial strain device is shown in Figure A.3. Load from the ram is transmitted through three columns to a piston which compresses a fluid to uniformly load the soil specimen. Pressure is measured in the fluid so that O-ring friction and piston inertia do not create applied stress measurement problems. The specimen is kept thin or wafered in order to minimize sidewall friction effects and to permit a uniform state of stress to develop within the specimen due to multiple internal stress reflections. Specimens are 10 inches in diameter and may be either 1-inch or 2-1/2-inch thick, depending upon the anticipated compressibility and gradation of the soil being tested. Surface deflections are measured at four points across the specimen using linear

variable differential transformers (LVDT's); special provisions have been incorporated into this measurement system to eliminate core rod friction and chamber fluid leakage while permitting calibration of the magnetically sensitive coils in the actual test environment.

An oscillogram recording of the applied vertical pressure and deflection response versus time for a typical dynamic test is shown in Figure A.4. Strain is calculated from the surface deflection and the height of the soil chamber by the usual assumption that strain within the specimen is uniform from top to bottom. The 10-inch-diameter device is extremely versatile; it can be used to conduct static and dynamic tests for purposes of fundamental research as well as for practical engineering applications, on either laboratory-prepared or field-sampled specimens of all soil types, under pressures ranging up to 2000 psi. Design and evaluation of this device and its high-quality performance have been described in considerable detail by Schindler (1968).

A.1.2 5-Inch-Diameter Device. When a soil sample is removed from the ground, its geostatic overburden stresses are relieved resulting in some volumetric expansion of the sample. Since a principal boundary condition of the uniaxial strain test involves the absence of strain in the lateral direction, special procedures (to be described later) have been devised for preparing test specimens without extruding them from the 1/8-inch-wall-thickness steel tubes used to extract the samples from the field site. Although the lateral expansion of such specimens is restricted, they can readily expand axially and thus, prior to live loading, must be recompressed under a static axial pressure approximately equal to the geostatic overburden stress at the depth from which the sample was obtained. When the specimen is unloaded, all stress

(including both the live stress and the overburden prestress) is removed dynamically. This permits measurement of the response of the specimen to live tension stresses up to the limit set by the overburden.

The 5-inch-diameter uniaxial strain device is simply an adaption of the basic 10-inch-diameter device modified for the express purpose of testing undisturbed specimens lathed from 5-1/4-inch-OD by 5-inch-ID Shelby tubes. A cutaway drawing of the 5-inch-diameter device is shown in Figure A.5. Doughnut-shaped inserts were machined for the 1- and 2-1/2-inch-deep soil containers to receive the Shelby-tube ring specimens; a similarly shaped insert was made to adapt the fluid container for a 5-inch-diameter piston loading assembly. New upper container and LVDT coil support plates were also required. Strain measurement is made by a single, centrally located LVDT.

A.1.3 15,000-Psi Device. For nuclear weapons effects related problems, there is a need for meaningful soil constitutive property data obtained under controlled states of stress much higher than the 2000-psi capability of the previously described devices. A cutaway drawing of a 15,000-psi device is shown in Figure A.6. Although this device is similar in principal to other WES devices, there are perhaps three distinguishing features which should be pointed out. First, since at 15,000-psi pressures even steel deforms significantly, the chamber wall thickness has been increased substantially to limit the radial strain and thus maintain an essentially uniaxial strain condition. The second factor results from the fact that one cannot generate 15,000 psi on a 5-inch-diameter piston with a 100-kip loading machine. Thus, a force multiplier technique had to be devised wherein a loading piston smaller in diameter than the soil sample was used to pressurize the fluid

chamber. The third and most crucial factor is that the unique LVDT strain measurement system currently being used with the other WES devices is not suitable for use at this extremely high pressure since the increased wall thickness required for the core housing would prevent an acceptable coil response. A new strain measurement system is employed in which the LVDT is completely contained within the pressurized fluid chamber.

A.2 UNDISTURBED SPECIMEN PREPARATION PROCEDURES

The tube or ring containing the soil specimen is carefully machined and the specimen trimmed to a length exactly equal to the depth of the test device soil container. For tests in the 10-inch-diameter device, the specimen and ring are placed in the center of the soil container and the volume between the ring and the container wall is filled with compacted sand as shown in Figure A.7. Although the specimen container ring does not contact the wall of the basic soil container, the tendency of soil particles and moisture from the specimen to be squeezed out under the confining ring or for the confining ring to strain radially is resisted by the same pressure in the sand that surrounds it. For tests in the 5-inch-diameter device, the specimen ring is restrained directly by the steel soil container insert or doughnut as shown in Figure A.8. Thin steel shims are used as necessary to ensure a snug fit between the specimen ring and the doughnut insert.

A.2.1 Shelby-Tube Ring. A procedure for preparing uniaxial strain test specimens within Shelby-tube rings was devised to prevent specimen disturbance by extrusion from the sample tubes used to extract them from the field. However, disturbance from all aspects of preparation and trimming must be kept to a minimum; therefore, any metal cutting

prodecure used to get a specimen into the desired configuration must keep vibration and heat to a minimum.

The possible metal cutting procedures considered were (1) sawing with a band saw, (2) cutting on a lathe using a parting tool, and (3) machining on a lathe. Sawing with a band saw (1) caused an undesirable level of vibration and a relatively rough metal edge that would possibly rupture the rubber membrane sealing the specimen from the pressurized fluid; this option was therefore abandoned. The parting tool method (2) consisted of using the tool in a longitudinally fixed position on the lathe and rotating the Shelby tube fastened in the lathe chucks. As the tube rotated, the parting tool moved into the tube and made a cut directly into the Shelby tube, the width of the cut depending on the tool used. In this process, three faces of the tool contributed friction and caused rather severe chatter or vibration as well as heating of the sample; this method was also abandoned. The machining or turning technique (3) utilizes the same lathe setup as the parting tool method except that the machining tool makes a cut into the tube, and as the tube rotates, the tool moves longitudinally down the tube at a feed rate. In this process, only one face of the tool is in contact with metal. The lathe settings governing the operation are chuck revolutions per minute, feed rate of the machine tool down the lathe, and depth of each cut. These settings are controlled by the machine operator, and after extensive practice and investigation, settings have been found which result in an insignificant level of vibration and heat.

Figure A.9 shows a full-length (37-inch) Shelby tube chucked in the lathe for the first rough machine cut about 3/4 inch away from the desired finished edge of the test specimen. After the rough machine cut

through the steel tube, a wire saw is used to cut through the soil sample as shown in Figure A.10. A separated rough-cut specimen, which is immediately coated with a protective wax, is shown in Figure A.11. The rough-cut specimen is then chucked in the lathe and fine-machined on each end to obtain the desired final 1-inch or 2-1/2-inch dimension; this leaves a protective thickness of soil protruding from each end (see Figure A.12) which is waxed prior to storage in a temperature- and humidity-controlled room. Finally, the specimen is trimmed flush with the machined faces of the Shelby-tube ring as shown in Figure A.13 just prior to the uniaxial strain test. This specimen preparation procedure has been extensively used and has proved to be quite satisfactory for most soils encountered during a variety of site investigations.

A.2.2 3.6-Inch-Diameter Ring. The machining procedure described above is, of course, limited to soils with sufficient cohesive strength to remain stable during machining while chucked in a lathe and turned about a horizontal axis. Relatively cohesionless samples fall apart or pour out of the steel Shelby tube when the lathe cut is made. This limitation has been encountered in several testing programs that included lacustrine deposits of fine sandy silts (ML) and silty sands (SM). Fortunately, however, good-quality 5-inch-diameter undisturbed samples of these materials were obtained in the usual manner by immediate extrusion from the Shelby tube in the field, placement in 6-inch-diameter cardboard containers, and encasement in paraffin or wax.

A 3.6-inch-diameter laboratory sampler was designed for obtaining uniaxial strain test specimens from these 5-inch-diameter wax-encased undisturbed soil samples. The sampler essentially consists of an inner specimen container ring surrounded by an outer driving sleeve and a

beveled cutting shoe; a cutaway drawing of the sampler is shown in Figure A.14. After the specimen has been extracted from the sample by jacking or advance trimming (Figure A.15), the driving sleeve, small support sleeve, and upper collar are removed so that the top of the specimen is exposed (Figure A.16). The soil is then trimmed flush with the top of the 3.6-inch-diameter specimen container ring (Figure A.17), and a uniaxial strain device adapter is placed over it (Figure A.18). Supported by the adapter, the specimen is then inverted; the beveled cutting shoe, large support sleeve, and lower collar are removed; and the second exposed soil surface is trimmed flush with the specimen container ring and test device adapter (Figure A.19). Figure A.20 shows the 1-inch-high by 5-1/4-inch-diameter adapter containing a 0.9-inch-deep by 3.6-inch-diameter soil specimen just prior to its insertion into the soil container for the previously described 5-inch-diameter uniaxial strain test device.

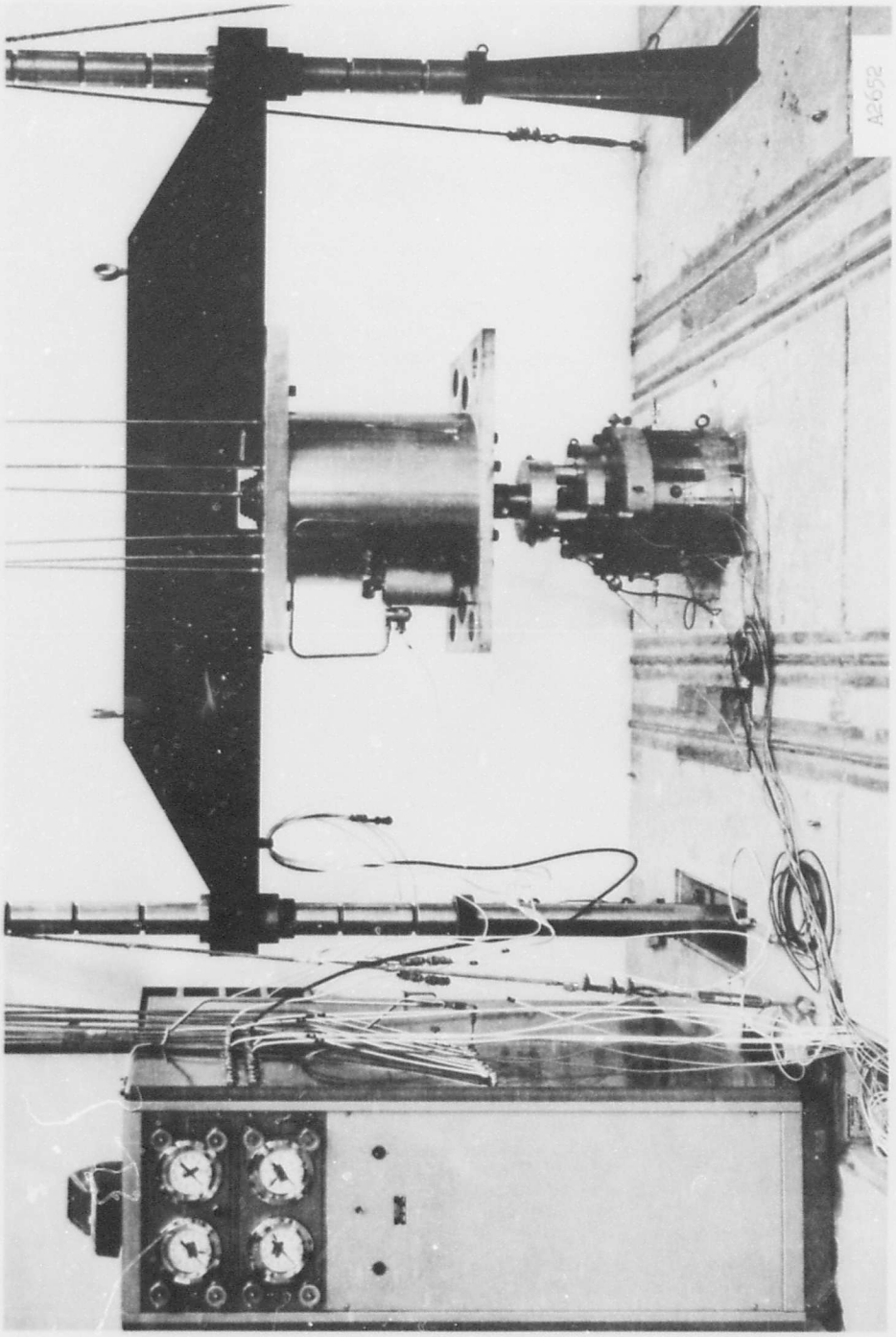

Figure A.1 Dynapak ram loader with 10-inch-diameter uniaxial strain test device.

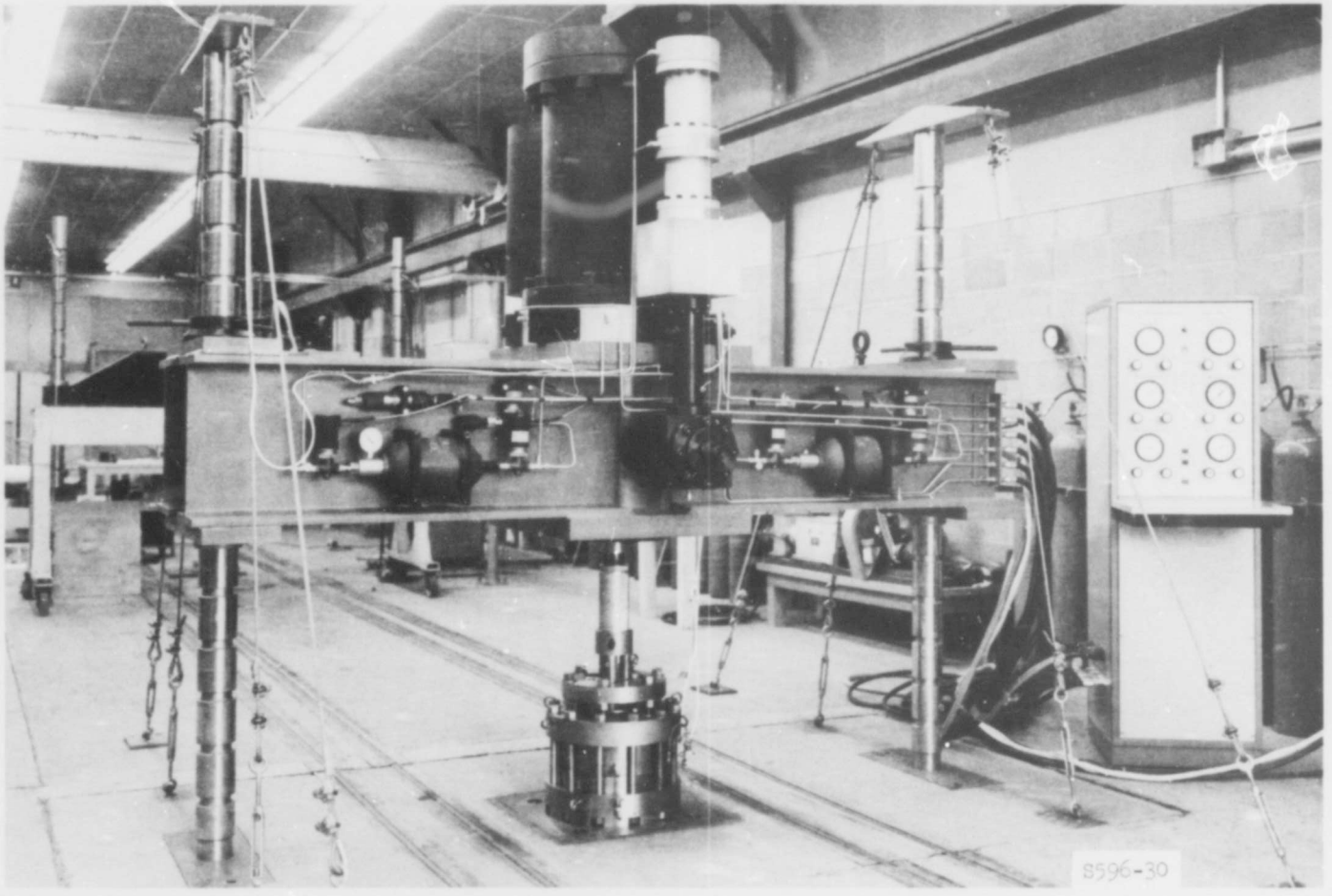

Figure A.2 SECO ram loader with 5-inch-diameter uniaxial strain test device.

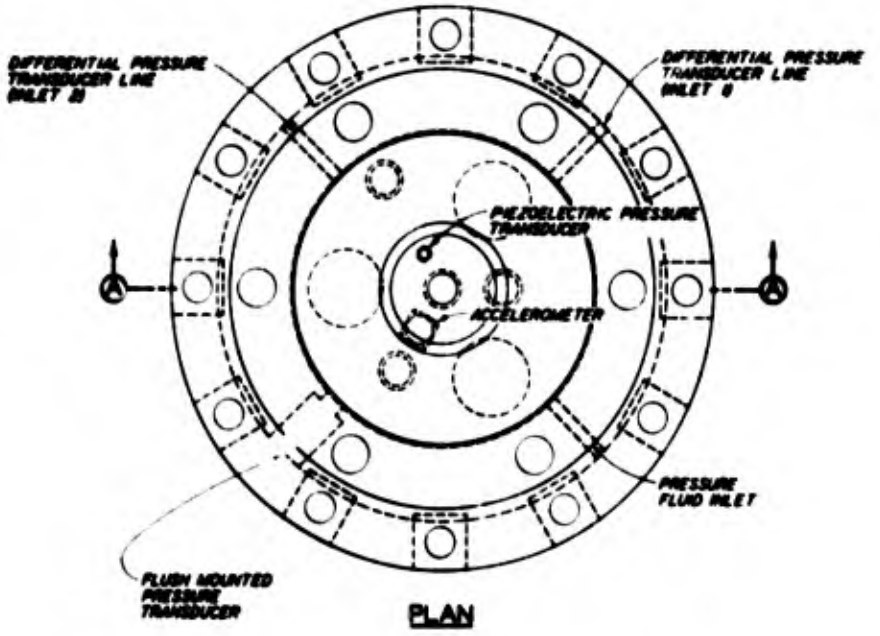

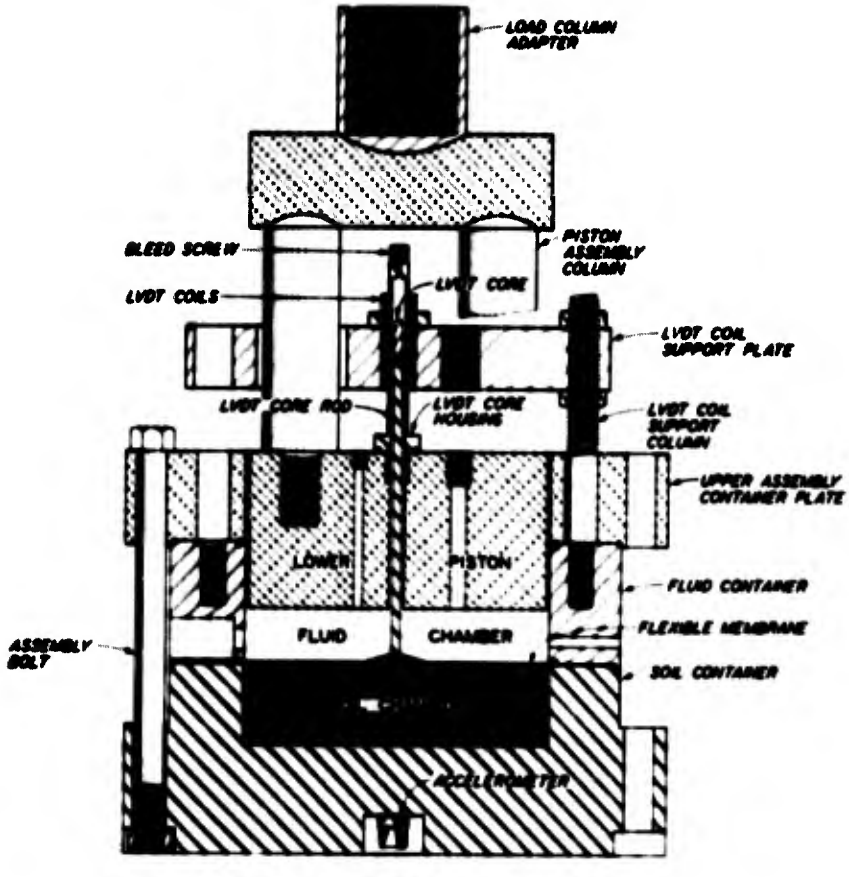

Figure A.3 10-inch-diameter uniaxial strain test device.

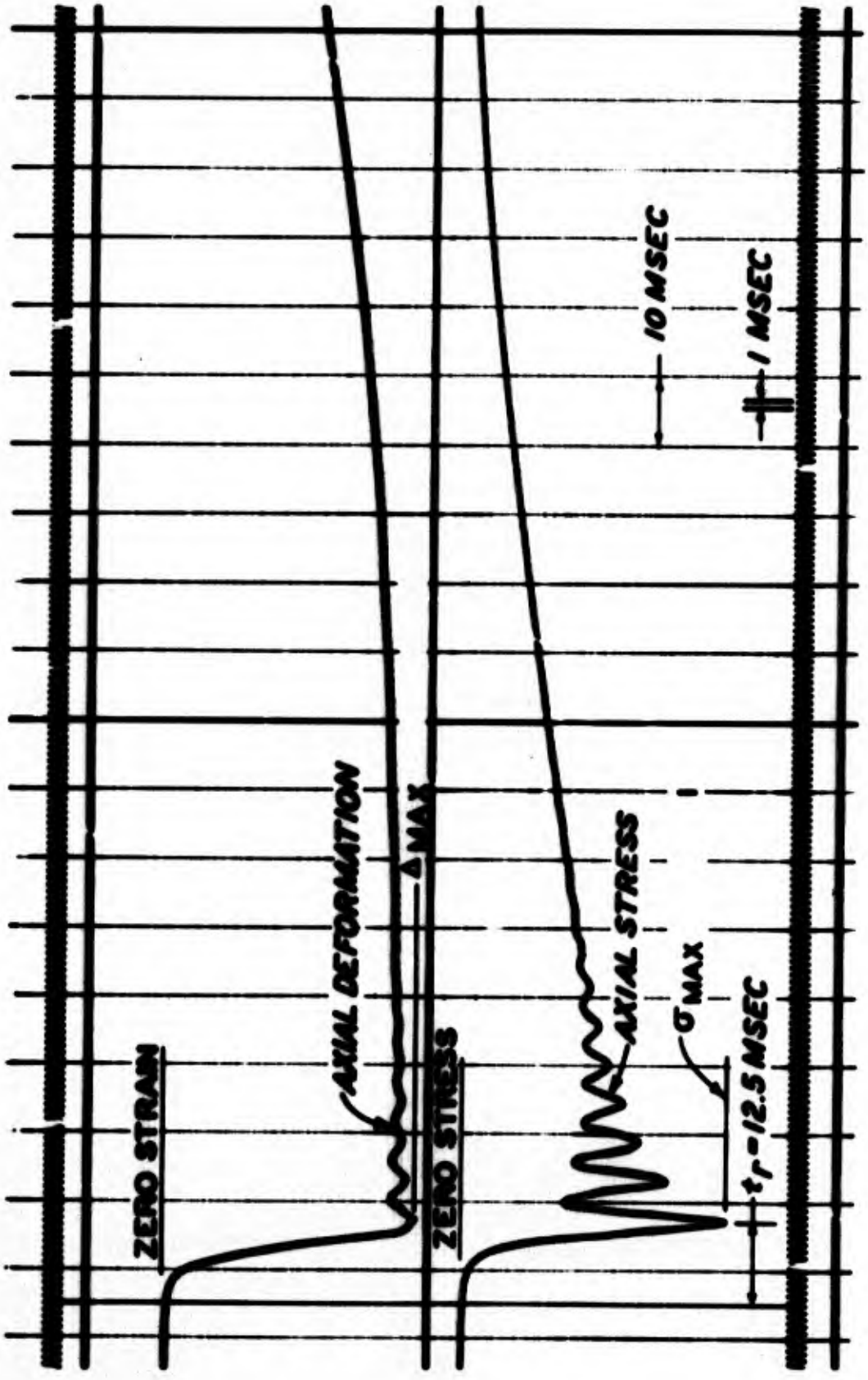

Figure A.4 Typical oscillogram for a dynamic uniaxial strain test.

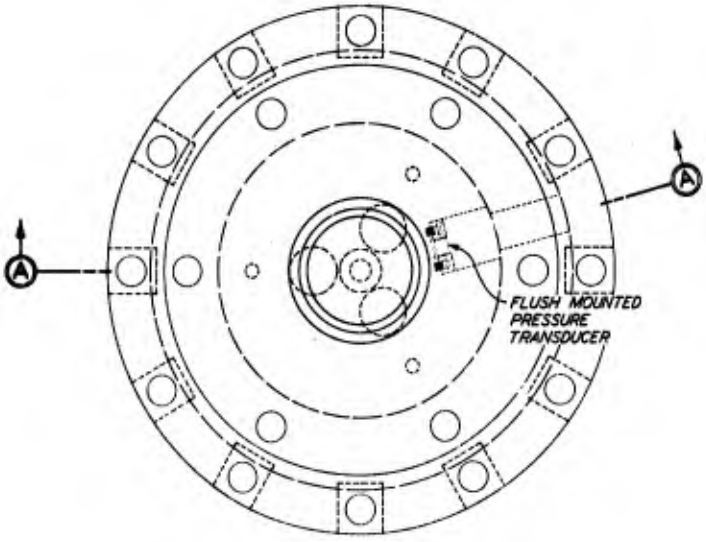

PLAN

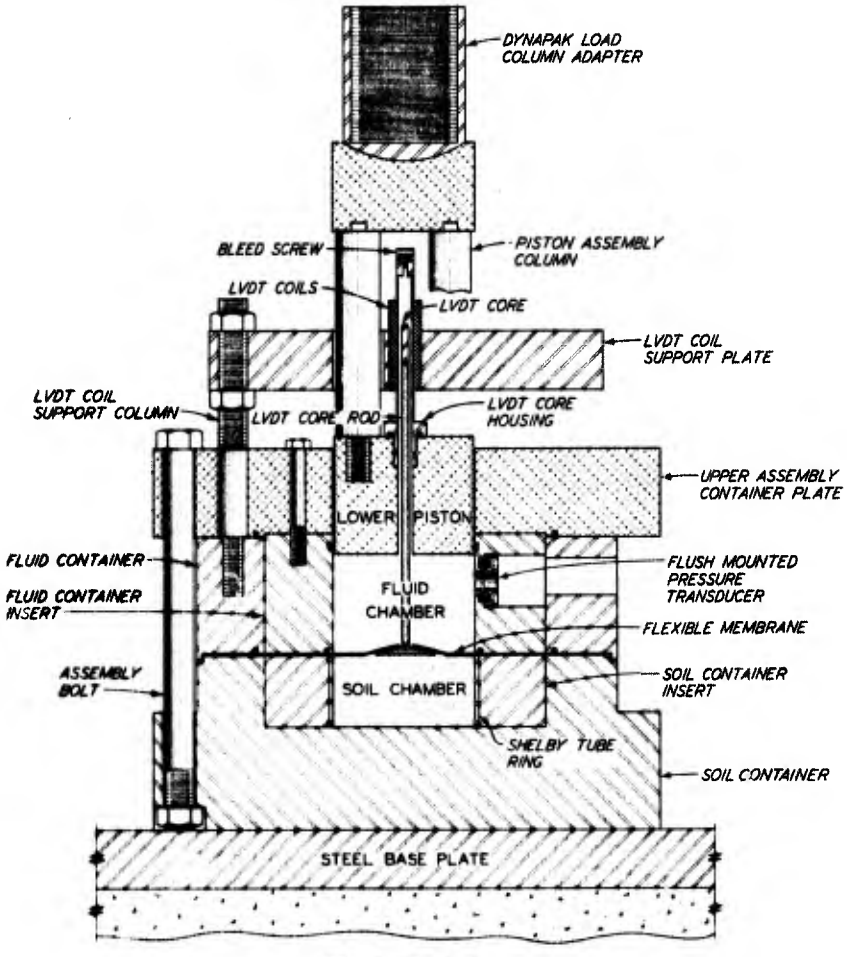

SECTION A-A

Figure A.5 5-inch-diameter uniaxial strain test device.

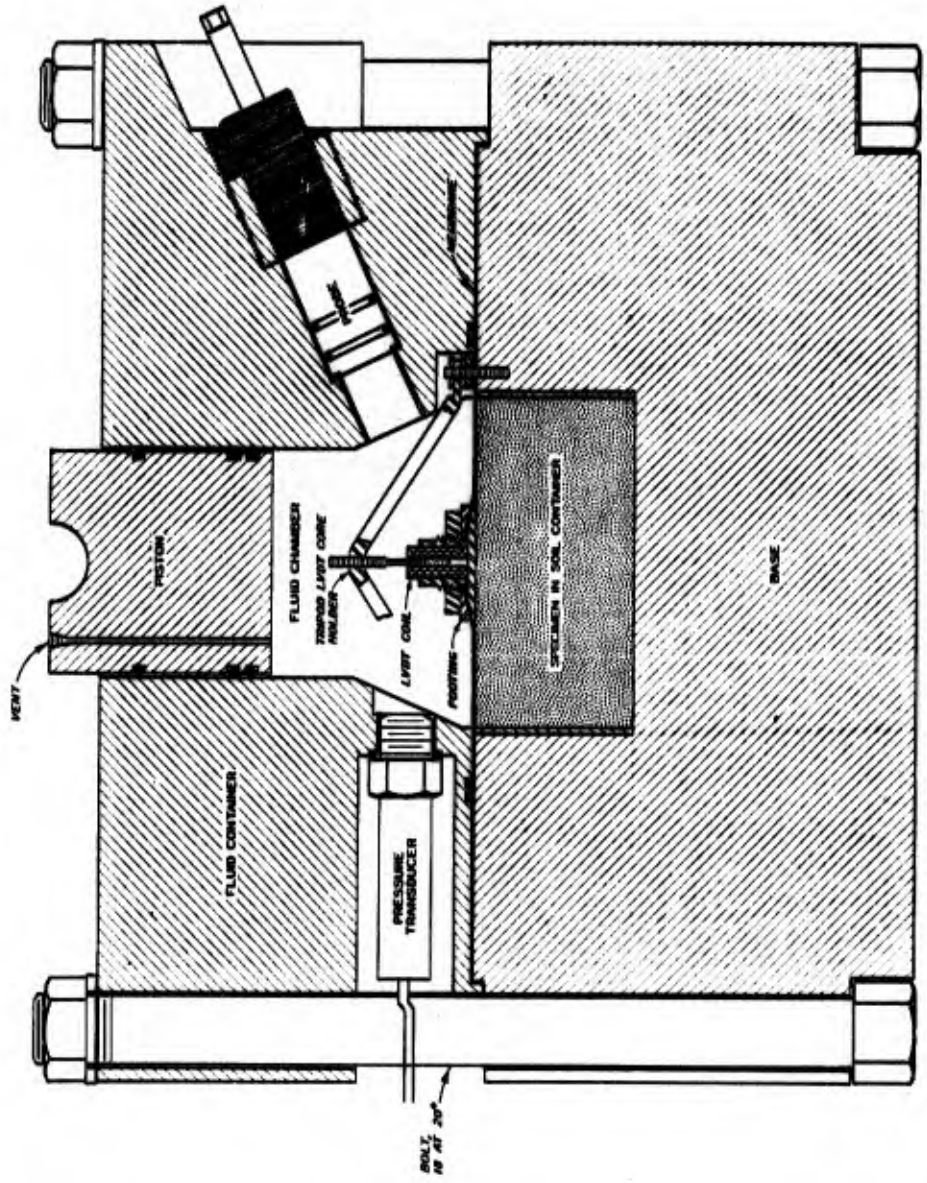

Figure A.6 15,000-psi uniaxial strain test device.

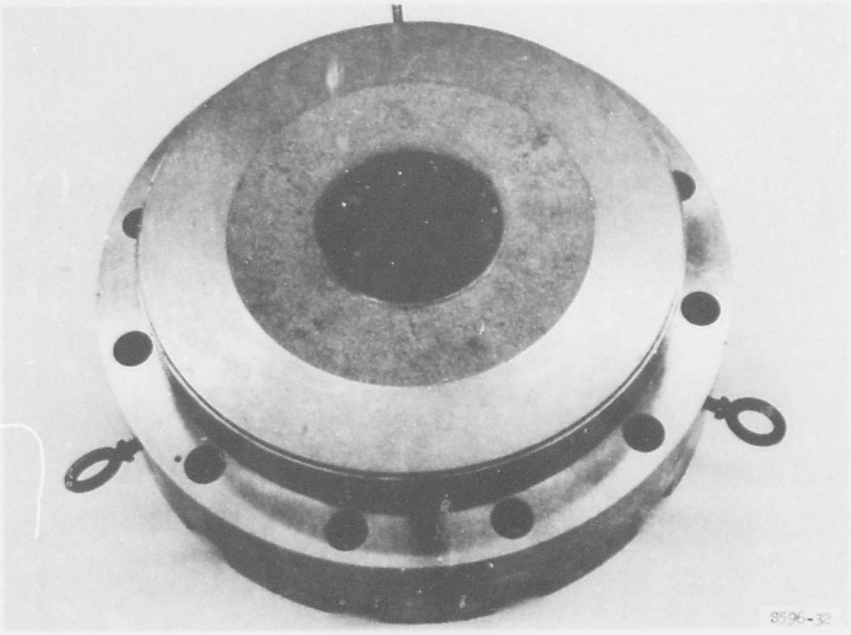

Figure A.7 Compacted sand surrounding undisturbed specimen in soil container for 10-inch-diameter test device.

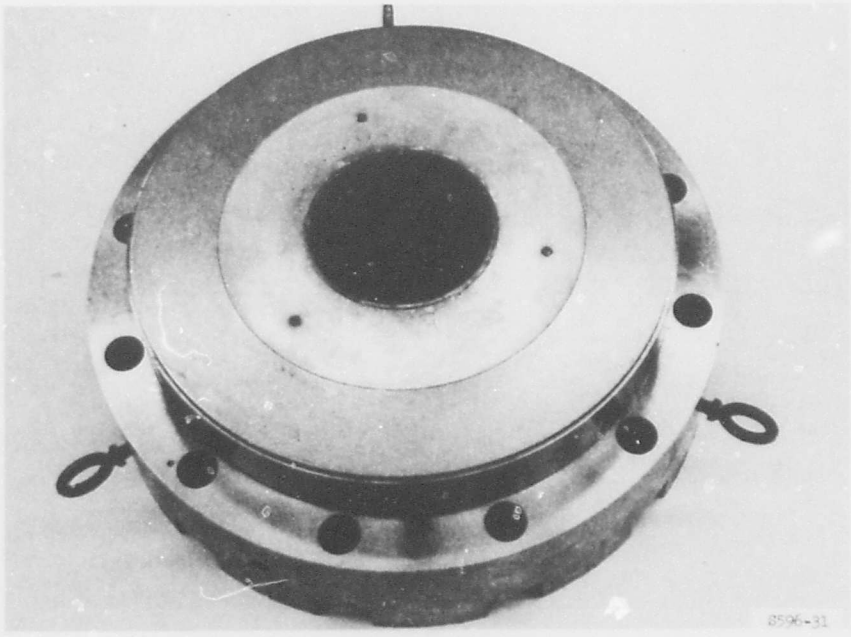

Figure A.8 Steel doughnut surrounding undisturbed specimen in soil container for 5-inch-diameter test device.

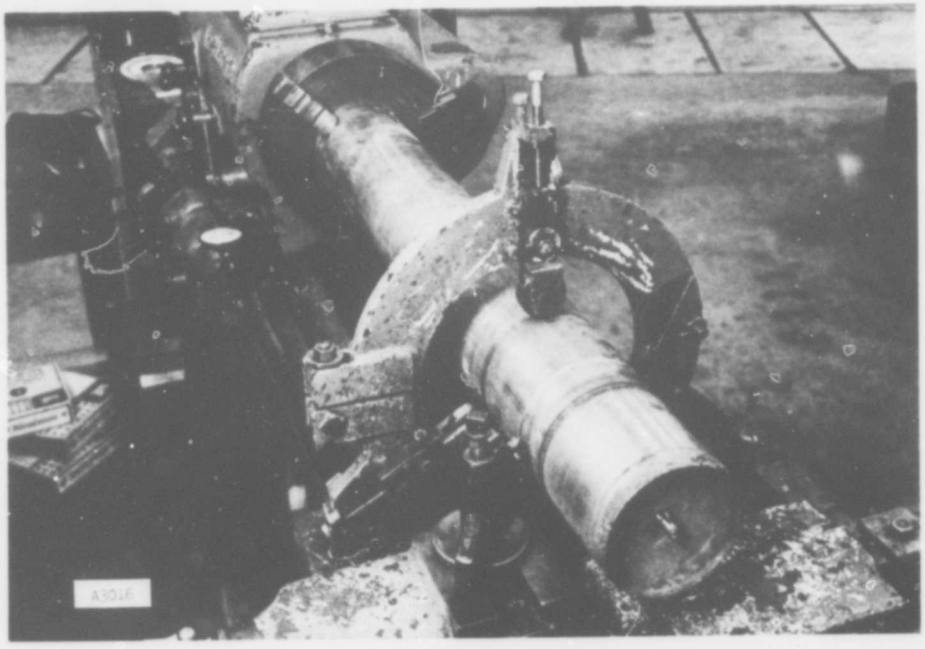

Figure A.9 Shelby tube chucked in lathe for first rough machine cut.

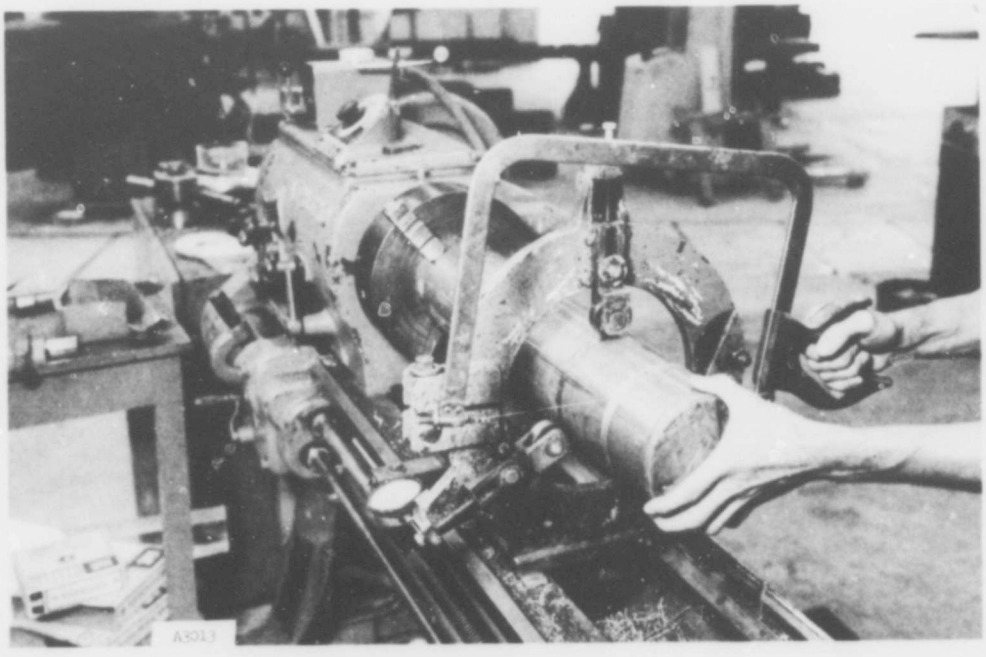

Figure A.10 Wire saw being used to separate soil sample after rough machine cuts through steel Shelby tube.

Figure A.11 Rough-cut Shelby-tube ring specimen with exposed soil partially coated with protective wax.

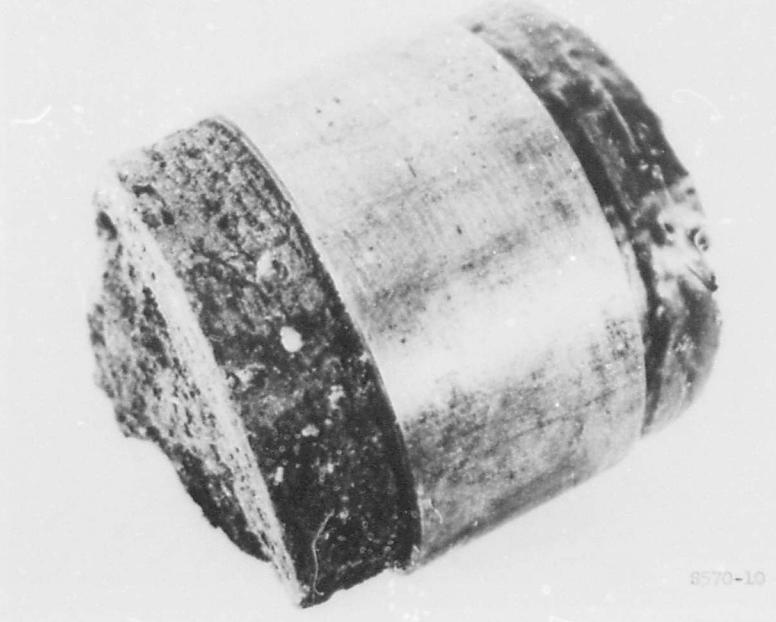

Figure A.12 Fine-machined Shelby-tube ring specimen with protruding ends of exposed and wax-protected soil.

S570-12

Figure A.13 5-inch-diameter by 2-1/2-inch-high Shelby-tube ring-encased specimen ready for uniaxial strain test.

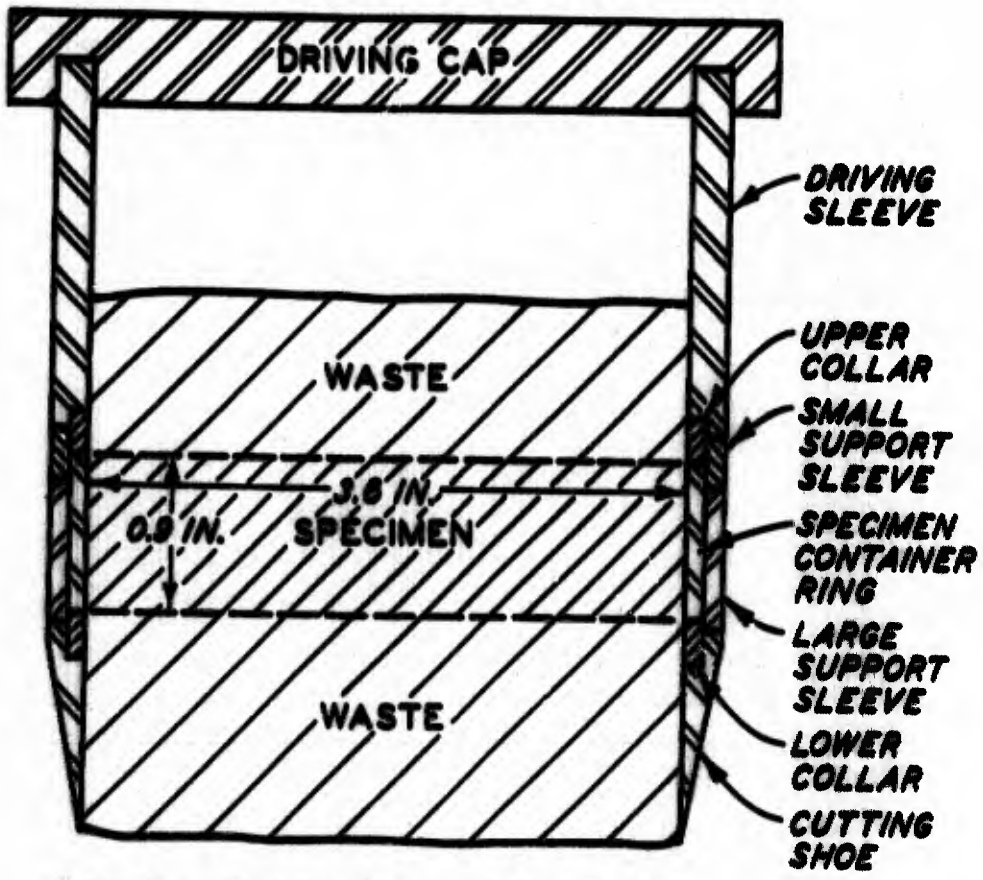

3.6-IN.-DIAM SOIL SAMPLER

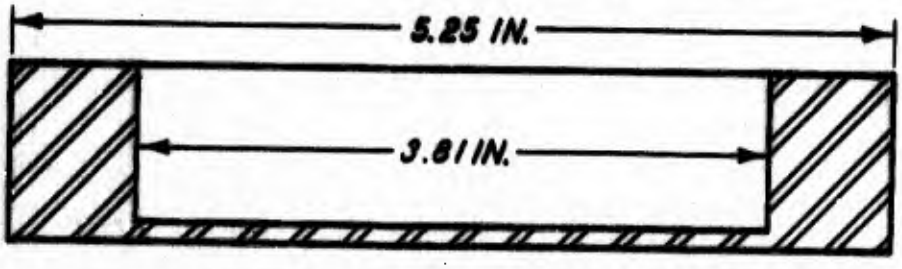

ADAPTER FOR 5-IN.-DIAM UNIAXIAL STRAIN TEST DEVICE

Figure A.14 Sampler for obtaining 3.6-inch-diameter by 0.9-inch-high ring-encased soil specimens and adapter for 5-inch-diameter uniaxial strain test device.

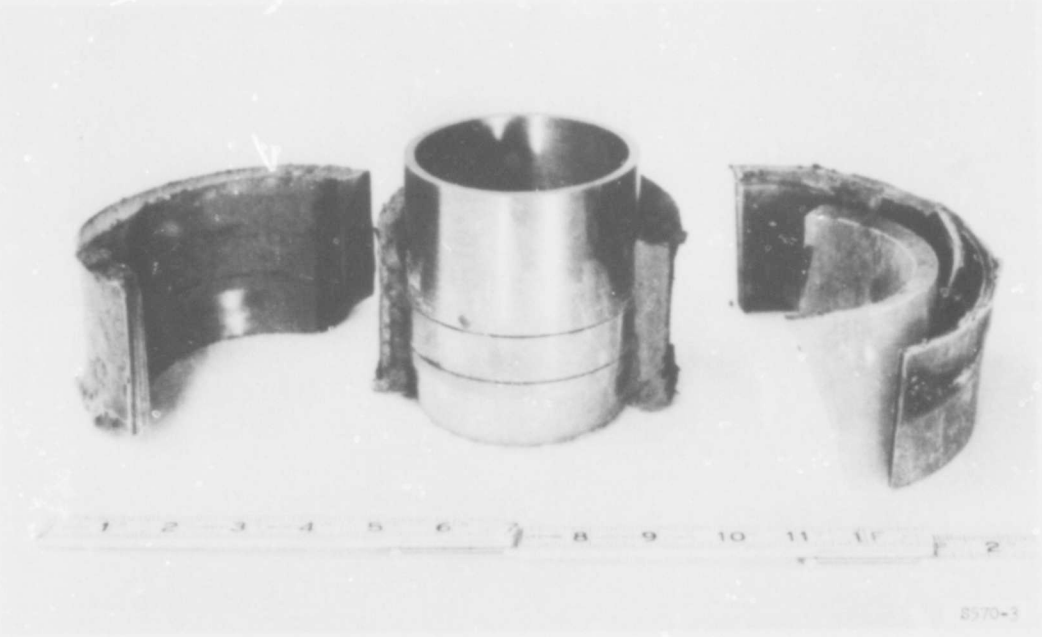

Figure A.15 3.6-inch-diameter ring sampler after jacking into wax- and cardboard-encased undisturbed soil sample.

Figure A.16 3.6-inch-diameter ring sampler after removal of driving sleeve, small support sleeve, and upper collar.

Figure A.17 Soil specimen being trimmed flush with top of 3.6-inch-diameter specimen container ring.

Figure A.18 Uniaxial strain device adapter being placed over 3.6-inch-diameter soil specimen.

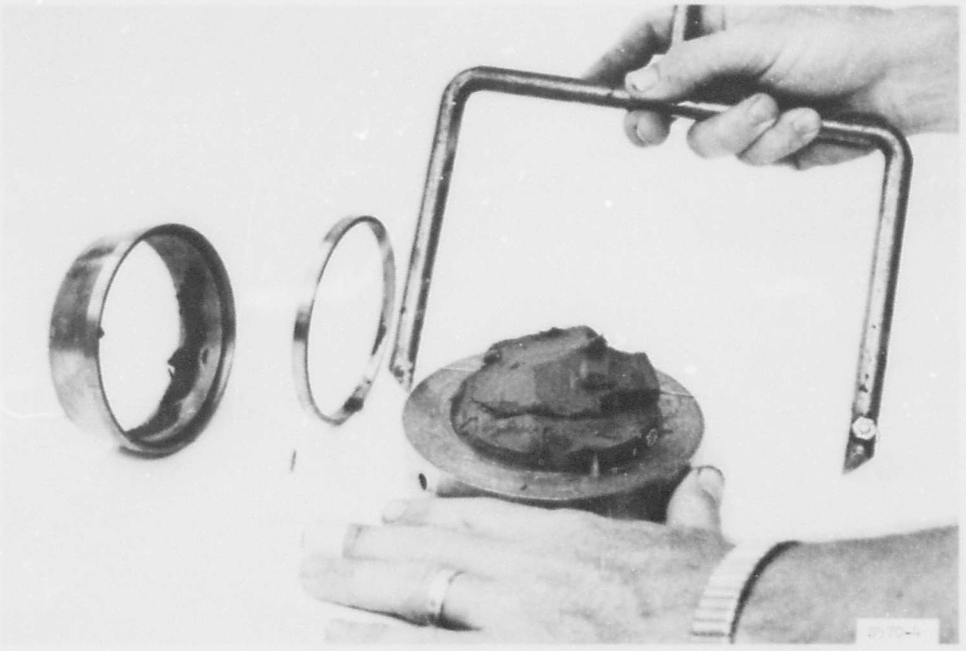

Figure A.19 3.6-inch-diameter specimen being trimmed flush with container ring and test device adapter after removal of cutting shoe, large support sleeve, and lower collar.

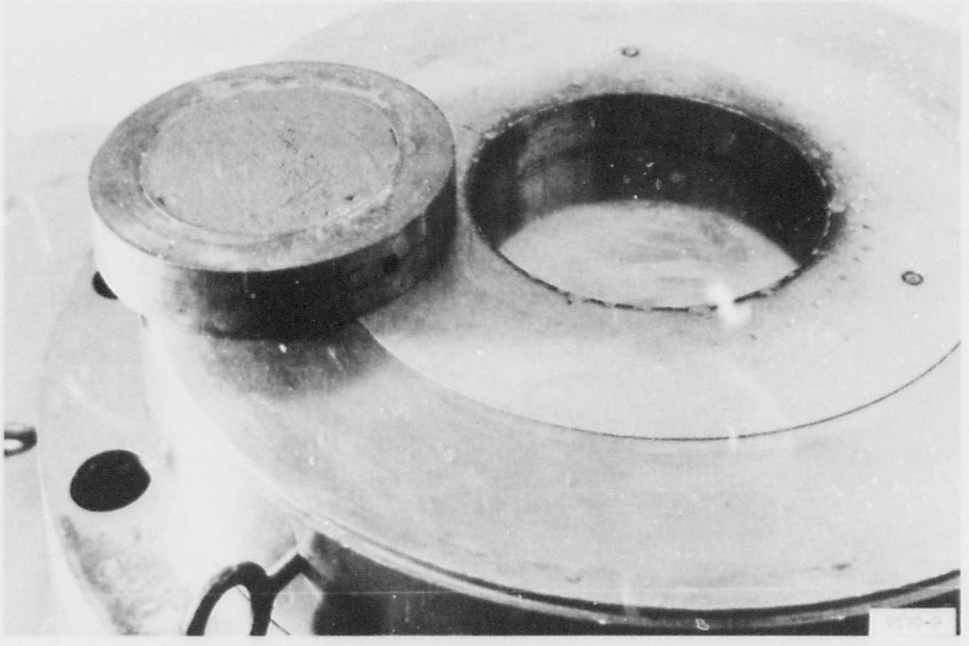

Figure A.20 3.6-inch-diameter specimen and adapter ready for insertion into 5-inch-diameter uniaxial strain test device.